# Fabrication of Fly Ash Based Ceramic Membrane for Tomato Juice Clarification and Water Treatment




*Murchana Changmai*

# Fabrication of Fly Ash Based Ceramic Membrane for Tomato Juice Clarification and Water Treatment

*Thesis submitted in partial fulfillment of the requirement for the degree of*

*Doctor of Philosophy*

*By*

*Murchana Changmai*

*Roll No.: 146107004*


**Department of Chemical Engineering**

**Indian Institute of Technology Guwahati, Assam 781039**

**May 2018**

*Dedicated to my Parents and the Almighty. Their Uncountable Blessings and Support has Helped Me to be the Better Person that I am Today.*

**Department of Chemical Engineering**

**Indian Institute of Technology Guwahati**

**Guwahati 781039, India**

# CERTIFICATE

It is certified that the work contained in the thesis entitled "**Fabrication of fly ash based ceramic membrane for tomato juice clarification and water treatment**", by **Ms. Murchana Changmai**, has been carried out under my supervision. The work documented in this thesis has not been submitted to any other University or Institute for the award of any degree or diploma.

**Dr. Mihir Kumar Purkait**

Professor

Department of Chemical Engineering

Indian Institute of Technology Guwahati

Guwahati 781039, India

Date

# Acknowledgements

I owe a debt of gratitude to many people who have helped me in completing this research work directly or indirectly throughout my stay in IITG. To begin with, I wish to express my sincere acknowledgement and respect to my supervisor, **Dr. Mihir Kumar Purkait** for being a source of my inspiration and guidance all throughout my research work. I am thankful to him for his useful suggestions and constant encouragement throughout my entire work period and feel fortunate enough to have worked under him all these years. The calm demeanour, dedication towards work and ease of handling the toughest of situations are the traits that I hope to inculcate from my supervisor. He has been a moral support throughout my bad times and has always provided me with the freedom to carry out my work without any pressure in the most amicable manner. For this I shall forever be indebted to him.

I would like to thank my doctoral committee members, **Dr. Subrata K. Majumder**, **Dr. Pallab Ghosh** (Department of Chemical Engineering), and **Dr. Lal Mohan Kundu** (Department of Chemistry) for their valuable suggestions and constructive criticism during the project evaluations, which helped me to make necessary improvements in various stages of my research work. I would specially like to thank **Dr. Subrata K. Majumder** and **Dr. Pallab Ghosh** for the rigorous and remarkable questions that they raised during the seminar presentations which had helped me a lot in understanding many facts related to my work as well as in improving my presentation and writing skills.

I am also thankful to all the faculty members of the Chemical Engineering Department for their encouragement and help at various stages during my stay in this Department. In this regard, I would specially like to mention the names of **Dr. Das, Dr. Uppaluri** and **Dr. Majumdar**

I would also like to extend my sincere gratitude to the technical officers of my Department specially, Mr. **Harsaraj Biswanath** and **Mrs. Ritumoni Kalita,** senior technical

superintendents **Mr. Lukumoni Borah** and **Mr. Dipak K. Barman,** technical superintendent **Mr. Jayanta K. Mout,** junior technical superintendents **Mr. Balen C. Mahanta, Mr. Debajit Borah** and **Mr. Pankaj S. Baruah** and the office staff, **Mr. Sailen Das, Mr. Deep J. Sinha** and **Mr. Bhagya Boro**. The experimental works presented in this thesis as well as all the official paper work would never have been possible without the help of these proficient technicians. I am also very thankful to **Mr. Bijoy Kumar Choudhury** (Senior Technician, Department of Mechanical Engineering), who helped me in installing my experimental setup. I would also like to express my gratitude to the **Central Instruments Facility, IITG** for analysing all my samples with the utmost precision and timely disposition.

I extend my sincere thanks to the lab seniors **Dr. Nilay Sharma**, **Dr V. Shyam K. Yadav**, **Mr. Abhik Bhattacharjee** and **Mr. Somnath Chanda** for helping me out innumerable times with my work. My juniors **Mr. Piyal Mondal**, **Mr. Sooraj P. Mohan** and **Ms. Deepti Nair** were constant supports in all my work and helped me in having a pleasant work environment in the lab with their untimely help, support and valuable cooperation. My junior **Mr. Mithelesh Pasawan** has been of immense help and I could not thank him enough for his contributions towards my work. I would like to take the opportunity to thank the research scholars in the RL 3 for helping me out whenever I approached them with any queries or requirements. I would also like to extend my heartfelt thanks to all of my Ph.D. batch mates and the other research scholars at Chemical engineering department, my IITG friends and my childhood friends who have shared their thoughts and views with me.

I would also like to extend my heartfelt thanks to **Department of Biotechnology (DBT), New Delhi, under DBT INNO INDIGO joint call** and **Tata Steel Limited** for giving me the opportunity to work with them in creating a better sustainable water environment.

**Acknowledgements**

I have no words to thank **Lord Krishna, Lord Shiva** and **Lord Ganesha** who are my strength and wisdom.

Last but not the least; I would like to thank my father **Mr. Biren K. Changmai**, my mother, **Mrs. Juri Changmai** and my younger sibling **Mr. Gaurav Changmai** for supporting me to do my Ph.D. My father and mother have always believed in me and moulded me into the strong and independent woman that I am today. My brother has been a moral support during my emotional breakdowns and I could not thank God enough for bestowing me with such a supportive family. Their love, affection, blessings and sacrifices made me stronger to overcome my huddles and achieve my target. I would also like to mention my dog **Pigu** who acted as my stress buster whenever I paid a visit back home.

*Murchana Changmai*

# *Abstract*

A rapid growth in the field of industries and academia has resulted in the immense development and amplification of the membrane technology market. Over the past few decades a rapid transformation has been witnessed with the development of new methods and technologies related to membranes science which cover a wide range of applications such as microfiltration, ultrafiltration, reverse osmosis, gas separations, artificial human organs to name a few. The scientific and engineering disciplines such as electro chemistry, physical chemistry, polymer chemistry and chemical engineering play a major role in this perspective. Thus membrane separation acts as a bridge connecting the varied applications with the respective disciplines. Microfiltration and ultrafiltration with the progress of time have emerged as good replacements for previously existing separation techniques such as a gravity filtration and clarification systems. The main advantages of membrane systems is that they occupy very less space with better operational durability. Recent research have pointed out the advantages of ceramic membrane over polymeric membranes over a wide range of applications which include properties such as stability at high operating temperatures and pressures, good chemical stability, relatively narrow pore size distribution and a higher porosity, higher hydrophilicity with high fluxes at very low pressures and a good mechanical stability, longer working life and impressive defouling properties. However, there still remains certain limitations associated with ceramic membranes which still needs to be acted upon. Large scale fabrications face a tremendous issue with the production of such functional membrane due to high fabrication costs along with the existence of a complicated fabrication process. Thus, it is of utmost necessity to come up with a simple and easily available fabrication technique for ceramic membranes which can be utilized on a large scale. The present work discusses a simple and easy method for the preparation of ceramic membrane suitable mainly for microfiltration applications. The prepared ceramic membrane was modified using a temperature responsive polymer to prepare a specially surface modified ceramic membrane Various applications carried out in the present work include microfiltration of tomato juice, utilization of carrot water from microfiltration process into a novel adsorbent for the treatment of Co (II) contaminated water, utilization of a composite temperature responsive ceramic membrane for BSA rejection, treatment of fluoride water, treatment of steel industry wastewater, treatment of drilling wastewater,

Fly ash based ceramic membranes having a varying pore size were prepared using the paste casting method. Variation in pore size was brought about by the reduction in size of the precursor powder using three different grinding medium viz. the ball mill, the mono mill and the planetary mill. The particle size were successfully reduced from the existing 170 µm (without grinding) to 102.4 µm (ball mill grinded), 78.38 µm (mono mill grinded) and 1 - 2.40 µm (planetary mill grinded). Thus three different membranes MB1, MB2 and MB3 with pore sizes 20-21µm, 1-2.29 µm and 227-450 nm respectively. The membrane thus prepared were used in the clarification of tomato juice to eliminate pectin like compounds responsible for deteriorating its quality with time. The resistance-in-series model was used to evaluate the decline in flux of tomato juice during microfiltration. Individual resistance profile with time were plotted and the changes were observed for the three membrane. The contribution of fouling resistance was in between 98 % and 96 %, adsorption resistance 0.09 % to 0.33 %, pore plugging resistance from 0.33 % to 0.91 % and membrane resistance from 0.6 % to 2 % of overall total resistance. The fouling resistance was thus found to be the main resistance involved in the flux decline of all the three membranes. Various physical and chemical properties of clarified and unclarified tomato juice were also estimated and analyzed.

The prepared ceramic membranes using the paste casting method were then surface modified using a special temperature responsive polymer poly (2-ethyl-2-oxazoline). Thus this thermo-responsive polymer-ceramic composite membrane was able to achieve opening and closing of pores by itself. This novel composite membrane was prepared by coating the polymer poly (2-ethyl-2-oxazoline) on ceramic membrane using the dip coating technique. Different parameters such as polymer concentration (5-20 wt %) and dip coating time (20-60) were considered while preparing the membrane. Extensive study of the physical and chemical properties of the membrane were carried out. Temperature responsiveness was utilized for studying the variation in water flux and BSA rejection. For temperatures above LCST (lower critical solution temperature) the flux achieved was highest at about 5.58×103 L/h.m$^2$ than at temperatures below LCST. A very good rejection of 68% was observed for membrane M-15 (coated with 15 wt % polymer). Hydraulic permeability of the membrane M-15 decreased with an increase in dip coating time and increased with an increase in operating temperature.

The waste from the clarification of tomato juice in the previous work was utilized in the preparation of a novel adsorbent for the treatment of Co (II) contaminated water. Heavy metal ions in waste water are known to affect human health, aquatic life and the

overall ecosystem in adverse ways. It has been found that chemically activated organic wastes from tomato and carrot can be utilized to remove toxic metal ions and organic pollutants from aqueous solution. Adsorbents from organic wastes such as tomato and carrot were prepared by chemical activation method. To increase their adsorption capacity the prepared adsorbents were combined with PET bottle leftovers to create a new composite adsorbent. All the prepared adsorbents were used to adsorb Co (II) from water. Effects of various factors were taken into consideration to study the uptake of Co (II). An optimum adsorbent dosage of 1.2, 0.6 and 0.8 g/L for ACW, ATW and APTC respectively was found to give the maximum amount of adsorption. The synthesized adsorbent particles were characterized using Fourier transform infrared spectroscopy (FTIR), X-ray diffractometer (XRD), Field emission scanning electron microscope (FESEM), Electron dispersive x-ray (EDX) and thermogravimetric analysis (TGA). The effect of all the three adsorbents on the physicochemical properties of Co (II) adsorption was studied by varying different parameters such as contact time, adsorbent dose and pH. Kinetic behavior of the three adsorbents for the uptake of Co (II) were studied. Freundlich model was best suited for the composite adsorbent with an adsorption capacity 312.50 mg/g.

The prepared ceramic membranes were also utilized in the field of treatment of fluoride contaminated drinking water in combination with the electrocoagulation process. A hybrid technique (electrocoagulation followed by microfiltration) was adopted for the efficient removal of fluoride from contaminated drinking water. Three samples of drinking water with fluoride concentration of 7.89, 4.79 and 1.78 mg/L were collected from the from hand tube well located in Karbi Anglong, Assam. The contaminated water was first pretreated using the electrocoagulation technique. Samples of water were studied utilizing the variation in applied current density and pH on the removal of fluoride from water. Effect of current density in the range of 15, 10 and 5 $A/m^2$ and an inter-electrode distance of 0.005 m was considered. A decrease in concentration to 0.0097, 0.335 and 0.656 mg/L for initial fluoride concentration of 1.78, 4.79 and 7.89 mg/L respectively were observed. The pretreated water was then transferred to a microfiltration setup consisting of the previously prepared ceramic membrane. Filtration studies suggested an increase in flux from 287.28 to 690.84 $L/m^2.h$ when the pressure increased from 196 to 509 kPa. Produced flocks were characterized to confirm the presence of fluoride. The proposed hybrid technique was able to reduce the fluoride concentration of contaminated drinking water to below permissible limit of 1.5 mg/L (WHO).

The ceramic membrane were also utilized for the electrocoagulation-microfiltration in the treatment of oil water effluents collected from a drilling site in Barekuri, Assam. Effluent water from the drilling site having oil and grease along with metals like Na, Cr, Cu, Pb and Ni were treated using the electrocoagulation technique and the treated effluent was then filtered through the LD-Slag membrane to remove the flocks produced during the electrocoagulation process. Pretreatment was carried out by varying the current density (20-80 $A/m^2$), electrode distance (0.005-0.2 m) and initial pH (3.6-8.7). The concentration of oil and grease was reduced from 35 mg/L to 10.2 mg/L in just 25 min. TDS values decreased from 3230 to 2780 mg/L. Conductivity of the feed increased from 2.65 to 6.19 which was due to the addition of NaCl, salinity remained more or less the same. Once electro-coagulated, microfiltration was carried out to remove the flocks from the treated water. Four different membranes prepared at sintering temperatures of 700, 800, 900 and 1000 $^oC$ were utilized for the microfiltration studies. Trans-membrane pressures were maintained at three different pressures of 98,196 and 194 kPa. At a pressure of 98 kPa the permeate flux increased from 264 to 423 $L/h.m^2$ when sintering temperatures increased from 700 to 1000 $^oC$. Again, with an increase in pressure, permeate flux increased due to more driving force. It was also observed that 75-85 % of the initial flux was lost during the microfiltration of the electro-coagulated samples. A detailed study was also done on the corrosion of the electrodes and the operating cost of the electrocoagulation process. The electrode cost and energy cost increased with increasing current density. The total cost as a result increased from 0.0502 to 0.253 $US\$/m^3$ when current density increased from 20 to 80 $A/m^2$. Flocks produced during the EC process were characterized using FESEM, EDX, XRD and FTIR.

Effluent water from Tata Steel Limited had chloride, sodium, potassium, manganese, magnesium, pH, TDS, sulphate, calcium and iron. This reject water was treated by a lab scale batch process of electrocoagulation followed by microfiltration of the electro-coagulated sample. The microfiltration process utilized a membrane prepared from fly ash. Removal studies were performed considering the operating parameters current density, run time and electrode distance. At a current density of 50 $A/m^2$, inter-electrode distance of 0.005 m and run time of 20 min the concentrations of Na, Mg, K and Ca were reduced to 449, 54, 35 and 18 ppm respectively, whereas Mn and Fe were found to be completely removed. The TDS concentrations were lowered to 2100, 2092 and 2070 ppm from an initial concentration of at current densities of 20, 30 and 50 $A/m^2$. A detailed study was also done on the corrosion of the electrodes and the operating cost of the

electrocoagulation process. Microfiltration studies were carried out at pressures of 103, 117 and 196 kPa. Membrane resistance contributed to about 71.8 % of the total offered resistance. Produced flocks were analyzed using EDX to confirm the removal of the metals by the electrocoagulation process. Sample electro-coagulated at 10 $A/m^2$ the steady state permeate flux increased from 122 to 1146 $L/m^2.h$ with increase in TMP from 103 to 196 kPa. Membrane resistance contributed to 71.8 % of the total resistance existing during the microfiltration process.

# Research Publications

**Published**

1. V.L. Dhadge, C.R. Medhi, **M. Changmai**, M.K. Purkait, "House hold unit for the treatment of fluoride, iron, arsenic and microorganism contaminated drinking water" Chemosphere 199 (2018) 728-736.
2. **M. Changmai**, P. Banerjee, K. Nahar, M.K. Purkait, "A novel adsorbent from carrot, tomato and polyethylene terephthalate waste as a potential adsorbent for Co (II) from aqueous solution: Kinetic and equilibrium studies" Journal of Environmental Chemical Engineering 6 (2018) 246-257.
3. **M. Changmai**, M.K. Purkait, "Detailed study of temperature-responsive composite membranes prepared by dip coating poly (2-ethyl-2-oxazoline) onto a ceramic membrane" Ceramics International 44 (2018) 959-968.
4. **M. Changmai**, J.P. Priyesh, M.K. Purkait, "$Al_2O_3$ nanoparticles synthesized using various oxidising agents: Defluoridation performance" Journal of Science: Advanced Materials and Devices 2 (2017) 483-492.
5. **M. Changmai**, M.K. Purkait, "Interaction of fatty acid chain length with $NiFe_2O_4$ nanoparticles" Surfaces and Interfaces 8 (2017) 45–53
6. **M. Changmai**, M.K. Purkait, "Kinetics, equilibrium and thermodynamic study of phenol adsorption using $NiFe_2O_4$ nanoparticles aggregated on PAC" Journal of Water Process Engineering 16 (2017) 90–97.

**Submitted**

1. **M. Changmai**, M. Pasawan, M.K. Purkait, " A hybrid method for the removal of fluoride from drinking water: Parametric study and Cost estimation" Separation and Purification Technology. (**Under review**)

2. **M. Changmai**, M. Pasawan, M.K. Purkait, "Treatment of drilling effluent using electrocoagulation followed by microfiltration" Chemosphere. (**Under review**)

3. **M. Changmai**, M.K. Purkait, "Understanding of resistance-in-series model during microfiltration of tomato juice utilizing fly ash based membrane fabricated from mechanically varied precursor powder" LWT – Food Science and Technology. (**Under review**)

4. **M. Changmai,** M. Pasawan, M.K. Purkait, "Application of electrocoagulation-microfiltration process for the treatment of reject water from steel plant" Journal of Hazardous materials. (**Submitted**)

## Conferences/ Seminars or workshops

1. M. Changmai, P. Banerjee, K. Nahar, M.K. Purkait, "A novel adsorbent from carrot, tomato and polyethylene terephthalate waste as a potential adsorbent for Co (II) from aqueous solution: Kinetic and equilibrium studies" **Indo- Japan bilateral symposium (IJBS) on Future Perspective of Bio resources** "in North-East India", 1-4 February 2018, **Indian Institute of Technology Guwahati**.

2. M. Changmai, M. Pasawan and M.K. Purkait, "A hybrid method for the removal of fluoride from water" **7th International conference on Chemical, Agriculture,**

**Environment and Natural Sciences (CAENS-2017)**, 20-21 November 2017, **Kuala Lumpur, Malaysia.**

3. M. Changmai and M.K. Purkait, Fly ash based membrane for the clarification of tomato juice: Resistance-in-series model, **REFLUX 2017**, 24-26 March, 2017, **Indian Institute of Technology Guwahati.**

4. M. Changmai and M.K. Purkait, "Defluoridation performance of Al2O3 nanoparticles synthesized using various oxidising agents" **International Conference on Nano for Energy and Water (NEW) Indo French Workshop on Water Networking 2017)**, 22-24 February, **University of Petroleum and Energy Studies Dehradun**.

5. M. Changmai and M.K. Purkait, "Effect of fatty acid chain length on the structural properties of the coated NiFe2O4 nanoparticles" **International Conference on Nano for Energy and Water (NEW) Indo French Workshop on Water Networking 2017)**, 22-24 February, **University of Petroleum and Energy Studies Dehradun**.

6. M. Changmai and M.K. Purkait, "Detailed study on the variation of particle size of precursor powder with pore size distribution of ceramic membranes" **Emerging trends in separation science and technology-SESTEC 2016**, 17-20 May, 2016, **Indian Institute of Technology Guwahati**.

7. Course by **Indian Institute of Technology Bombay** on "Technical Communication for Scientists and Engineers", 11 January - 02 May 2016.

8. M. Changmai and M.K. Purkait, "Microfiltration of tomato juice: Resistance in series model" **3rd Indo-German Workshop on "Advances in materials,**

**reaction and separation processes"** 23-26 February, 2016, **Indian Institute of Technology Guwahati**.

9. M. Changmai and M.K. Purkait, "Investigation on the variation of particle size of precursor powder with pore size distribution of membrane" **CHEMCON-2015**, 27-30 December, 2015, **Indian Institute of Technology Guwahati.**

# CONTENTS

**CONTENTS**

# LIST OF FIGURES

# LIST OF TABLES

# Nomenclature

## Notations

| | |
|---|---|
| $A$ | Area of the electrodes |
| $A_m$ | Membrane area available for filtration |
| $C_e$ | Initial concentration of Co (II) |
| $C_{Electrode}$ | Consumption quantities of electrode material |
| $C_{Energy}$ | Consumption quantities of and electricity |
| $C_o$ | Equilibrium concentration of Co (II) |
| $F$ | Faraday's constant |
| $I$ | Current |
| $J_F$ | Steady state permeate flux |
| $J_h$ | Heat flux |
| $J_i$ | Electrical flux |
| $J_I$ | Initial permeate flux |
| $J_m$ | Mass flux |
| $J_n$ | Momentum flux |
| $J_p$ | Permeate flux |
| $J_v$ | Volume flux |
| $J_W$ | Pure water flux |
| $K_1$ | Rate constant pseudo-first-order adsorption |
| $K_2$ | Rate constant of the pseudo-second-order adsorption |
| $K_F$ | Freundlich constant |
| $K_L$ | Langmuir constants related to rate of adsorption |
| $L$ | Length of pore in equations |
| $L_p$ | Hydraulic permeability |

| | |
|---|---|
| $m_1$ | Weight of the electrodes immediately after the electrocoagulation experiment |
| $m_2$ | Weight of the electrodes after the electrocoagulation experiment after cleaning |
| $M$ | Mass of adsorbent taken |
| $M_d$ | Dry mass of the ceramic membrane |
| $M_s$ | Mass of the suspended membrane |
| $M_w$ | Molecular mass of Aluminium |
| $M_c$ | Mass of the ceramic membrane saturated with water |
| $n$ | Freundlich constant |
| $p$ | Price of electrical energy |
| $\Delta P$ | Transmembrane pressure in equations |
| $q$ | Price of electrode |
| $q_e$ | Amount of Co (II) adsorbed onto the adsorbent at equilibrium |
| $q_m$ | Langmuir constants related to adsorption capacity |
| $q_t$ | Amount of Co (II) adsorbed onto the adsorbent at any time t |
| $Q_P$ | The flow rate of permeate across the membrane |
| $r$ | Radius of pores |
| $r_m$ | Mean pore radius |
| $\%R$ | Percentage removal |
| $R_{ad}$ | Adsorption resistance |
| $R_f$ | Fouling layer membrane resistance |
| $R_m$ | Resistance offered by the fresh membrane |
| $R_{pp}$ | Resistance due to pore blocking of membrane |
| $R_t$ | Total resistance |
| $t$ | Film-thickness |

| | |
|---|---|
| $T$ | Electrolysis time |
| $V$ | Volume of solution taken |
| $Vi$ | Applied voltage |
| $V_L$ | Volume of EC solution. |
| $W_1$ /$W_4$ | Weight of the sample + crucible before change |
| $W_2$ /$W_5$ | Weight of the sample + crucible after change |
| $W_3$ /$W_4$ | Weight of the sample before change |
| $W_A$ | Weight of membrane in air |
| $W_S$ | Soaked weight of membrane |
| $W_{SW}$ | Suspended weight of membrane |
| $\mu_p$ | Viscosity of water |
| $W_W$ | Wet weight |
| z | Number of electron transferred |
| ε | Porosity |
| $\rho$ | Density of the film formed over the electrode surface |
| $\mu$ | Viscosity of water |

## Abbreviations

| | |
|---|---|
| AAS | Atomic absorption spectroscopy |
| ACW | Activated carrot waste |
| APTC | Activated composite |
| APET | Activated PET |
| ATW | Activated tomato waste |
| BD | Bulk density |
| BIS | Bureau of Indian Standards |

| | |
|---|---|
| BM | Bare ceramic membrane |
| BSA | Bovine serum albumin |
| CA | Cellulose acetate |
| CW | Dried carrot waste |
| D.O. | Dissolved oxygen |
| EC | Electrocoagulation |
| EDX | Energy-dispersive X-ray spectroscopy |
| EPA | Environmental protection agency |
| FDR | Flux decline ratio |
| FESEM | Field emission scanning electron microscope |
| FRR | Flux recovery ratio |
| FTIR | Fourier transform infrared |
| KBr | Potassium bromide |
| LCST | Lower critical solution temperature |
| MF | Microfiltration |
| PAI | Polyamide-imide |
| PAN | Polyacrylonitrile |
| PES | Polyethersulfone |
| PET | Polyethylene pterepthalate |
| PM | Polymer coated ceramic membrane |
| PNM | Polymer-nanoparticle coated ceramic membrane |
| PP | Polypropylene |
| PSF | Polysulfone |
| PVDF | Polyvinylidene fluoride |
| RO | Reverse osmosis |

| | |
|---|---|
| SPCB | State pollution control board |
| TDS | Total dissolved solids |
| TGA | Thermogravimetric analysis |
| TMP | Transmembrane pressure |
| TSS | Total suspended solids |
| UF | Ultrafiltration |
| UV-Vis | Ultraviolet-visible spectrophotometry |
| WCA | Water contact angle |
| WHO | World health organization |
| XRD | X-ray diffraction analysis |

# Chapter 1
# Introduction

# *Chapter 1*

## Introduction

*This chapter gives the overview of the method adopted for the preparation of ceramic membrane using different raw materials and its application in the field of microfiltration. The basic objective of the applications include fruit juice clarifications, the provision of clean drinking water and clean surface water and. The microfiltration process has been clubbed with an electrocoagulation process to create a reliable and an efficient technique for the treatment of drinking water and industrial wastewater. The work also deals with the utilization of the waste left behind from the clarification of fruit juice into a novel adsorbent. A detailed characterization study has been performed on all the prepared membranes. The chapter subsequently presents detailed literature review that includes study of various resistances existing during the microfiltration process.*

## 1.1 Background

Membrane technology has become one of the most amicable separation technology over the past few decades and are now one of the most competitive replacements for conventional techniques. In simple words, a membrane can be defined as a semi-permeable barrier that prevent intimate contact between two homogeneous phases, but allow a favoured transit of certain selected species across its structure. The main reason that membrane technology has attracted so much attraction in the recent years is due to the fact that it works without the addition of extra chemicals, with low energy usage, low cost and maintenance and ease of usage. The membrane has the ability to aid in the transfer of certain species more readily than others because of certain chemical or physical properties existing between the membrane used and the permeating species. The simple principle being that the membrane acts as a very

specific filter that will let water flow through, while it catches the suspended solids and other substances. In order to ensure the penetration of these specific substances, various methods have been identified. Examples of such methods include the concentration gradients maintained across a membrane, introduction of high pressure, maintaining a temperature gradient across the membrane surfaces and the existence of an electrical potential. Each of these methods correspond to the respective driving force that aids in the separation process. Thus, the driving force (pressure, concentration, electrical potential and/or temperature) helps in separating a particular component through a membrane. The liquid that is able to pass through the membrane is known as "permeate" and the retained liquid is known as "retentate" or "concentrate. The **Table 1.1** below shows the various phenomenological equations that may exist during a membrane transportation process [1-2].

**Table 1.1: Phenomenological equations in a membrane transport process**

| **Flux type** | **Equation** | **Obeyed law** |
|---|---|---|
| Mass flux | $J_m = -D\frac{dC}{dx}$ | Fick's law |
| Volume flux | $J_v = -L_p\frac{dP}{dx}$ | Darcy's law |
| Electrical flux | $J_i = -\frac{1}{R}\frac{dE}{dx}$ | Ohm's law |
| Heat flux | $J_h = -\lambda\frac{dT}{dx}$ | Fourier's law |
| Momentum flux | $J_n = -\vartheta\frac{dV}{dx}$ | Newton's law |

Membrane filtration thus emerges as a new alternative for various conventional processes such as flocculation, adsorption via the use of activated carbon filters or the age old sand filters, purification by sedimentation, ion exchange and distillation. Membranes are used more and more often for the creation of process water from groundwater, surface water or wastewater. A majority of industrial processes mainly utilize the organic membranes which are membranes synthesized from synthetic and or natural polymers. The most common synthetic polymers include polyvinylidene fluoride (PVDF), polysulfone (PSF), polyethersulfone (PES), polyacrylonitrile (PAN), polypropylene (PP), polyamide-imide (PAI) to name a few. Whereas natural polymers include cellulose, rubber and wool. The selection of the polymer depends largely on the intended application and the fabrication technique to be utilized along with factors such as chain interactions, functional group polarity, chain rigidity and stereoisomerism of the selected polymer. Certain membrane separation may require the use of a polymer with a very low affinity towards the permeate, whereas in other cases the opposite may be desirable. Although polymeric membranes find their usage in a wide array of applications, however they have a wide range of disadvantages associated with them such as low solvent resistance, low pH and temperature resistance and lower mechanical strength. To overcome these disadvantages inorganic membranes (ceramic) were fabricated which compensated the drawbacks associated with the polymeric membrane. The ceramic membranes consisting of a metal and a non-metal oxide provide a favorable use in highly acidic or basic environments due to their inherent inertness. They are usually prepared by molding into definite shapes followed by high temperature sintering. Certain ceramic membranes which are prepared from zeolites possess catalytic properties and are widely used in highly-selective gas separation process. In addition to the benefits mentioned above, inorganic membranes offer high resistance to corrosion with a longer working life span. **Table 1.2** shows the basic advantages and disadvantages associated with both organic and inorganic membranes [2-4].

**Table 1.2: Features of polymeric and ceramic membranes.**

| Polymeric membrane | | Ceramic membrane | |
|---|---|---|---|
| **Advantages** | **Disadvantages** | **Advantages** | **Disadvantages** |
| Wide pore size<br>Low cost<br>Ease of fabrication | Low solvent resistance.<br>Low pH resistance<br>Low temperature range.<br>Low mechanical strength. | Corrosion resistance<br>pH resistant<br>High temperature resistant<br>Longer life span<br>Low fouling<br>Higher mechanical strength | Limited pore size<br>Higher cost<br>Brittle in nature |

## 1.2 Membrane classification

In the simpest terms, a membrane is a barrier with specific pore size ratings and retain particles or microorganisms larger than their pore size primarily by surface capture. Thus, the membrane can be classified into various subdivisions based on different viewpoints such as nature of the membrane, separation regime and membrane geometry. The membrane as such may be synthetic or natural, homogenous or heterogeneous, aiding in active or passive transportation process. The first and the most common classification is based on the nature of the membrane i.e. Synthetic or biological membrane. Synthetic membranes can be further divided into organic (polymeric or liquid) and inorganic (e.g. ceramic, metal) membranes whereas biological membranes can be living or non-living. Synthetic membranes display a broad range of physical structure based on the material they are made from. On the basis of separation regime, membranes may be classified as homogeneous and heterogeneous. The first group is

dense homogeneous polymer membranes (uniform in composition and structure) which are usually prepared from solution by solvent evaporation or by extrusion of the melted polymer. However, being dense in nature, their application becomes rather limited. The fact being that a minimal membrane thickness is required for the flow of permeate across the membrane to maintain the membrane stability. The majority of heterogeneous membrane are porous with pores of definite dimensions or consist of a dense top layer on a porous structure. Another classification of solid membranes is on the basis of their morphology or structure i.e. symmetric and asymmetric membrane. The symmetric (isotropic membranes are subdivided into microporous membranes, non-porous dense membrane and electrically charged membrane. Asymmetric (anisotropic) membrane on the other hand are subdivided into Loeb-Sourirajan membrane, thin-film (composite) membrane and liquid membranes. Symmetric membranes refer to the membranes with uniform structure throughout the membrane thickness and are mainly used in dialysis and electrodialysis. The total resistance of the mass transfer through the membrane relies on the total thickness of the membranes. Hence, the lesser the membrane thickness the higher is the permeation rate. Within the asymmetric membranes, there are the integrally skinned membranes where the pore structure gradually changes from very large pores to very fine pores resulting in a "skin" like structure on top of the membrane and named as "integrally skinned". Whereas, many a times the skin may also be nonporous. The thin-film composite membrane is one of the most important type of asymmetric membrane. Asymmetric membranes are primarily utilized in pressure driven processes such as reverse osmosis, gas separation, microfiltration and ultrafiltration. The preference of asymmetric membrane over the rest is because of the fact that it provides a high permeate flow per unit area and a very high mechanical stability. Another category of membranes is that of the porous membranes, which can also be divided into the following main groups. They are divided according to their pore diameter: microporous ($d_p$ < 2 nm), mesoporous (2 nm < $d_p$ < 50 nm) and macroporous ($d_p$ >

50 nm). A classification of the membrane may also be done on the geometry of the membrane. This geometry exists as per requirement in a particular application and can be tubular, hollow fiber, flat sheet etc [1-4].

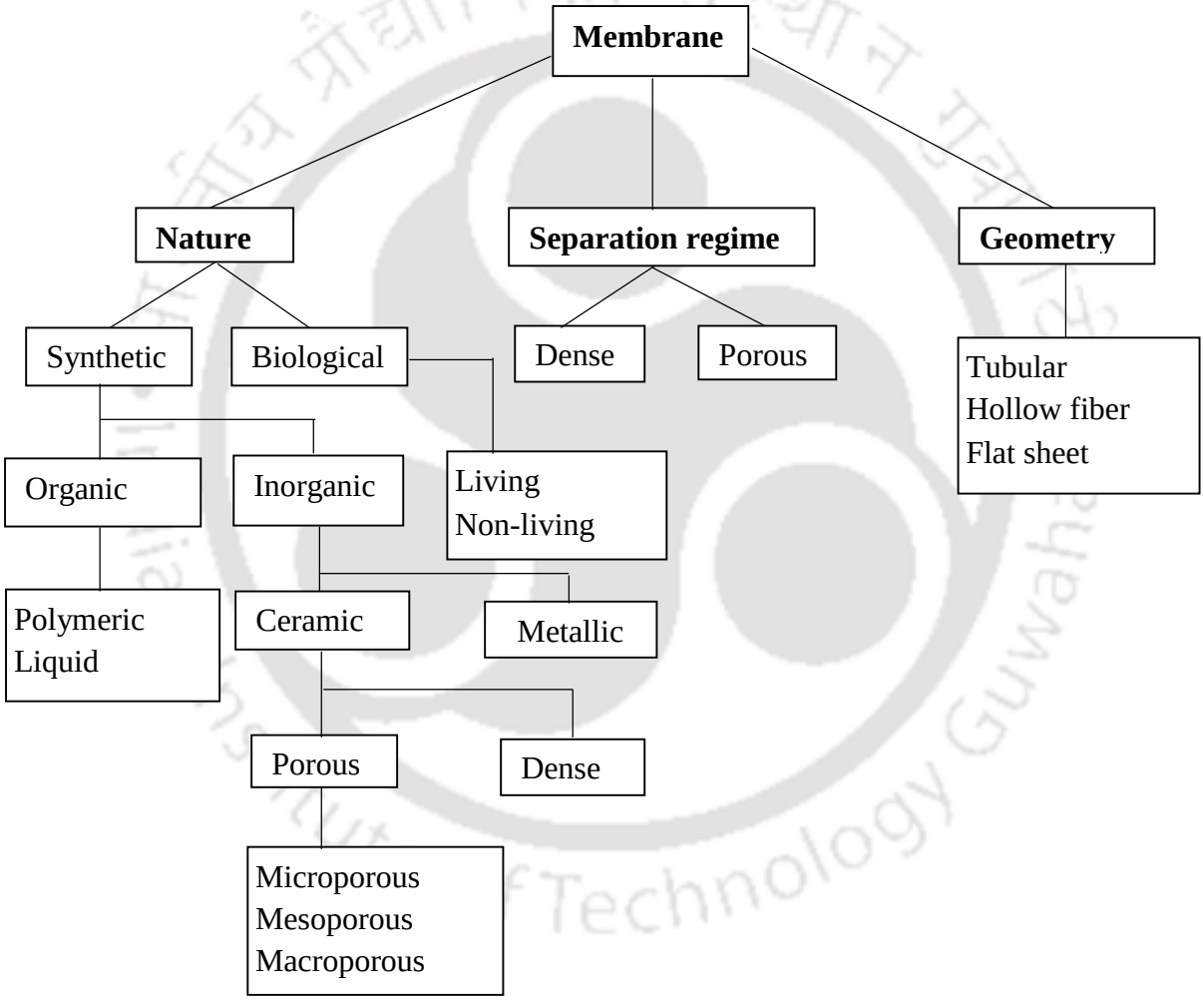


**Fig. 1.1: Schematic diagram showing the general classification of membranes.**

## 1.3 Membrane separation process

Membrane separation process are of a wide variety based on the configuration, driving force acting on the separation process, mechanism of transport of various components through the membrane and many other such specific features. Membrane separation involves separating components from liquid, fluid or gaseous streams by means of forcing the stream to flow under pressure over the surface of a membrane. Species smaller than the membrane pore size pass through the membrane while the larger species are retained. Hence, large volumes can be treated with remarkable energy efficiency. For pressure driven process, the pore size of them membrane of the membrane plays a major role. Reverse osmosis (RO) is one of the most complex technique in membrane separation which concentrate low molecular weight organic materials and salts while allowing water and solvents to pass. Hence, it is extensively utilized in the removal ionic species including the desalination of sea water and reclaiming of brackish well water. Nanofiltration (NF) also referred as "loose reverse osmosis" separates liquid in a region between reverse osmosis (RO) and ultrafiltration (UF) displaying an excellent rejection of divalent ions. Hence, NF applications include demineralization, color removal and desalting. Ultrafiltration (UF) is a low pressure fractionation of selected components by size and are mainly used in numerous industries for concentration, clarification and dia-filtration of large process streams. The UF membrane is more porous compared to reverse osmosis process. Hence, colloids, suspended solids and organic molecules like BSA are retained back by the UF membrane. The porous nature of the UF membranes aids in the operation of the membranes at high fluxes and low pressures. Microfiltration (MF) separates macro materials and suspended solids in the size range of about 0.05-2.0 microns. Typical materials removed by MF are starch, bacteria, fat, molds, yeast and emulsified oils. MF offers unlimited new process opportunities in the industrial market [1-4].

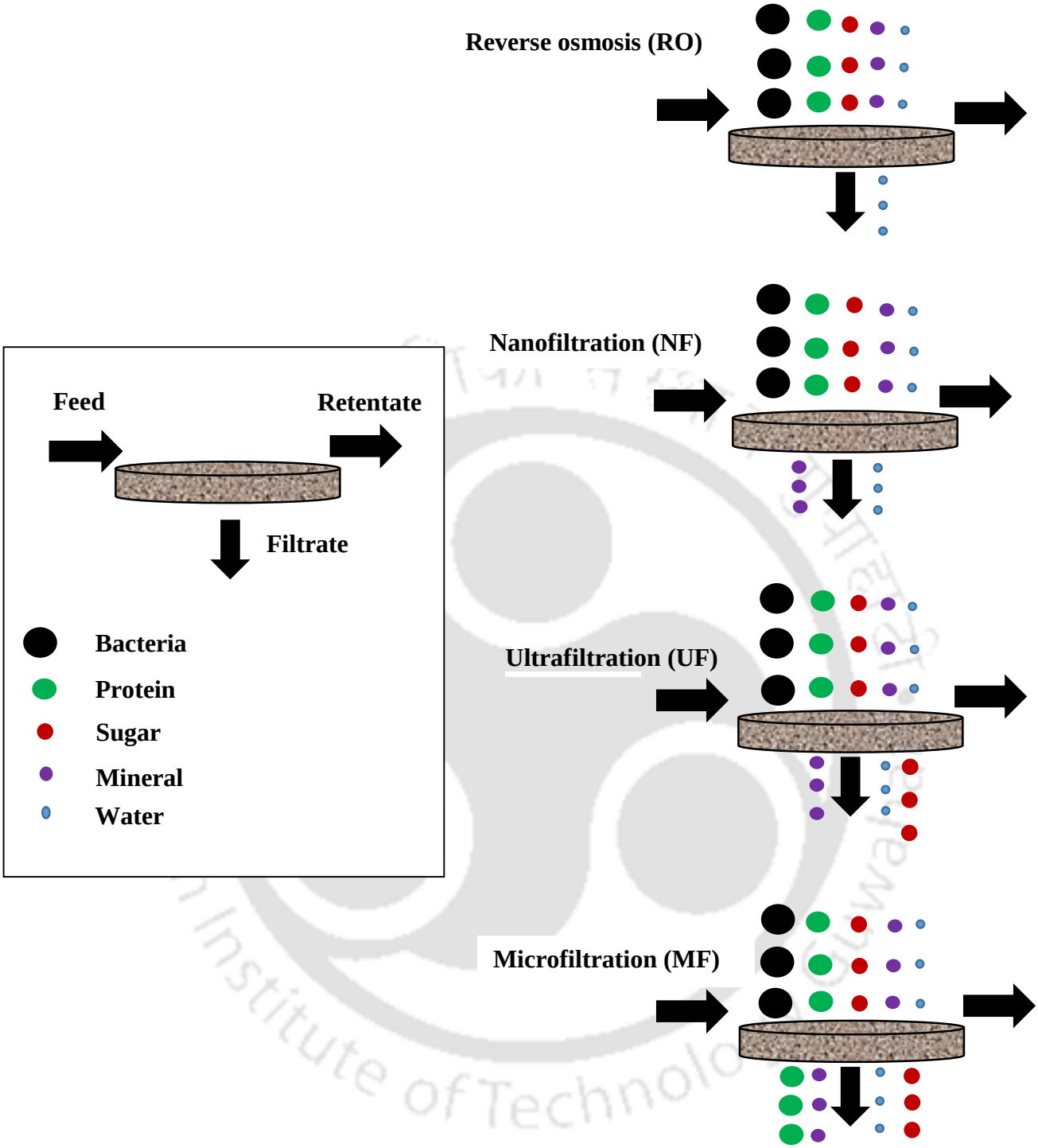


**Fig 1.2: Schematic diagram showing the description of reverse osmosis, nanofiltration, ultrafiltration and microfiltration.**

## 1.4 Fabrication of ceramic membranes

With increasing protocols being established for environment protection and an increasing demand in desalinated water, membrane separation process finds a huge demand in the present scenario. Membranes find a wide range of application especially in the treatment of water and wastewater via the use of microfiltration, ultrafiltration, nanofiltration and reverse osmosis. Another reason for membranes being in high demand is because of the fact that they reduce the waste disposal expenditure to a very large extent and allow the easy recovery of materials. The ceramic/inorganic membranes are usually fabricated form materials such as alumina, clay, zirconia and titania. Despite the high costs encountered during the fabrication process of the ceramic membranes their long term durability, resistivity to harsh chemicals, higher mechanical strength along with high thermal stability finds their way into a widespread application in both industrial and household. Researchers have found that ceramic membranes are in fact more advantageous and effective in the treatment of water in comparison to conventional techniques such as sedimentation and floatation. A ceramic membrane possess three distinct layers each having its own specific function. The top layer is responsible for carrying out separation, the intermediate layer is characterized by pores of lower sizes acting as a bridge between the top layer and the support layer. The last layer is the porous support which is responsible for providing the mechanical strength to the fabricated ceramic membrane. Various methods have been identified for the fabrication of ceramic membranes. These methods include slip casting, tape casting, powder pressing, paste processing, extrusion, sol-gel process, dip coating, chemical vapour deposition, and anodic oxidation. The selection of any preparation method depends on the application and the desired membrane structure [5,6]. The slip casting method involves the poring of a suspension of clay or ceramic materials in water into a mold. The main disadvantage associated with this method is the preparation of a stable colloidal suspension which includes the controlling various factors such as controlling

the interactive forces of van der Waals, electrostatic and interparticle force. Widely stable slips can be obtained by controlling the pH at a particular value. The colloids prepared for the fabrication of the membrane are usually in the dispersed or flocculated state.

Powder pressing involves the compaction of ceramic powder into a specific form. During the compaction process, the ceramic powder are made cohesive through mechanical densification under the effect of temperature. There are mainly two types of powder pressing techniques, axial pressing and isotactic pressing. The axial pressing process is the most economically viable pressing methods and is extensively used in large scale production of flat and circular supports. Axial pressing may be of two types, wet pressing and dry pressing, wet pressing which utilizes the use of a fluid and the dry pressing only involves dry ceramic powder. In case of isotactic pressing a greater uniformity of compaction is obtained due to the application of pressure from multiple directions. Therefore, a better shape is obtained in the case of isotactic pressing. Isotactic pressing can be further subdivided into isotactic hot pressing, where the isotactic pressure is created by heating an encapsulated fluid like argon gas to the working temperature resulting in the ceramic support of desired shape and isotactic cold pressing, where the isostatic pressure is created by applying external pressure onto the fluid, normally water or oil. This pressure is uniformly applied to ceramic powder to form the required shape of the membrane support.

Another traditional method utilized in the fabrication of ceramic membrane is the paste pressing method. In this process a mixture of the ceramic powder is prepared using water and then it is casted onto a mold of desired shape placed on a flat porous (gypsum) or a nonporous support. The paste usually consists of additives providing mechanical strength to the membrane such as metasilicates and boric acid along with the presence of pore forming agents such as the carbonates. The pressure is applied as per the required shape. It is in fact one of the simplest of all the methods for the fabrication of ceramic membrane and does not require the use of any

machines for the fabrication process. Although a large number of researchers have already fabricated membranes utilizing kaolin and clay yet one the problem persisting is the control of microstructure during the fabrication process.

Another method that has been utilized in the fabrication of ceramic membrane is the extrusion method. Fabricated membranes are mainly extruded using clay as the starting medium due to the fact that clay possess excellent rheological properties. This clay is then mixed with the required plasticizers (PVA, PAA, PEG, etc.), binders (methylcellulose, carboxymethylcellulose, hydroxyethyl cellulose, etc.) and lubricants as the additives which gives it the required plastic properties providing excellent shape-forming capabilities without losing its cohesion. . In the extrusion method, the homogeneous paste is forced through the opening of a die with the help of a screw, especially an extruder in industries or a piston in the laboratory. Tubular and multichannel membrane supports have been widely prepared by this method. Based on the number of channels, inner diameter and the external diameter of ceramic tubes required the diameter of the die is adjusted to obtain the membrane of desired specification. Other important parameters that should be kept in mind whole fabricating such membranes are the particle size of the ceramic or clay powder, organic additives required, pugging and ageing of the paste, extrusion pressure, and velocity [7].

## 1.5 Applications of ceramic membranes

Ceramic membranes often form an asymmetric structure consisting of a microporous top layer and a mesoporous intermediate layer to ensure mechanical resistance during application of the fabricated membrane. These membrane modules can withstand high temperatures extreme acidity or alkalinity and high operating pressures, making them suitable for many applications overcoming the disadvantages associated with the polymeric membranes. To show the wide

array of available application of ceramic membranes, few applications have been briefed down below [8]

**Chemical and petrochemical industry**

Product seperation and cleaning

Concentration of polymeric suspensions, latex and metal hydroxide solutions

Catalyst recovery

Brine recycling

Recovery of dyes and pigments

Desalination of products (optical brighteners, surfactants, and dyestuffs)

Cleaning, rrecovery and recycling of organic solvents

Fuel oil and ethanol processing

**Textiles/pulp and paper industry**

Lignosulfonate fractionation

COD reduction of bleach plant effluents

Whitewater recovery from paper machines

Paper coating recovery

Colour removal

Dye bath recovery and reuse

Spin bath finish and size recovery

**Pharmaceutical/cosmetic and biotechnology**

Concentration, fractionation, isolation of pharmaceutical active agents (antibiotics, enzymes, proteins, amino acids and vitamins) and plant extracts and sterilization

Separation and fractionation of milk and whey ingredients

Desalination of whey

Purification of spirits

Separation of soybean protein

Vegetable oil processing

Purification of drinking water

Sugars and starches processing

Recovery of product from beer and cider tank bottoms

Recovery of water from waste stream

**Water recycling and environment**

RO pretreatment

Wastewaters and potable water treatment

COD, BOD and suspended solids reduction by membrane bioreactor

Separation, concentration and dewatering of biomass and algae

Processing of alginates

Disposal of fat emulsions

Desalination

Fermentation broth clarification, separation of yeast, concentration of bacterial suspension

Vaccine production

High purity process water (pvrogen and bacteria-free)

**Automotive/mechanical/mineral/metal industry and surface engineering**

Recycling and disposal of degreasing and rinsing bathes

Treatment of oil/water emulsions

Recovery of heavy metals

Cleaning of wastewater from grinding processes

Treatment of wastewater from glass and glass fiber production

Pretreatment cleaner

Washing machine tanks

Oil wastewater

**Food, dairy and beverages**

Clarification and stabilization of wine, beer, cider, soy sauce and vinegar

Concentration of juice

Removal or microorganisms from milk and whey

Removal of suspended solids

Emulsified oil removal, edible oils, waste oil treatment

Recycling of water from swimming pools, sewage palnts etc

Sewer overflow treatment

Methane digester water recovery

Upgrading Vacuum residual oil

Radioactive waste treatment

## 1.6 State of the art

With a brief overview of the contemporary research, this section outlines the research outcome of various literatures so as to identify few promising areas of research that needs to be addressed in this thesis. The state of the art has been presented for microfiltration membrane and its application in different fields.

### 1.6.1 Fabrication of fly ash based ceramic membrane using mechanically varied precursor powder for the clarification of tomato juice

In the past two decades, considerable efforts have been made to reduce energy demands. The use of membrane technology to replace a separation or purification step in an industrial process

may reduce the overall consumption of energy [9]. Porous ceramic membranes have been widely employed in many industrial fields owing to their significant advantages, such as excellent thermal, chemical, and mechanical resistances [10]. Usually, a porous structure can be achieved by a conventional powder-processing route with the incorporation of some pore-forming agents, such as sawdust, starch, graphite or organic particulates [11] or by injection molding [12] or gelcasting [13]. It is observed that the pore size increased with increased particle size and decreased with decreasing particle size. Another important parameter observed was the relation of pore size with the sintering temperature. Higher sintering temperature resulted in large sized pores, hence it is also important for us to maintain low sintering temperature, thereby reducing the operating costs, in order to obtain membranes with lower diameter pores. It was seen that there was no specific dependence on the pore size of the membrane with the preparation method.

Depending upon the size of particles to be retained, the pressure-driven processes namely micro-filtration, ultra-filtration, nanofiltration and reverse osmosis are used [14]. Membrane technology is continuously going through the advancement phase in the development of membranes that can be used in a wide variety of applications, keeping in mind the cost implications. Existing and continuing research in membrane technology aims at the fabrication of ceramic membranes that are suitable for high temperature applications [15]. More attention is given membranes prepared from the low cost of abundant raw materials available worldwide. For example coal fly ash emerges as a by-product from the combustion of raw coal in thermal powerplants [16-28].Without suitable treatment, fly ash may be a source of dust which adversely affects our environment. Therefore, it is necessary to utilize this waste not only to decrease environmental pollution but to produce high added-value products from it. Especially fly ash containing $Al_2O_3$ and $SiO_2$ is suitable for the fabrication of dense mullite-based ceramics, as has been proven. Global production of tomato is around 163.4 million tons as in

2013 with China having a share of 31% followed by India, United States and Turkey in tomato production [29].

Tomatoes are rich in carbohydrates (Sugar, Dietary fiber), fat, protein, vitamins, lycopene etc. Consumption of tomatoes may be in various forms including salads, processed ketchup, processed soups, pickles, juice etc. Since they are acidic in nature, making them and especially preserving them in home canning has become extremely easy. However, of all the varieties of food products available the juice of tomatoes is one of the most popular products. Juice is usually obtained by peeling of the skin, crushing and removing the seeds and passing through a sieve. Due to the presence of constituents such as cellulose, hemicellulose and protein, the juice tends to become highly dense and viscous thereby causing difficulty in the subsequent clarification processes. Clarification is one of the most essential steps for the recovery of natural color substance and concentration by membrane technology. The more these suspended solids are removed from the juice the more will be the efficiency of the juice post clarification [30-35].

Few methods used in the pretreatment of fruit juice include treatment by pectinase enzyme, centrifugation of fruit juice in presence of a fining agent, enzymes or both. However, processes like these are costly and the main aim is to develop a process which would give us products equivalent to these processes but at much lower costs. Membrane processes, including micro-filtration (MF) and ultra-filtration (UF), are a good alternative to traditional methods requiring lower energy and capital costs; these processes are non-thermal separation methods which cause no phase change and minimal loss of proteins, vitamins, sugars and salts [36-40]. Micro-filtration and ultra-filtration are widely used for the clarification of various fruit juices such as pomegranate [41], apple [42, 43], melon [44], carrot [45], tomato [46, 47], pear [48], pineapple [49], umbu [50], blood orange [51] and black currant [52-53].

**Table 1.3: Literature review showing the comparison of variation of pore size of fabricated membrane based on the precursor particle size**

| Raw material | Particle size ( µm) | Pore size (µm) | Sintering temperature (°C) | Reference |
|---|---|---|---|---|
| Fly ash, Calcined bauxite | 15.09 | 6.55-7.28 | 1450 | [16] |
| $Al_2O_3$, $TiO_2$,PVA | 20-100 | 8.65-10.37 | 1650 | [19] |
| $Al(OH)_3$, Kaolinite, Gangue, $MgCO_3$ | 30.8 | 0.326, 3.535 | 1500 | [20] |
| Kaoline, $CaCO_3$, Quartz | 14.24 | 1.42, 1.60, 2.72 | 900, 950, 1000 | [23] |
| Kaoline, $CaCO_3$, Quartz | 4.9 | 0.31, 0.45, 0.45, 0.56 | 850, 900, 950, 1000 | [24] |
| $Al(OH)_3$, Microsilica | 2 | 0.2 | 1500 | [30] |
| Fly ash , Bauxite | 1.52 | 0.93, 1.03, 1.25, 1.80, 2.20 | 1300, 1350, 1400, 1450, 1500 | [34] |
| Fly ash | 0.5 | 0.25 | 800 | [35] |

**Literature review**

The importance of porous ceramic membranes is increasing in water purification, because monomodal and narrow pore size distributions in the mesoporous and macroporous range can be tailored depending on applied processing parameters (e.g. initial ceramic particle size, shaping technique, drying and sintering conditions). Because of their high mechanical strength ceramic membranes can withstand high pressure loads and therefore, they are able to endure high water permeate flux rates. Another advantage of ceramic membranes is that they can easily be cleaned by back-flushing, thermal, acidic or basic treatment without affecting the pore morphology. A literature review was done in order to see the variation of pore size of a membrane with the particle size of the raw materials. It is already known by the Kozeny equation that the mean pore size and the mean particle size are directly proportional to each other.

A literature review was done in order to see if the method of preparation had any effect on the resultant pore size of the produced membrane. The two methods studied extensively were the uniaxial method and the paste method. As observed from the **Table 1.4**, it can be seen that the final pore size in the fabricated ceramic membrane is independent of the fabrication method used.

**Table 1.4: Table showing the pore sizes of the ceramic membrane based on the type of fabrication method adopted**

| Preparation method | Average pore size (μm) | References |
|---|---|---|
| Uniaxial | 1.01 | [6] |
| Paste | 1.30 | [9] |
| Uniaxial | _ | [22] |
| Uniaxial | 1.91 | [23] |
| Uniaxial | 1.32 | [23] |
| Paste | 6.30 | [24] |
| Paste | 10.20 | [26] |
| Paste | _ | [27] |
| Uniaxial | 26.20 | [34] |
| Paste | 0.5–0.8 | [30] |
| Paste | 0.9–1.2 | [80] |
| Paste<br>Paste<br>Paste | 0.28<br>0.443<br>3.16 | [30] |

**Possible scope for further research and work done**

From the above literature review it may be envisaged that several authors have reported the preparation of inorganic membrane and the pore size of these membranes were controlled mainly by maintaining the sintering temperature. It is observed that the pore size increased with increased particle size of the precursor powder and decreased with decreasing particle size. Moreover, the use of fly ash based membrane has not been utilized in the field of fruit juice clarification. Therefore, in the present work, the effect of initial size of the precursor powder on the pore size of the resultant membrane was investigated. The precursor powder contains fly ash along with various additives such as binding agents, pore forming agents and strength providing agents. The prepared membranes were thus utilized in the microfiltration of tomato juice to remove pectin like compounds which were responsible for degrading the quality of tomato juice in the long run. Detailed studies were performed on the resistances acting on the membrane during the process of microfiltration.

### 1.6.2 Fabrication of temperature responsive composite ceramic membrane

The composite polymer–ceramic membranes are characterized with excellent properties such as structural integrity [54], fouling resistance [55], flux [56] and selectivity [57]. Inorganic membranes have always gained preference over polymeric membranes due to their robust nature including the capability to operate at high temperature and pressure, thus came the application of coating the inorganic membranes with layer of polymer where the separation is entirely governed by the polymeric with controlled permeation and improved selectivity [58]. These membranes thus have a great potential in application for drug delivery, chemical separations, chemical valve, per-vaporation etc. Despite numerous attractive properties the usage of polymer-ceramic composites has not gained much

appreciation, the preparation of responsive membrane from ceramic membranes has been rarely reported. One of the many reasons being that the ceramic membranes are two to three fold times costlier in comparison to their counterpart of organic membranes [59].

Several methods have been reported till date for preparing composite polymer-ceramic membranes which mainly includes the physical attachment of the polymer to the inorganic substrate via methods such as solution casting [60], coating [61, 62], dip-coating a porous ceramic substrate [63], asymmetric incorporation of inorganic materials as a powder in a polymer matrix [64], or pore-filling of a porous ceramic substrate with acrylamide, followed by cross-linking [65].

Environmental sensitive membranes have numerous remarkable properties which has made them an interesting topic of discussion in the recent years. Stimulus-responsive membranes that are sensitive to environmental stimuli such as temperature [66-68], pH [69], electric fields [70], magnetic field [71], light [72] and ionic strength [74] have recently gained much attention, focusing mainly on the development of an environmentally sensitive polymer composite membrane with sensitivity. Shrinking–swelling stimuli-responsive polymer brushes which are sensitive to environmental stimuli such as pH, temperature, light, electric fields and ionic strength present a new and promising platform for the development of membranes with easy- cleaning and anti-fouling properties. Reports have been made on polymers that undergo a discontinuous phase transition and to change their configurations in response to a small change in temperature [77]. Temperature-sensitive membranes have an added advantages over other stimuli responsive membranes mainly because of the fact that the former allows easy manipulation with precise adjustment of temperature. If such polymers could be grafted onto a porous membrane such as an inorganic membrane, it is possible to obtain a composite polymer ceramic membrane which would be sensitive to temperature. Numerous work on temperature responsive polymer PNIPAAm has been done

till date which mainly includes depositing a layer of the polymer on the inorganic surface by methods such as graft polymerization, microwave supported polymerization [78-81].

There are two main types of thermoresponsive polymers; the first present a lower critical solution temperature (LCST) while the second present an upper critical solution temperature (UCST). LCST and UCST are the respective critical temperature points below and above which the polymer and solvent are completely miscible [82-85]. A polymer solution below the LCST is a clear, homogeneous solution while a polymer solution above the LCST appears cloudy. As the volume-phase transition brings about dramatic changes in the physical properties of the polymer gels. When the operating temperature is lower than the LCST, the grafted polymer branches in the membrane has extended conformation filling the membrane structure, causing a closed flow membrane structure [86, 87]. When the operating temperature is higher than the LCST, the grafted chains collapse due to the hydrophobic interactions of polymer branches at temperatures above its LCST, which cause a more open flow membrane structure [89, 90]. Therefore, the separation factor decreases, while the flux increases with an increase in operating temperature [91].

**Literature review**

Poly (N-isopropylacrylamide) brushes grafted with $ZrO_2$ (PNIPAAm-g-$ZrO_2$) composite membranes has been prepared for humic acid (HA) removal. The PNIPAAm-g-$ZrO_2$ membrane had a high rejection of 98.0% with a steady flux of 111.9 L $m^{-2}$ $h^{-1}$ at 25 $^oC$. This membrane exhibited good anti-fouling properties along with improved membrane performance during filtration of HA [77].

A thermo-responsive, poly (N-isopropylacrylamide) (PNIPAAm) grafted poly (vinyl alcohol) (PVA-g-PNIPAAm) copolymer membranes was developed for separation of isopropyl alcohol (IPA)/water mixtures via pervaporation. PVA-g-PNIPAAm copolymers

were synthesized by microwave supported graft copolymerization. Structure of copolymers was characterized by element analysis, FTIR, TGA/DTG/DSC, 13C NMR and SEC. PVA-g-PNIPAAm membranes prepared with casting technique were characterized by SEM-AFM. Effects of grafting yield, operation temperature, and feed concentration on separation factor and flux were investigated to determine the membrane performance [78].

Poly (N-isopropylacrylamide) (PNIPAAm), grafted into tubular type porous polyethylene (PE) membranes were prepared by the plasma-induced graft polymerization technique. A wide range of grafting was achieved by varying grafting conditions such as monomer concentration and graft-reaction medium. Different solvent compositions such as water, methanol, methanol/water mixed solvents, and benzene, were used as reaction media, among which water showed a much higher polymerization rate than organic solvents. A mechanism explaining the solvent effect in the plasma-induced graft polymerization was proposed based on the polarity of the solvents. Characterizations using SEM and micro FT-IR suggested that the grafted polymers were located simultaneously on the outer surface, the inner surface, and the surface of pore wall of the tubular-type membrane [79]. The water permeability of the grafted membrane showed a sharp change around the LCST, and the grafted PNIPAAm could respond instantly to environmental temperature changes. Novel multifunctional membranes were prepared by ultraviolet photopolymerization of N-isopropylacrylamide (NIPAAm) on the surface of porous hydrophilic polypropylene microfltration membranes. The poly N-isopropylacrylamide PNIPAAm gels were generated on the surface of the membrane through a covalent bond in the presence of a crosslinking agent, N,N-l- methylenebisacrylamide. The cross-linked PNIPAAm gels were temperature-responsive hydrogels and could swell and deswell reversibly in aqueous solution at lower critical solution temperature (LCST) of PNIPAAm. With a change of temperature, the effective pore size of the membrane surface increased or decreased as the PNIPAAm gels

swell or deswell. Above the LCST of PNIPAAm, the fluxes of water and solution containing 500 ppm of dextran (molecular weight: $1.67\times10^5$ g/mol) through the temperature-sensitive membranes are about 6 and 85 times higher than those below the LCST of PNIPAAm, respectively. The changeable flux makes due to changes in pore sizes made it possible to employ the temperature-sensitive membranes as a sensor or valve that regulates filtration properties by responding to temperature. Solutions of dextran with a molecular weight from 6300 to 2,000,000 were used to evaluate the separation performance of the temperature-sensitive membranes as the ultrafiltration membrane. The ranges of rejection of dextran and the flux of solution are from 0 to 90 and 8 to 32 $l/m^2.h$, respectively, depending on the temperature, pressure, and molecular weight of dextran. It is clear that the temperature-sensitive membrane exhibits multifunctional characteristics; that is, the microfiltration membrane is above the LCST of PNIPAAm, and the ultrafiltration membrane is below the LCST of PNIPAAm [80].

A series of thermo-responsive polyvinylidene fluoride (PVDF)/poly (stearyl methacrylate) (PSMA) composite membranes with a highly hydrophobic surface were fabricated using a non-solvent induced phase separation method. The introduction of comb-like polymer-PSMA endowed the composite membranes with hydrophobicity and thermoresponsive characteristics, and the transition response to temperature were adjusted as a result of the PSMA content in the composite membranes. The effects of PSMA on membrane morphology, hydrophobicity, and oil-water separation performance were studied. Further, the thermo-responsive and crystallographic characteristics of the membranes were investigated. Anorthogonal experiment design (OED) was applied in this study to evaluate the separation performance of membranes for water-in-oil emulsions with different solution compositions and casting conditions. The unique property of thermoresponsivity along with

high flux and separation efficiency rendered these membrane as a promising option for the separation of oil-water mixtures and solutes with small core size differences [81].

Reduce in the pore size of microporous ceramic tubular membranes was brought about by coating their inner surfaces using cellulose acetate solution forming a thin coating of ~35 μm. Three tubular membrane configurations viz., 1-channel, 7-channel and 19-channel, hollow tubular having an identical pore size of 1.2 μm and apparent porosity of 35 vol.% were tested for pollutants collected from different industrial discharge sources in addition to simulated effluent mixtures under cross-flow filtration mode. Filtration experiments were performed by varying feed pressure, feed concentration and permeate flux [83].

Composite ultrafiltration membranes were prepared by applying thin coating of polyvinyl acetate (PVAc) over ceramic support by using a modified dip-coating method. Since the polymer solution (N,N-di-methyl acetamide solvent), was not viscous enough for uniform coating, the technique was modified using a secondary solvent (water) for the removal of DMAc rather than drying it from the solution. For studying the effect of polymer concentration and dipping time over membrane parameters, twelve different membranes were prepared using four different concentrations (10 %, 20 %, 30 % and 40 %) and three dipping time (30 s, 60 s and 120 s). Membranes were characterized with TGA, SEM, air and hydraulic permeability and acid/base treatment. From gas permeability study, the pore sizes were found between 150 and 9 nm. The lowest pore size membrane (9 nm) was applied for the purification of lysozyme from chicken egg white (CEW) using three different concentrations. pH 11.0 was found as most suitable for the purification using the prepared membrane and over 98 % of transmission of LS were found [88].

A cellulose acetate (CA)-ceramic composite membranes was prepared by using dip coating technique. Ceramic supports used in this work were prepared from kaolin with an average pore size of 560 nm and total porosity of 33 %. The dip coating parameters studied

experimentally were the concentration of CA solution (varying from 2 wt % to 8 wt %) in acetone and dipping time (varying from 30 s to 150 s). The fabricated composite membranes were characterized using scanning electron microscope, gas permeation, pure water flux and ultrafiltration (UF) experiments using bovine serum albumin (BSA). It was observed that the membrane prepared with 2 wt % and 4 wt % CA were suitable for microfiltration applications and those with 6 wt % and 8 wt % were for ultrafiltration applications. Theoretical investigation was conducted to know the macroporous and mesoporous structure of the prepared membranes using Knudsen and viscous permeability analysis of air. Phenomenological models were proposed to illustrate the dependency of hydraulic resistance of membrane on the structural parameters such as average pore size, effective porosity as well as dip coating parameters like dipping time and concentration of CA. It was found that, the growth rate of CA film on the ceramic support followed exponential growth law with respect to dipping time. The total hydraulic resistance of the membrane was evaluated to be inversely proportional to the ratio of pore sizes of top layer and ceramic support. The resistance due to the CA film was found to be depended to the order of 1.73 with respect to concentration of CA. An increase in the concentration of CA was found to be more effective than dipping time to reduce the membrane pore size [89].

In addition to the above composite ceramic membranes prepared, chitosan coted α-alumina composite membranes, m-phenylenediamine trymesoylchoride coated α-Alumina, $ZrO_2/Al_2O_3$ coated with poly dimethyl siloxane by the dip-coating method. Similar composite membranes were prepared by where α-alumina was dip coated by poly dimethyl siloxane polymer. Aluminum oxide-Polyimide and Polycarbonate composite membranes were prepared by the casting method. Composite poly (vinyl acetate) and poly (vinyl pyrrolidone) grafted onto α –alumina membrane. Similarly Poly acryl amide grafted ceramic

membranes and polyvinyl alcohol-chitosan dip coated ceramic membrane were also fabricated [90-92].

**Table 1.5: Table showing existing composite ceramic membrane**

| **Support membrane** | **Modification** | **Technique** | **Reference** |
|---|---|---|---|
| α -alumina | Poly(vinyl acetate)<br>Poly(vinyl pyrrolidone) | Graft polymerization | [58] |
| $ZrO_2$<br>Ceramic | Poly (N-isopropylacrylamide)<br>Cellulose acetate | Graft polymerization<br>Graft polymerization | [77]<br>[83] |
| α-Alumina | Chitosan | Coating | [84] |
| α-Alumina | M-phenylenediamine<br>trymesoylchoride | Interfacial<br>polymerization | [85] |
| α-alumina | PDMS coating | Dip-coating | [86] |
| Aluminum oxide | Polyimide and Polycarbonate coating | Casting | [87] |
| Ceramic | Polyvinyl acetate | Dip coating | [88] |
| Ceramic | Cellulose acetate | Dip coating | [89] |
| Ceramic | PAA grafting | Graft polymerization | [90] |
| Ceramic | Polyvinyl alcohol-Chitosan | Dip coating | [91] |

**Possible scope for further research and work done**

Studies suggest that most of the composite stimuli responsive membrane prepared are of polymeric nature. Thus a vast field of composite ceramic membrane still remain unexplored. A review on the above **Table 1.5** suggests that a wide variety of responsive composite membranes have been prepared but the application of a responsive polymer coated ceramic membrane is rather limited. The main focus was on the temperature responsive polymers that have not been used till date as a coating agent and thereby create a composite responsive membrane. The present work deals with the preparation of a composite polymer ceramic membrane keeping in mind factors such as cost effectiveness and performance of the resultant membrane. A polymer poly (2-ethyl-2-oxazoline) is utilized in the present work which has not been used for coating a membrane anywhere else till date. The polymer was coated onto the surface of the fly ash based ceramic membrane using a simple dip-coating technique. The prepared membranes were the characterized and a detailed study on the effects of temperature was made considering various parameters such as polymer coating concentration and dipping time. Rejection of BSA protein by the composite membrane was also studied.

### 1.6.3 Fabricating a novel adsorbent from tomato waste and carrot waste left from microfiltration process for treatment of Co (II) contaminated water

The necessity of heavy metal pollution control has been of significant concern in last few decades. Environmentalists are primarily concerned due their high toxicity and impact on human health and environment. To overcome this problem researchers have developed alternative technologies for the removal of these pollutants from aqueous effluents. The use

of low-cost and waste biomaterials as adsorbents of dissolved metal ions are a promising alternative and an economic solution to this global problem. Among them, activated carbon is gaining more prominence in industrial sectors due to its high specific surface area, favorable pore size distribution and high surface reactivity [93]. Numerous technologies have been developed over the past few years to remove toxic cobalt from water. These mainly include chemical precipitation, electro flotation, ion exchange, reverse osmosis and adsorption on activated carbon [94–98]. However, to make the technology available to the common masses a cost effective alternative system for the treatment of metal contaminated waste streams are required. Natural materials such as waste from fruits or vegetables may have potential to be used as low cost adsorbents as these are unused resources, widely available and environmentally friendly [99]. Agricultural wastes such as orange peel, mango peel and tomato residue have been reported as probable sources of low cost adsorbents due to their easy availability, inherent porosity, filterability and high carbon content [100, 101]. Also, the use of bio waste for activated carbon synthesis has an advantage of being renewable and less expensive. The high content of volatile matters existing in the biomass has been ideal to produce a highly porous structure of activated carbon which can be utilized for water treatment [102]. The process of activation takes place either through chemical activation, or through physical activation. Chemical activation presents a greater advantage over the later due to requirement of a lower temperature for pyrolysis, higher yield and higher surface area. The chemical reagents used are dehydrating agents that influence pyrolytic decomposition and prevent the formation of tar [103-106]. With the increase in global plastic market, the disposal of plastic wastes with their low bio and photo degradability pose a serious challenge [107-109]. Numerous research have been performed in the last few years to develop innovative technologies for the conversion of the excessive amounts of waste into useful value-added products [110-113]. The most common way to

eliminate polyethylene terephthalate (PET) waste is production of activated carbon and it is one of the most environment friendly solutions for recycling of this type of carbons rich wastes [114-118]. In carbon manufacturing, polymer precursors are used when carbon of low inorganic impurity content is needed. PET consists of different formulations and combinations of hydrocarbon derivatives [119-120]. The high carbon content and low amounts of mineral matters and impurities in PET have made them a promising precursor for activated carbons which can be utilized for the adsorption of heavy metals from aqueous solutions [121].

**Literature review**

Numerous adsorbents have been utilized for Co (II) adsorption. Recently, a major attention has been given to the utilization of agricultural wastes into value added products mainly in the synthesis of bioadsorbents. The major advantages of biosorption over conventional treatment techniques include low cost, high efficiency, minimal sludge production and ease of regeneration of biosorbents. Agricultural wastes are extremely rich hemicellulose, lignin, extractives, lipids, proteins, simple sugars, water hydrocarbons and starch containing a variety of functional groups that facilitates metal complexation. Chemical activation is one of the main methods utilized in the activation of agricultural wastes for the removal of cobalt from aqueous solutions. Sulphurised activated carbon has been utilized with an adsorption capacity of 153.6 mg/g [24]. Fungal based bioadsorbent had a very high adsorption capacity of 190 mg/g for Co (II) ions from aqueous solution [25]. Shells and peels of various nuts and fruits such as almond hull [26], lemon peel [27], fruit nut shell [28], watermelon rind [29], orange peel [34] have also been utilized in Co (II) adsorption providing adsorption capacities of 45.5 mg/L, 27 mg/L, 98 mg/L, 175 mg/L and 1.23 mg/L, respectively. The orange peel mentioned have been used directly without any activation.

**Possible scope for further research and work done**

A critical insight into the above literatures suggest that agricultural waste have a huge potential for being used as an adsorbent due to their inherent porosity, filterability and high carbon content. Based on the studies above it was found that tomato waste can act as a potential adsorbent for Co (II) in aqueous solutions. Therefore, in this study, obtained tomato waste including the pulp, skin along with carrot waste and polyethylene terephthalate (PET) were used to prepare a composite adsorbent using the chemical activation technique. This work focused on the fabrication and characterization along with the kinetics and equilibrium studies. The composite adsorbent was prepared by combining the activated carrot and tomato waste with activated PET waste. Activated PET has a very high adsorption capacity and mixing it with other adsorbents would further enhance the adsorption of Co (II) form aqueous solutions. A cost estimation of the prepared composite adsorbent was also carried out.

## 1.6.4 Developing a hybrid method for the removal of fluoride from drinking water

Fluoride is an inorganic, monatomic anion of fluorine and is the most electronegative element representing about 0.06 to 0.09 % of earth's crust in the form of minerals like topaz, fluorite, rock phosphate, mica hornblende, sellaite ($MgF_2$), fluorspar ($CaF_2$), sodium fluoride (NaF), cryolite ($Na_3AlF_6$) and fluorapatite [$3Ca_3(PO_4)_2\ CaF_2$] [128-130]. Fluoride contaminated groundwater has been a major issue with concentrations existing as high as 4 mg/L and is considered as a serious problem throughout India and the world [131-133]. Thus to differentiate the effects of fluoride concentration on human health, various limits have been determined. For an instance, the secure limit of fluoride in drinking water must

be less than 1.5 mg/L. A fluoride concentration of 1.5-3.0 mg/L results in dental fluorosis, concentrations of 3.0-4.0 mg/L causes stiffened brittle bones, whereas a concentration higher than 4.0 mg/L results in crippling fluorosis [131]. High fluoride concentration may also cause bone deformation, spotting/ flaking of teeth and bruising of the thyroid, liver and other organs [132]. The United States standards limit ranges between 0.6 to 0.9 mg/L [134, 135]. The permissible upper limit of fluoride in a tropical country like India is 1.00 mg $L^{-1}$ as issued by the Bureau of Indian Standards (BIS) for drinking water [136].

Fluorosis effects a vast majority of the population in India with 17 out of the 32 states being under the influence of fluoride problems either directly or indirectly. Highly effected states in India include Assam, Rajasthan, Andhra Pradesh, Orissa, Gujarat, Madhya Pradesh, Bihar, Delhi, Gujarat, Haryana, Jammu and Kashmir, Karnataka, Kerala, Maharashtra, Manipur, Punjab, Rajasthan, Tamil Nadu, Chhattisgarh and Uttar Pradesh [137, 138]. Groundwater in the Karbi Anglong district of Assam was found to have fluoride content as high as 15-20 mg/L whereas in certain regions of Kamrup district fluoride levels were at 6.88 mg/L. 30% area of Assam faces issues with fluoride with ranges as 1.6 - 23.4 mg/L [139].

**Literature review**

Numerous techniques have been reported for the elimination of fluoride like; adsorption [140], electrocoagulation [141], waste carbon slurry [142], donnan dialysis [143], nanofiltration [144], anion-exchange membrane [145], defluoridation of ground water utilizing the combination of adsorption and donnan analysis in physicochemical and biological treatment [146], activated carbon[147, 148], and reverse osmosis [149]. Traditional methods such as precipitation with NaCl (33.6 mM) compounds have been utilized widely in the past. Electrocoagulation (EC) is an in-situ method meant for removing

of the flocculating agent by flotation and generating the electro-oxidation of sacrificial anode and simultaneous evolution of hydrogen cathode with the formation of the $Al(OH)_3$ flocks. This technique combines three main interdependent process that includes electrochemistry, coagulation and hydrodynamics [150, 151].

**Possible scope for future research and work done**

From the review of above literatures it may be concluded that although several authors have reported various techniques for the defluoridation of water [152-155], however a technique combining the advantages of electrocoagulation and microfiltration has not been performed as of yet [156-158]. Hence, the present study included a hybrid method which is a combination of electrocoagulation and microfiltration for fluoride removal from contaminated drinking water. Experiments in batch mode have been performed to investigate the parametric effects such as initial concentration, current density and initial pH on the electrocoagulation process. Studies on corrosion of electrode and the sludge formed during the experiment (bipolar connection) were determined. Operating cost for the removal of fluoride was calculated material and energy costs. Furthermore, the electrocoagulated water were filtered using ceramic membranes to make the water suitable for drinking purpose. Microfiltration was carried out to remove the flocks generated during electrocoagulation process. Membrane used for filtration and the sludge produced during the electrocoagulation process were characterized by FESEM, EDX and FTIR analysis.

### 1.6.5 Treatment of drilling effluent using electrocoagulation followed by microfiltration

Drilling effluents from oil and gas well sites heave a potential impact on the environment. The chemical and physical properties associated with these fluids influences the environmental impact ability. Drilling fluids wastewater and drill cuts are the two most important wastes generated during the drilling process. Some of the additives present in these wastes introduce potentially toxic compounds into the fluids thereby increasing the toxic levels to a great extent [165]. Oil-water emulsions through discharge from several industrial work in machining, automotive shops, oil-drilling, refineries, off shore oil explorations, oil transportation and distribution have been one of the major causes of water pollution [166,167]. Moreover, emulsions of oil-in-water have also been widely used in metal processing industry such as in industrial work of cooling and lubrication which are later replaced and discharged due to substantial degradation of certain components. This oil discharged into the environment may be of different forms such as free (oil and grease), dispersed and emulsions [168].

**Literature review**

Till date a large number of methods have been proposed by various researchers from all over the world to treat such forms of oil in water. It is a necessity, in the present times, to identify new technologies which would be efficient enough in separating oil form such oil-in water emulsions. Methods such as adsorption [169], coagulation [170, 171], anaerobic treatment [172], reverse osmosis [173], ultrafiltration [174], chemical destabilization by using inorganic salts [175,176], flocculation [176], dissolved air flotation [177] and membrane processes [178, 179] have been widely used in the past to treat such water. Previous research studies have suggested that electrocoagulation process has a high

rate of success in the separation of oil from oily rejects in comparison to other available processes [180-182]. For this purpose, electrocoagulation process plays a more prominent role in the treatment of oily wastewaters [183-185]. This process in combination with other techniques can be an effective method for a highly efficient process [186-192]. The main advantages being the non-requirement of any additive chemicals to enhance the process of destabilizing the emulsion, a simple and easy to use working set-up, lower investment and lower operating costs and most importantly a decreased amount of sludge production [191, 192]. The process of electrocoagulation involves the dissolution of the sacrificial anode due to the application of potential difference across the electrodes. This dissolution of anode results in the production of flocks in the form of metallic hydroxides within the sample of water to be treated. This in-situ process mainly includes three major steps i.e. an electrolytic reaction at the electrode surface, formation of coagulants and finally the adsorption of the colloidal particles onto the produced flocks which gets removed either by sedimentation of floatation. It is also of utmost importance that a proper electrode material is selected for carrying out the process of electrocoagulation. Materials such as aluminium and iron are frequently used and have been found to give good results in comparison to other electrode materials [191-193].

Combination of electrocoagulation (EC) with processes such as electro-floatation, reverse-osmosis and nanofiltration have already been reported previously. These methods were basically utilized for the treatment of contaminated drinking water, like the removal of fluoride from drinking water, treatment of textile wastewater (electrocoagulation-nanofiltration), removal of silica from brackish water (electrocoagulation-reverse osmosis) [165-168]. In order to use the combination of electrocoagulation along with filtration it is very important to know the particle size of the flocks generated during electrocoagulation process [169-172]. The particle size would in turn determine the type of filtration process

that can be combined with the existing would definitely determine the type of filtration process to be combined with the existing EC process [172-175]. In addition to the synthetically prepared oil water, EC process has been utilized in the treatment of oily wastewater such as refectory oily wastewater, vegetable oil refinery industry wastewater, palm oil mill effluent, vegetable oil wastewater, crude oil and restaurant oil water [195, 196]. With increasing threat to the aquatic life due to high toxic levels of the drilling effluents, it has become an utmost necessity to treat the effluents before being discharged into the environment. Different standards have been set up to control the water pollution scenario due to such industrial effluents. As per central pollution board of India (CPCB) the permissible limit for oil and grease stands at 35 mg/l [197-204]. Hence it has become an utmost importance to develop a method to maintain the permissible limits of drilling effluents before being released into the environment.

**Possible scope for further research and work done**

From the review of the above literatures it may be concluded that although several authors have reported the treatment of oily water using electrocoagulation technique, however, the use of a hybrid electrocoagulation (EC) and microfiltration (MF) technique has not been explored for the treatment of oily wastewater. In view to this, EC process was utilized with a microfiltration (MF) set up so as to remove the flocks produced during the EC process. Effluent water from the drilling site of Barekuri, Oil India Limited (OIL) was collected on 29$^{th}$ August, 2017. The obtained sample was from a drilling location TAU having a well depth of 3364 m. Obtained effluent samples had very high quantity of suspended solids, TDS, sulphates, chlorides, COD and BOD. The oil and grease content was around 35 mg/L. Electrocoagulation process was carried out on these effluent samples varying operating parameters such as current density, electrode distance and initial pH. Once

electrocoagulated the sample was filtered using indigenously prepared fly ash based membranes. Four different sintering temperatures were chosen for investigating its effect over different morphological properties of the membrane. The performance of prepared microfiltration membrane was investigated to separate electrocoagulated byproduct. A cost estimation on the electrocoagulation process was also done to investigate the power consumption and electrode material utilized during each process. Detailed flux studies were done to study the performance of the membrane during the microfiltration process.

### 1.6.6 Application of electrocoagulation-microfiltration process for the treatment of effluent water from steel plant

Heavy metal wastewater are directly or indirectly discharged from the industries such as steel plants, mining, fertilizer plants, paper mill tanneries etc. which are non-biodegradable and tend to accumulate in the environment. Toxic heavy metals in industrial wastewater include mainly chloride, sodium, potassium, manganese, magnesium, sulphate, calcium, iron, zinc, nickel, mercury, cadmium, lead, chromium etc. Chloride in the form of $Cl^-$ ion is one of the major inorganic anions in water and wastewater constituting approximately 0.05% of the earth's crust with concentrations between 1 to 100 ppm being normal in freshwater. A high chloride contents may harm metallic pipes, structures and cause dissolution of the electrode material by pitting corrosion, reducing soil water potential leading to osmotic stress [207, 208]. Iron above 0.3 mg/l can affect appearance affecting domestic water supplies, promoting iron bacteria and staining of laundry cloths [199-201]. Removal of sulfide, sulfate and sulfite ions in drinking water is also necessary [209]. Manganese (Mn) is the second most abundant metal in nature Mn contamination in ground water affects the intelligent quotient, effects the central nervous system and lungs [210, 211]. Permissible limit for Mn in the ground water is 0.05 mg/L.

**Literature review**

To remove such toxic heavy metals from industrial effluents numerous treatment methods are available. Lime-soda softening is generally applied in water with high concentrations of dissolved solids such as high calcium and magnesium species [211]. Treatments such as ion exchange, electrocoagulation [212], adsorption [213], membrane processes such as ultrafiltration [214], nanofiltration [215, 216], coagulation-flocculation [217], donnan exclusion [218, 218]. Desalination, distillation and bio-sorption are some techniques used to decease the salinity of water [219, 220]. Chemical treatments are not used due to disadvantages like high costs of maintenance, problems of sludge handling and its disposal and neutralisation of effluent [221, 222]. High contamination of water bodies by pollutants is characterized by biochemical oxygen demand (BOD), chemical oxygen demand (COD), suspended solids (SS), toxicity and colorants which cause bacterial and algal slime growths, thermal impacts, scum formation, color problems and a loss of both biodiversity and aesthetic beauty of the environment [223-224].

Electrocoagulation (EC) is a promising technology that can be utilized for the treatment of industrial effluents due to its high efficiency. The conventional method used for the EC is an in-situ method meant for removing of the flocculating agent by flotation and generating the electro-oxidation of sacrificial anode and simultaneous evolution of hydrogen cathode with the formation of the $Al(OH)_3$ flocks. This technique combines three main interdependent process that includes electrochemistry, coagulation and hydrodynamics. Combining the EC process with filtration can further enhance the removal efficiencies.

**Possible scope for work and work done**

In this part of the thesis, we utilize the benefits of electrocoagulation and microfiltration in the treatment of effluent water from steel industry. In the present study, nanofiltration reject

water from Tata Steel Limited Jamshedpur was collected which had high concentration of heavy metals such as MG, Mn, Fe, Na, Ca etc. Experiments in batch mode have been performed to investigate the effects of current density and inter-electrode distance. The performance of membrane has been studied at various at different transmembrane pressure. Studies on removal efficiency of contaminants, corrosion of electrode, film thickness, permeate flux as well as the sludge formed during the experiment (bipolar connection) were estimated. Washing and flux recovery analysis of various series resistances, energy consumption and operating cost for the removal of contaminate wastewater was calculated material and energy costs. Microfiltration was carried out to remove the flocks generated during electrocoagulation process and suggested the reduction in flux from electro-coagulated samples. Flock and membrane characterization (before and after filtration) were done using UV, FESEM, and EDX analysis.to confirm the removal of the metals by the electrocoagulation process.

## 1.7 Objectives and scope of work

This thesis is focused on microfiltration membrane preparation using fly ash as the major precursor and its use in vegetable juice clarification and water treatment. The main objectives are

1. Fly ash based membrane fabricated from mechanically varied precursor powder for the clarification of tomato juice: Resistance-in-series model
2. Detailed study of temperature-responsive composite membranes prepared by dip coating poly (2-ethyl-2-oxazoline) onto a ceramic membrane
3. A novel adsorbent from carrot, tomato and polyethylene terephthalate waste as a potential adsorbent for Co (II) from aqueous solution: Kinetic and equilibrium studies

4. A hybrid method for the removal of fluoride from drinking water: Parametric study and Cost estimation
5. Treatment of drilling effluent using electrocoagulation followed by microfiltration
6. Application of electrocoagulation-microfiltration process for the treatment of effluent water from steel plant.

## 1.8 Organization of the thesis

In order to fulfil the above objectives the thesis is organized in eight chapters. The content of each chapter is given below.

**Chapter 1** addresses the state of the art, research motivation of present work, possible scope of research, objectives and organization of the thesis. **Chapter 2** discusses the application of fly ash based low cost membranes for the clarification of tomato juice in batch mode operation. Various resistances existing during the microfiltration process were studied along with an analysis on the quality of the treated juice. The prepared fly ash based membrane was modified by a polymer layer coating and discussed in **Chapter 3**. A composite ceramic membrane was prepared and a thermo-responsive polymer Poly (2-ethyl-2-oxazoline) was dip coated. The fabricated composite membranes were characterized and applied in the filtration of BSA protein. **Chapter 4** describes the utilization of waste generated after tomato juice clarification (Chapter 2) to prepare an adsorbent for the removal of Co (II) contaminated water. **Chapter 5** describes the application of selected fabricated membrane in **Chapter 1** for the microfiltration of electrocoagulated by-product obtained during treatment of fluoride contaminated drinking water using electrocoagulation. **Chapter 6** presents the application of the fabricated ceramic membrane for the microfiltration of electro coagulated drilling fluids for the removal of oil, grease and other heavy metals. In addition to a detailed characterization, studies were also done on the corrosion and operating costs

of the electrocoagulation process. **Chapter 7** presents the application of the prepared membrane in the microfiltration of electrocoagulated effluent water from the steel industry**.** Finally, **Chapter 8** contains the inferences drawn from various chapters presented in this thesis and some suggestions towards scope for future work.

# Chapter 2

# Fly ash based membrane fabricated from mechanically varied precursor powder for the clarification of tomato juice: Resistance-in-series model

# *Chapter 2*

# Fly ash based membrane fabricated from mechanically varied precursor powder for the clarification of tomato juice: Resistance-in-series model

*This chapter discusses the preparation and characterization of low cost ceramic membranes for microfiltration application. Fly ash based ceramic membranes MB1, MB2 and MB3 having varying pore size were prepared using the paste casting method. Variation in pore size was brought about by the reduction in size of the precursor powder using the ball mill, the mono mill and the planetary mill. The prepared membrane was used to clarify tomato juice to eliminate pectin like compounds responsible for deteriorating its quality with time. The resistance-in-series model was used to evaluate the decline in flux of tomato juice during microfiltration. Individual resistance profile with time were plotted and the changes were observed for the three membrane. The profile of different resistances occurring during the filtration process and corresponding flux decline were calculated for each membrane. Various physical and chemical properties of clarified and unclarified tomato juice was reported well.*

## 2.1 Experimental

### 2.1.1 Raw materials

The raw materials used for the preparation of the ceramic membranes are fly ash from National Thermal Power Corporation (NTPC), Calcium carbonate (Merck), Sodium carbonate (Merck), Boric acid (CDH), Sodium metasilicate (CDH) and egg shell powder. All the materials considered for membrane preparation were used without any further purification. Compositions of three membranes are shown in the **Table 2.1.** Three composition were

considered as shown in the Table 1. Optimization for the best composition was carried out experimentally and it was found that composition C3 had the best membranes which were defect free as compared to compositions C1 and C2. Hence, the succeeding membrane preparations were carried out using composition C3.

**Table 2.1: Composition of the membranes**

| Raw materials | Composition 1 (C1) | Composition 2 (C2) | Composition 3 (C3) |
|---|---|---|---|
| Fly ash | 63 | 70 | 70 |
| $CaCO_3$ | 18 | 15 | 14 |
| $Na_2CO_3$ | 12 | 10 | 7 |
| Boric acid | 3.5 | 2.5 | 4.5 |
| Sodium metasilicate | 3.5 | 2.5 | 4.5 |

### 2.1.2 Experimental apparatus and procedures

Three different grinding machines were used to reduce the particle size as well as to mix precursor mixture properly. The ball mill (Richa equipments), the mono mill and the planetary mill (Make: Insmart systems) were used as three different grinding equipment. Hence three precursor powders were obtained of different sizes of which three varieties of ceramic membranes were prepared. All the three mills were run at 250-450 rpm for 6 h.

–Rotational speed: 250-450 rpm.

–Grinding time: 6 h

–Sample mass: 500 g

The powder product thus obtained after the prescribed operation mode was carefully removed from the mill and then stored in a desiccator for the subsequent characterization.

### 2.1.3 Ceramic membrane fabrication

The fly ash obtained from National Thermal Power Corporation Limited (NTPC India) was sufficiently rich in Silica ($SiO_2$) and Alumina ($Al_2O_3$). Combining the fly ash with additives such as a binding agent, pore forming agent and strength providing agent, we can obtain a precursor powder viable for preparing ceramic membrane for carrying out microfiltration. The membrane fabrication process involved thorough mixing and grinding of the raw materials in a ball mill, mono mill and planetary mill. Once the mixed and grinded raw material was obtained, a definite amount of Millipore water was used to obtain a paste which was then casted on an MS ring with a diameter of 52 mm and thickness of 7 mm. The casted membrane was kept so to dry overnight under the application of uniform weight (2 kg) to prevent any structural defect in the membrane. The obtained circular disk shaped membrane was dried in the oven for 12 h at 120 °C and then sintered at 850 °C for 5 h. The membrane obtained were hard, rigid and porous.

The membrane was then polished with silicon carbide abrasive paper (C-220) to obtain a smooth and flat membrane of diameter 51.75 mm and thickness 6.5 mm. Finally, the membrane was cleaned in a sonicator for 15 min to remove loose particles from the membrane and dried at 120 °C. Thus, three membranes MB1, MB2 and MB3 were prepared for the three different sized precursor powder. The obtained membranes thus had different pore size as confirmed below by FESEM analysis.

### 2.1.4 Tomato juice preparation

Fresh tomatoes were purchased from the market near IITG and were washed thoroughly with running water to remove any foreign particles. The juice was then extracted using a fruit juice extractor and filtered by nylon fine mesh cloth for removal of suspended solids. The obtained extract was refrigerated at 4 - 5 °C for further experiments.

### 2.1.5 Analytical methods

The obtained juice was then analyzed to determine the pH, color, clarity, density, suspended solids, total solid and metals like sodium (Na), potassium (K), calcium (Ca) and magnesium (Mg). UV - Vis Spectroscopy was used to measure the color and clarity of the juice. The solids were determined by weighing the pre-weighed sample after removing the supernatant. Metal concentration was done using atomic absorption spectroscopy. The analytical procedures utilized in the measurement of particle size distribution was DelsaNano (Beckman Coulter); pH using a pH meter and density using pycnometer.

### 2.1.6 Micro-filtration studies

The membrane was fixed on the experimental setup having a capacity of 280 ml using m-seal and then each fresh membrane were examined for the pure water flux at a transmembrane pressure of 4 bar .The clarified tomato juice was filtered through the ceramic membrane MB1, MB2 and MB3. The results obtained from the three membranes were then fitted in fouling models to find out which of the three prepared membranes could be used against fouling in clarified tomato juice. The permeation flux i.e. permeate flux through the membrane is given by the formula.

$$J_p = \frac{Q_P}{A_m} = \frac{\Delta P}{\mu_P(R_m + R_f)} \quad 2.1$$

Where,

$Q_p$= The flow rate of the permeate across the membrane

$A_m$= Membrane area available for filtration

$R_f$ = Fouling layer membrane resistance ($m^2/m^3$)

$\mu_p$= Viscosity of the solution (Pa.s)

The pure water flux for a fresh membrane is expressed as

$$J_w = \frac{\Delta P}{\mu_W R_m} \quad 2.2$$

$\mu_w$ = viscosity of water (Pa.s)

$R_m$= Resistance offered by the fresh membrane ($m^{-1}$)

**2.2. Results and discussion**

Structural characterization of prepared membranes were performed and reported well in the subsequent section. Characterization techniques involved the thermogravimetric analysis (TGA) of the raw material paste to identify the weight change of the precursor powder at different thermal conditions, structural characterization of membranes by X-ray diffraction (XRD) (Bruker, Model-D8- Advance) to investigate the extent of phase transformations. Scanning was performed from 2θ value between 10 - 70° at a speed of 0.5 sec/° in an uninterrupted mode at an increment of 0.05. The analytical procedures involved the measurement of particle size distribution using DelsaNano (Beckman Coulter); pH using a pH meter. The precursor powder was analyzed for the presence of various functional groups by the FTIR (Make: Perkin Elmer, USA, Model: LR 64912C). FTIR analysis was performed with the KBr -supported technique in the range of 400 - 4000 $cm^{-1}$ with a scanning rate of 40 and a

resolution of 4 $cm^{-1}$. The surface morphology of the prepared membrane was analyzed using FESEM (JEOL JSM-6400F, Zeiss LEO) which examined the morphological structure and measure the average pore size. Working temperature regimes were analyzed using the TGA and EDX was used to analyze the composition of the particle.

### 2.2.1 Characterization

#### 2.2.1.1 Fourier Transform infrared spectroscopy (FTIR)

The FTIR analysis was carried out to study the chemical composition of the membrane. The **Fig. 2.1 (a)** below shows the peaks corresponding to certain vibrations in each material. The peaks for fly ash at 1028 $cm^{-1}$ occurs due to Si-O-Si asymmetric stretching, peaks at 657 $cm^{-1}$ is for Al-O stretching. The peaks of boric acid at 550 - 400 $cm^{-1}$ represents B-O-B stretching whereas the peaks near 700 - 800 $cm^{-1}$ stand for B-O stretching. In $CaCO_3$ the bands at 717 $cm^{-1}$ represents symmetric stretching and 879 $cm^{-1}$ and 1481 $cm^{-1}$ represents the asymmetric stretching of $CO_3$ group. Similar is the vibrational peaks for $Na_2CO_3$ with vibrations representing the $CO_3$ groups. In $Na_2SiO_3$ peaks at around 700 and 1000 $cm^{-1}$ represents O-Si-O and Si-O vibrations respectively.

The IR spectrum for various membrane mixtures at different compositions were also analyzed. The **Fig. 2.1 (b, c)** below shows the spectrum for membrane MB1 at the three compositions C1, C2 and C3 are shown below. The comparison of two graphs shows that there is a disappearance in the peaks at 1481 $cm^{-1}$ for the sintered samples which suggests the conversion of the carbonates to $CO_2$ and thus assists in the pore formation of the membrane.

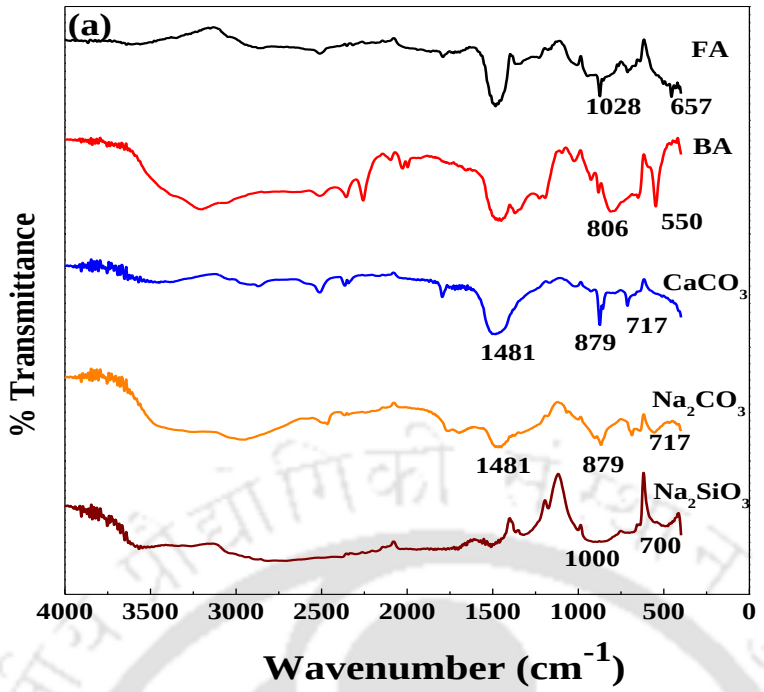


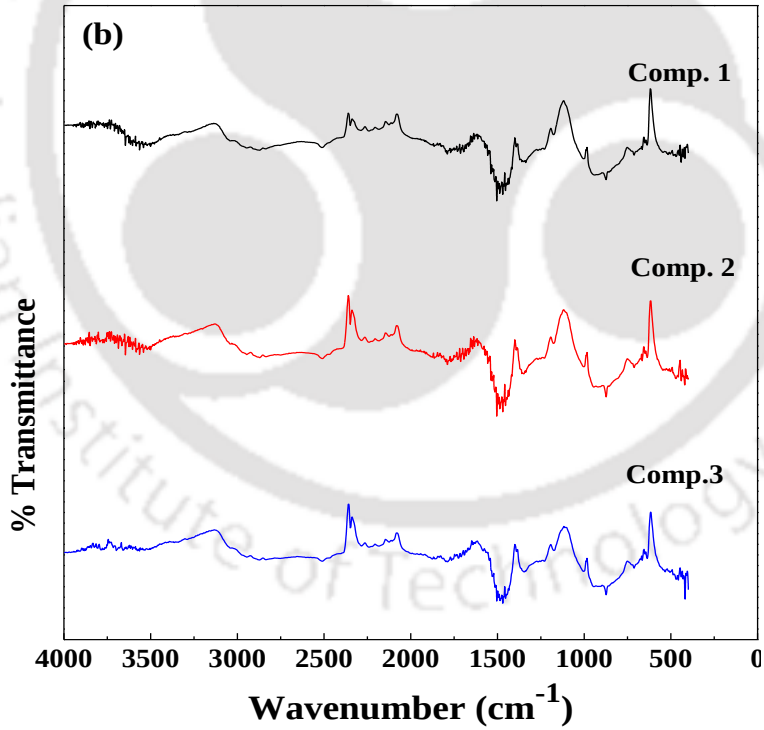

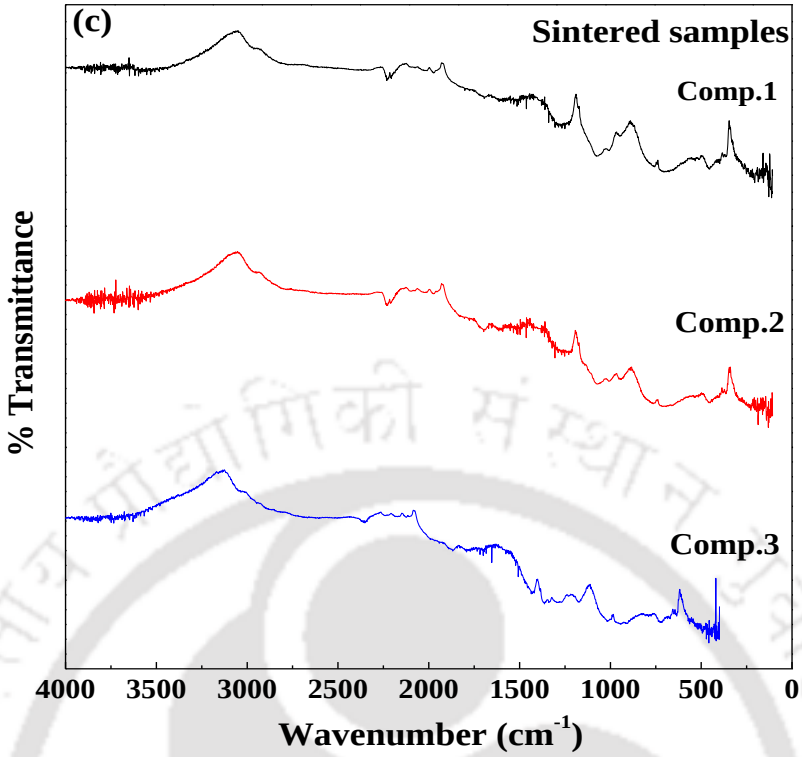


**Fig. 2.1: FTIR spectrum of (a) individual raw materials of ceramic membrane (b) Ceramic membrane MB1 at compositions C1, C2 and C3 before sintering and (c) Ceramic membrane MB1 at compositions C1, C2 and C3 after sintering.**

### 2.2.1.2 X-ray diffraction (XRD)

Crystallographic characterization of various compositions of membrane powder were examined by XRD measurements The **Fig. 2.2 (a)** below shows the major crystalline phases of fly ash sintered at 850°C.The main crystalline phases identified were quartz (Q), hematite (H) and mullite (M). A minute amount of anhydrite (A) can be seen also on the spectrum.

Analysis for the samples of membrane MB1 and its three compositions were performed without any sintering. As seen from the **Fig. 2.2 (b)** below there was observation of quartz (Q), mullite (M), calcite (C) and silicate (S) evident from the graph below.

The samples were then sintered at 850 °C for 5 h and then examined for determining the phase transformations. A detailed observation of the peaks revealed that there is a significant phase transformation at higher temperature. An observation of peaks and trends in the XRD patterns **Fig. 2.2 (c)** conveys that the major dominating phase present is anorthite ($CaAl_2Si_2O_8$) while the other important phase present is mullite ($2Al_2O_3.SiO_2$).

The xrd patterns of the sample at composition C1 for different grinding mediums were examined. As it can be seen from the **Fig. 2.2 (d)** below changes in peak height can be observed. The patterns showed a decrease in the height of the peaks as well as the broadening of peaks due to a decrease in crystalline size which is brought about due to the reduction in particle size.

### 2.2.1.3 Thermogravimetric analysis (TGA)

TGA analysis was performed to identify temperature regimes where major weight losses (and phase transformations) occur in the membrane and thereby obtain the minimum sintering temperature. As seen from the **Fig. 2.3 (inset)** below, the change in weight is evident for the membrane MB1. At 111 °C a dip in the curve is observed which is mainly due to the removal of the water molecule weakly bonded to the sample mixture. The weight loss of the sample between 113 and 545 °C was 8 %, which can be attributed to burning of small impurities and unburned mineral coal powder and also because of evaporation of boric acid whose boiling point is 300 °C. The maximum weight loss of about 13 % occurred in the temperature regime between 545 and 966 °C. This is the region where the formation of $CO_2$ occurred due to the calcination of $CaCO_3$.

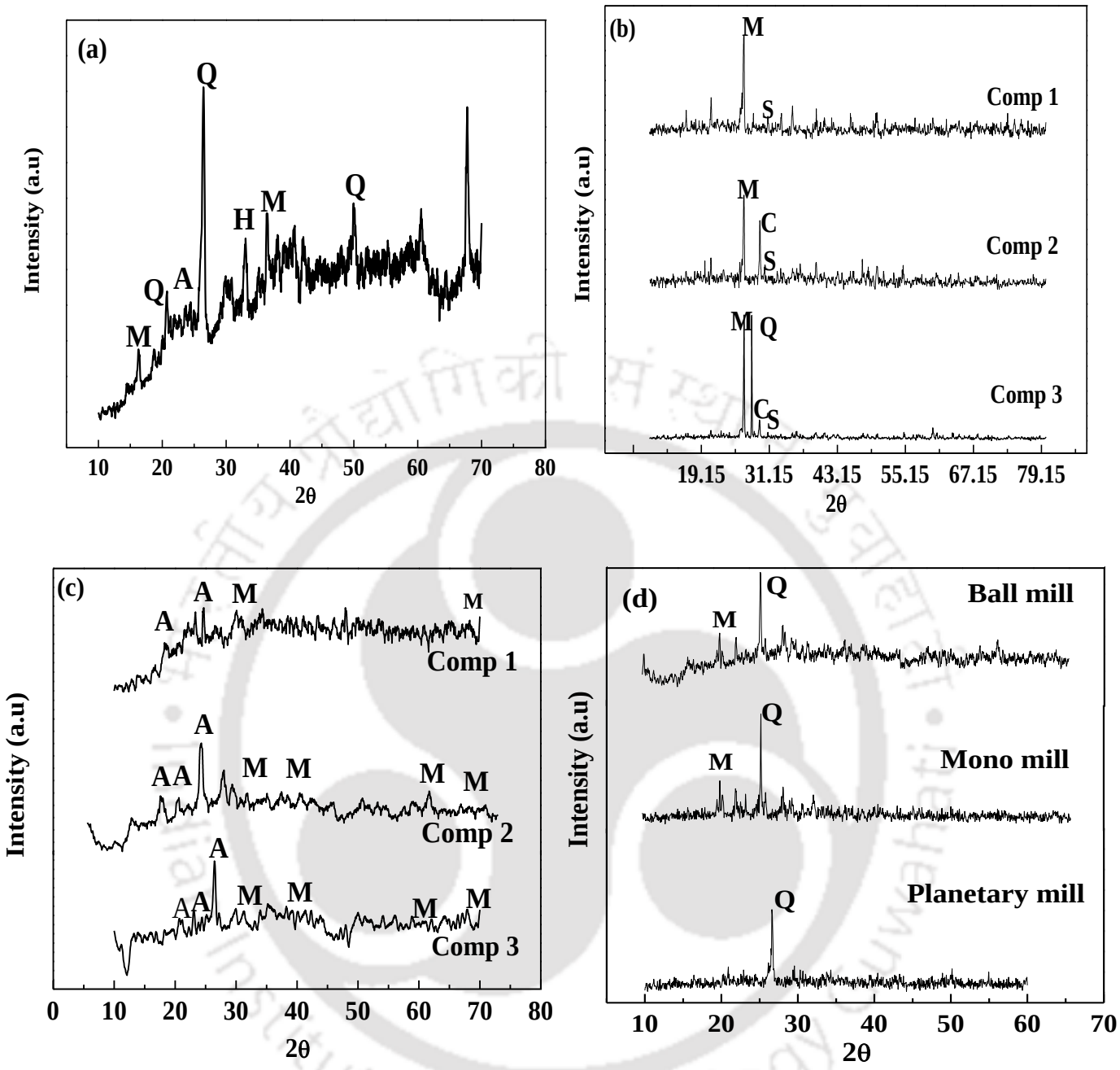


**Fig. 2.2: XRD analysis of (a) Fly ash sintered at 850°C (b) non-sintered ceramic membrane MB1 at compositions C1, C2 and C3 (c) sintered at 850°C ceramic membrane MB1 at compositions C1, C2 and C3 (d) Ceramic membrane with different grinding mediums of the precursor powder.**

Release of $CO_2$ gas creates vacant spaces and imparts porous structure to the membrane. A maximum weight loss of around 25 % was observed. Similar results were evident from the TGA analysis of membrane MB2 at composition C2**.** A dip in the curve at around 98 – 103 °C was observed due to evaporation of water. From 111 °C to 720 °C which was again due to the burning of impurities, unburnt mineral coal powder and evaporation of fly ash. From 720 °C to 820 °C maximum weight loss occurred due to the formation of $CO_2$ in the calcination of $CaCO_3$ and $Na_2CO_3$ a change in mass percentage of 24 % was observed. We thus selected our sintering temperature as 850 °C based on the mass % change with temperature from the above graphs. Similarly, TGA analysis were carried out for precursor powder prepared using the ball mill, the mono mill and the planetary mill as the grinding medium **Fig. 2.3**. As discussed before the lowest particle size was available for the planetary mill as the grinding medium with the order of particle size decreasing as ball mill> mono mill> planetary mill .It was observed that with decreasing particle size the sintering temperature also decreased as 850 °C> 750 °C > 650 °C.

The reason for this change can be explained keeping in mind the steps involved in effective grain coarsening i.e. thorough surface diffusion, grain boundaries and thermal evaporation and condensation. The smaller the particle size, the faster it is going to be grain coarsening due to high surface energy of the particles.

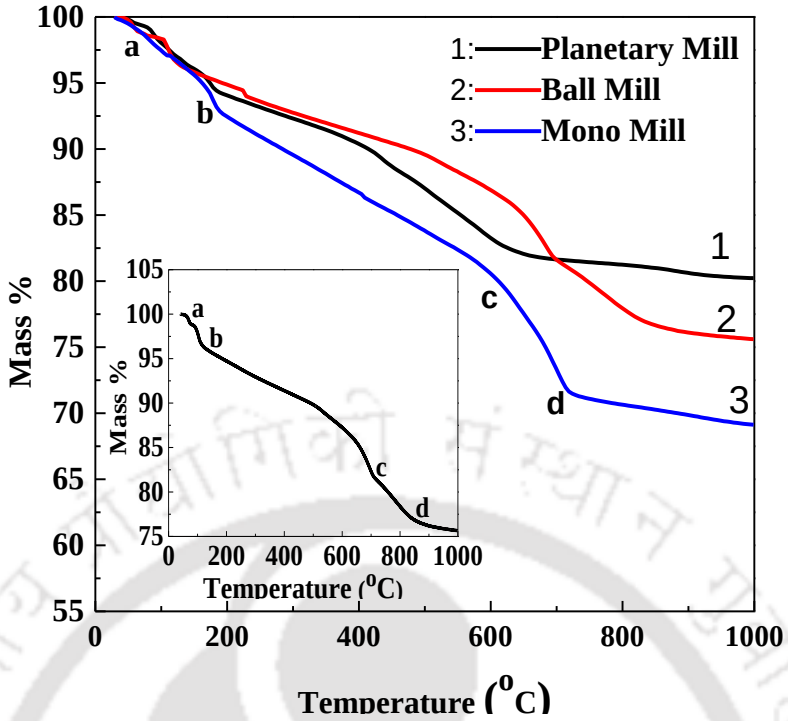


**Fig. 2.3: TGA of precursor powder prepared using ball mill, mono mill and planetary mill, (inset): TGA analysis of precursor powder at composition C1. a-b: removal of water molecule weakly bonded, b-c: burning of small impurities, unburned mineral coal powder and evaporation of boric acid, c-d: formation of $CO_2$ occurred due to the calcination of $CaCO_3$.**

### 2.2.1.4 Particle size distribution

The particle size distribution of the ball mill ground, mono mill ground and planetary mill ground particles are shown in the **Fig. 2.4** below. It is seen that the normal Gaussian distribution is not obtained rather the graphs show a log - normal and rosin - rammler distribution which shows an irregular particle size distribution [53].

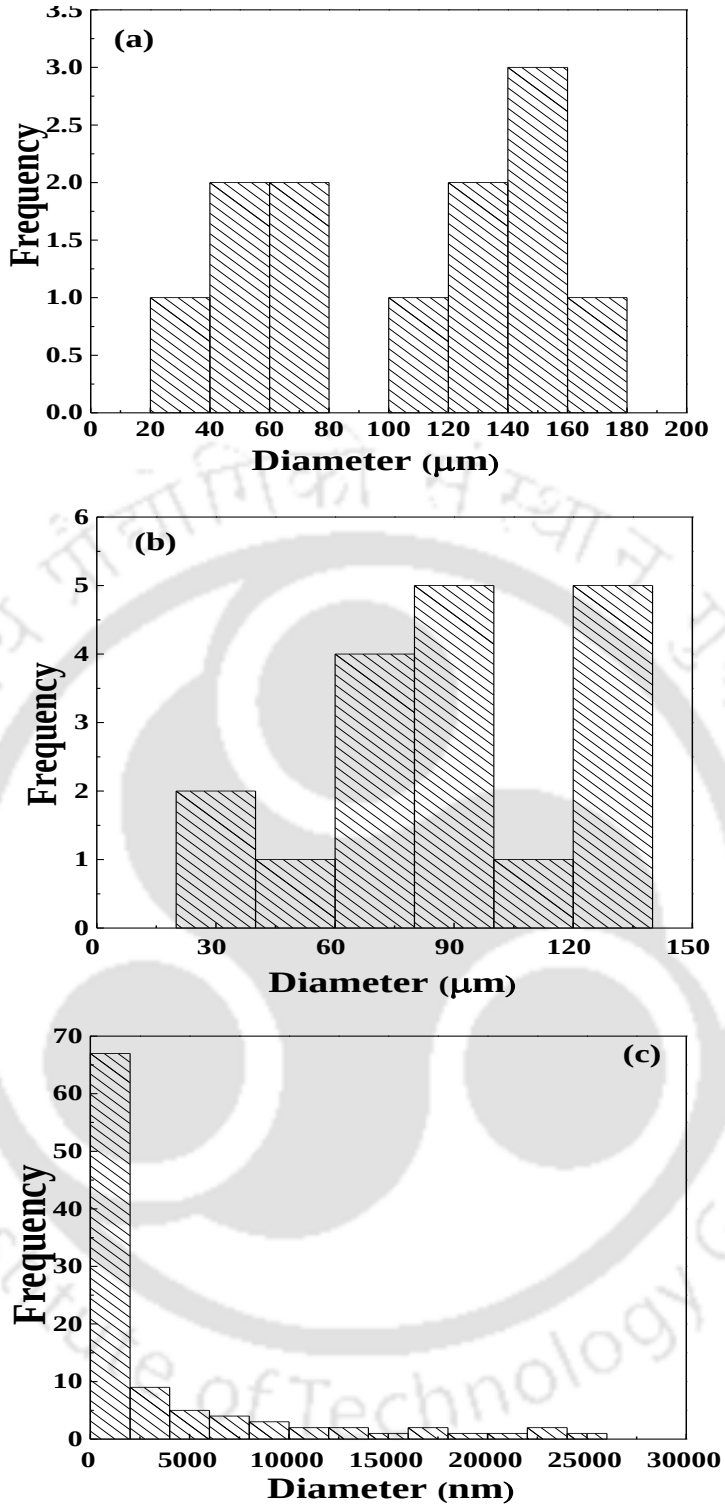


**Fig. 2.4: Particle size analysis of precursor powder for membrane (a) MB1 (b) MB2 and (c) MB3.**

### 2.2.1.5 Field emission scanning electron microscope (FESEM)

The ceramic membranes prepared were then viewed under FESEM to determine the pore size of the membranes. Membranes with sintering temperature 850 °C, 750 °C and 650 °C were examined. It was found that the membranes prepared using ball mill grounded raw materials Fig. 2.5 (a, b) had a pore size range of about 20 - 21µm.

Membranes prepared using mono mill grounded raw materials were examined Fig. 2.5 (c, d) and was found that the pore size reduced to 1 - 2.29 µm. It was also observed that the pores developed were almost uniform in size.

The membranes prepared by planetary ball mill grounded raw materials Fig. 2.5 (e, f) showed pore size in the range of 227 - 450 nm.

Thus, reducing the pore size of the starting powder clearly reduces the pore sizes of the resulting membrane. This is because of the reason that with a reduction in particle size of the precursor powder, the distance between the nearby particles reduces and hence the resulting pores also gets reduced in size.

### 2.2.1.6 Electron dispersive X-ray (EDX) analysis

The Composition of particles were analyzed in individual as well as larger crystals using Energy dispersive X-ray spectroscopy (EDX). The EDX analysis Fig. 2.6 consisted of spectra showing peaks corresponding to the presence of the elements O, Si, Al, Fe, Ti, K, Mg, Ca and Na. We have an electron image of the sample powder and the corresponding EDX pattern for that particular scanned sample area. The elements analyzed by EDX suggests proper mixing of the precursor powder for membrane preparation.

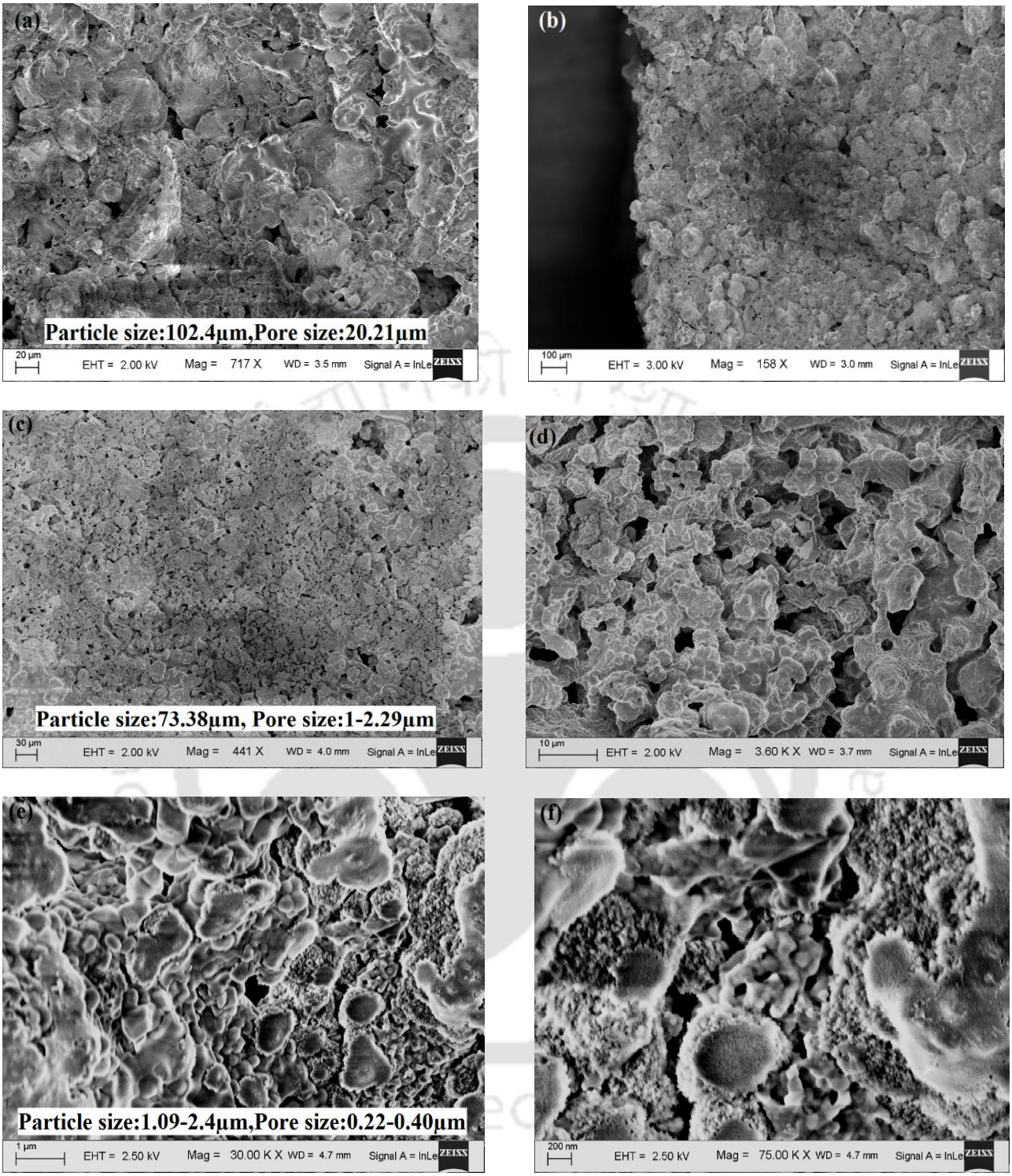


**Fig. 2.5: FESEM figures of membrane prepared by (a, b) Ball mill grounded raw materials, (c, d) Mono mill grounded raw material FESEM and (e, f) Planetary ball mill grounded raw materials.**

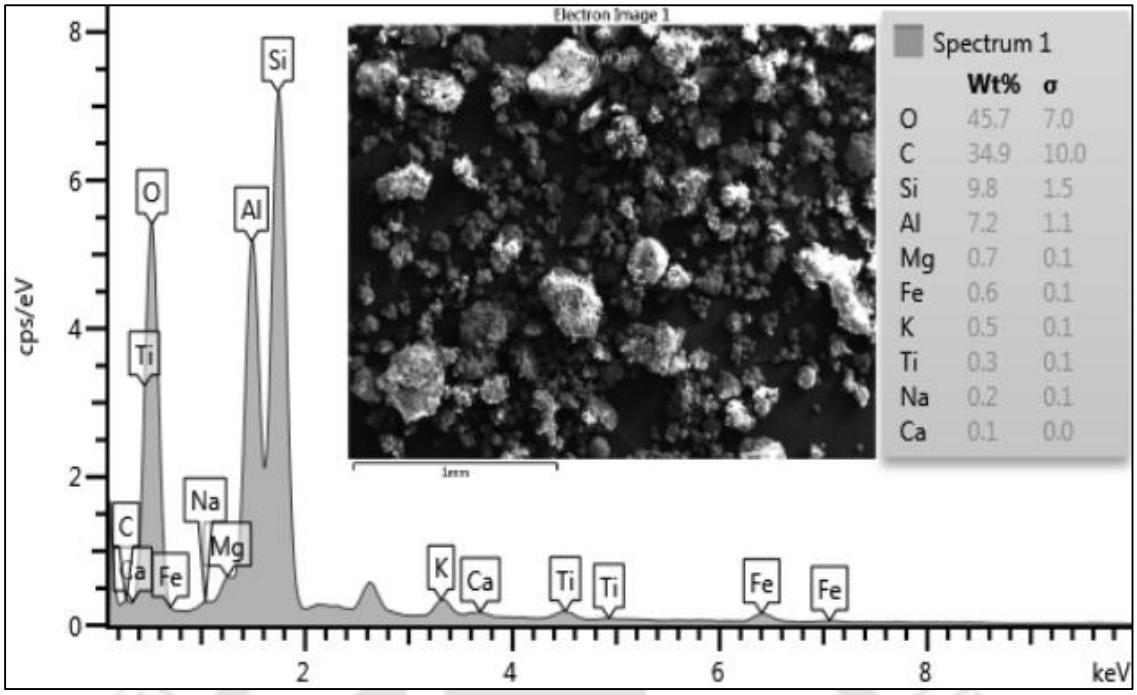


**Fig. 2.6: EDX figures of grounded raw materials for membrane.**

### 2.2.2 Physical properties

#### 2.2.2.1 Apparent porosity (%)

The apparent porosity (A.P.) was measured to determine the pores present in our prepared samples. The membranes were first weighed in the air followed by suspending the membranes in water to measure the suspended weight .The membranes were then soaked in water for 24 h, removed from water and measured again for the soaked weight.

$$\% \text{ A.P.} = \frac{W_S - W_A}{W_S - W_{SW}} \times 100\ \% \qquad 2.3$$

Where, $W_A$ is the weight in air (g), $W_S$ is the soaked weight (g), $W_{SW}$ is the suspended weight (g). An apparent porosity of 51.39 % was obtained for membrane MB1, 44.43 % for membrane MB2 and 29.50 % for membrane MB3.

### 2.2.2.2 Water absorption (%)

To obtain the water absorption (W.A.) weight of the membrane in air was measured followed by soaking the sample in water for 24 h. The membrane was removed from water after 24 h, pat dried to remove excess surface water and the wet weight was measured.

$$\% \text{ W.A.} = \frac{W_W - W_A}{W_A} \times 100\ \% \qquad 2.4$$

Where, $W_A$ is the weight in air (g), $W_W$ is the wet weight (g). The % water absorption of 28 % was obtained for membrane MB1, 32.19 % for membrane MB2 22.57 % for membrane MB3.

### 2.2.2.3 Bulk density

Bulk density (B.D.) is the dry weight of the solid per unit volume of the solid. It was determined by obtaining the amount of water displaced in a beaker using the Archimedes principle. It can be calculated as

$$\text{B.D.} = \frac{Mass\ in\ air\ (g)}{Volume\ of\ water\ displaced\ (ml)} \qquad 2.5$$

The bulk density of 0.96 was obtained for membrane MB1, 1.06 for membrane MB2 and 1.391 for membrane MB3.

The **Fig. 2.7** shows the changes of % apparent porosity, % water absorption and bilk density for the membranes MB1, MB2 and MB3. As it can be seen from the figure above the % apparent porosity and the %water absorption decreases with decreasing pore size. The % water absorption increased with increasing % apparent porosity and the bulk density increased somewhat for the membrane MB3 in comparison to membrane MB1 and MB2. Bulk density is the amount of powder by weight in a definite volume. Finer is the particle size, more the amount of powder shall accommodate in the same volume, thereby increasing the B.D. with compaction. Thereby, MB3 had higher bulk density than MB1 and MB2.

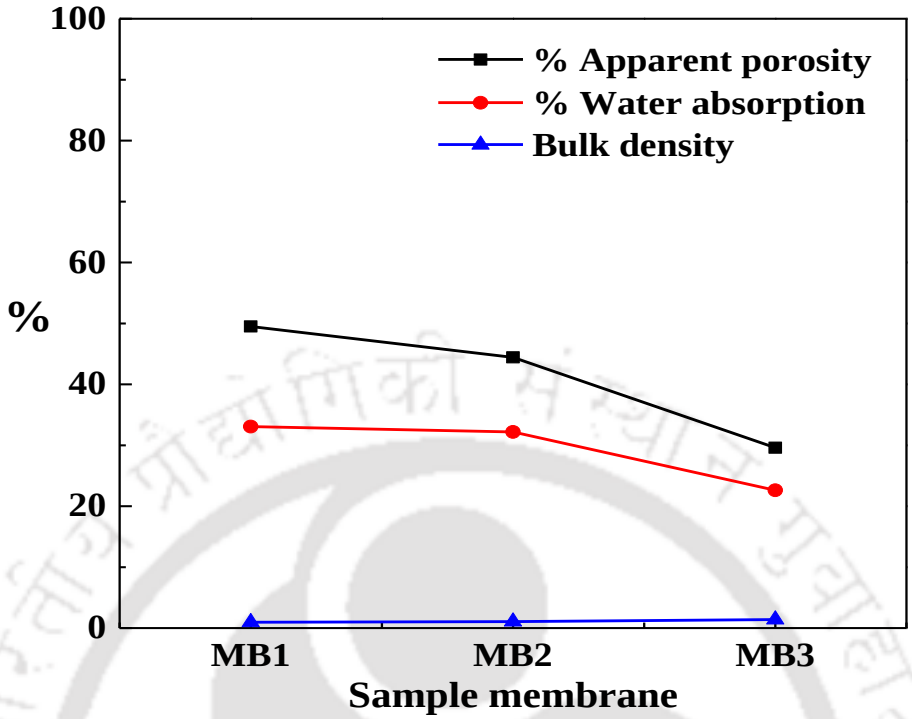


**Fig. 2.7: Graph showing the physical properties of sample membrane.**

### 2.3 Determination of various resistances

The overall flux decline associated with the ceramic membranes over time during the given operating conditions can be expressed as [49-51]

$$J_w = \frac{\Delta P}{\mu(R_m + R_{ad} + R_{pp} + R_f)} \qquad 2.6$$

Where, $R_T = R_m + R_{ad} + R_{pp} + R_f$

The individual resistances can be determined as explained below.

**Membrane resistance ($R_m$)** is mainly used to determine the initial membrane resistance. Pure water is permeated through the membrane with the application of pressure which is noted by reading the value on the pressure gauge. The membrane resistance is expressed as

$$R_m = \frac{\Delta P}{\mu v_w} \quad 2.7$$

The membrane resistances were obtained as $1.2 \times 10^{12}$ $m^{-1}$, $3.5 \times 10^{12}$ $m^{-1}$ and $6.3 \times 10^{12}$ $m^{-1}$ for membrane MB1, MB2 and MB3 respectively

The tomato juice was then charged into the membrane setup without the application of any pressure and allowed to stay as such for around 10 - 20 min. After the mentioned time period the juice was withdrawn from the setup and the membrane was meticulously cleaned with pure water to remove any adhering solid particles that may be present in the juice sample stuck on to the membrane. The cleaned membrane was again placed in the setup and the permeate flux for pure water was calculated at different pressures. The new resistance $R_m$ is thus obtained by calculating the slope of the permeate flux and operating pressure graph

$$R'_m = \frac{\Delta P}{\mu v_w^{ad}} \quad 2.8$$

The adsorption resistance ($R_{ad}$) is calculated after a period of 16 min for each membrane and is expressed as

$$R_{ad} = R'_m + R_m \quad 2.9$$

The plot of adsorption resistance with time is shown in the Fig. **2.8 (b).** As seen from the figure the adsorption resistance increases initially until reaching a certain time beyond which it becomes constant and remains the same with increasing time. As seen from the graphs it is evident that the adsorption resistances are 15.67 % of the membrane resistance for MB1, 21.51 % for MB2 and 17 % for MB3 which is mainly because of the hydrophobic

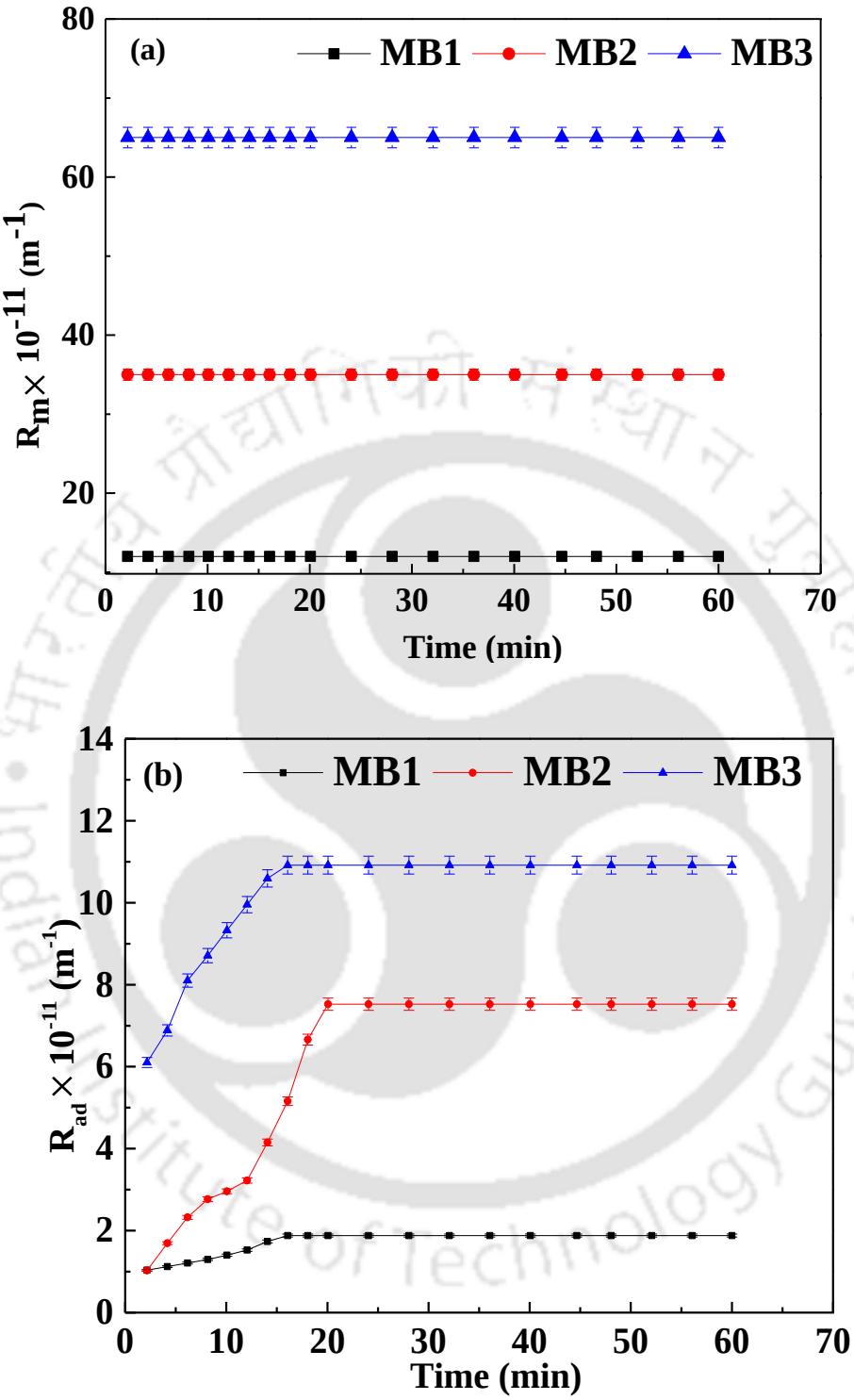


**Fig. 2.8: Variation of (a) Membrane resistance (b) Adsorption resistance as a function of time.**

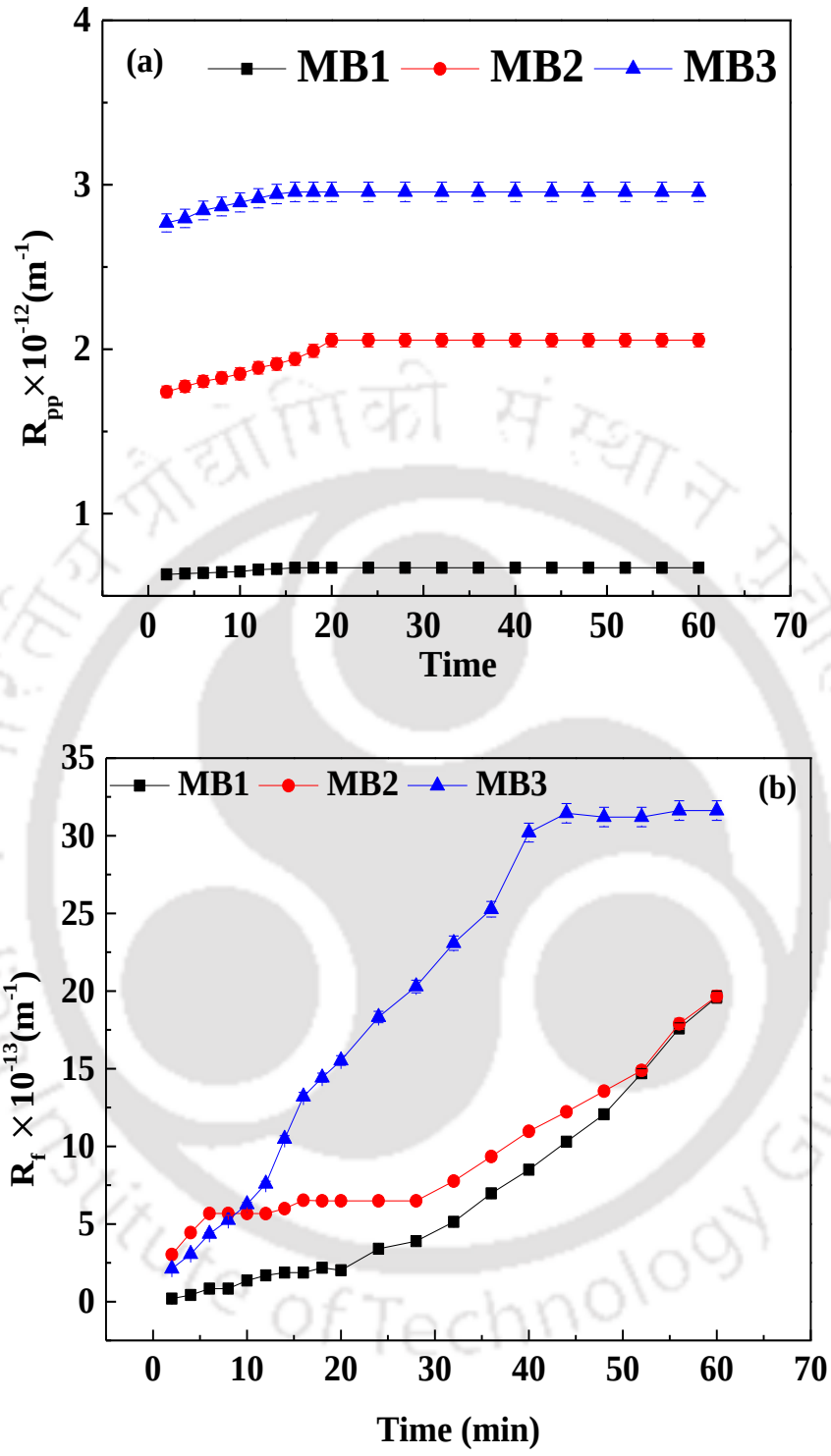


**Fig. 2.9: Variation of (a) Pore blocking resistance and (b) Fouling resistance as a function of time.**

interactions, polar interactions and charge transfers starting immediately as the membrane comes in contact with the feed solution.

Using a clean membrane, fresh tomato juice was again charged in the setup and the microfiltration experiment was conducted under mentioned operating conditions for 16 min. During this 16 min of operation, the permeate flux was calculated by noting down the decline in the value of permeate weights with time. The permeate flux is calculated as shown in eq. (2.6).

The flux is usually calculated during the initial microfiltration period of 16 min is expressed as

$$J_w^{16} = \frac{\Delta P}{\mu(R_m + R_{ad}^{16} + R_{pp}^{16} + R_f^{16})} \qquad 2.10$$

After the end of 16 min the membrane is removed from the setup and washed with pure water to eliminate any deposition on the membrane surface as a result of which the term $R_f$ is

eliminated. The membrane is thus allowed to pass pure water under suitable operating conditions which can be expressed as

$$\nu_w = \frac{\Delta P}{\mu(R_m + R_{ad}^{16} + R_{pp}^{16})} \qquad 2.11$$

The values of $R_m$ and $R_{ad}^{16}$ have already been calculated from the eq. (2.7) and (2.9) above. Incorporating these values in eq. (2.11) will give us the value of the pore plugging resistance, $R_{pp}^{16}$. The calculated value of the pore plugging resistance is then incorporated into eq. (2.10) to give us the value of reversible fouling resistance, $R_f^{16}$. This value of resistance helps us to know the growth of the reversible fouling layer on the ceramic membrane surface with time.

The plot of pore plugging resistance, $R_{pp}$ with time shows that the resistance value increases gradually upto a certain time of around 16 min and then obtains a constant value (**Fig. 2.9a)**.

It should be noted that the pore blocking mechanism depends on the relationship between solute size and the diameter of the membrane pores. If the solute size is larger than the pore size, the process

begins with complete blocking as further particle deposition shall be on those that have already adhered to the membrane.

The plot of fouling resistance with time shows that the fouling increases rapidly during the first initial stage of the experiment and then as the filtration process continues the rate of cake deposition becomes slower **Fig. 2.9b**. This is mainly because of the reason that the heavier particles settle first on the surface of the membrane followed by the light weight particles which shall deposit at later stages of the experiment.

At the end of 60 min of operation time, the various resistances occurring all throughout the filtration process were calculated. The fouling resistance was in between 98 % and 96 %, the adsorption resistance 0.09 % to 0.33 %, the pore plugging resistance from 0.33 % to 0.91 % and the membrane resistance from 0.6 % to 2 % of overall total resistance. Thus, the reversible fouling resistance was found to be the major resistance prevailing during the filtration process. Each of the experimental work were repeated at least 3 times in order to ascertain the accuracy of results. An error of around ± 2% to ± 3 % were observed. The alterations of the flux decline profile for the given operating conditions were in sync with the expected trends i.e. they decreased with increasing time.

The flux profile for the three membranes MB1, MB2 and MB3 are also shown in **Figure. 2.10.** Following the normal trend of flux decline, it can be seen that MB2 has the highest steady state flux value of 56.2 L/h.m$^2$. Preceding studies suggested $R_f$ to be the major resistance existing during the microfiltration process hence the decline in flux can be associated with the formation of cake layer owing to deposition of higher molecular weight solids in the fruit juice.

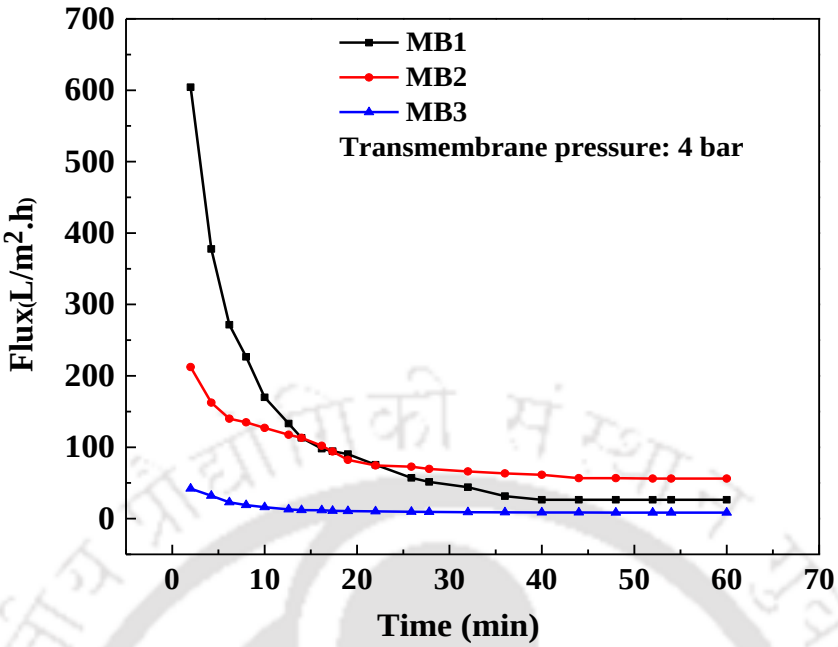


**Fig. 8: Variation of permeate flux with time for membranes MB1, MB2 and MB3.**

### 2.4 Juice Analysis

The juice (feed and permeate) was analyzed for physical properties such as color, clarity, density, pH, total solids, viscosity, total soluble sugar, density, alcohol insoluble solid, water insoluble solid content and metals like Na, K, Ca and Mg as shown in **Table 2.2** below.

The main properties studied included the color which was higher for the feed at 0.75 and lowest for the permeate 3 at 0.45. This is because of the fact that the suspended solids are removed during the microfiltration process, hence a lower absorbance value for low concentration of suspended solids i.e. intensity of color decreased with filtration.

The density of the feed was around 0.91 g/cm$^3$ and decreased with filtration with the permeate 3 having the lowest density of 0.80 g/cm$^3$. Tomato juice was acidic in nature which was mainly due to the presence of various acids like citric acid and malic acid. pH values of the permeate remained almost the same as the feed.

Total soluble sugar (TSS) of the feed was the highest at 26.66 $^{o}$Brix and that for permeate 3 was the lowest at 0.10 $^{o}$Brix. Turbidity measurements suggested that membrane MB3 retained the highest suspended solids present in the feed and provided us a turbid free tomato juice having turbidity values of 0.2 NTU. Similarly Total solids (TS) were also the least for permeate 3 obtained using MB3 at 0.01 g/100 mL.

AIS and WIS values were the lowest for permeate 3 with values of 0.04 and 0.01 %, respectively.

A slight decrease in the concentration of metals like Na, K, Ca and Mg was also evident which might be associated with the fact that some amount of the metals are retained by the cake layer formed on the membrane surface during the microfiltration process. Moisture content, total solids, ash content and organic matter were also calculated (**Table 2.3**).

The permeate juice were then analyzed after 7, 12 and 30 days to see if any changes were visible in the physical properties. It was found that properties like color, clarity, density and suspended solids almost had a change of about 2 - 3 % from fresh juice properties. However, the viscosity of the juice was found to increase with an increase in the number of days, the highest viscosity being for 45 days. Hence the clarified juice could be used for storage without any preservatives in refrigeration for 30 days at least.

The average particle size of feed and permeates from membranes MB1, MB2 and MB3 (**Fig. 2.11**) were also determined. It was found that the feed had an average particle size of 117.48 µm, whereas the particle sizes for the permeates 1, 2 and 3 are found to be 10.36 µm, 1.04 µm and 220 nm. A bimodal nature is observed in the Fig. 10. This is because of the fact that the smaller sized solids tend to agglomerate with time resulting in the second mode in the figure. It can be also observed that larger colloidal particles are successfully eliminated as a result of the filtration process.

The permeate juice were then analyzed after 7, 12 and 30 days to see if any changes were visible in the physical properties. It was found that properties like color, clarity, density and suspended solids almost had a change of about 2-3 % from fresh juice properties. However, the viscosity of the juice was found to increase with an increase in the number of days, the highest viscosity being for 30 days. The increase in viscosity of juice stored at low temperature might be due to the development of dextran by bacteria such as *Leuconostoc mesenteroides*.

**Table 2.2: Physical properties of tomato juice**

| **Characteristics** | **Feed** | **Permeate 1 (MB1)** | **Permeate 2 (MB2)** | **Permeate 3 (MB3)** |
|---|---|---|---|---|
| Color (A) | 0.75 | 0.73 | 0.51 | 0.45 |
| Clarity (% ) | 0.25 | 1.35 | 35.7 | 55.2 |
| Density ($g/cm^3$) | 0.95 | 0.90 | 0.89 | 0.80 |
| pH | 4.56 | 4.50 | 4.76 | 4.89 |
| Total soluble sugar ($^oBrix$) | 26.66 | 3.91 | 1.04 | 0.10 |
| Turbidity (NTU) | 50 | 2.1 | 0.8 | 0.2 |
| Total solids (g/100 mL) | 0.89 | 0.80 | 0.25 | 0.11 |
| Water insoluble solid (%) | 0.16 | 0.12 | 0.06 | 0.01 |
| Alcohol insoluble solid (%) | 0.64 | 0.20 | 0.01 | 0.04 |
| Na (mg/L) | 35 | 34 | 33 | 31 |
| K (mg/L) | 998 | 997 | 995 | 992 |
| Ca (mg/L) | 85 | 82 | 81 | 80 |
| Mg (mg/L) | 75 | 73 | 72 | 71 |

***Waste (Skin+ Pulp + Seeds) consisted of 82.4 % and 87 % of WIS and AIS respectively**

**Table 2.3: Physical properties of tomato waste**

| Chemical composition (%) | Tomato waste |
|---|---|
| Moisture | 75.21 |
| Total solids | 24.79 |
| Volatile solids | 91.18 |
| Ash | 8.82 |
| Organic matter | 91.18 |

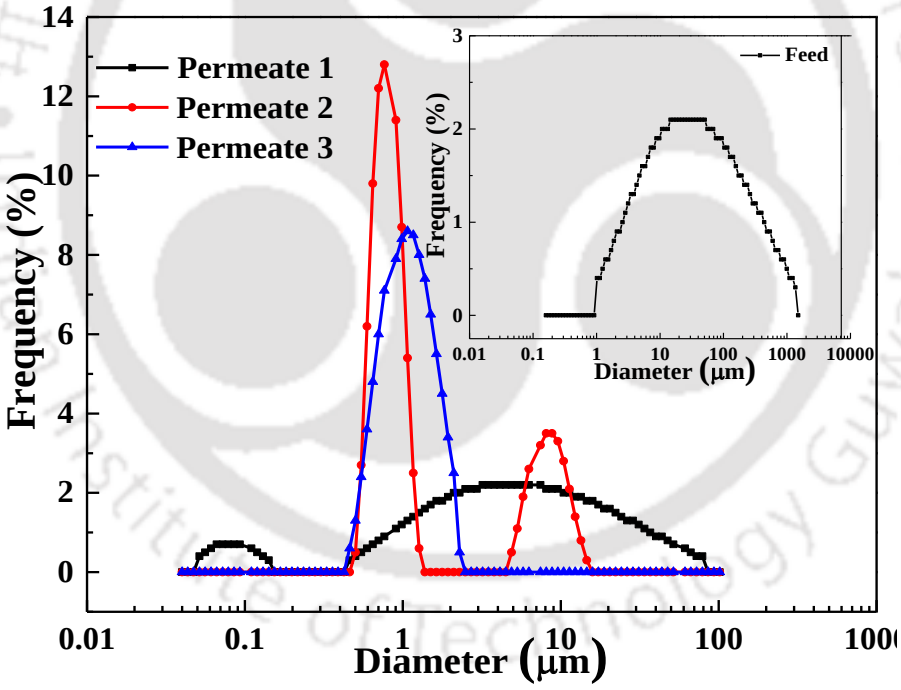


**Fig. 2.11: Graphs showing average particle size of the feed and the permeate for the membranes MB1, MB2 and MB3.**

# Chapter 3

# Detailed study of temperature-responsive composite membranes prepared by dip coating poly (2-ethyl-2-oxazoline) onto a ceramic membrane

# *Chapter 3*

# Detailed study of temperature-responsive composite membranes prepared by dip coating poly (2-ethyl-2-oxazoline) onto a ceramic membrane

*This chapter discusses the preparation and characterization of a thermo-responsive polymer-ceramic composite membrane that achieves opening and closing of pores by itself. This novel composite membrane was prepared by coating the polymer poly (2-ethyl-2-oxazoline) on ceramic membrane using the dip coating technique. Different parameters such as polymer concentration (5 - 20 wt %) and dip coating time (20 - 60 s) were considered while preparing the membrane. Special emphasis has been laid down on an extensive study of the physical and chemical properties of the membrane. Temperature responsiveness was utilized for studying the variation in water flux and BSA rejection. It was found that at temperatures above lower critical solution temperature (LCST) the flux achieved was highest than at temperatures below LCST.*

## 3.1 Experimental

### 3.1.1 Raw materials

The raw materials used for the preparation of the ceramic membrane are Fly ash from National Thermal Power Corporation Limited (NTPC), Calcium Carbonate (Merck**)**, Sodium carbonate (Merck), Boric acid (CDH), Sodium metasilicate (CDH), poly (2-ethyl-2-oxazoline) (Sigma Aldrich) and acetone. All the materials used for membrane preparation were used without any further purification. The desired composition used in the preparation of the membrane is shown in **Table 3.1** which was obtained after repeated trial and error experiments as discussed in **section 2.1.1** of **Chapter 2**.

**Table 3.1: Composition of the membranes**

| Raw materials | Composition (dry weight %) |
|---|---|
| Fly ash | 70 |
| $CaCO_3$ | 14 |
| $Na_2CO_3$ | 7 |
| Boric acid | 4.5 |
| Sodium metasilicate | 4.5 |

### 3.1.2 Ceramic membrane fabrication

The membrane fabrication process involved thorough mixing and grinding of raw materials like fly ash, sodium carbonate, sodium metasilicate, calcium carbonate and boric acid in a ball mill at 180 rpm for 1 h. Once the mixed and grinded raw material was obtained, a definite amount of millipore water was used to obtain a paste which was then casted on an MS ring with diameter of 52 mm and thickness of 7 mm. The casted membrane was kept to dry overnight under the application of uniform weight to prevent any structural defect in the membrane. The obtained circular disk shaped membrane was dried in the oven for 12 h at 120 $^oC$ and then sintered at 750 $^oC$ for 5 h. After the sintering process, the membrane turned hard, rigid and had a porous texture. Eventually, the membrane was polished with silicon carbide abrasive paper (C - 220) to obtain a smooth, flat membrane of diameter 51.75 mm and thickness 6.5 mm. Finally, the membrane was cleaned in a sonicator for 15 min to remove loose particles from the membrane and dried at 120 $^oC$ [87, 88].

Poly (2-ethyl-2-oxazoline) solution was prepared by dissolving the polymer of 5, 10, 15 and 20 wt % in acetone separately in beakers. The mixtures were stirred using a magnetic stirrer for 24 h to ensure uniform and complete dissolution of poly (2-ethyl-2-oxazoline) in acetone. Prior to the dip coating process, the ceramic supports were kept immersed in acetone for 3 h to displace air bubbles that may be present in the membrane porous structure which would restrict the penetration of poly (2-ethyl-2-oxazoline) solution into the membrane pores during dip coating. Surfaces other than the top surface of the support were covered using Teflon tape to prevent polymer deposition. Coating of poly (2-ethyl-2-oxazoline) over the support was carried out by dipping the support in the poly (2-ethyl-2-oxazoline) solution with dipping time varying from 20 s to 60 s. After the coating process, the composite membranes were kept on a flat glass surface at ambient temperature for 24 h to yield a thin coating of poly (2-ethyl-2-oxazoline) on the ceramic support. During this time, acetone of the top layer evaporates and thereby contributes to the pore formation, membrane morphology and separation capabilities. The composite membrane thus prepared constituted a ceramic support that was dominated with macroporous structure and a poly (2-ethyl-2-oxazoline) top layer that was dominated with mesoporous structure. Finally, the composite membrane was dried at 45 $^{o}$C for 3 h in a hot air oven to accomplish complete removal of acetone from the membrane structure. The nomenclature of various composite membranes fabricated with varying polymer concentration in acetone (5-20 wt %) and dipping time (20–60 s) are presented in **Table 3.2** [87, 88].

**Table 3.2: Nomenclature of fabricated membranes based on polymer concentration**

| Polymer concentration (wt %) | Membrane type | Dipping time (s) | Membrane type |
|---|---|---|---|
| 5 | M-5 | 0 | M-15-0 |
| 10 | M-10 | 20 | M-15-20 |
| 15 | M-15 | 40 | M-15-40 |
| 20 | M-20 | 60 | M-15-60 |

### 3.2 Results and discussion

Structural characterization of prepared membranes were performed and reported well in the subsequent section. Characterization techniques involved the thermo gravimetric analysis (TGA) of the raw materials paste to identify the weight transformations of the material at different thermal conditions, structural characterization of membranes by X-ray diffraction (XRD) Bruker, Model-D8-Advance to investigate the extent of phase transformations. Scanning was done from high angle 2θ value between 10 - 70° at a speed of 0.5 sec/° in continuous mode at an increment of 0.05. Delsa-nano was used to determine the particle size of the polymer with changing temperature. FTIR (Make: Perkin Elmer, USA, Model: LR 64912C) analysis was performed with the KBr supported technique in the range of 450 - 4000 $cm^{-1}$, to study the chemical composition of the membrane. Structural characterization of the support were carried out using FESEM (Make: Zeiss, Model: Sigma) for the evaluation of membrane morphology, presence of surface/cross-sectional defects such as pinholes and cracks (if any) and estimation of membrane thickness for those cases where substantial films were deposited.

The membrane was attached onto the holder using m-seal which was in turn fixed to the steel casing having a capacity of 300 ml as shown in **Fig. 3.1**. Each freshly prepared membrane

were examined for pure water flux at a transmembrane pressure of 1 bar. The permeation flux was determined using the formula 3.1 as shown below.

$$J_P = \frac{Q_P}{A_m} \qquad 3.1$$

Where, $Q_P$ = The flow rate of permeate across the membrane and $A_m$ = The membrane area available for filtration.

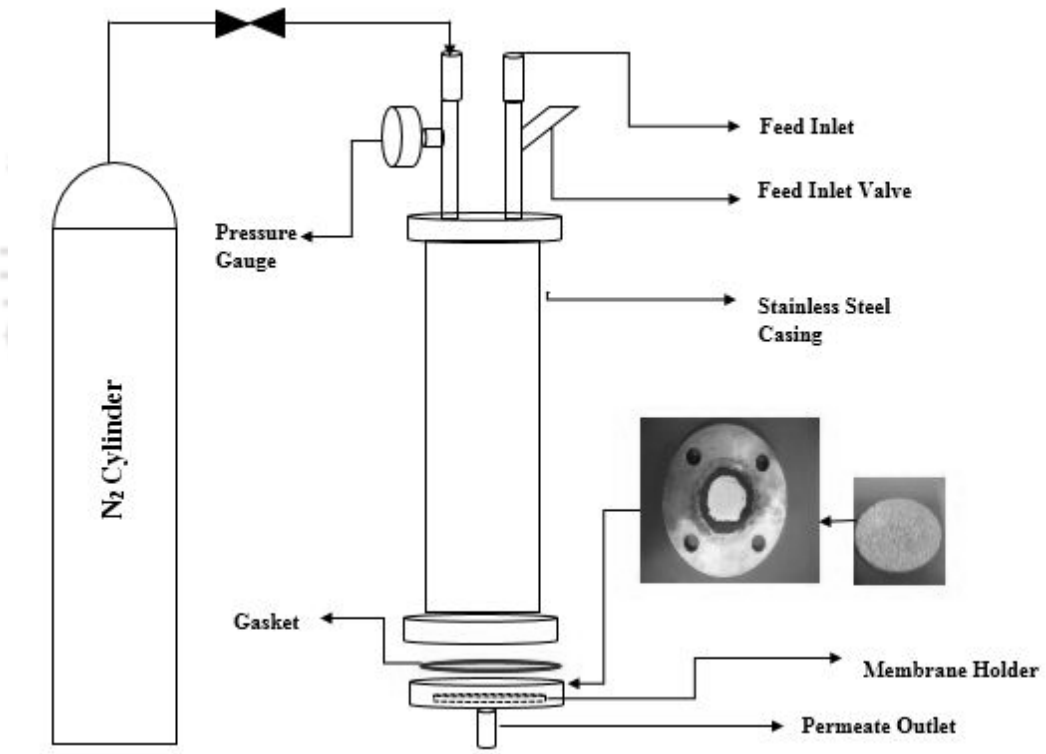


**Fig. 3.1: Experimental setup for permeation experiments**

### 3.2.1 Characterization

#### 3.2.1.1 Fourier transfer infrared spectroscopy (FT-IR)

**Figure 3.2** shows the FT-IR results of bare ceramic membrane, polymer poly (2-ethyl-2-oxazoline) and the composite membrane. For the bare ceramic membrane, peaks at 550 - 400 $cm^{-1}$ represents B-O-B stretching, peaks at 700 - 800 $cm^{-1}$ stand for B-O stretching and O-Si-O vibrations due to the presence of boric acid and $Na_2SiO_3$, peaks at 657 $cm^{-1}$ is for Al-O stretching. Peaks at 717 $cm^{-1}$ and 879 $cm^{-1}$ due to symmetric and asymmetric stretching of $CO_3$ group in $CaCO_3$. Peak at 1481 $cm^{-1}$ represents the asymmetric stretching of $CO_3$ group for $Na_2CO_3$ and 1000 $cm^{-1}$ represents Si-O vibrations of $Na_2SiO_3$. In the spectrum of poly (2-ethyl-2-oxazoline), the sharp peaks at 1680 and 1110 $cm^{-1}$ were assigned to the stretching of C-N and C–O groups, respectively. The characteristic band at 980 $cm^{-1}$ could be attributed to the skeletal vibration of the pendant 2-oxazoline rings. The weak shoulders at 2855 and 2962 $cm^{-1}$ were associated with the symmetric and asymmetric vibrations of $CH_2$ [84]. The composite ceramic membrane spectrum exhibited the spectrums from both the poly (2-ethyl-2-oxazoline) polymer and the ceramic membrane **Fig. 3.2,** thereby suggesting a well coated layer of the polymer on the membrane surface.

#### 3.2.1.2 Thermogravimetric analysis (TGA)

The main purpose of thermal analysis is to identify the various temperature regimes in which the major weight losses and phase transformations occur in the membrane. As seen from the **Fig. 3.3 inset** below, the change in weight is evident for the ceramic membrane. From 26-153 $^oC$ a dip in the curve is observed which is mainly due to the removal of water molecule weakly bonded to the sample mixture having a weight loss of 4 %. The weight loss of sample between 153-182 °C

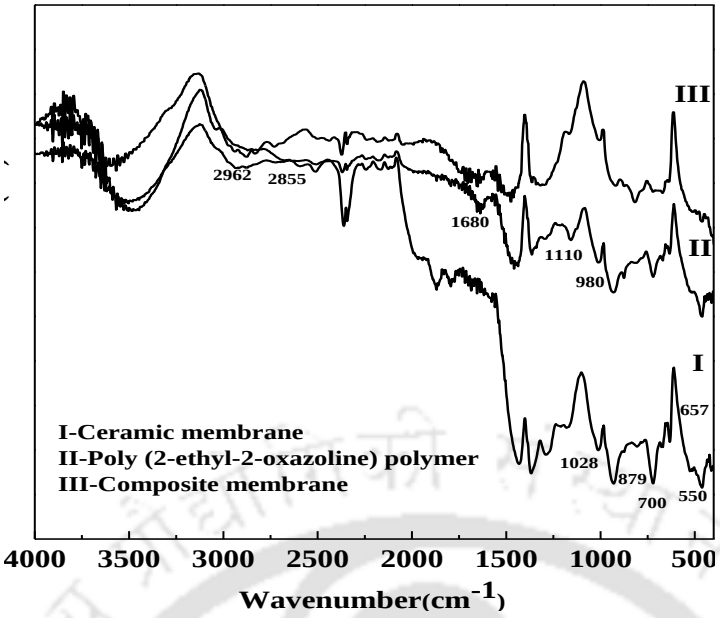


**Fig. 3.2: FTIR spectrum of ceramic membrane, poly (2-ethyl-2-oxazoline) and polymer-ceramic composite membrane**

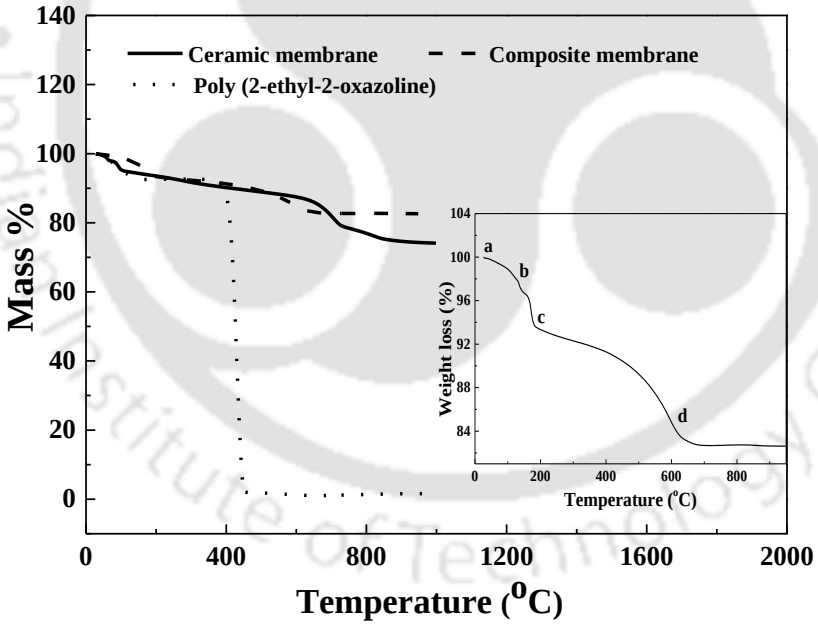


**Fig. 3.3: TGA graph of ceramic membrane, poly (2-ethyl-2-oxazoline) polymer and ceramic/ poly (2-ethyl-2-oxazoline) polymer composites, inset: TGA graph of ceramic membrane a-b: Evaporation of weakly bonded water, b-c: Burning of impurities, c-d: Calcination of CaCO3 along with evaporation of boric acid**

was 3 %, which can be attributed to burning of small impurities and unburned mineral coal powder. The maximum weight loss of about 11 % occurred at the temperature regime between 182-681 °C. This is the region where the formation of $CO_2$ occurred due to the calcination of $CaCO_3$ and also because of the evaporation of boric acid whose boiling point is 300 °C. Release of $CO_2$ gas creates vacant spaces and imparts porous structure to the membrane.

As seen from **Fig. 3.3**, for neat poly (2-ethyl-2-oxazoline) polymer, the first major weight loss occurred at 250$^{o}$C and the second at 350 $^{o}$C. The ceramic – poly (2-ethyl-2-oxazoline) polymer composites showed a major weight loss between 280 and 350 $^{o}$C, associated with the decomposition of poly (2-ethyl-2-oxazoline) chains grafted on the ceramic membrane surfaces. The TGA results revealed that the ceramic-poly (2-ethyl-2-oxazoline) polymer composites showed a thermal stability less than the ceramic membrane which was mainly because of the polymer coating on the top surface of the membrane.

#### 3.2.1.3 X-ray diffractometer (XRD)

Analysis for the ceramic membrane samples were performed both before and after sintering. As seen from the **Figure 3.4** below there was observation of quartz (Q), mullite (M), calcite (C) and silicate (S) evident from the graph. Planes (100) and (101) for quartz, (110) and (121) for mullite, (100), (110) and (200) for silicate and (110), (104), (012), (110) and (202) for calcite were observed [86].

The samples were then sintered at 750 $^{o}$C for 5 h and then examined for determining the phase transformations. A critical observation of the peaks reveals that there is significant phase transformation occurring at higher temperature. An observation of peaks and trends in the XRD patterns (**Fig. 3.4 a)** conveys that the major phase present are mullite (M), Zirconite (Z) and

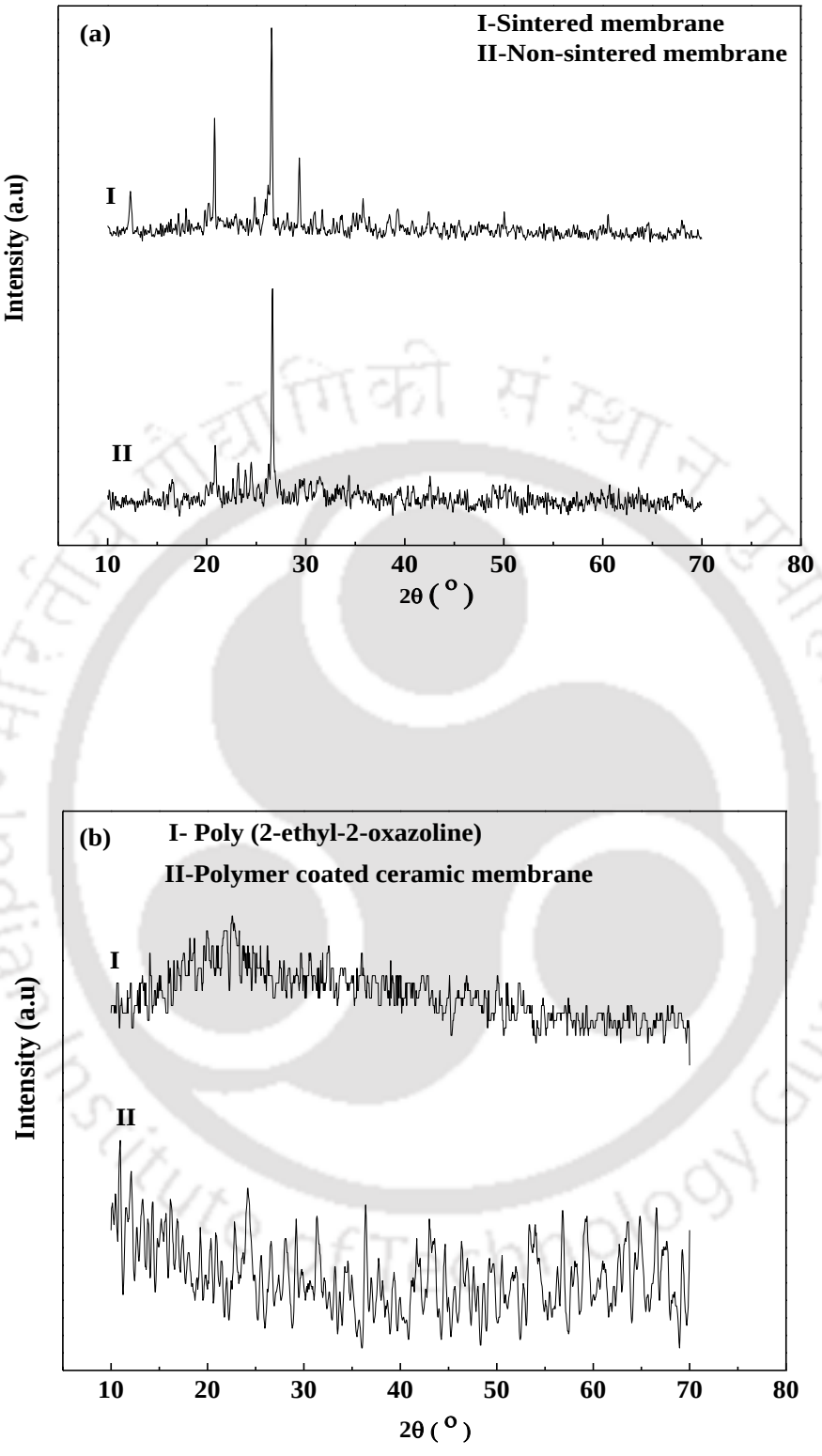


**Fig. 3.4: (a) XRD spectrum of the non-sintered ceramic membrane and ceramic membrane sintered at 750ºC (b) XRD spectrum of (b) Poly (2-ethyl-2-oxazoline) polymer and (c) Ceramic/ poly (2-ethyl-2-oxazoline) polymer composite**

anorthite (A). Planes (110) and (121) were observed for mullite, (001), ($10\bar{1}$), (010) and (100) for anorthite and (002), (040), (240), (244)) for zirconite according the JCPDS data [87, 88].

The poly (2-ethyl-2-oxazoline) polymer did not show any clear peaks in XRD, indicating its amorphous structure. However, the XRD pattern of the ceramic-poly (2-ethyl-2-oxazoline) polymer composites was nearly same as the neat poly (2-ethyl-2-oxazoline), implying that a well formed layer of the polymer was deposited on the surface of the ceramic membrane **Fig. 3.4 b**.

### 3.2.1.4 Electron dispersive X-ray analysis (EDX)

The EDX analysis of the sintered ceramic membranes without any coating shows a spectra mainly consisting of peaks corresponding to the presence of elements O, Si, Al, Fe, Ti, K, Mg, Ca and Na. The EDX spectra of poly (2-ethyl-2-oxazoline) polymer consisted of peaks corresponding to the presence of elements C, O and N. The Al detected maybe because of the Al present in the ceramic membrane **(Fig. 3.5a).**

The EDX analysis of ceramic-poly (2-ethyl-2-oxazoline) polymer composite consisted of peaks corresponding to the presence of elements C, O, Si, Al, Fe, Ti, K, Mg, Ca and Na. The high C weight % corresponds to the C-chains in the polymer and the presence of N also corresponds to

the N present in the ring structure of poly (2-ethyl-2-oxazoline) (**Fig. 3.5b**).

### 3.2.1.5 Field emission scanning electron microscope (FESEM)

The main purpose for the analysis of the surface and cross-sectional FESEM study was to visualize various possible mechanisms involved in poly (2-ethyl-2-oxazoline) deposition on the ceramic support. Besides identifying surface defects and surface morphology, the study is aimed

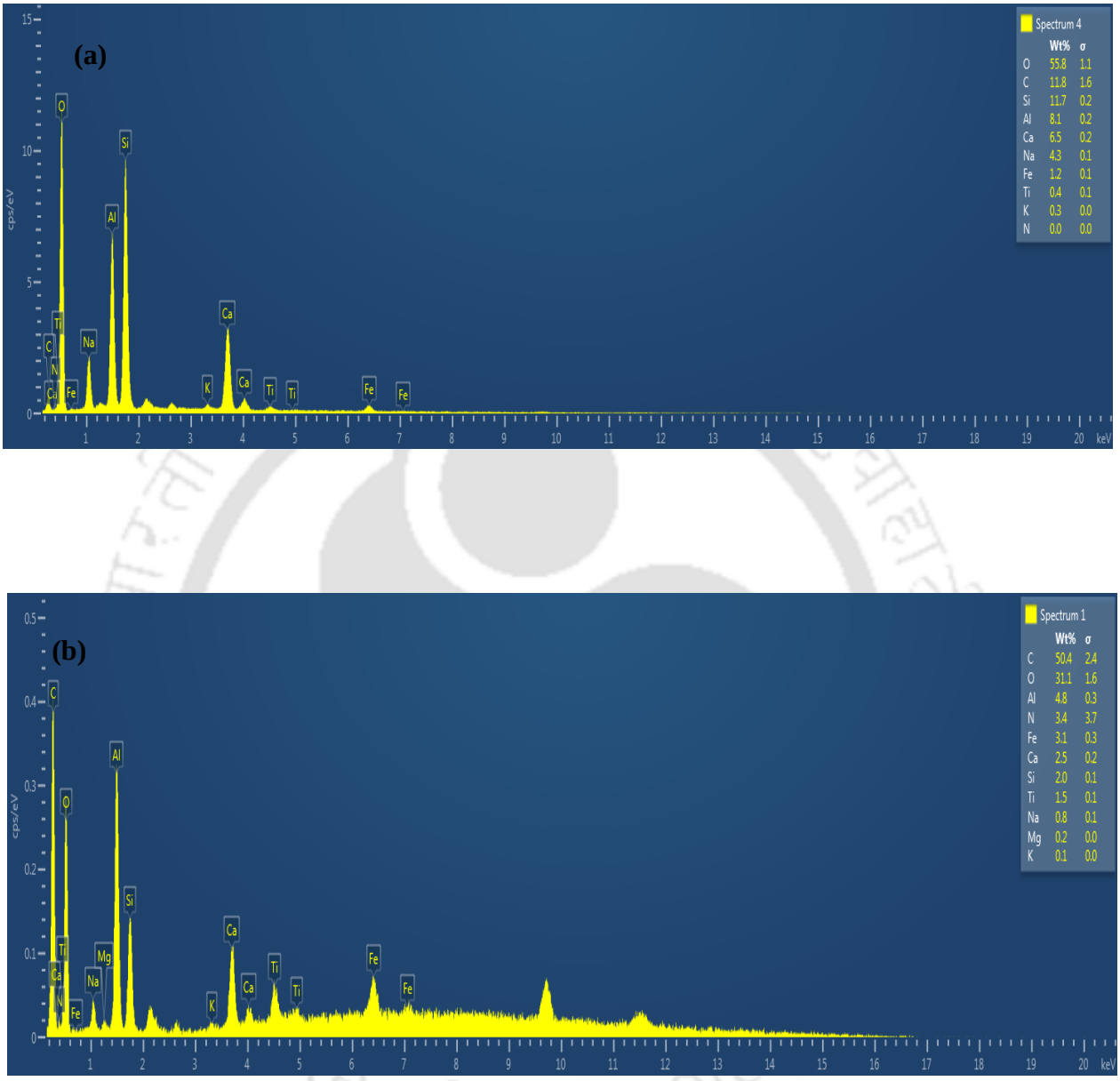


**Figure 3.5: EDX analysis (a) Bare ceramic membrane (b) Ceramic-poly (2-ethyl-2-oxazoline) polymer composite membrane**

to evaluate the effect of dip coating parameters (polymer concentration and dipping time) on ceramic membrane. The ceramic membranes prepared without any top coating were viewed under FESEM to determine the pore size of the membranes. Membranes were sintered at 750 $^{o}$C which were then analyzed under FESEM to investigate the presence of pores on the surface of the membrane. It was found that the membranes prepared using ball mill grounded raw materials had a pore size range of about 6.61µm.

**Fig. 3.6** presents FESEM images of the top surface of composite membranes prepared by varying poly (2-ethyl-2-oxazoline) concentration (5–20 wt %). From the figure it was observed that with increase in both polymer concentration and dipping time, the pore size of the membrane decreases. The FESEM image of 5 wt % poly (2-ethyl-2-oxazoline) membrane (M-5) indicates that almost no layer of polymer is deposited on the ceramic surface. When the concentration of polymer was increased to 10 wt %, the top surface was totally covered by the poly (2-ethyl-2-oxazoline) layer and created a porous polymeric structure (M-10). The porous structure of the polymeric film was attributed to the evaporation of the solvent (acetone) from the membrane surface. Membranes prepared with 15 wt % polymer concentration (M-15) indicated a stable porous structure.When the concentration of the polymer was increased to 20 wt % (M-20), it was observed that the membrane top surface had a very fine porous structure. The size of the pores decreased from 2.31 µm to 0.08 µm **Table 3.3**. This decrease in average pore size with an increase in polymer concentration could be due to viscosity changes.As the polymer concentratio n increases, the viscosity of the polymer solution also increases resulting in a decrease in the droplet growth rate of the membrane pores [88].

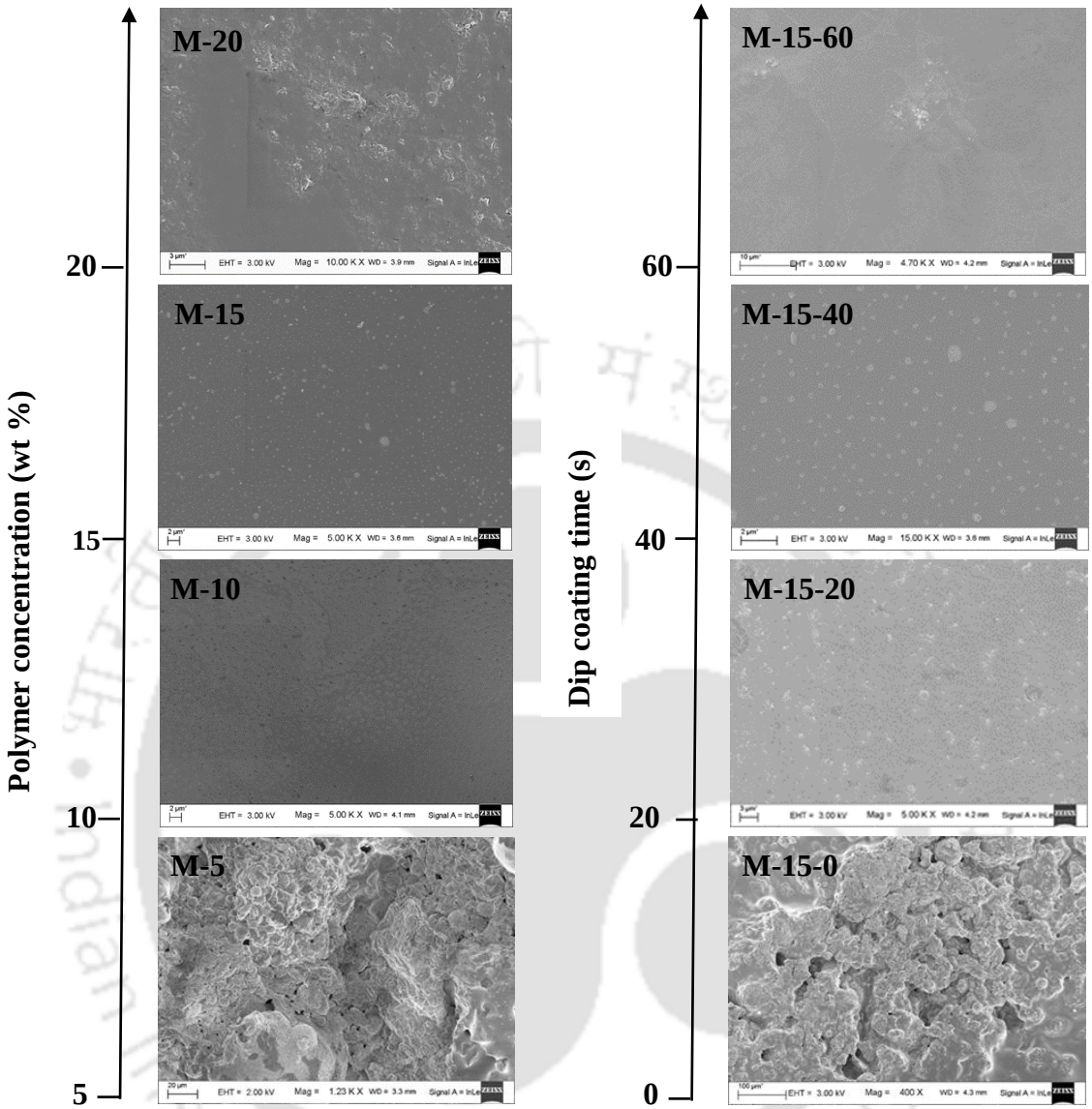


**Fig. 3.6: FESEM images of top surface of composite membranes at varying composition and varying dipping time**

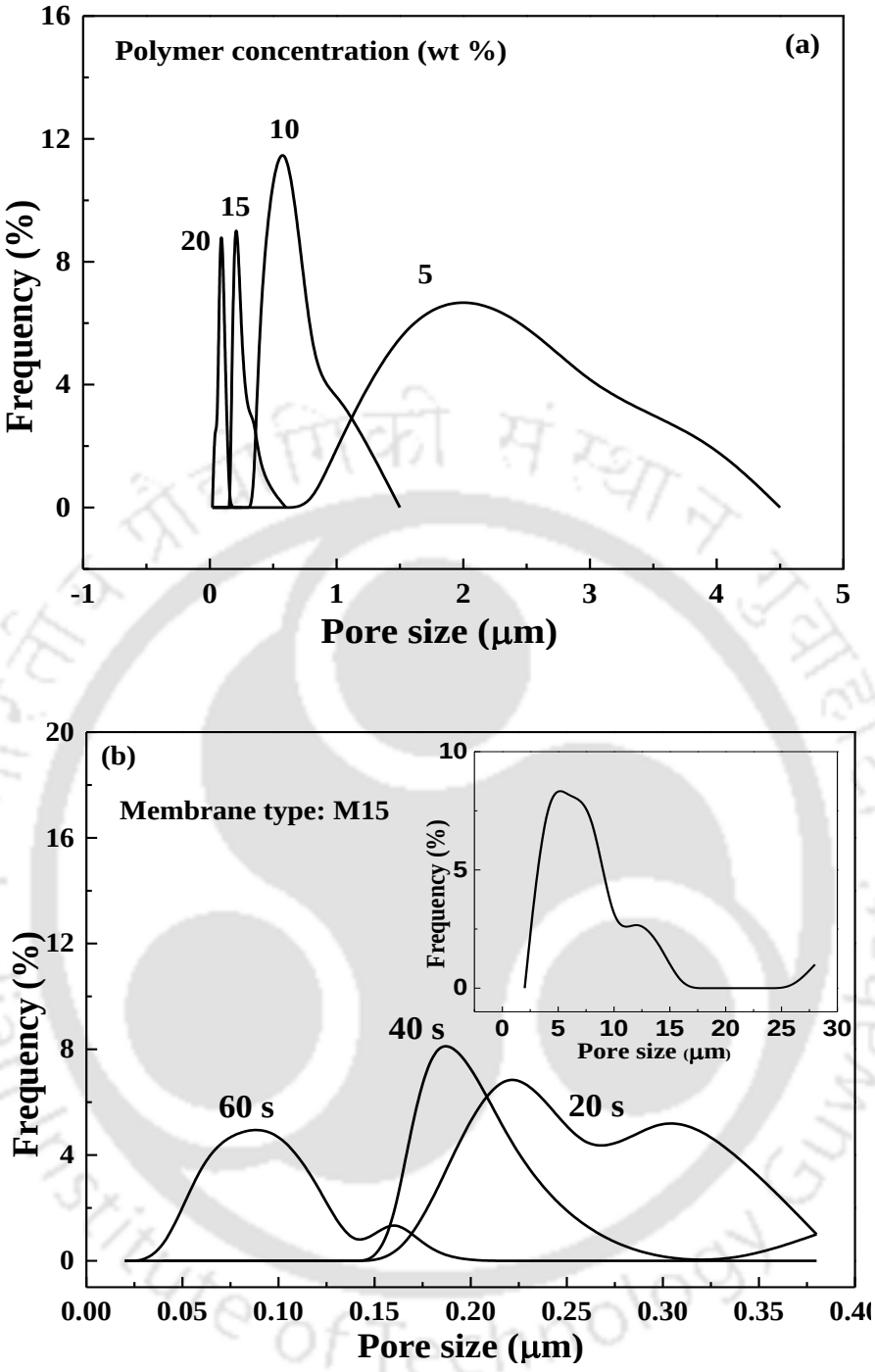


**Fig. 3.7: Pore size distribution of composite membrane at (a) Varying polymer concentration and (b) Varying dipping time, inset: Pore size of uncoated ceramic membrane**

**Figure 3.6** illustrates the variation of average pore size of the membranes with different dipping time. It was also found that with increase in dipping time from 20 to 60 s, the pore size of the membranes decreased significantly due to deposition of more poly (2-ethyl-2-oxazoline) on the support. **Figure 3.7a and 3.7b** shows the particle size distributions of the composite membranes prepared at varying polymer concentartion and varying dipping time. Initially, the average pore size of the support was 20.21 µm. The average pore size of the composite membrane decreased to 0.24 µm when the support was subjected to dip coating at 15 wt % polymer concentration and 20 s of dipping time (M-15-20). With increase in dipping time to 40 s, the pore size of the membrane further decreased to 0.15 µm (M-15-40). A further increase of dipping time to 60 s resulted in a membarne with pore size of 0.07 µm (M-15-60). With an increase in dipping time, the ceramic membrane surface was exposed to the polymer solution for more time. This resulted in the acccumulation of polymer soltion on the membrane surface thereby increasing the viscosity due to increased contact time. As discussed above an increase in viscosity resulted in the decrease of droplet growth rate thereby decreasing the membranbe pore size.

**Table 3.3: Pore size of composite membrane at varying polymer concentration and varying dipping time**

| Membrane ty | Pore size (µm) | Thickness (µm) | Membrane type | Pore size (µm) | Thickness (µm) |
|---|---|---|---|---|---|
| M | 20.21 | 0 | M-0-0 | 20.21 | 0 |
| M-5 | 2.31 | 2.80 | M-15-20 | 0.24 | 15.41 |
| M-10 | 0.48 | 11.74 | M-15-40 | 0.15 | 16.52 |
| M-15 | 0.18 | 117.38 | M-15-60 | 0.07 | 38.58 |
| M-20 | 0.08 | 277.11 | | | |

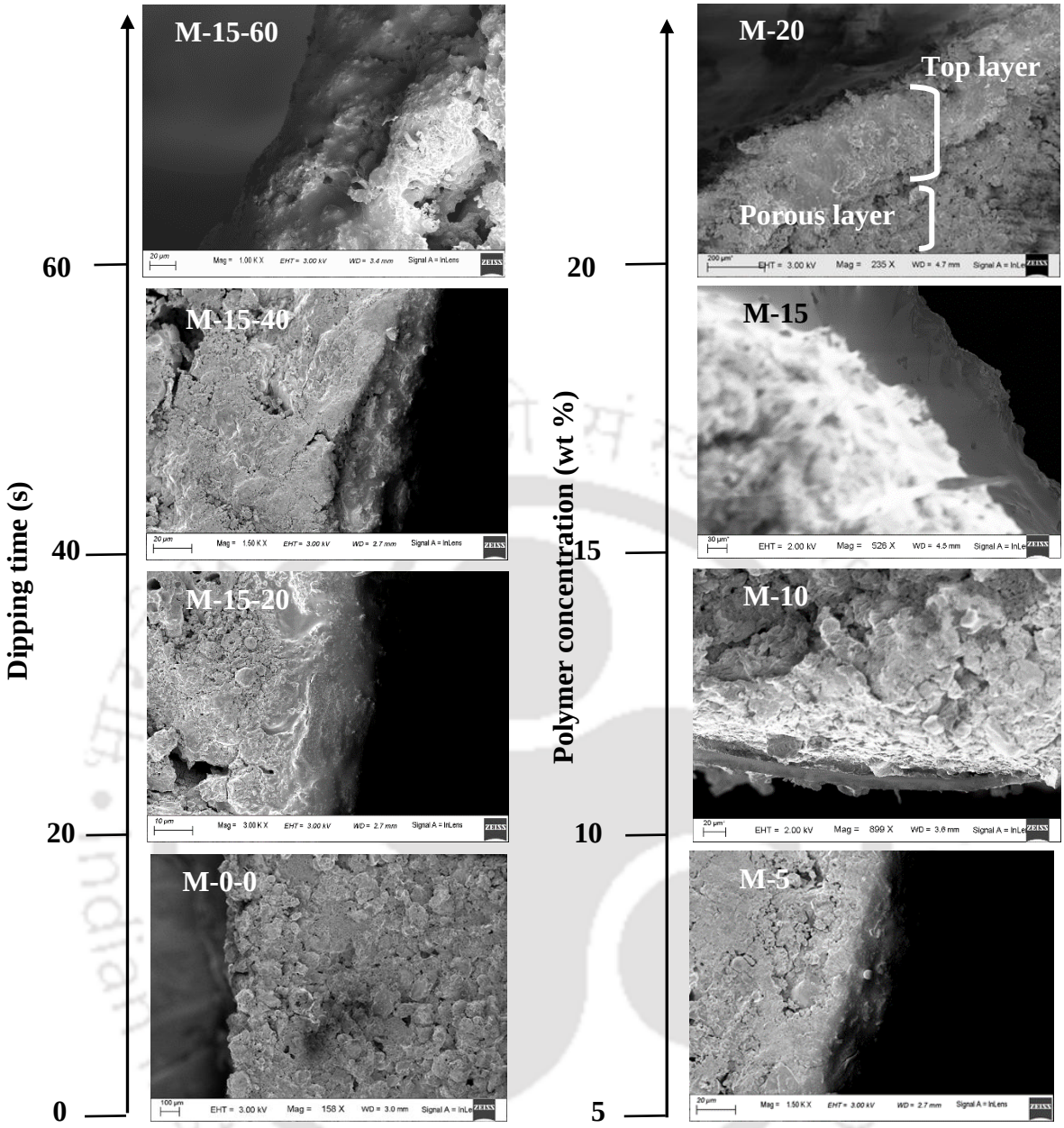


**Fig. 3.8: FESEM images of cross-section of composite membrane at varying dipping time and varying polymer concentration**

**Fig. 3.8 and Table 3.3** gives details about the thickness of the polymer layer deposited with variation in polymer concentration and dipping time**.**With increase in dipping time a definite layer of polymer was observed on the ceramic membrane surace. We considered the membrane M-15 for dipping time studies as the pores were observed to be formed uniformly on the surface without any blockage of the ceramic pores. Initially a very thin layer of film growth was observed for membrane M-15-20 with thickness of 2.8 µm. With an increase in dipping time, a stable film was formed for M-15-40 and M-15-60. The measured film thickness for these membranes was 16.5 µm and 38.5 µm, respectively. For increasing polymer concentration from 5-20 wt % the thickness of the polymer coating was seen to increase for M-5 to M-20 from 2.8 to 277.1 µm.

### 3.2.1.6 Zeta Potential

The zeta potential of membrane surfaces and the resulting electrostatic interactions are determining factors of membrane fouling. This study investigates the influence of pH value on the zeta potential of the polymer poly (2-ethyl-2-oxazoline). From the **Figure 3.9** below it is seen that the membrane surface is negatively charged and the charge increases with increasing pH. These results can be explained by a compression of the electrochemical double layer (EDL). On increasing the ionic strength of the solution has an effect of compressing of the EDL. This happens as the counter-ions are pushed closer to the surface of the particle in consideration resulting in repulsive forces due to Van der Waals forces.

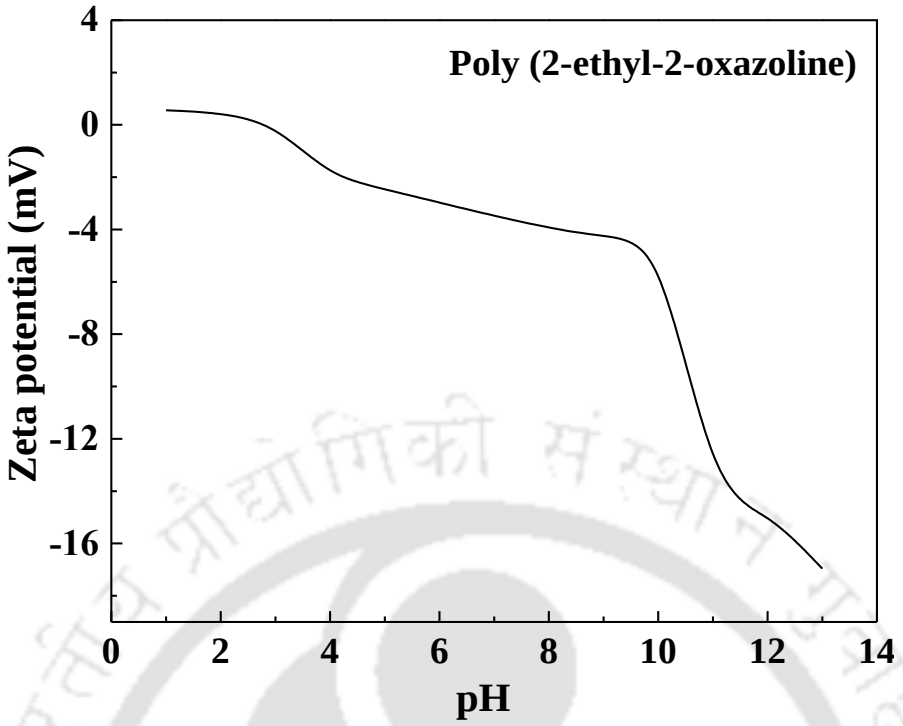


**Fig. 3.9: Zeta potential curve of poly (2-ethyl-2-oxazoline)**

### 3.2.1.7 Compression test

The mechanical resistance test was performed using the compressive strength. Two membrane samples were examined which included non-sintered uncoated membrane and sintered (750ºC) coated membrane. The effect of sintering on the mechanical properties of the membrane supports was highly evident from the analysis. It was observed that sintered samples offered much higher strength in comparison to unsintered samples. The load vs displacement graphs (**Fig 3.10a and b**) clearly indicated the failure of non-sintered membrane at 12.44 KN and whereas the sintered and coated membrane had a failure at 17.662 KN. The compressive strengths of specimens progressively increased with the increase in sintering temperature up to 750°C. Compared to the porosity, the nature of phases plays a more significant influence on strength [85]. Presence of

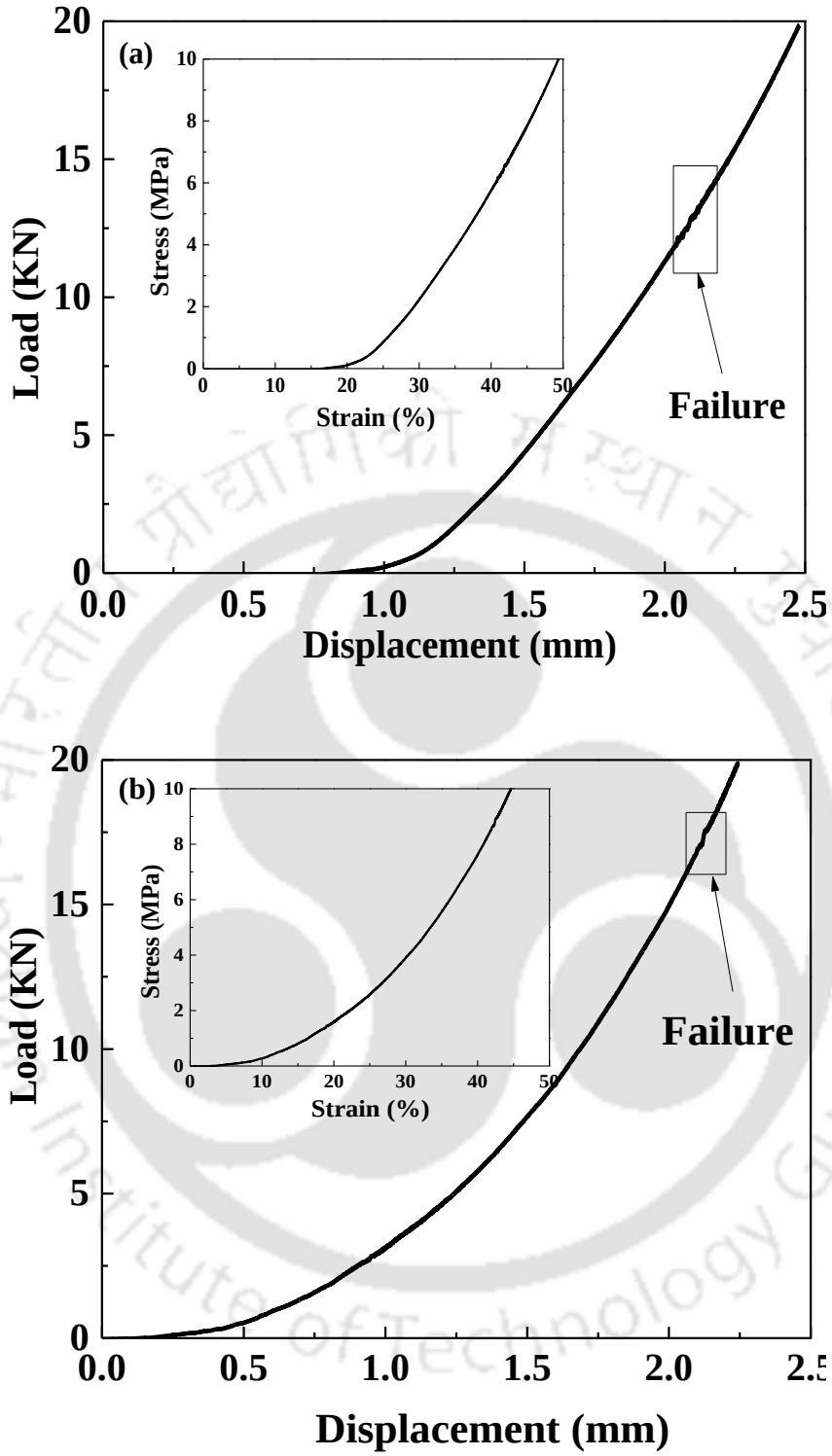


**Fig. 3.10: Load vs displacement, inset: stress vs strain graph for (a) Uncoated non-sintered membrane (b) Sintered (750 ºC) and coated membrane**

phases like anorthite were found to be helpful in increasing the strength of the membrane. XRD results of sintered samples in section 3.1.3 suggested the presence of anorthite in our samples thus an increase in strength was evident. The relationship between compressive stress and compressive strain is shown by **Fig 3.10a and b inset.** As seen from the figure, the fabricated membranes have the ability to withstand external loads during the compression test.

### 3.2.1.8 Contact angle

The uncoated ceramic membranes are highly hydrophilic in nature and thus considerable efforts has been made to improve the hydrophobicity of the membrane by incorporating a layer of polymer on the ceramic membrane surface. For poly (2-ethyl-2-oxazoline) coated ceramic membrane (M-15), under steady state conditions, the water contact angle varied from $37.4^{o}$ to $76.98^{o}$ (**Table 3.4**) as the operating temperatures varied from 25 $^{o}$C to 90 $^{o}$C. This is mainly because of the reason that the polymer is in swollen and hydrophilic state at temperatures below LCST whereas at temperatures at and above LCST they become shrunken and hydrophobic in nature [86].

## 3.3 Filtration studies

The effect of temperature on the flux of water through the temperature-sensitive membrane is shown in **Fig. 3.11**. The LCST of a polymer plays a significant role in controlling the rate of filtration through a membrane. At temperature higher than 60°C, the LCST of poly (2-ethyl-2-oxazoline), the flux of water increases significantly with the rise of temperature. Below LCST, the polymer forms hydrogen bonds with water and exists in solution form. However, above LCST, inter and intramolecular interaction in polymer is much stronger resulting in the breakage of the hydrogen bonding. The polymer chain thus shrinks, leading to an increase of the effective

**Table 3.4: Contact angle of membrane M-15 at different temperatures**

| Temperature (°C) | Contact angle (°) | Image |
|---|---|---|
| 25 | 37 | 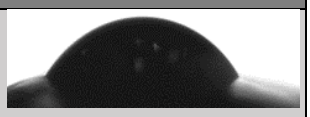 |
| 50 | 47.6 | 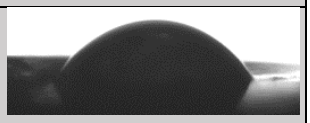 |
| 60 | 51.42 |  |
| 70 | 58.25 | 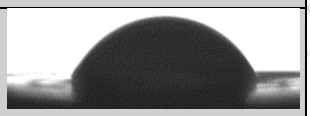 |
| 80 | 68.97 | 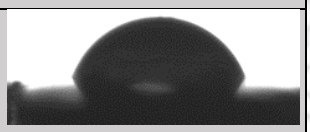 |
| 90 | 76.98 | 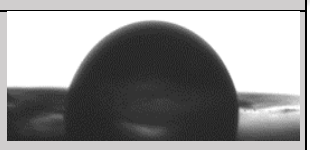 |

pore size in porous membrane [84]. The change of polymer above and below LCST is depicted in **Fig. 3.11 a and b**. It is probable that the pentagonal water structure is generated among water molecules adjacent to the hydrophobic molecular groups of poly (2-ethyl-2-oxazoline). Hydration of water molecules surrounding the polymer chain causes an extension of the polymer chain thereby shrinking the effective pore size, and thus, the flux of water decreases. This pentagonal structure is stable at low temperatures and unstable at high temperatures resulting in the deswelling process of poly (2-ethyl-2-oxazoline) gel above the LCST. The deswelling of polymer gels leads to the enlargement of the effective pore size; subsequently, the flux of water increases **Fig. 3.12**. The changeable flux of water indicates that the temperature-sensitive membrane can be employed as the sensor or valve to respond to temperature and control the liquid-transfer processes [80].

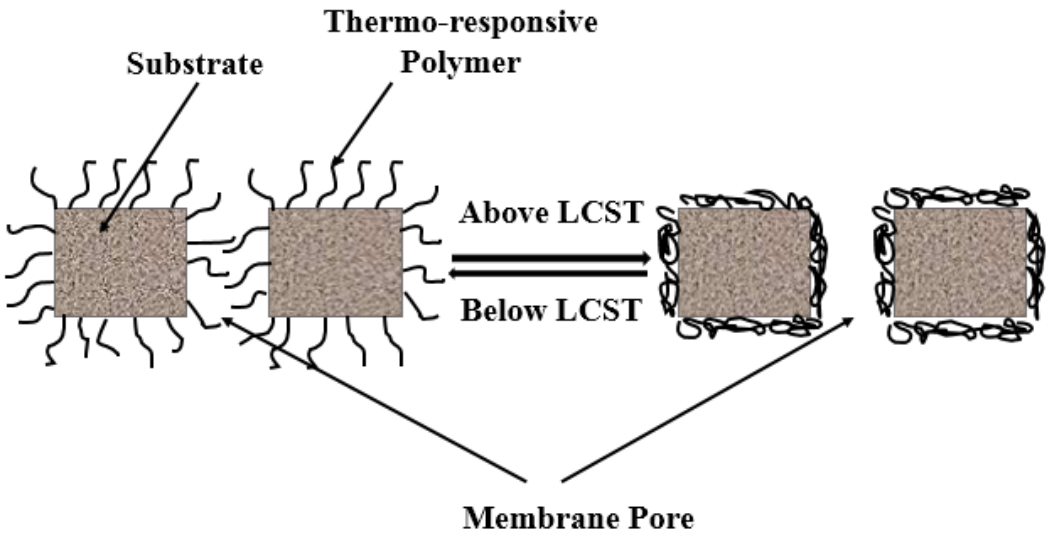


**Fig. 3.11 b: Schematic diagram showing the effect of LCST**

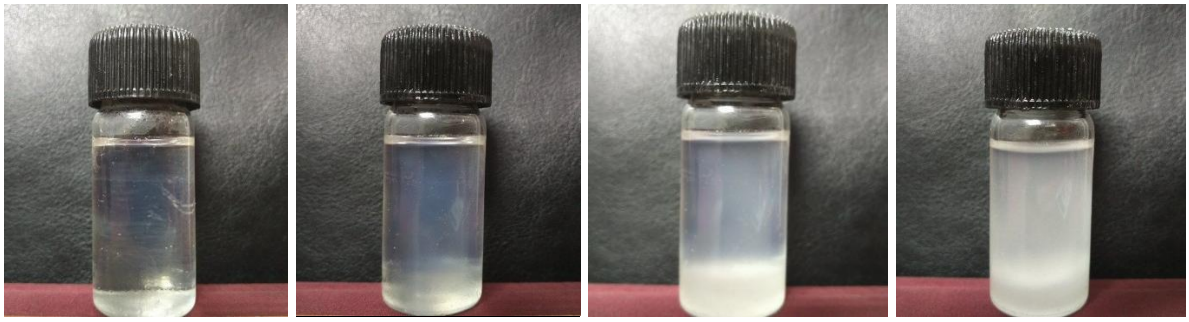

**Fig. 3.11 a: Picture showing the effect of LCST on poly (2-ethyl-2-oxazoline)**

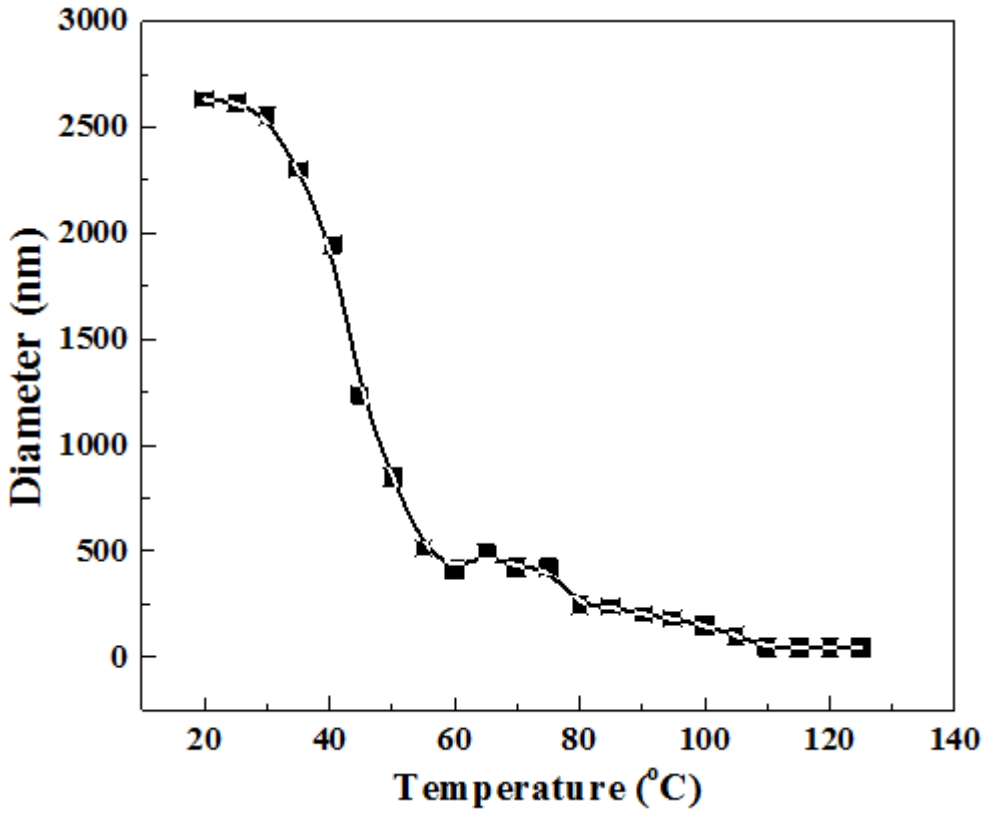


**Fig. 3.12: Temperature vs particle diameter of poly (2-ethyl-2-oxazoline)**

The remarkable change of effective pore size on the surface of the temperature-sensitive membrane makes it possible to separate species of varying size. To evaluate the effect of temperature on the separation behavior, the flux of water was determined at different concentrations of polymer coating (5, 10, 15 and 20 wt %) at different operating temperatures (25, 60 and 90 $^{o}$C). It appears that with increasing temperature, the flux of the solution increases because higher temperatures increase effective pore size, surface of membrane is enlarges, increasing the flux of pure water.

For the membrane M-5 the flux remained more or less the same at all the three operating temperatures. The reason being that the coating on the membrane surface is minimal which does not contribute much on the filtration process. A change in flux for membrane M-5 was observed from $1.35 \times 10^{3}$ to $0.03 \times 10^{3}$ L/h. m$^2$ at 25 $^{o}$C, $1.58 \times 10^{3}$ to $0.03 \times 10^{3}$ L/h. m$^2$ at 60 $^{o}$C and $1.89 \times 10^{3}$ to $0.49 \times 10^{3}$ L/h. m$^2$ at 90 $^{o}$C **(Fig 3.13a)**. For membrane M-10 the flux increased with an increase in temperature from 25$^{o}$C to 90 $^{o}$C. A change in flux for membrane M-10 was observed as $0.89 \times 10^{3}$ to $0.1 \times 10^{3}$ L/h. m$^2$ at 25 $^{o}$C, $1.98 \times 10^{3}$ to $0.12 \times 10^{3}$ L/h. m$^2$ at 60 $^{o}$C and $3.98 \times 10^{3}$ to $0.14 \times 10^{3}$ L/h. m$^2$ at 90 $^{o}$C **(Fig 3.13b)**. Similar were the cases for membranes M-15 and M-20 as seen from **Fig 3.13c and 3.13d** below. Change in flux for membrane M-15 was observed to decrease from $1.75 \times 10^{3}$ to $0.19 \times 10^{3}$ L/h. m$^2$ at 25 $^{o}$C, $2.42 \times 10^{3}$ to $0.26 \times 10^{3}$ L/h. m$^2$ at 60 $^{o}$C and $4.9 \times 10^{3}$ to $1.39 \times 10^{3}$ L/h. m$^2$ at 90 $^{o}$C whereas flux for membrane M-20 was observed to change from $2.66 \times 10^{3}$ to $0.7 \times 10^{3}$ L/h. m$^2$ at 25 $^{o}$C, $3.42 \times 10^{3}$ to $1.37 \times 10^{3}$ L/h. m$^2$ at 60 $^{o}$C and $5.59\times 10^{3}$ to $1.682 \times 10^{3}$ L/h. m$^2$ at 90 $^{o}$C. However, as observed from FESEM data, pore formation was more precise for the membrane M-15 in comparison to the membranes M-5, M-10 and M-20. Hence, further experiments on the study of effects of contact time was done for the membrane M-15**.**

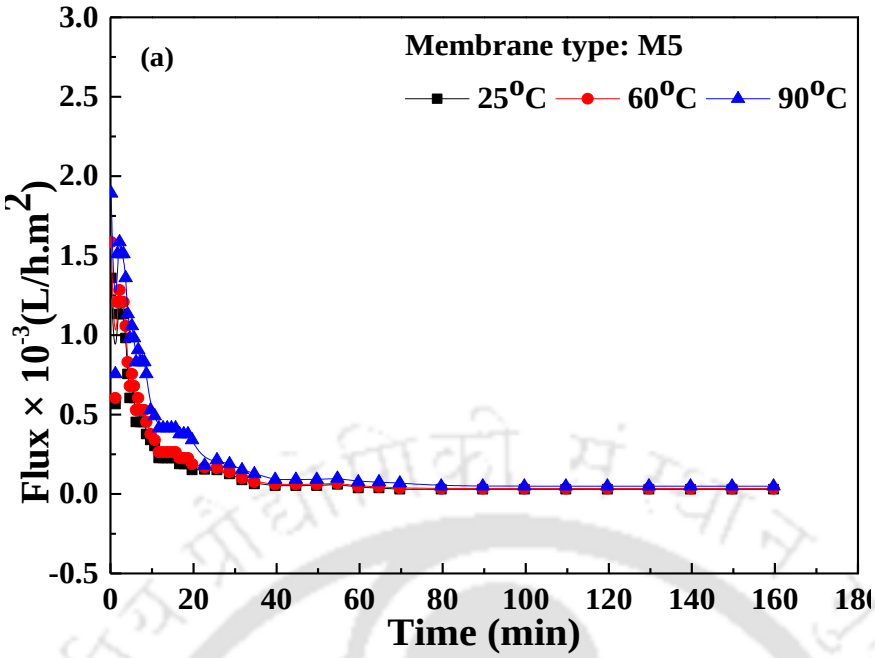


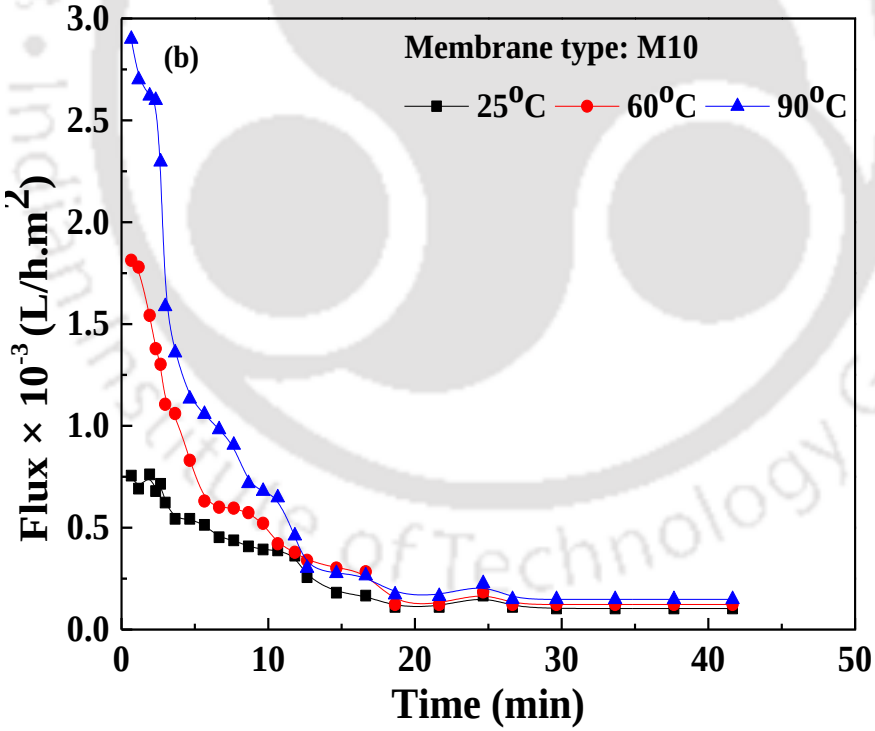

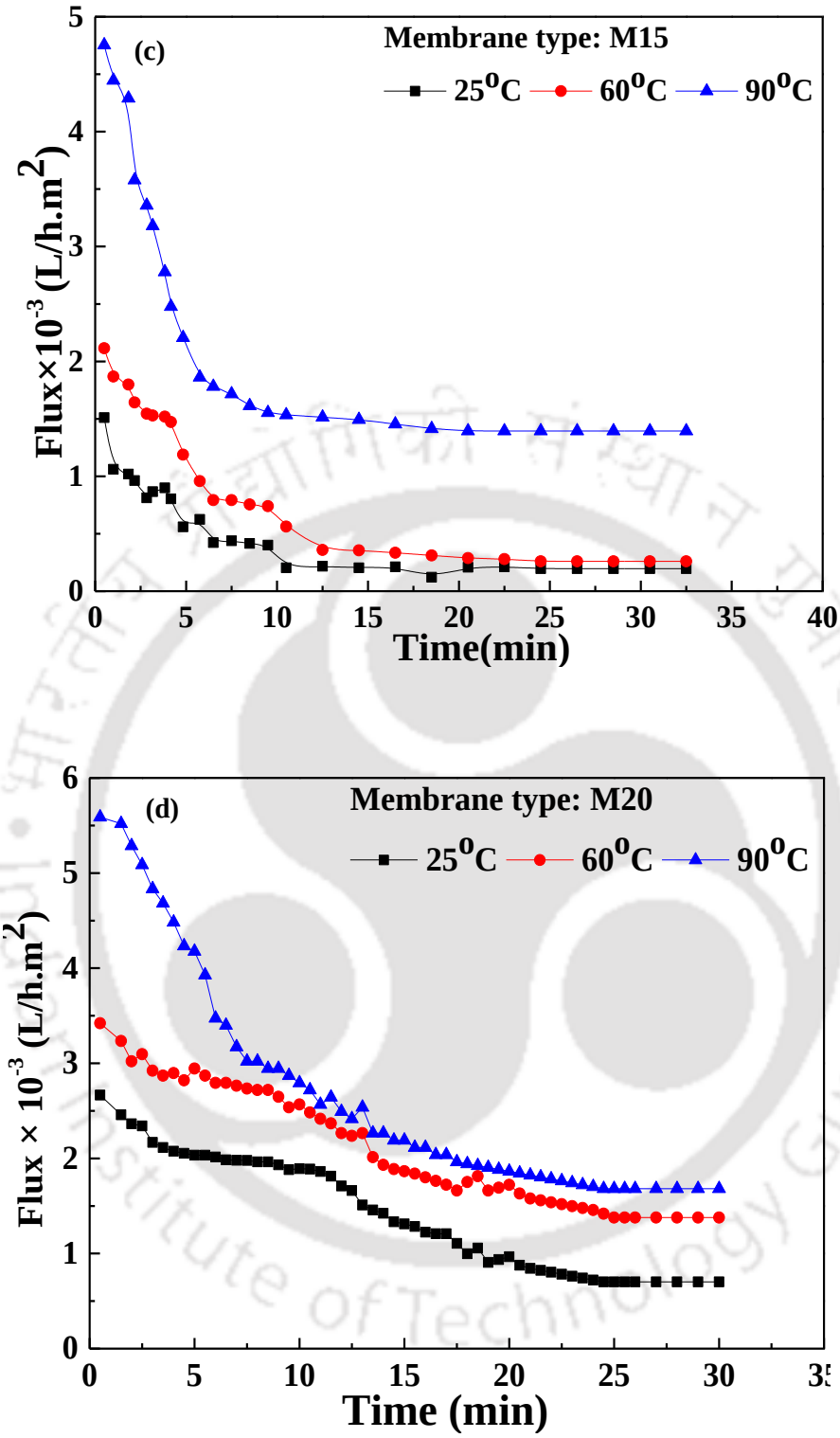


**Fig. 3.13: Variation of PWF with time and temperature during compaction of composite membranes with poly (2-ethyl-2-oxazoline) concentration of (a) 5 wt %, (b) 10 wt % , (c) 15 wt % and (d) 20 wt %.**

The effect of contact time on membrane M15 was studied along with the effect of temperature. Membranes were prepared at different coating time (20, 40 and 60 sec) and studied their effect at different operating temperatures (below and above LCST) of 25 $^{o}$C and 90 $^{o}$C. As seen from the **Fig. 3.14** below the flux decreased with an increase in dip coating time, because a thicker layer formed on the membrane surface which thereby resulted a reduction in flux. However, with an increase in the operating temperatures from 25 $^{o}$C to 90 $^{o}$C the flux increased. As seen for M-15-20 s, when the temperature increase from 25 $^{o}$C to 90 $^{o}$C, the flux increased from 0.53 × $10^3$ L/h.$m^2$ to 0.85 × $10^3$ L/h.$m^2$, respectively. Similar observations were made for membrane M-15-40 s and M-15-60 s.

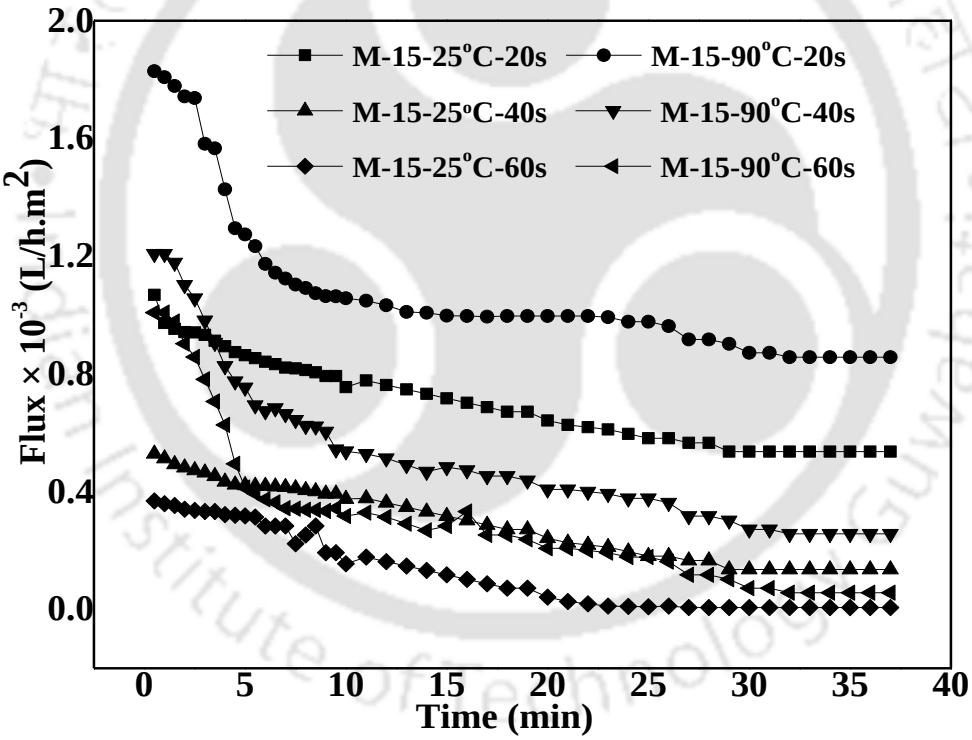


**Fig. 3.14: Effects of dip coating time on PWF of membrane M-15 at operating temperatures of 25 $^{o}$C and 90 $^{o}$C**

### 3.4 Hydraulic permeability

**Figure 3.15** shows the effect of dip coating parameters on the hydraulic permeability (*Pm*) of the prepared membranes. From the figure it can be seen that for M-15 membrane permeability, $P_m$ decrease from $72.09 \times 10^{-6} - 0.81 \times 10^{-6}$ m/s.kPa at 25°C with an increase in dipping time from 20 – 60 s. Similarly, permeability decreased from $115.5 \times 10^{-6} - 7.56 \times 10^{-6}$ m/s.kPa as dipping time increased from 20 – 60 s. This was due to the fact that, with increase in dipping time the average pore size of the membrane decreases and top layer thickness increases thereby resulting in the decrease of membrane permeability. The membrane permeability can be determined using the relation "$PWF = P_m \Delta P$", where PWF: Pure water flux, $P_m$=Permeability and ΔP: Transmembrane pressure.

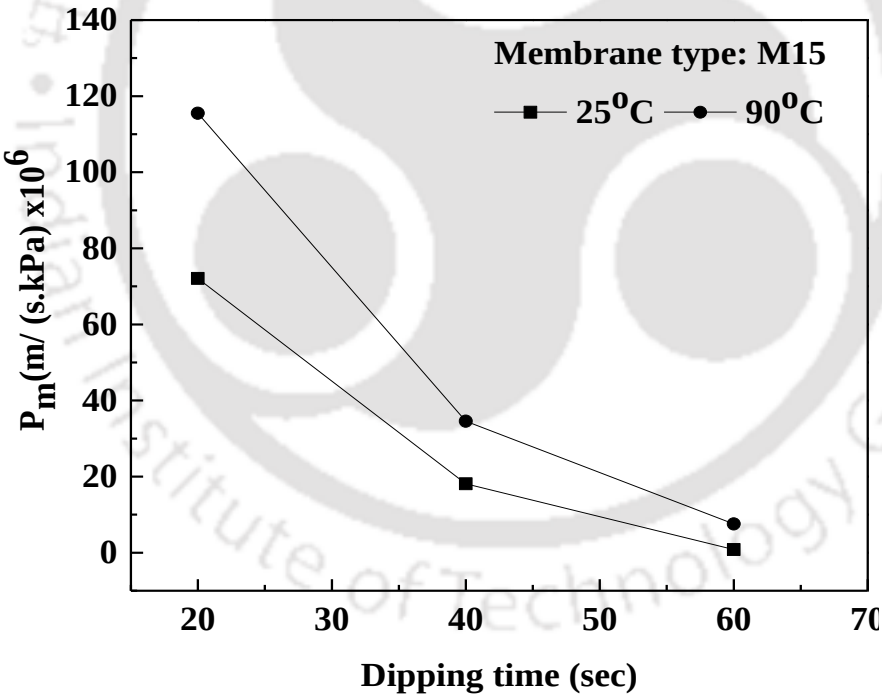


**Fig. 3.15: Effect of poly (2-ethyl-2-oxazoline) dipping time on the hydraulic permeability of different composite membranes.**

### 3.5 Protein rejection

**Figure 3.16** presents the variation of permeate flux and rejection (%) of BSA with membrane fabricated at different polymer concentrations (5, 10, 15 and 20 wt %) and also at different dipping time (20, 40 and 60 s). As shown, percent BSA rejection decreases with an increase in dipping time and polymer concentration. However, the rejection decreased with an increase in operating temperatures. This is because of the transformation occurring above LCST. When temperature is below LCST, pores existing on the surface of the membrane are smaller hence a higher rejection is offered. However, at a temperature higher than LCST deswelling of polymer leads to the enlargement of the effective pore size offering a lower rejection of the protein. Percent BSA rejection was found to vary from 15 % to 5 % for membrane M-5 as the temperature changed from 25 $^{o}$C to 90 $^{o}$C. Similar changes were observed for membrane M-10 with % rejection changing from 21 % to 7 %, membrane M-15 from 68 % to 27.8 % and membrane M-20 from 69 % to 30 %. As seen from the rejection studies at different polymeric concentration, Although M-20 provided the highest rejection of BSA yet M-15 provided the same rejection property with minimal usage of polymer coating. The pore size of membrane M-15 as seen in **Fig. 3.6b** was sufficient enough to retain the BSA protein which had a particle size of around 100-200 nm. Thus the effect of dipping time on protein rejection were carried out for membrane M-15. As seen from **Fig. 3.16b** % rejection decreased with increasing dipping time. The % rejection were found to change from 51 to 25.71 % for membrane M-15-20, 53 to 35.28 % for membrane M-15-40 and 68 to 28.6 % for membrane M-15-60 as the temperature increased from 25 $^{o}$C to 90 $^{o}$C.

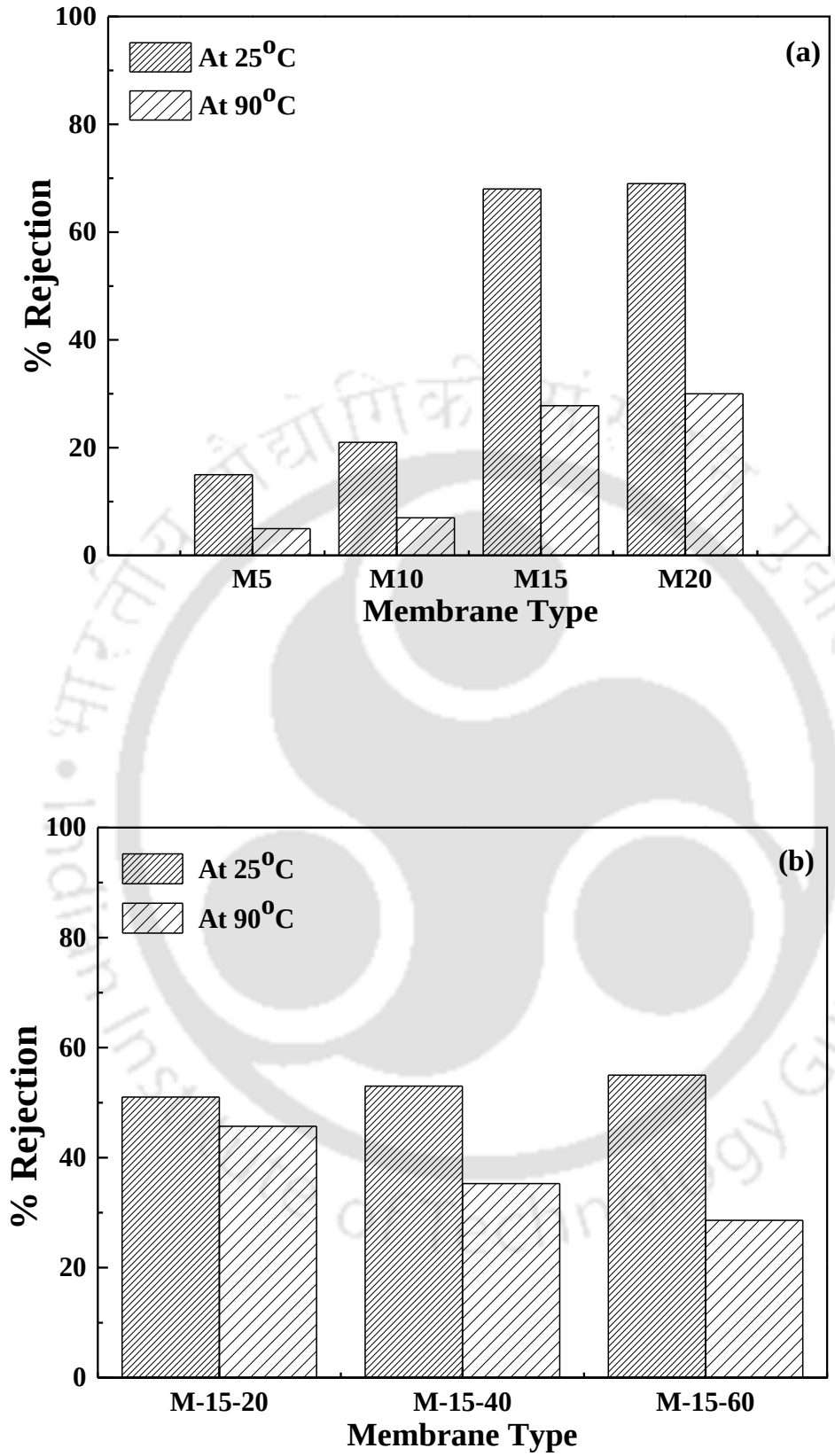


**Fig. 3.16: BSA rejection profile for membrane fabricated by varying (a) Polymer concentration (b) Dipping time**

The rejection of BSA could not be carried out with the bare ceramic membrane because of extremely large pore sizes of about 20.21 µm and very low MWCO of BSA. Hence coated ceramic membrane were used which had a reduced pore size of as low as 0.07 µm (Table 3.3) were successful enough in rejecting almost 69 % of BSA protein for a membrane coated with 20 wt % of poly (2-ethyl-2-oxazoline).

# Chapter 4

# A novel adsorbent from carrot, tomato and polyethylene terephthalate waste as a potential adsorbent for Co (II) from aqueous solution: Kinetic and equilibrium studies

# *Chapter 4*

# A novel adsorbent from carrot, tomato and polyethylene terephthalate waste as a potential adsorbent for Co (II) from aqueous solution: Kinetic and equilibrium studies

*This chapter describes the preparation of novel adsorbents from carrot, tomato and PET. The developed adsorbents were used for the removal of Co (II) from aqueous solutions. The synthesized adsorbent particles were characterized using Fourier transform infrared spectroscopy (FTIR), X-ray diffractometer (XRD), Field emission scanning electron microscope (FESEM), Electron dispersive x-ray (EDX) and thermogravimetric analysis (TGA). The adsorption efficiency of all the three adsorbents for Co (II) adsorption was studied by varying different parameters such as contact time, adsorbent dose and pH. Kinetic behaviour of the three adsorbents for the uptake of Co (II) were studied. Langmuir and Freundlich isotherms were used to investigate the equilibrium behaviour of the system.*

## 4.1 Experimental

### 4.1.1 Materials

Tomato waste and carrot waste were procured from a local shop in the IITG market. Post consumption PET bottles were collected from IITG market; Chemical activators zinc chloride ($ZnCl_2$) and ferric chloride ($FeCl_3$) along with hydrochloric acid (HCl) were purchased from Merck, sodium hydroxide (NaOH) from Rankem and cobalt nitrate hexahydrate ($Co(NO_3)_2.6H_2O$) was procured from Merck. Deionized water was used for all the reactions including synthesis and adsorption study. All the chemicals obtained were of analytical grade and were used without any further purification.

## 4.2 Preparation of adsorbent

### 4.2.1 Adsorbent preparation from organic waste (tomato and carrot)

The tomato waste (peel, seeds and pulp) and carrot waste (peel and pulp) were collected, washed with de-ionized water to take off the impurities and subsequently dried in an air oven at 110$^{o}$C for 24 h. The resulting product was powdered and mixed with 150 mL water and $ZnCl_2$ to obtain $ZnCl_2$: tomato/carrot waste ratio of 1:1. The mixture was mechanically stirred at a temperature of 40$^{o}$C and 140 rpm for one day, after which it was filtered and dried at 110$^{o}$C for 12 h. The dried product was then subjected to thermal treatment in a muffle furnace at a temperature of 550$^{o}$C with a retention time of 2 h. The produced adsorbents were cooled to room temperature and 0.2 N HCl was added. They were washed sequentially several times with hot distillated water to remove residual chemical till a neutral pH(6-7) was achieved and again dried at 110$^{o}$C for 12 h (**Fig. 4.1)**.

### 4.2.2 Adsorbent preparation from PET-tomato waste-carrot waste

The PET-precursor was activated through incorporation of inorganic salt. Small PET pieces of size approx. 0.5 m × 0.5 cm were washed and boiled in an aqueous solution of 1.65 wt % of $FeCl_3$. This mixture was mechanically agitated for 24 h followed by sintering at a temperature of 500 $^{o}$C with a retention time of 2 h. The resulting product sample was cooled naturally.0.4 g of $ZnCl_2$-activated adsorbent from tomato and carrot waste and 0.8 g of $FeCl_3$ activated adsorbent from PET were mixed in 20 ml of distill water and stirred for 24 h. The mixture was then filtered and dried in an

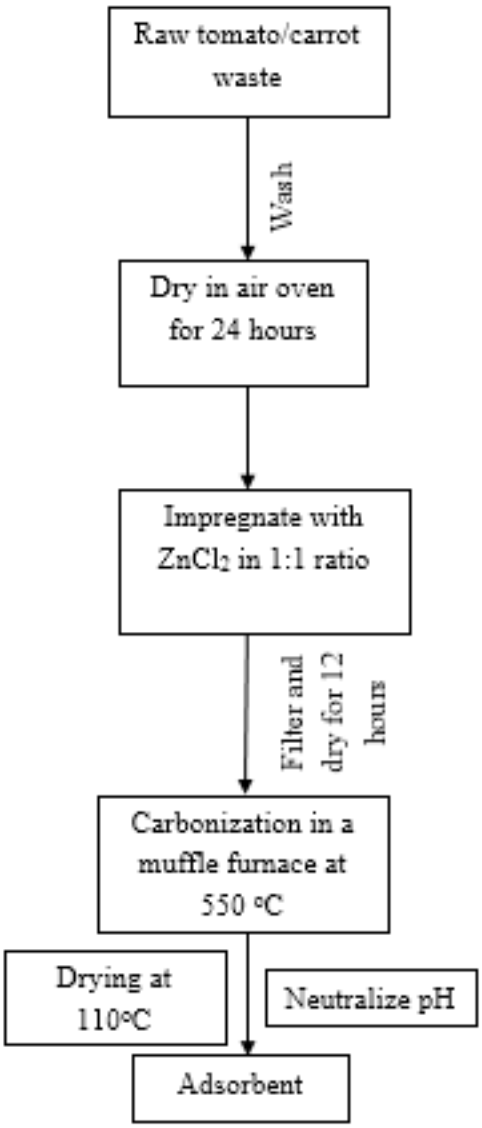


**Fig. 4.1**: Steps for preparation of activated carbon from carrot and tomato waste

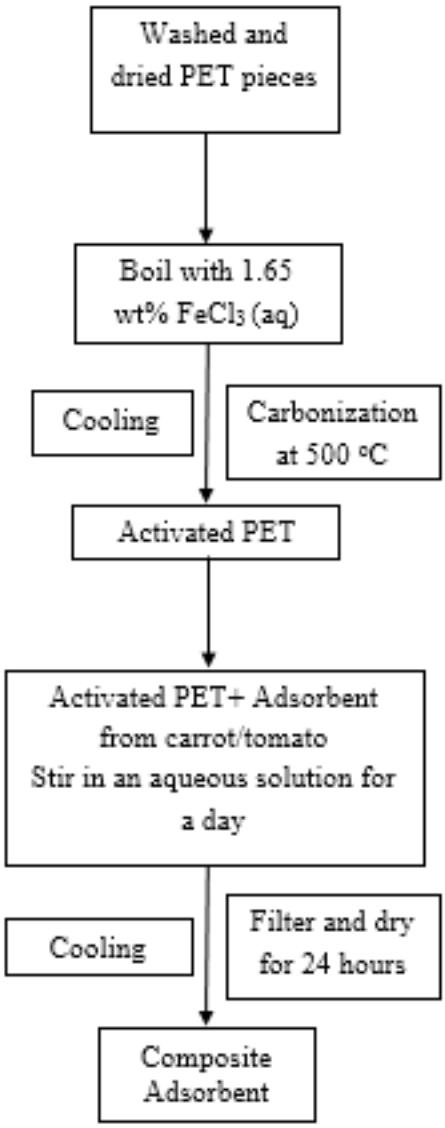


**Fig. 4.2**: Steps for preparation of composite activated carbon

air oven for one day. The resulting product obtained was a composite adsorbent with a combination of activated PET and activated carbon from carrot and tomato waste (**Fig. 4.2**).

### 4.3 Adsorption experiment

Batch adsorption experiments were performed by the prepared adsorbents i.e. activated carbon from carrot waste, tomato waste and activated composite for the adsorption of Co (II) from solution. 0.2 moles/L stock solution of Co $(NO_3)_2.6H_2O$ was prepared using Millipore water. The initial experimental solution of 0.01 moles/L was prepared from the stock solution with dilution. All stock solution and standard solution preparations were carried out in a volumetric flask. Calibration curves were prepared by analysing the standard solutions of different concentration obtained by diluting the stock solution with the help of atomic absorption spectroscopy, AAS (Varian). All the adsorption experiments were carried out in a 250 ml Erlenmeyer flask. The flasks were kept in a lab shaker for a designated period of time before being analyzed. Each sample was filtered prior to analysis so as to prevent the interference of the adsorbent powder with the analysis. Studies were performed to identify the best among the three prepared adsorbents for the adsorption of Co (II). Experiments were designed to determine the efficacy of adsorption with contact time for 2 h. The effect of adsorbent doses ranging from 0.1 to 2 g/L were considered. Effect of pH on the extent of adsorption was also investigated. Adjustment of pH was done by using 0.1 M HCl and 0.1 M NaOH.

The removal efficiency (% *R*) was calculated by

$$\% R = \frac{C_o - C_e}{C_o} \times 100\ \% \qquad 4.1$$

The adsorption capacity $q_e$ was calculated by

$$q_e = \frac{(C_o - C_e)V}{m} \qquad 4.2$$

Where, $C_o$ = Initial concentration of Co (II), mg/L

$C_e$ = Equilibrium concentration of Co (II), mg/L

V = Volume of solution taken, L

M = Mass of adsorbent taken, g

### 4.4 Characterization techniques

The thermal behaviour of tomato waste and carrot waste were measured with a thermo gravimetric analyzer (TGA; Mettler Toledo). About 10 mg of sample material was heated from 25 $^oC$ to 1000 $^oC$ at a ramping rate of 10 $^oC$/min under nitrogen gas atmosphere with the low rate of 200 mL/min, and constantly weighed. Percent weight loss versus temperature plots were taken for the thermogravimetric analysis. Fourier transform infrared spectrometry (FTIR) (Perkin Elmer, USA, Model: LR 64912C) was utilized to determine the presence of various functional groups by the. FTIR analysis was performed with KBr - supported technique in the range of 400 – 4000 $cm^{-1}$ with a scanning rate of 40 and a resolution of 4 $cm^{-1}$. A wide angle x-ray diffractometer (XRD) (Bruker D8) was used to study the crystallite structure of dried waste and activated adsorbent for all the three samples. Scanning was done from high angle 2θ value between 10 – 70$^o$ at a speed of 0.5 s/$^o$. The X-ray source was operated using monochromatic copper radiation (Cu Kα λ = 0.1541 nm) at 40 kV and 40 mA. Elemental analysis was performed using the Electron diffractometer (EDX) (Zeiss). The surface morphology of these adsorbent were analyzed using JEOL JSM-6400F FESEM (field emission scanning electron microscopy) (Zeiss LEO). The samples were kept onto a conductive carbon tape above the metal stub and coated with a thin layer of silver for charge dissipation. Zeta potential of the adsorbents were determined using the Delsa Nano (Model No.: Delsa Nano C; Make: M/s Beckman Coulter,

Swtizerland) apparatus. Samples were suspended in Millipore water using a sonicator and then placed in the zeta potential cell for further analysis.

### 4.5 Proximate and ultimate analysis

Proximate analysis such as moisture content, volatile impurities, ash content, % fixed carbon and % burn-off was determined for the activated carbon samples to know the quantity of usable charcoal product through the following procedures. Moisture content of each sample adsorbent was determined by measuring its weight ($W_1$). The sample was then placed in an air oven at a temperature of 110 $^oC$ for 1 h followed by cooling in a desiccator for 15 min after which the weight is again measured ($W_2$) [128, 129].

$$\textbf{\% moisture} = \frac{\boldsymbol{W1-W2}}{\boldsymbol{W3}} \times \mathbf{100}\ \% \qquad 4.3$$

Where, $W_1$ = Weight of the sample + crucible before change, $W_2$ = Weight of the sample + crucible after change, $W_3$ = Weight of the sample before change.

The volatile content was measured by placing the sample in an air oven at a temperature of 150$^oC$ for 1 h followed by cooling in a desiccator for 15 min. Weights were measured before and after drying.

$$\textbf{\% volatile matter} = \frac{\boldsymbol{W4-W5}}{\boldsymbol{W6}} \times \mathbf{100}\ \% \qquad 4.4$$

Where, $W_4$ = Weight of the sample + crucible before change, $W_5$ = Weight of the sample + crucible after change, $W_6$ = Weight of the sample before change.

Similarly, for % ash content, samples were stepwise heated to 550 ± 5$^oC$ with a retention time of 8 h, or until a white ash was obtained. Once the samples cooled down to room temperature, weights were measured.

$$\%\ \boldsymbol{ASH} = \frac{\boldsymbol{wt.of\ crucible\ and\ ash - wt.of\ crucible}}{\boldsymbol{wt.of\ crucible\ and\ sample - wt.of\ crucible}} \times \mathbf{100}\ \% \qquad 4.5$$

The percent carbon content is given as

$$\%\boldsymbol{C} = \mathbf{100} - \%(\boldsymbol{volatile} + \boldsymbol{moisture} + \boldsymbol{Ash}) \qquad 4.6$$

## 4.6 Results and discussion

### 4.6.1 Thermogravimetric analysis (TGA)

The thermograms obtained for carrot and tomato waste depicted decomposition in three different steps (**Fig. 4.3**). The first step occurred at temperature range of 28 to 150 $^{o}$C with a weight loss of 3.85 % which was due to the moisture present in the sample. The second weight loss step of 7.99 % occurred at 150 to 280 $^{o}$C. This weight loss was related to the release of volatiles resulting from the decomposition of hemicelluloses. The third step at 280 to 480 $^{o}$C was characterized by the decomposition of cellulose and lignin which had a maximum rate of weight loss of 30.88 %. Therefore, this temperature can be said to be the lowest carbonization temperature for the production of adsorbent.

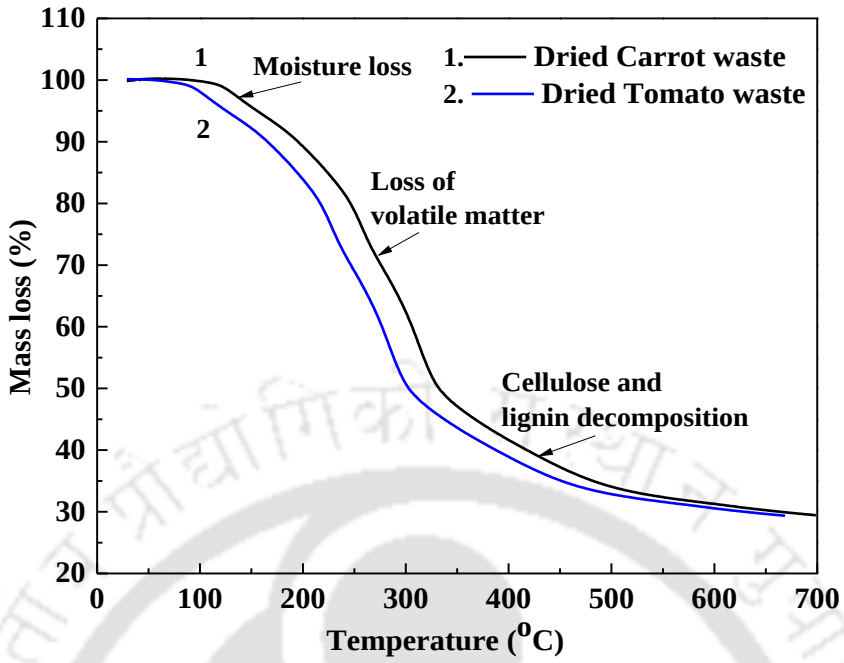


**Fig. 4.3: TGA curve for dried tomato waste and carrot waste**

### 4.6.2 Fourier transform infrared spectroscopy (FTIR)

In the spectra of dried tomato waste (TW), the presence of the broad and intense absorption peak at 3323.17 $cm^{-1}$ indicates the O-H stretching vibrations of absorbed water in the sample. The peak observed at 3053.96 $cm^{-1}$ can be attributed to the aliphatic saturated C - H stretching vibrations of in lignin polysaccharides including cellulose and hemicellulose. The two notable peaks are located at 2903 $cm^{-1}$ and 2833 $cm^{-1}$ due to the symmetric and asymmetric stretching vibration of methyl groups. The presence of the peak at 1743.27 $cm^{-1}$ indicates the carbonyl (C = O) stretching vibration of the carboxyl groups of pectin, hemicellulose and lignin. The peak at 1618.10 $cm^{-1}$corresponds to absorbed water H – O - H bends. The peak at 740.64 $cm^{-1}$ is related to the C-H bending with different degrees of substitution [95, 96].

After chemical activation, the FTIR spectrum of activated carbon from tomato waste (ATW) was markedly different from TW. The broad band located in the region of 3100 - 3400 $cm^{-1}$ related to O - H stretching vibrations existed but shifted to the high wave number. The band

located at about 1512.71 $cm^{-1}$, which could be attributed to C = C vibration in aromatic rings. The band at 1228.21 $cm^{-1}$ is due to the C-O stretching vibration of phenol group. The many absorption bands disappeared when the FTIR spectrum for the ATW are compared to that for TW. This is likely to be due to the vaporization of organic matter at high temperatures (**Fig. 4.4a)**.

The spectrum of the dried carrot waste (CW) samples revealed the presence of vibrational bands at 3700 - 3000 $cm^{-1}$ due to the adsorbed water present in the sample, bands at 2327 - 2353 $cm^{-1}$ were due to symmetric and asymmetric stretching of methylene groups, bands at 1649 - 1544 $cm^{-1}$ was due to the presence of amide groups. Vibrational bands at 1442 - 1326 $cm^{-1}$ was due to the C-H bending whereas the bands at 1262 $cm^{-1}$ were due to the C - C and C – C - H, bands at 1025 $cm^{-1}$ was due to the C - O stretching and the bands at 800 $cm^{-1}$ was related to aromatic C-H bending with different degrees of substitution. Activated carbon from carrot waste (ACW) had relatively lesser peaks in comparison to the dried carrot waste peaks [104, 105]. Further many peaks also disappeared due to the vaporization of organic matter at high temperatures (**Fig. 4.4b)**.

The FTIR spectra of powder obtained from activated polymer waste displayed bands at 3688 and 3629 $cm^{-1}$ from the O-H stretching vibration in alcohols; 3447 and 3428 $cm^{-1}$ from the N-H stretching vibration in primary amines; 2950 $cm^{-1}$ from the –CH stretch of a methylene; and 1694 $cm^{-1}$ from the C = O stretching vibration in carboxylic acid. Strong bands around 1650, 1536 and 1514-1450 $cm^{-1}$, due to C = C stretching in an aromatic ring, and peaks around 1412 $cm^{-1}$, indicated the presence of pyrones and aromatic groups. The peaks around 920 and 756-662 $cm^{-1}$ indicated

C-H out-of-plane bending in an aromatic ring. The FTIR spectra of composite adsorbent (APTC)

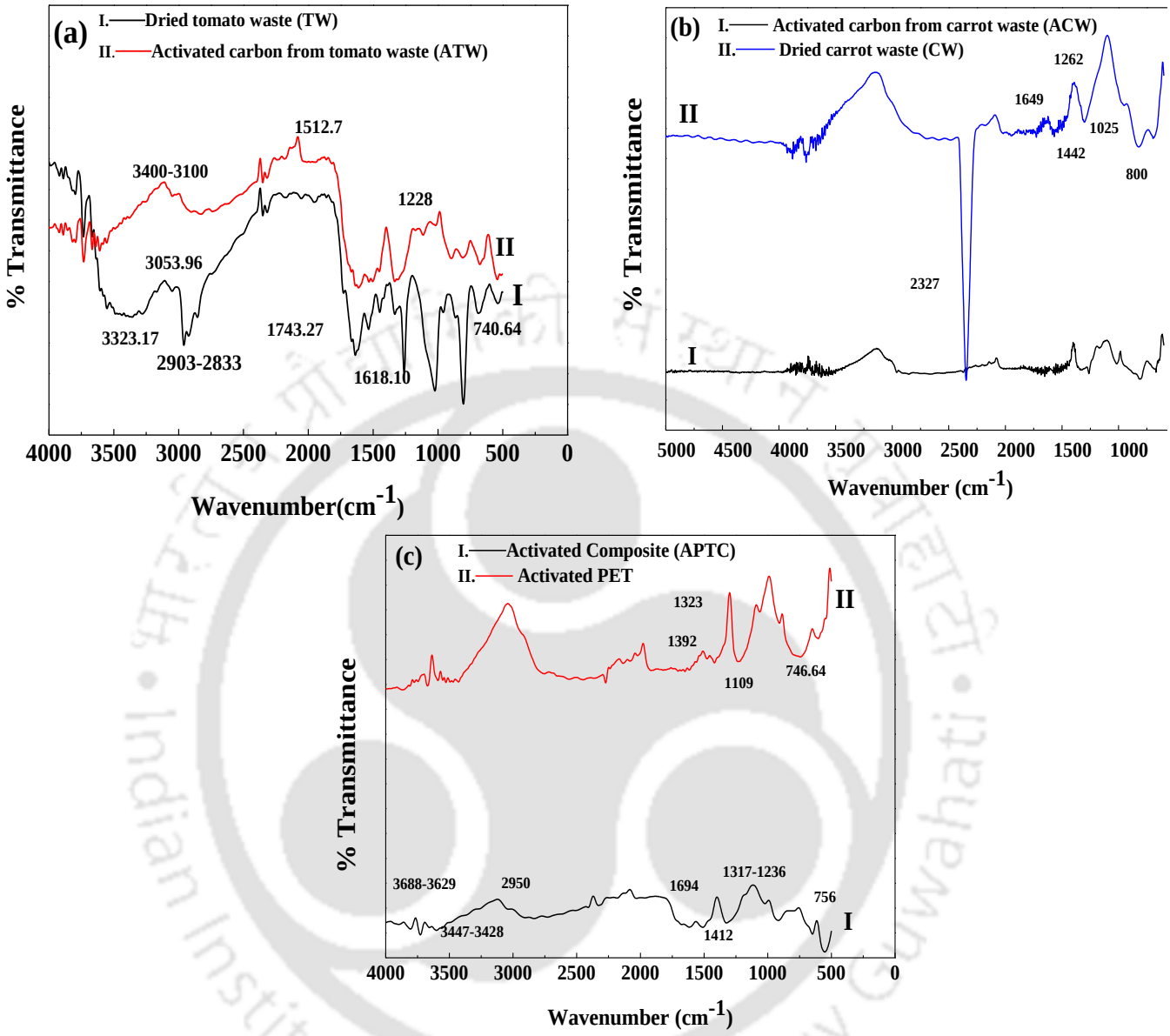


**Fig. 4.4: FT-IR graph for (a) Dried tomato and activated carbon from tomato waste (b) Dried carrot and activated carbon from carrot waste (c) Activated PET and activated composite**

bands at 1554 $cm^{-1}$ were due to C = C stretching in an aromatic ring, indicating the presence of pyrones and aromatic groups. Peaks at 1392 $cm^{-1}$ and 1323 $cm^{-1}$ were due to deformation of C - H alkane. The peak at 1109 $cm^{-1}$ was due to C-O stretching vibration of carboxylic acids and alcohols. The band at 746.64 $cm^{-1}$ was related to aromatic, out of plane C - H bending with different degrees of substitution (**Fig. 4.4c**).

### 4.6.3 X-ray diffraction analysis (XRD)

**Figure 4.5a** shows the x-ray diffraction (XRD) patterns of the dried tomato waste (TW) and activated carbon from tomato waste (ATW). In TW, a broad peak appeared at $2\theta = 21.8^{o}$ which was attributed to the characteristic crystal structure of cellulose. The intensity of the peak largely decreased after carbonization due to the decomposition of the cellulose. Two broad peaks appeared at approximately $2\theta = 25^{o}$ and $43^{o}$ after activation with $ZnCl_2$ in ATW. They corresponded to the formation of hexagonal graphite structures (0 0 2) and (1 0 0) (overlapped 1 0 0 and 1 0 1). In addition, the XRD pattern of ATW contained a sharp peak at $2\theta = 35.3^{o}$ which was due to the presence of zinc oxide and zinc carbides on the washed ATW surface. The sharpness of the peak that the zinc present was comparatively large, though still in the micro range.

**Fig. 4.5b** shows the XRD patterns of the dried carrot waste (CW) and activated carbon from carrot waste (ACW) with crystal structure similar to tomato waste. Moreover, the intensity of the peak largely decreased after carbonization due to the decomposition of the cellulose. The diffraction pattern of PET polymer had three crystalline peaks superimposed on the scattered curve due to amorphous regions. These peaks are at $2\theta = 17.0$, 22.5, and $25.5^{o}$ which corresponded to side spacing in the crystal structure of 5.21, 3.49, 3.51 Å, respectively. These were the reflections from the (1 0 0), (0 $\bar{1}$ 0) and (1 1 0) crystal planes. APET had weak and

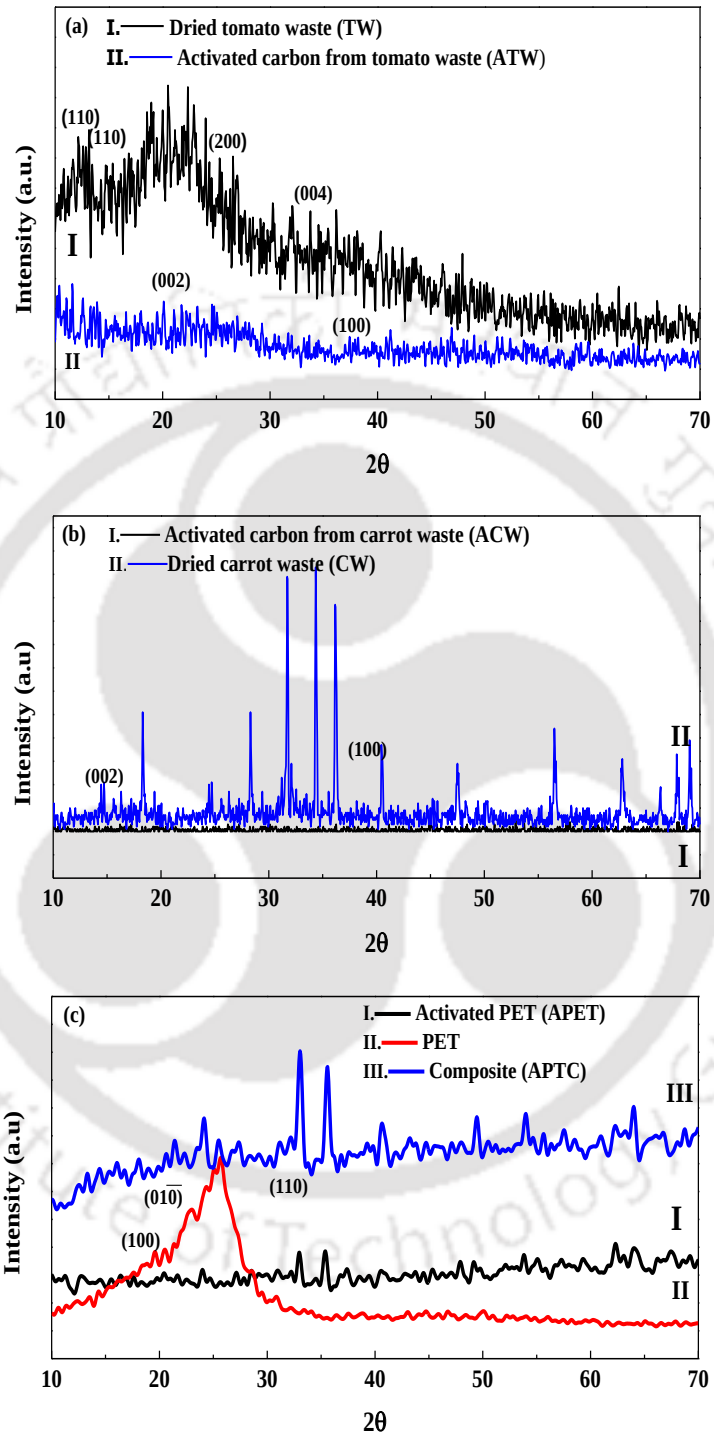


**Fig. 4.5: XRD graph for (a) Dried tomato and activated carbon from tomato waste (b) Dried carrot and activated carbon from carrot waste (c) Activated PET and activated composite**

broad diffraction at 2θ = 15 - 30° which was attributed to poorly organized carbon. In this diffraction spectrum, some reflexes may correspond to phases of Fe, $Fe_3O_4$, $Fe_2O_3$ and $Fe_2C$. The peaks at 32.93° and 35.4° with a d-spacing of 2.71 Å and 2.53 Å were due to superimposition of carbon tetrachloride, 3, 5 - Dibromopyridine, 2 - Adamantanol and other such compounds. The diffraction pattern of the composite adsorbent (APTC) prepared from the APET, ATW and ACW showed similar yet elevated intensity of diffraction than the individual separate samples, indicating a higher adsorptive power of the composite. The peaks at 33.2 and 35.7° are due to 1, 1-Trimethyltriphenyldisiloxane and Pyrrol-1-yl potassium, indicating a d-spacing of 2.706 Å and 2.522 Å respectively (**Fig. 4.5c**).

### 4.6.4 Energy dispersive X-ray spectroscopy (EDX)

**Figure 4.6a** and **4.6b** shows the EDX micrograph of activated carbon from carrot waste (ACW) and activated carbon from tomato waste (ATW) respectively. The micrographs showed the presence of carbon (C), oxygen (O) due to carbonization, phosphorus (P), Copper (Cu), Magnesium (Mg), Chlorine (Cl) and Zinc (Zn) due to activation, along with Manganese (Mn) and other elements such as Sulphur (S), Calcium (Ca), Potassium (K) and Sodium (Na) in trace amounts. The Energy dispersive spectroscopy (EDX) of the $FeCl_3$ activated carbon produced from PET (APET) showed a higher percentage of oxygen (O) due to carbonization process, along with the presence of iron (Fe), carbon (C) and chlorine (Cl). Elements such as zinc (Zn), Copper (Cu), Hydrogen (H) were present in trace amounts and hence not detected by the instrument (**Fig. 4.6c)**. Micrograph for APTC showed elements that were a combination of those present in the constituent $ZnCl_2$ activated carbon from tomato waste and $FeCl_3$ activated carbon from PET. Elements like iron (Fe), Oxygen (O) along with sodium (Na), Copper (Cu), Calcium (Ca), Magnesium (Mg), Phosphorus (P), Potassium (K) and Manganese (Mn) were detected in trace amounts (**Fig. 4.6d).**

**(a)**

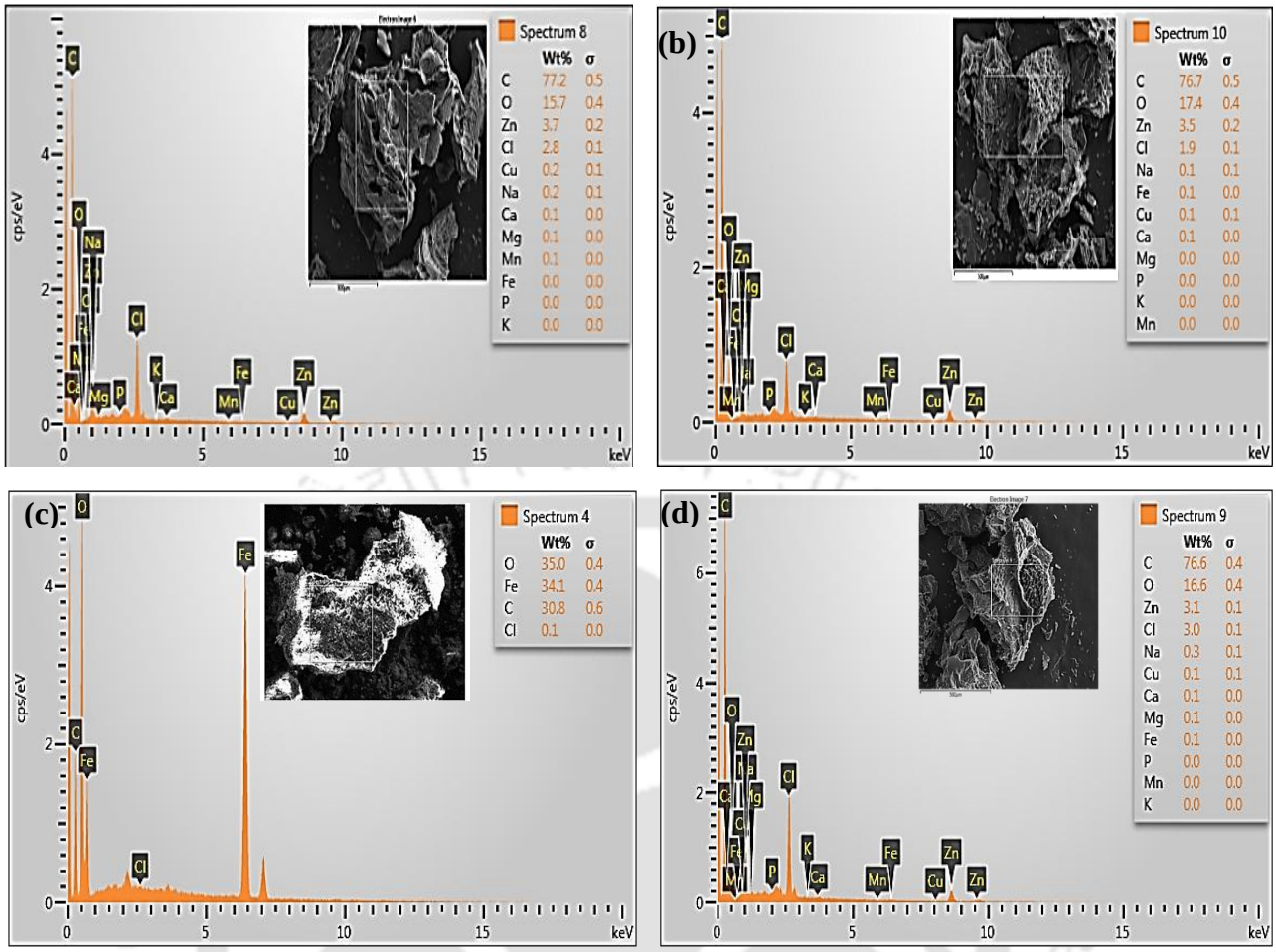


**Fig. 4.6: EDX graph for (a) Activated carbon from carrot waste (b) Activated carbon from tomato waste (c) Activated PET (d) Activated composite**

### 4.6.5 Field emission scanning electron microscopy (FESEM)

The FESEM micrographs of $ZnCl_2$ activated carbon from tomato waste showed a highly porous structure as evident from **Fig. 4.7a** and **4.7b**. The cavities on the surfaces of the adsorbent were from the evaporation of the activating agent along with the conversion of cellulose and lignin

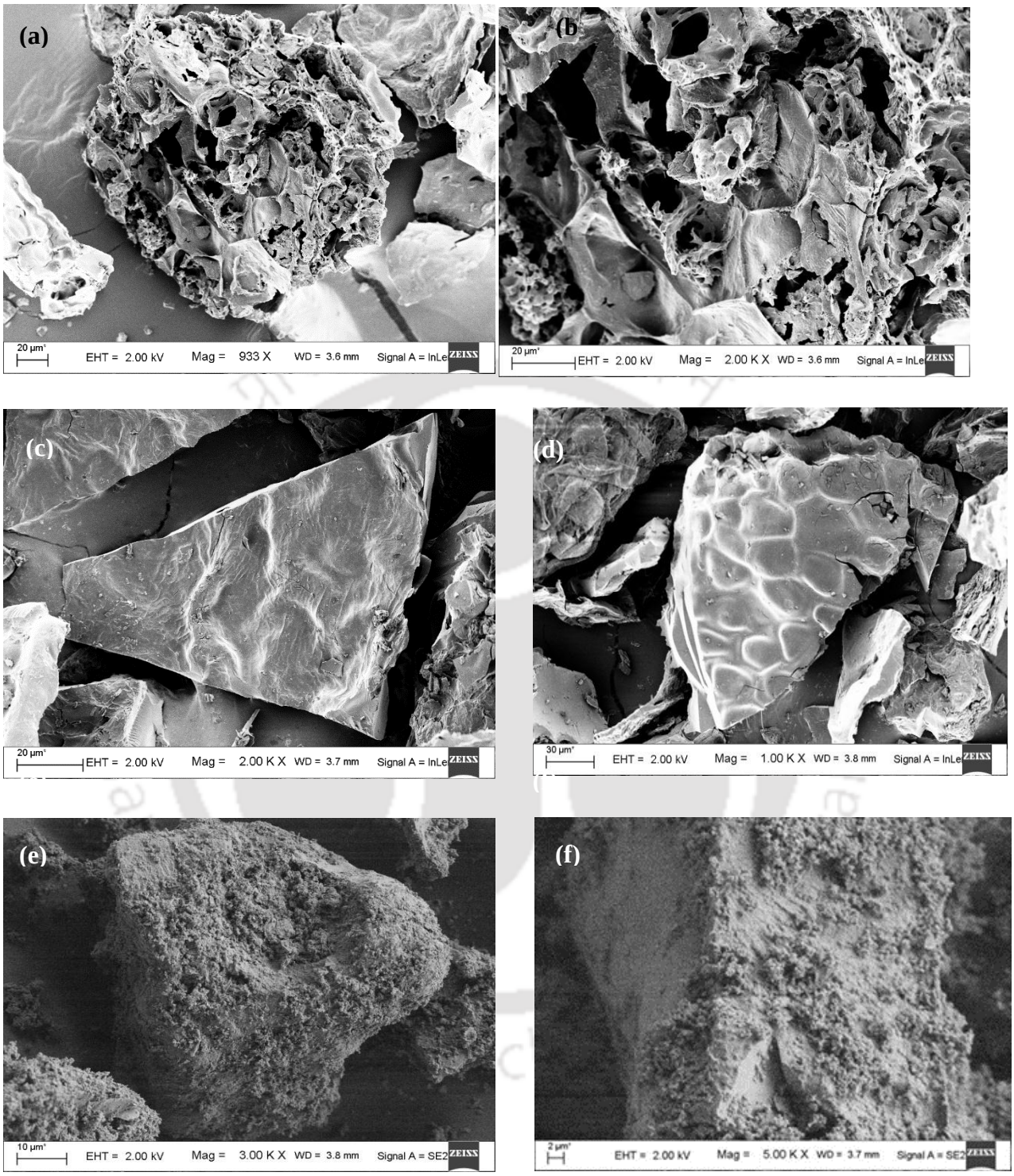


**Fig. 4.7: FESEM figures (a) and (b) Activated carbon from tomato waste, (c) and (d) Activated carbon from carrot waste, (e) and (f) Activated composite**

to $CO_2$ during the sintering process leaving the space previously occupied by the activating agent. The impregnation with $ZnCl_2$ followed by a thermal treatment under inert atmosphere involves a remarkable degradation of the microstructure. Such degradation is coupled to relatively important mass losses. Whereas for the activated carbon from carrot waste, a rather smoothened and scaled outer surface was observed as in **Fig. 4.7c and 4.7d**. However, the internal structure showed the presence of roughness with crevices like structure. The composite (APTC) on the other hand showed the structure of a well distributed fine particles on the surface of a large particle. Previous microstructure studies revealed that the larger particle is that of $ZnCl_2$ activated carbon from tomato and carrot waste, and therefore the smaller particles must definitely be those of $FeCl_3$ activated carbon from PET (**Fig. 4.7e and 4.7f**).

### 4.6.6 Proximate analysis

The % moisture, % volatile matter, % ash content and % fixed carbon from the proximate analyses are shown in **Table 4.1**.

**Table 4.1: Showing proximate values of activated carbon samples**

| Samples/Proximate analysis | % Moisture | % Volatile matter | % Ash content | % Fixed carbon |
|---|---|---|---|---|
| Activated carbon from tomato waste | 4.67 | 9.46 | 25.6 | 60.27 |
| Activated carbon from carrot waste | 2.13 | 2.47 | 62.8 | 32.6 |
| Activated Composite (Polymer + Tomato + Carrot) | 3.86 | 5.42 | 21.6 | 69.12 |

Moisture content and volatile matter was found to be the highest in activated carbon from tomato waste at 4.67 and 9.46 %, respectively, ash content was the highest for carrot at 62.8 % whereas the % fixed carbon was highest activated composite adsorbent at 69.12 %.

## 4.7 Adsorption studies

### 4.7.1 Effect of adsorbent dose

Variation of extent of adsorption with adsorbent dose is shown in **Fig. 4.8.** The adsorption experiments were carried out for a time period of 24 h to see the maximum adsorption capacity of each adsorbent at a given dosage maintain a pH of 7. It may be seen from the figure that an increase in adsorbent dose resulted in increase in adsorption. This can be attributed to the fact that large surface is available for adsorption when the doses increases [112]. However, all the three adsorbents offered different removal efficiencies. As seen from the Figure, activated carbon from carrot waste (ACW) the maximum removal obtained was 24 % at an adsorbent dose of 1.2 g/L, for activated carbon from tomato waste (ATW) the maximum removal obtained was 37 % at an adsorbent dose of 0.6 g/L and for the composite (ATPC) a removal of 67 % at an adsorbent dose of 0.8 g/L was obtained. This variation of adsorbent dosage can be justified from the results obtained in FESEM studies. FESEM figures suggested ATW to be more porous on the surface than ACW, hence a large number of active sites were available on ATW surface for adsorption of Co (II). Thus adsorbent dosage required was less in comparison to ACW to obtain a maximum adsorption. Whereas APTC was a composite of ATW, ACW and activated PET hence a slight increase in dosage may be an acceptable reason.

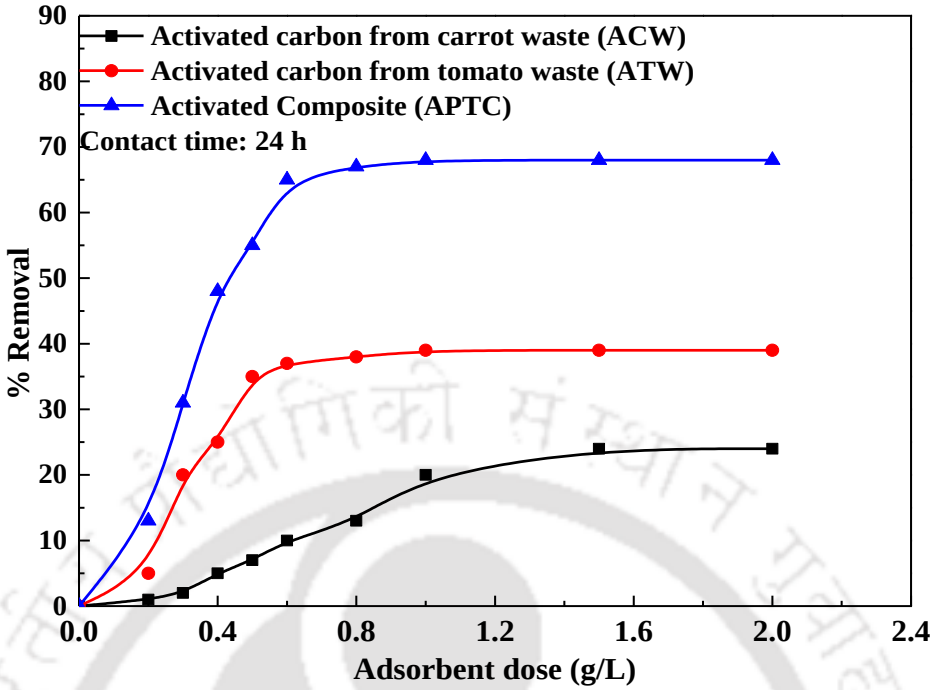


**Fig. 4.8: Effect of adsorbent dose on adsorption of Co (II)**

### 4.7.2 Effect of contact time

**Figure 4.9** shows the effect of contact time on the removal of Co (II). As seen, the curve rises at the initial stages with increasing contact time because of the large amounts of vacant sites available for adsorption. However, after a particular period the curve tends to become consistent without any further increase This plateau reached is because of the fact that all the sites which were available initially for the uptake of Co (II) ions have been filled or occupied in due time i.e. saturation of Co (II) on the adsorbent surface takes place. The equilibrium time thus obtained were around 75, 99 and 99 min for ACW, ATW and APTC, respectively. The dosages of the prepared adsorbents which gave the maximum adsorption ($q_{e,APTC}$ = 264.72 mg/g, $q_{e,ATW}$ = 214.11 mg/g and $q_{e,ACW}$ = 52.99 mg/g) at the given operating conditions as suggested in the previous section have been used, hence three different adsorbent dosages are considered. FESEM figures already suggested that ACW were less porous and hence the lesser uptake of

Co (II). Furthermore, the ACW got saturated with the adsorbed Co (II) ions must faster due to no availability of sites. However, ATW and APTC had much more available surface sites for the uptake of Co (II) and hence more time is required to reach the equilibrium stage.

### 4.7.3 Effect of pH and zeta potential

The pH of a solution plays a very crucial role on the adsorption of Co (II) from water. With changes in the pH, the surface charge of the adsorbents also changed [108]. The variation of zeta potential of the adsorbents with pH is shown in **Fig. 4.10**. The figure clearly shows that the charge on the surface of the adsorbent is significantly changed with pH of the solution. The values of $pH_{zpc}$ for ACW, ATW and ATPC were found to be 7.6, 8.9 and 9.74, respectively. It is seen that with an

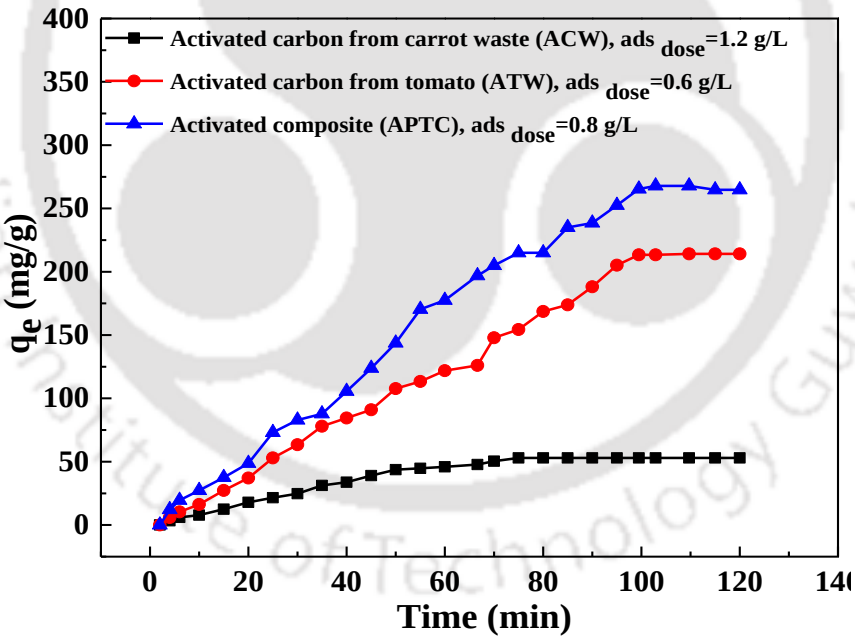


**Fig. 4.9: Effect of contact time on the adsorption of Co (II) by the prepared adsorbents**

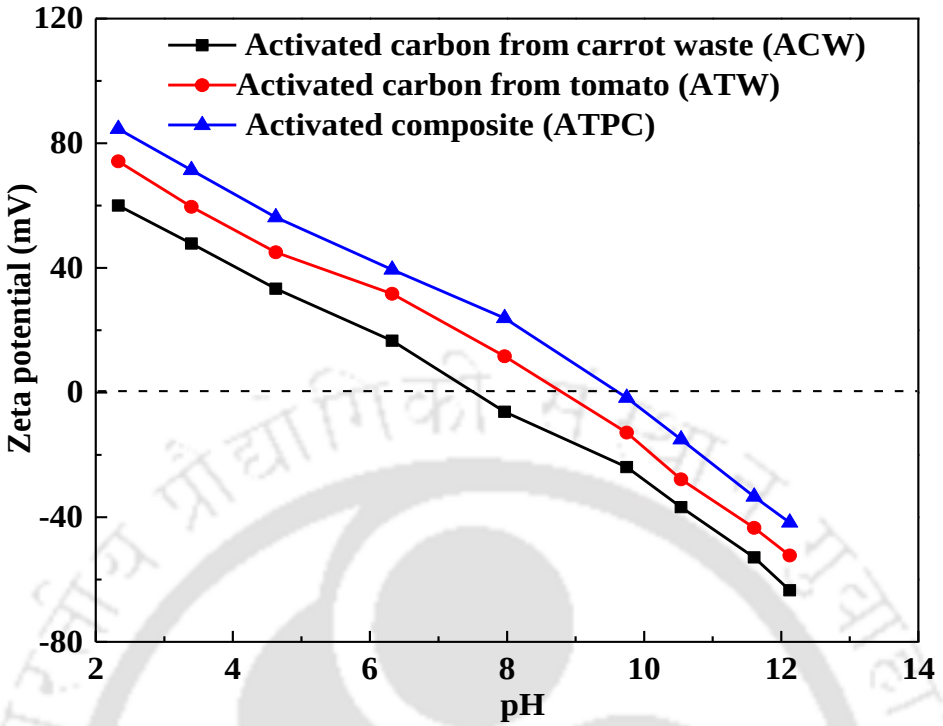


**Fig. 4.10: Effect of pH on zeta potential of the prepared adsorbents**

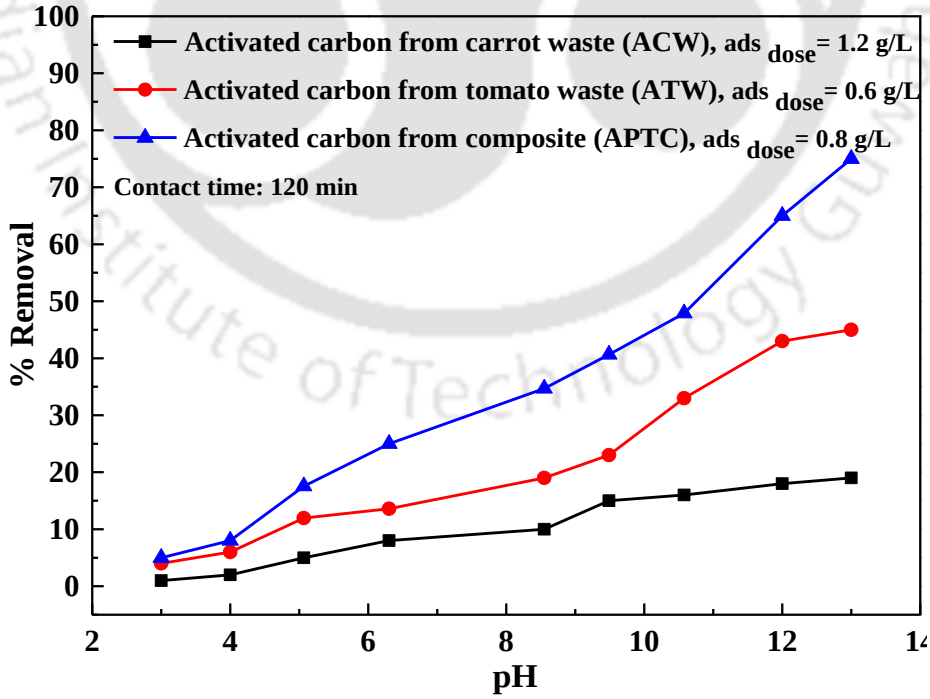


**Fig. 4.11: Effect of pH on zeta potential of the prepared adsorbents on % Removal**

increase in pH, the zeta potential value goes down. At low pH, the surface of the adsorbents would be surrounded by large amounts of hydronium ions ($H_3O^+$). On the other hand, at higher pH values, the surface of the adsorbents would be surrounded by large amounts of hydroxide ions ($OH^-$). Since Co (II) is cationic in nature, it is natural that its adsorption on the surface of the adsorbents would increase with an increasing pH. Another important observation from **Fig. 4.10** is that the adsorbent ATPC had the highest negative zeta potential in comparison to the other two adsorbents. Hence, it may also be seen that the highest removal of Co (II) would be carried out by the composite ATPC. This is evidenced by analyzing the % removal at different pH values for the three adsorbents (**Fig. 4.11**). The figure shows the increase in % removal with increasing pH and the highest removal being offered by the composite. As evident when the pH increased beyond 7.6, 8.9 and 9.74 for ACW, ATW and ATPC respectively, the % removal increased drastically. Below $pH_{zpc}$ the % removal was low and gradual however beyond the $pH_{zpc}$ value a drastic uptake of Co (II) was observed. As seen the % removal increased from 3 to 19 % for ACW, 4 to 45 % for ATW and 5 to 75 % for ATPC.

## 4.8 Anova test

The analysis of variance (ANOVA) gives knowledge about the validity of the parameters, contribution of each parameter in the adsorption experiment and their statistical significance [20 - 22]. The results of analysis of variance (ANOVA) are given in **Table 4.2**. The F-value for each process indicates which parameter had a significant effect on the adsorption process. Larger the F-value greater is the effect. When the probability P-value > 0.05, the variance is less suggesting our considered parameter to be insignificant. However, if the probability P-value < 0.05, the considered parameter is insignificant. Anova test of zeta potential at different pH values ranging from 2 - 12, % removal with adsorbent dose and % removal variation with contact time for the

three adsorbents had the P-value as 0.017, $2.63 \times 10^{-4}$ and $2.39 \times 10^{-7}$ , respectively, hence suggesting the significance of our considered parameters in the adsorption process. As seen from the table, the F-value was highest at 18.81 for contact time followed by adsorbent dose and pH. The sequential order of the process variables is given below for Co (II) removal onto ACW, ATW and APTC.

Contact time > Adsorbent dose > pH

**Table 4.2: ANOVA studies for various parameters for adsorption of Co (II) on the prepared adsorbents**

| Source | SS | df | MS | F | P-value | Inference |
|---|---|---|---|---|---|---|
| **Zeta potential variation with pH for different adsorbents** | | | | | | |
| Model | 2811 | 2 | 1405 | 4.84 | 0.017 | Significant |
| Error | 6960 | 24 | 290 | | | |
| Total | 9771 | 26 | | | | |
| **% Removal variation with adsorbent dose for different adsorbents** | | | | | | |
| Model | 7126 | 2 | 3563 | 11.35 | $2.63 \times 10^{-4}$ | Significant |
| Error | 8470 | 27 | 313 | | | |
| Total | 15597 | 29 | | | | |
| **Adsorption capacity variation with contact time for different adsorbents** | | | | | | |
| Model | 20170 | 2 | 10085 | 18.81 | $2.39 \times 10^{-7}$ | Significant |
| Error | 40210 | 75 | 536 | | | |
| Total | 60380 | 77 | | | | |

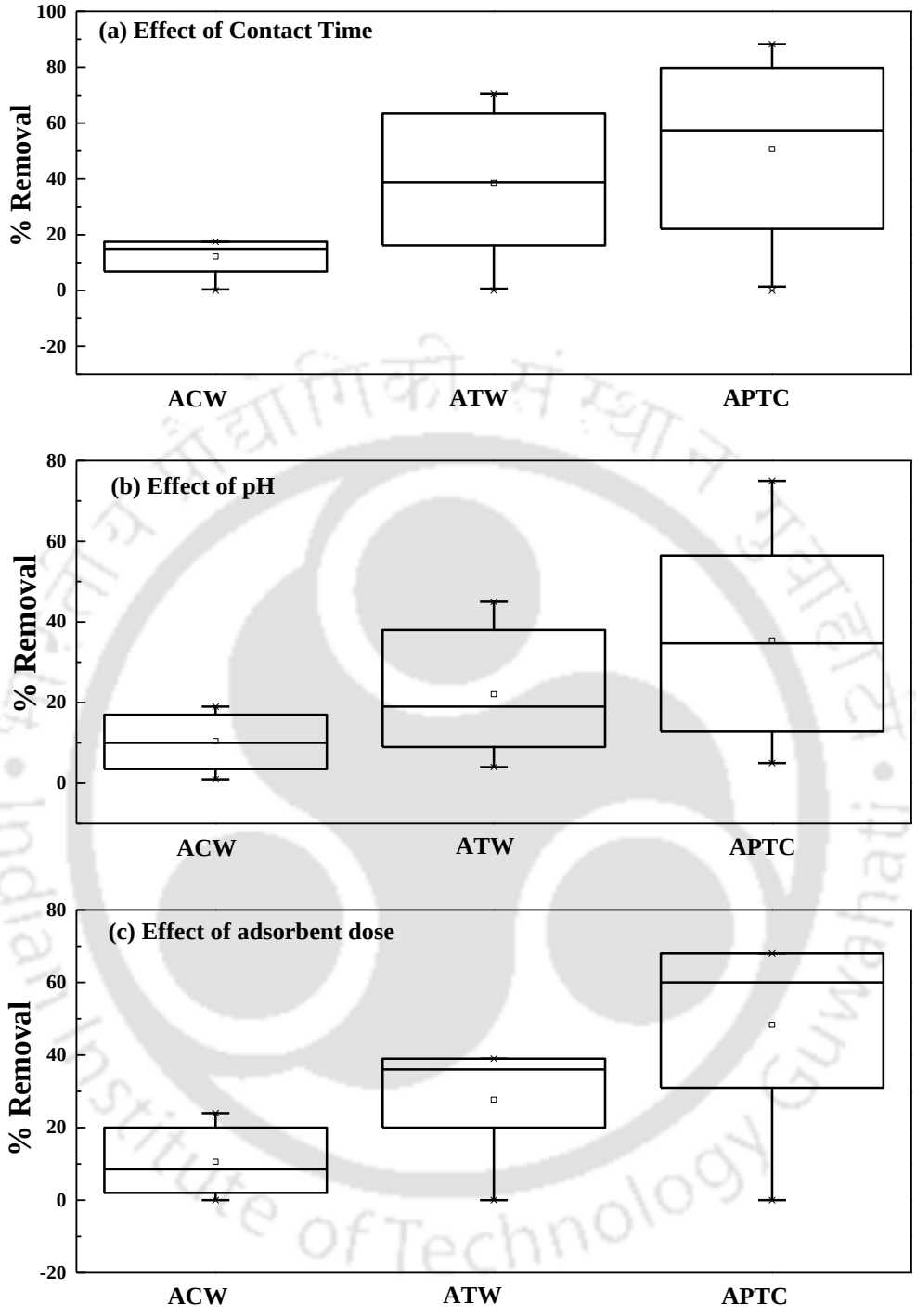


**Fig. 4.12: Box-plot statistical analyses of sampling distributions of the prepared adsorbents (ACW: Activated carrot waste, ATW: Activated tomato waste, APTC: Activated composite) (a) Effect of contact time (b) Effect of pH (c) Effect of adsorbent dose**

Box plots are used to show overall patterns of response for a group. They provide a useful way to visualize the range and other characteristics of responses for a large group. As indicated in **Fig. 4.12a,** the medians of all the three boxes lies at different level indicating the differences among the % removal at different contact time. The box corresponding to the activated carbon from carrot is smaller than the other two boxes suggesting a high level of agreement in the values. Similar interpretations can be made from **Fig. 4.12b**. Highly skewed distributions appear in box plot of activated carbon from tomato in **Fig. 4.12a** and activated composite in **Fig. 4.12c** suggesting a uniform distribution of values at varying pH**.** Another interesting observations made was the presence of very short whiskers for activated carbon from tomato waste and activated composite [116, 117] for Fig. 4.12c. The whiskers were missing from the upper region of the box suggesting that the upper quartile and the maximum value coincided.

## 4.9 Adsorption kinetics

The adsorption kinetics gives detail about the mechanism of Co (II) adsorption from aqueous solution. In this study, pseudo-first-order and pseudo-second–order are applied. The pseudo first order model is based on the first order Lagregren model [112-114] given in **Table 4.3.**

$$\boldsymbol{log\ (q_e - q_t) = log\ (q_e) - \frac{k_1}{2.303t}} \qquad 4.7$$

Where $q_e$ is the amount of Co (II) adsorbed onto the adsorbent at equilibrium (mg/g), $q_t$ is the amount of Co (II) adsorbed onto the adsorbent at any time t (mg/g), and $K_1$ ($min^{-1}$) is the rate constant.

A plot of *log* ($q_e$ - $q_t$) versus t shown in **Fig. 4.13a** gave us the values of the $K_1$ and $q_e$ which are shown in **Table 4.3**. Experiments were performed for the three adsorbents ACW, ATW and APTC and it was observed that the correlation coefficient ($R^2$) coefficient was the maximum for the

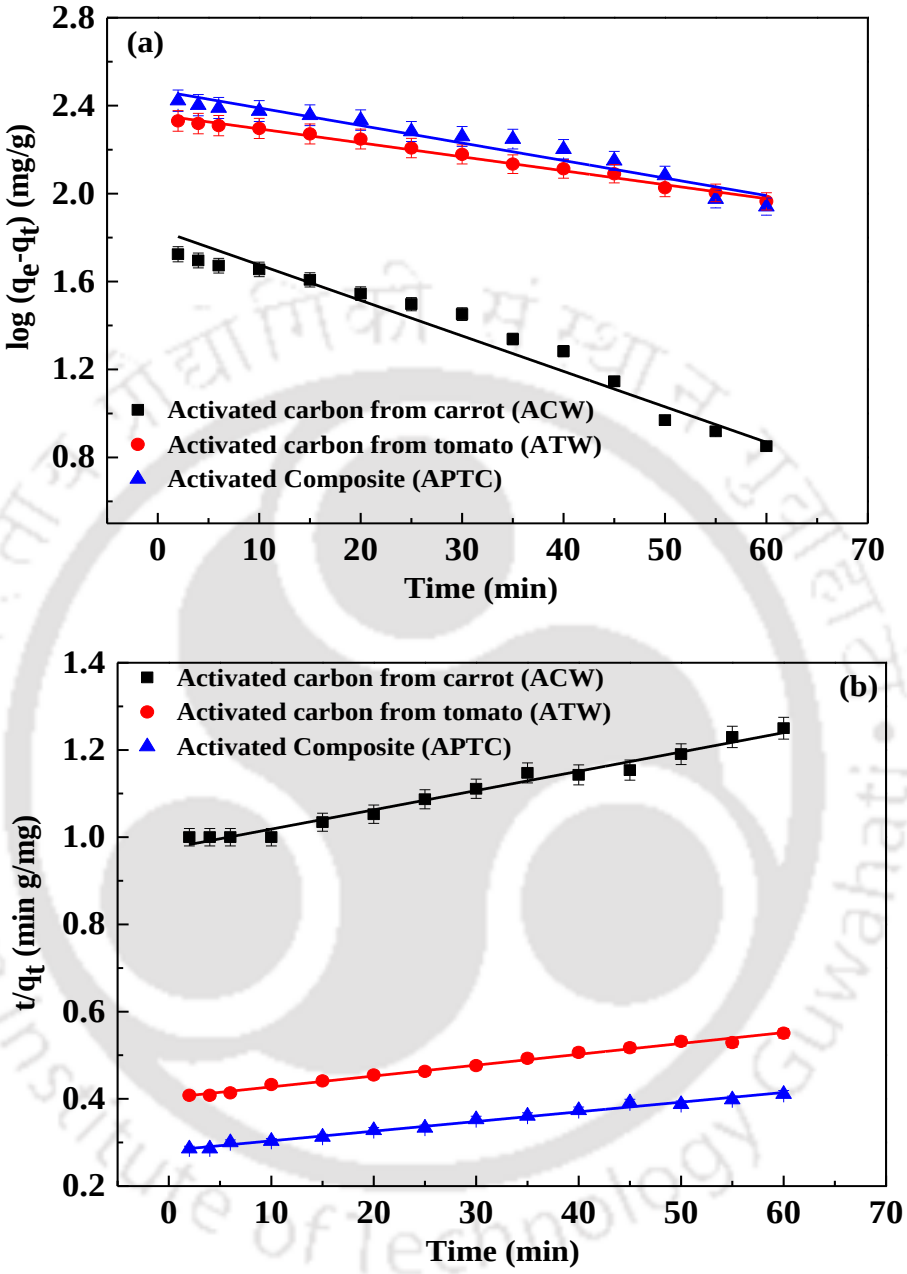


**Fig. 4.13: (a) Pseudo-First order kinetics (b) Pseudo-second order kinetics for adsorption of Co (II) onto prepared adsorbents.**

**Table 4.3: Kinetic parameters of Co (II) adsorption by prepared adsorbents**

| Model | Equation | Parameters | | | |
|---|---|---|---|---|---|
| First-order kinetic | $Log\ (q_e - q_t) = log(q_e) - k_1/2.303t$ | ***Adsorbent type*** | $q_e$ **(mg/g)** | $k_1$ **($min^{-1}$)** | $R^2$ |
| | | Carrot | 65.02±2 | 0.0349 | 0.96 |
| | | Tomato | 227.35±2 | 0.0145 | 0.98 |
| | | Composite | 290.97±2 | 0.0178 | 0.94 |
| Second-order kinetic | $(t/q_t) = 1/(k_2 q_e^2) + 1/q_e(t)$ | ***Adsorbent type*** | $q_e$ **(mg/g)** | $k_2$ **(g/mgmin)** | $R^2$ |
| | | Carrot | 227.27±2 | 0.00002 | 0.98 |
| | | Tomato | 400±2 | 0.000015 | 0.99 |
| | | Composite | 454.54±2 | 0.000017 | 0.99 |

activated carbon from tomato waste (ATW) with a value of 0.98 followed by the carrot adsorbent (APTC) at 0.96 and the activated composite (ACW) at 0.94.

The pseudo-second order model considers adsorption over the whole range and agrees with chemisorption mechanism. The equation is given as

$$\left(\frac{t}{q_t}\right) = \frac{1}{k_2 q_e^2} + \frac{1}{q_e t} \qquad 4.8$$

Where $K_2$ (g/mgmin) is the rate constant of the pseudo-second-order adsorption, $q_e$ is the amount of Co (II) adsorbed on the adsorbent at equilibrium (mg/g), and $q_t$ is the amount of Co (II) adsorbed in mg/g on the adsorbent at any time, $t$.

A plot of $t/q_t$ versus t shown in Fig. 4.13b gives the values of $K_2$ and $q_e$ as in the Table 4.3. The correlation coefficient ($R^2$) is calculated to determine the suitability of the model. As seen from

Table 4.3, the $R^2$ value was as follows 0.99 for APTC, 0.99 for ATW and 0.98 for ACW. This suggested that the prepared adsorbents followed the second order kinetics model

### 4.10 Adsorption equilibrium study

Adsorption isotherm studies were performed to determine the interaction between adsorbate and adsorbent. The most important isotherms to be considered are the Langmuir isotherm and Freundlich isotherm [27-30].

The Langmuir isotherm given in **Table 4.4** and is represented by the equation

$$\frac{C_e}{q_e} = \frac{1}{K_L q_m} + \frac{C_e}{q_m} \qquad 4.9$$

The isotherm is based on the assumption that adsorption takes place in a specific homogenous site i.e. once the adsorbate molecule occupies particular site further adsorption does not occurs. A plot of $C_e/q_e$ versus $C_e$ (**Fig. 4.14 a, b and c**) gave us the values of $q_m$ and $K_L$ are shown in **Table 4.4**.

Langmuir studies were done for ACW, ATW and APTC. As seen from the table the $R^2$ values obtained were 0.81, 0.90 and 0.96 for ACW, ATW and APTC, respectively.

The Freundlich isotherm is represented by the following equation

$$lnq_e = lnK_F + \frac{1}{n} lnC_e \qquad 4.10$$

$$ln\ q_e = ln\ K_F + 1/n\ ln\ C_e$$

A plot of $ln\ q_e$ versus $ln\ C_e$ gave us the values of $n$ and $K_F$ (**Fig. 4.14 d, e and f**). This isotherm considers adsorption to occur in multilayers. The calculated values of $K_F$ and n are given in **Table 4.4**.

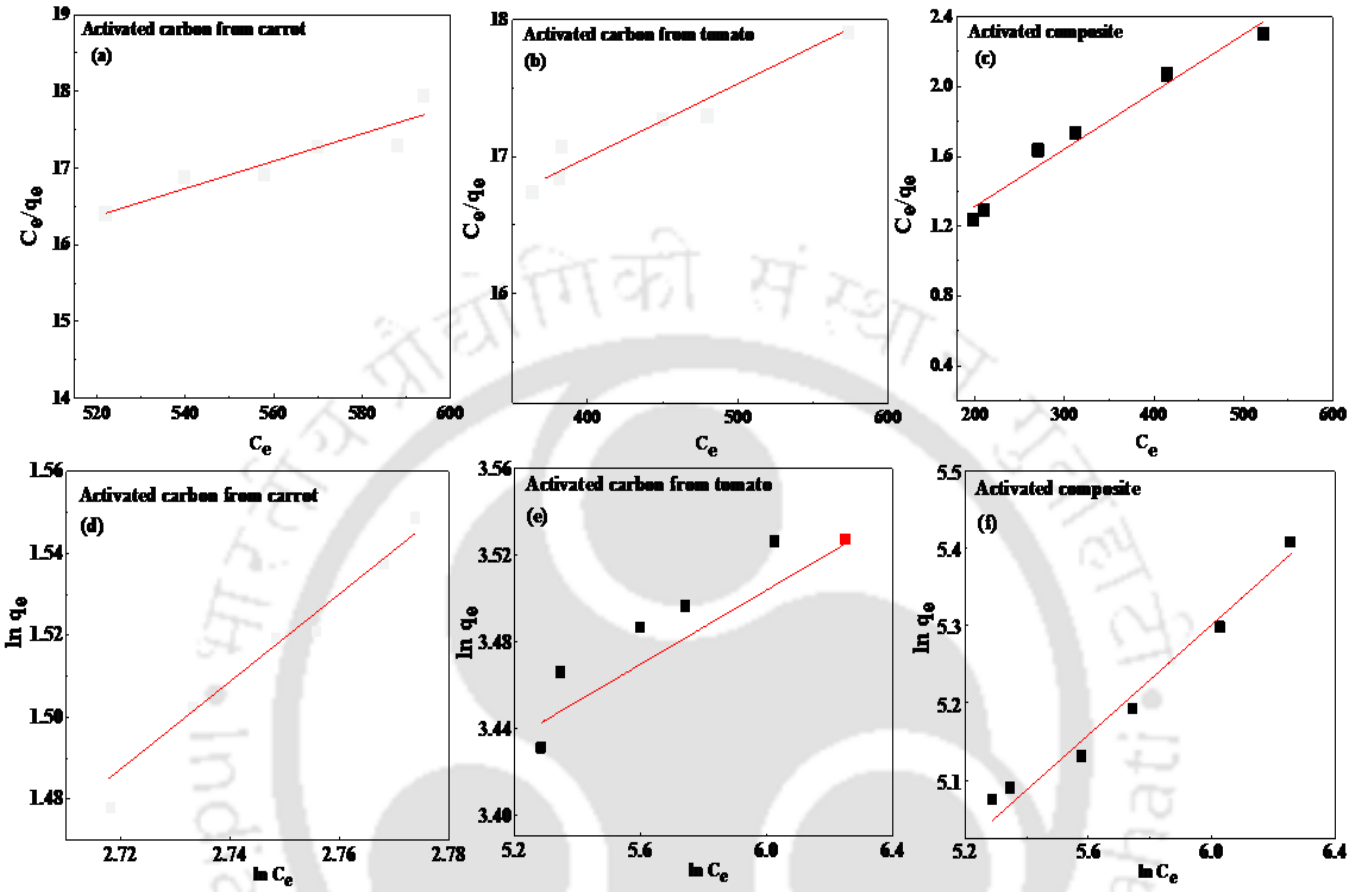


**Fig. 4.14: (a-c) Langmuir isotherm for adsorption of Co (II), (d-f) Freundlich isotherm for adsorption of Co (II)**

As seen from the table the composite adsorbent with a $R^2$ value of 0.98 favoured the Freundlich adsorption. **Table 4.5** shows numerous adsorbents that have been utilized for Co **(**II) adsorption.

**Table 4.4: Isotherm constants of Co (II) adsorption by prepared adsorbents**

| **Isotherm** | **Equation** | **Adsorbent type** | **Parameters** | | |
|---|---|---|---|---|---|
| | | | $q_m$ **(mg/g)** | $K_L$**(L/mg)** | $R^2$ |
| Langmuir | $C_e/q_e = 1/(K_L q_m) + (1/q_m)*C_e$ | Carrot | 56.17 | 0.0069 | 0.81 |
| | | Tomato | 170.06 | 0.0024 | 0.90 |
| | | Composite | 312.50 | 0.0016 | 0.97 |
| Freundlich | $ln\ q_e = ln\ K_F + 1/n\ ln\ C_e$ | | $K_F$ **(mg/g(l/mg)$^{1/n}$ )** | ***n*** | $R^2$ |
| | | Carrot | 0.176 | 0.845 | 0.97 |
| | | Tomato | 17.28 | 9.091 | 0.90 |
| | | Composite | 26.29 | 2.958 | 0.96 |

As seen from the table numerous adsorbents were used like sulphurised activated carbon, fungal based biosorbent, almond green hull, lemon peel, fruit nut shell, watermelon rind, natural zeolite, EDTA modified silica gel, coir pith and kaolinite and orange peel which clearly shows our adsorbent to be better than those already prepared. The highest adsorption was offered by fungal based biosorbent with an adsorption capacity of 190 mg/g. However, the composite

adsorbent prepared in the present was better than the individual adsorbents mentioned in the table with an adsorption capacity of 312.50 mg/g.

**Table 4.5: Table showing comparative capacities for CO (II) by various adsorbents**

| Adsorbent | Adsorption capacity (mg/g) | References |
|---|---|---|
| Sulphurised activated carbon | 153.6 | [24] |
| Fungal based biosorbent | 190 | [25] |
| Almond green hull | 45.5 | [26] |
| Lemon peel adsorbent | 22 | [27] |
| Fruit nut shell | 98 | [28] |
| Watermelon rind | 175 | [29] |
| Natural zeolite | 14.38 | [30] |
| EDTA modified silica gel | 20 | [31] |
| Coir pith | 12.82 | [32] |
| Kaolinite | 0.919 | [33] |
| Orange peel | 1.23 | [34] |
| Composite carrot, tomato and PET adsorbent | 312.50 | Present work |

## 4.11 Cost estimation

A brief cost estimation was done for the activated composite which offered us the maximum adsorption capacity for Co (II) **(Table 4.6).** Since PET bottles and tomato and carrot waste were collected free of cost from IITG market, their cost has not been included this work. Cost of power consumption and chemicals used suggested that the cost of present composite adsorbent was 58.93 US$ per kg which is far less than the activated carbon available in the market at 172.96 US$ per kg of adsorbent.

**Table 4.6: Cost analysis for activated composite (APTC)**

| **Parameters** | **Duration (h)** | **Unit cost (US$/kg)** | **Power rating (KWh)** | **Price (US$/kg)** |
|---|---|---|---|---|
| Cost of drying | 46 | 0.09 | 1.5 | 6.21 |
| Cost of activation | 5 | 0.09 | 1.4 | 0.63 |
| Cost of chemicals | _ | _ | - | 52.09 |
| Total cost | | | | 58.93 |

# Chapter 5

# A hybrid method for the removal of fluoride from drinking water: Parametric study and cost estimation

# *Chapter 5*

# A hybrid method for the removal of fluoride from drinking water: Parametric study and cost estimation

*The present study describes the application of selected fabricated membrane for the microfiltration of electrocoagulated by-product obtained during treatment of Fluoride contaminated drinking water using electrocoagulation. Three samples of drinking water with fluoride concentration of 7.89, 4.79 and 1.78 mg/L were collected from a hand tube well located in Karbi Anglong, Assam. Effects of initial concentration, current density and pH on the removal of fluoride were extensively investigated in the electrocoagulation chamber. Effect of current density in the range of 5-15 A/m$^2$ and an inter-electrode distance of 0.005 m was considered. Produced flocks were characterized to confirm the presence of fluoride. Microfiltration studies were carried out at three different pressures of 196, 392 and 509 kPa to remove the flocks from the pre-treated water. The proposed hybrid technique was able to reduce the fluoride concentration of contaminated drinking water to below permissible limit of 1.5 mg/L.*

## 5.1 Experimental

### 5.1.1 Materials and methods

Drinking water samples were collected from Karbi Anglong with fluoride concentrations of 7.89, 4.79 and 1.78 mg/L. All the experiments were performed at constant temperature of 25 $^oC$. A measured quantity (1.2 L) of the fluoride contaminated drinking water was taken into the electrochemical cell. Current density was maintained in the range of 5 - 15 A/m$^2$. The treated water samples were collected at different time intervals and analyzed. NaCl at 1.95 g/L was added to increase the conductivity of the sample. Electrodes were washed with $H_2SO_4$ and

rubbed with abrasive paper (C-220) in order to ensure the complete removal of impurities before every experiment. The used electrodes were replaced after a run of 5 experiments. Fly ash was collected from National thermal power corporation (NTPC). Calcium carbonate (Merck), Sodium carbonate (Merck), Boric acid (CDH) and Sodium metasilicate (CDH) were used for the preparation of ceramic membranes.

### 5.1.2 Membrane preparation

The membrane fabrication process included mixing and grinding of raw materials like fly ash, sodium carbonate, sodium metasilicate, calcium carbonate and boric acid in a ball mill at 200 rpm for 3 h. The grinded raw material was mixed with Millipore water to obtain a paste. The paste was then casted on an MS ring with a diameter of 52 mm and thickness of 7 mm and left to dry overnight under the application of uniform weight (4 kg). The obtained circular disk shaped membrane was dried in the oven for 12 h at 120 °C and then sintered at 700 °C for 6 h. The membrane obtained were very high in strength and porous in nature. The membrane was then polished with abrasive paper (C-220) to obtain a smooth and flat membrane of diameter 51.35 mm and thickness 6.7 mm. The final stage included the cleaning of membrane by sonication for 15 min to remove loose particles from the membrane followed by drying at 120 °C. The as obtained membrane were then coated with a polymer cellulose acetate and with polymer-nanoparticle solution. The main purpose of coating the sample membrane were to reduce the pore size of the membrane as the flocks obtained during electrocoagulation process would be very less in size. Hence, three types of membrane were prepared to be used for filtration purpose; bare ceramic membrane (BM), polymer coated ceramic membrane (PM) and polymer-nanoparticle coated ceramic membrane (PNM). Based on the size of the produced flocks a particular membrane would be utilized for the filtration process.

### 5.1.3 Measurement and analysis

The residual fluoride concentrations were measured with fluoride ion electrode (Make: CONSORT, Belgium). Water quality including pH, conductivity, and turbidity were determined using a microprocessor based water analyzer kit (VSI electronics Pvt. Ltd., Mohali, Chandigarh). Microscopic observation of flocks from the electrocoagulation unit as well as the membranes used for filtration were carried out by a scanning electron microscope (FESEM, Make: LEO) which provided details on the morphological characteristics. Energy dispersive X-ray (EDX) was performed to identify the elemental composition of the by-products obtained from the electrochemical unit. The analytical procedures utilized in the measurement of particle size distribution was Delsa Nano (Beckman Coulter), Fourier transform infrared spectroscopy (FTIR, Make: Perkin Elmer, USA) analysis was carried out to confirm the bond stretching of the flocks formed during the electrocoagulation process.

### 5.1.4 Electrocoagulation bath

A setup having dimension of 0.23 m × 0.12 m × 0.08 m with a working volume of about 1.2 L was used to carry out the electrocoagulation experiments. Aluminium sheets of 0.07 m × 0.77 m × 0.001 m were used as electrodes for electrocoagulation. A distance of 0.005 m was maintained between the electrodes with bipolar connection. Four electrodes were used out of which two ends of the electrodes were connected to a DC power source whereas the other two electrodes had no connections to a power source. Induced polarization occurred when a potential was applied to the end of the electrodes resulting in bipolarization of the total assembly. The set-up was then connected to DC power source (Crown, DC regulated power supply, 0-30 V/2A) to perform the electrocoagulation experiment. The EC set-up was kept in constant stirring mode using a magnetic stirrer to facilitate an enhanced adsorption of fluoride.

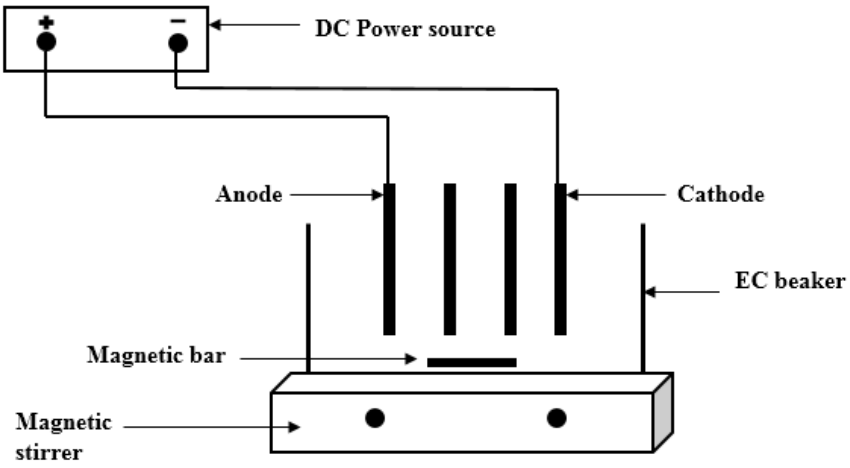


**Fig. 5.1: Electrocoagulation setup with bipolar connection**

The effects of initial fluoride concentration, current density and pH were studied at different conditions as listed in **Table 5.1**. Samples were taken at a definite interval of time for 20 min and the fluoride concentration was detected. Flocks produced during the electrocoagulation process were dried at 110 $^{o}$C for further characterization.

### 5.1.4 Fluoride removal mechanism by electrocoagulation

Electrocoagulation process has received increased attention in the recent years in comparison to other conventional methods. The fact being the high removal efficiency at lower operating costs and easily operable mechanism has led to the increased popularity of this process. Electrocoagulation basically consists of a pair of electrodes separated by a particular distance. When a potential is applied across the electrodes, it results in the in-situ generation of coagulant species as the sacrificial metal anode (aluminum or iron) dissolves, while hydrogen is simultaneously evolved at the cathode. These coagulant species (metal hydroxide) helps in removing fluoride by aggregating the suspended fluoride in water and adsorbing it on the metal

**Table 5.1: Range of operating parameters for arsenic and fluoride removal by electrocoagulation**

| Type of experiment | Initial fluoride concentration (mg/L) | Initial pH | NaCl concentration (mg/L) | Interelectrode distance (m) | Current density ($A/m^2$) | Run time (min) |
|---|---|---|---|---|---|---|
| Effect of initial concentration | 1.78<br>4.79<br>7.89 | 7.9<br>7.9<br>7.9 | 1.95<br>1.95<br>1.95 | 0.005<br>0.005<br>0.005 | 15<br>15<br>15 | 20<br>20<br>20 |
| Effect of current density | 1.46<br>7.89 | 7.9<br>7.9 | 1.95<br>1.95 | 0.005<br>0.005 | 5,10,15<br>5,10,15 | 20<br>20 |
| Effect of initial pH | 7.89<br>7.89 | 3.89<br>11.28 | 1.95<br>1.95 | 0.005<br>0.005 | 15<br>15 | 20<br>20 |

hydroxide. Bubbles of hydrogen and oxygen produced during the electrocoagulation process compels the pollutant particles to stay afloat. Apart from adsorption, processes such as sweep coagulation, bridge coagulation and co-precipitation are also play a vital role for the removal of fluoride in electrocoagulation process. The reactions occurring during the electrocoagulation are shown below.

**Reactions occurring at the anode**

$Al^{3+}(aq) + 3e^- \longrightarrow Al(s)$ $E^o = -1.662$ V 5.1

$O_2(g) + 4H^+ + 4e^- \longrightarrow 2H_2O$ $E^o = +1.229$ V 5.2

**Reactions occurring at the cathode**

$2H_2O + 2e^- \longrightarrow H_2(g) + 2OH^-(aq)$ $E^o = -0.83$ V 5.3

**Reactions occurring at bulk**

$Al^{3+} + 3H_2O \longrightarrow Al(OH)_3(s) + 3H^+$ 5.4

$Al(OH)_3 + xF^- \longleftrightarrow Al(OH)_{3-x}F_x + xOH^-$ 5.5

Flotation is the dominant pollutant removal path at high current densities, while sedimentation is dominant at lower current densities. This change is due to the fact that at lower current densities, bubble concentration is not sufficient enough to aid floatation of the pollutants as a result of which the pollutants aggregate among themselves and settle down at the bottom of the electrolytic tank. Various monomeric species such as $Al(OH)^{+2}$, $Al(OH)^{+}_2$, $Al_2(OH)_2^{4+}$, $Al(OH)_4^-$ and polymeric species such as $Al_6(OH)_{15}^{3+}$, $Al_7(OH)_{17}^{4+}$, $Al_8(OH)_{20}^{4+}$, $Al_{13}O_4(OH)^{7+}_{24}$, $Al_{13}(OH)_{34}^{5}$ are produce during the EC process which finally transform into $Al(OH)_{3(S)}$ [31].

## 5.2 Results and discussion

### 5.2.1 Effect of initial fluoride concentration and run time

The effect of initial fluoride concentration and run time are shown in **Fig. 5.2**. Experiments were carried with bipolar connection and at a current density of 15 A/m$^2$ with an electrode distance of 0.005 m. As seen from the **Fig. 5.2**, the concentration dropped gradually and then reached a steady state value after a 10, 16 and 17 min for a fluoride concentration of 1.78, 4.79 and 7.89 mg/L respectively. As electrocoagulation proceeds aluminium cation resulted in amorphous aluminium hydroxide precipitation. With increase in electrocoagulation time, more

amounts of aluminium hydroxide were produced which had a very high affinity for the fluoride ions. A sudden drop in concentration is evident from the **Fig. 5.2** and this is because of the fact that initially a high rate of mass transfer occurred due to largely available vacant sites on the generated flocks responsible for removal of fluoride. Moreover, the monomeric and polymeric species produced as discussed in **section 5.1.5** aid in the formation of various fluoride complexes enhancing the overall removal of fluoride. Thus, with an increase in initial fluoride concentration the electrocoagulation time required also increases to reach a steady state value. However, experiments showed that the fluoride concentrations were attained below WHO recommendations within 20 min of the experiment. Hence, rest of the experiments were carried out for a time period of 20 min. It may be seen from the figure that the concentration of fluoride reduced to 0.65, 0.335 and 0.0097 mg/L from initial concentrations of 7.89, 4.79 and 1.78 mg/L, respectively which is within the WHO limit of 1.5 mg/L.

### 5.2.2 Effect of current density

The effect of current density was studied for the two fluoride concentrations 7.89 mg/L and 1.78 mg/L. Current density was varied from 5 - 15 $A/m^2$ using bipolar electrode connection. **Fig. 5.3** shows that with an increase in current density the fluoride removal increased. With the increase in current density, anodic oxidation occurs more instantaneously, which in turn aids in the formation of amorphous aluminium hydroxides species sufficiently in the vicinity of the electrode as well as in the bulk resulting in the formation of a fine gelatinous film on the electrode surface. Fluoride ions present in the solution interacted at the vicinity of anode and formed a complex. For an initial fluoride concentration of 1.78 mg/L the concentrations reduced to 0.0097, 0.014 and 0.073 mg/L. for current densities 15, 10 and 5 A/m2, respectively at the end of 20 min.

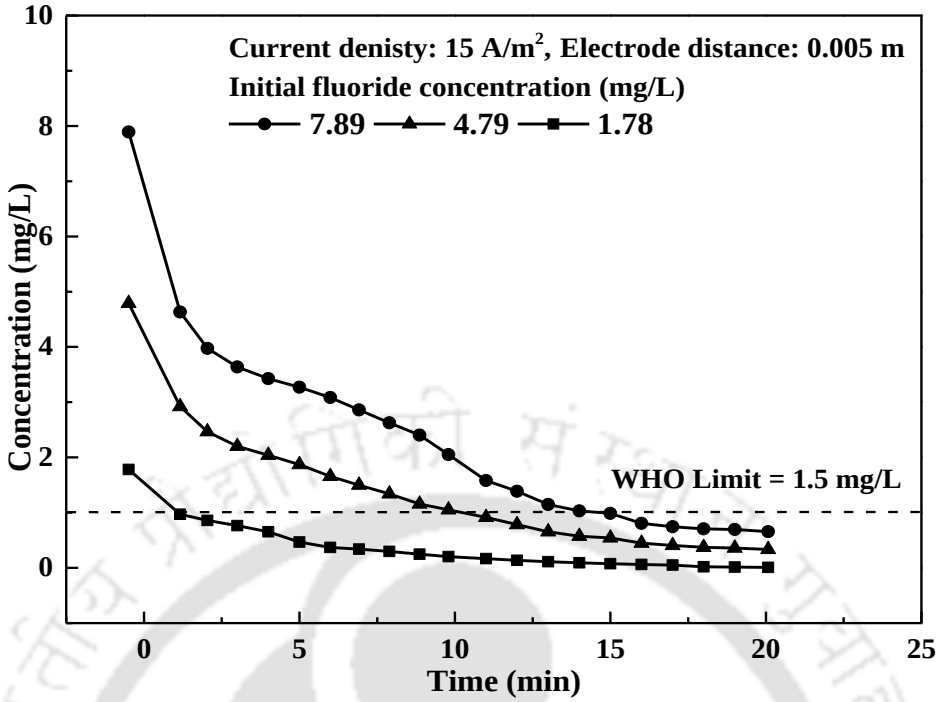


**Fig. 5.2: Effect on removal of fluoride at different initial concentration**

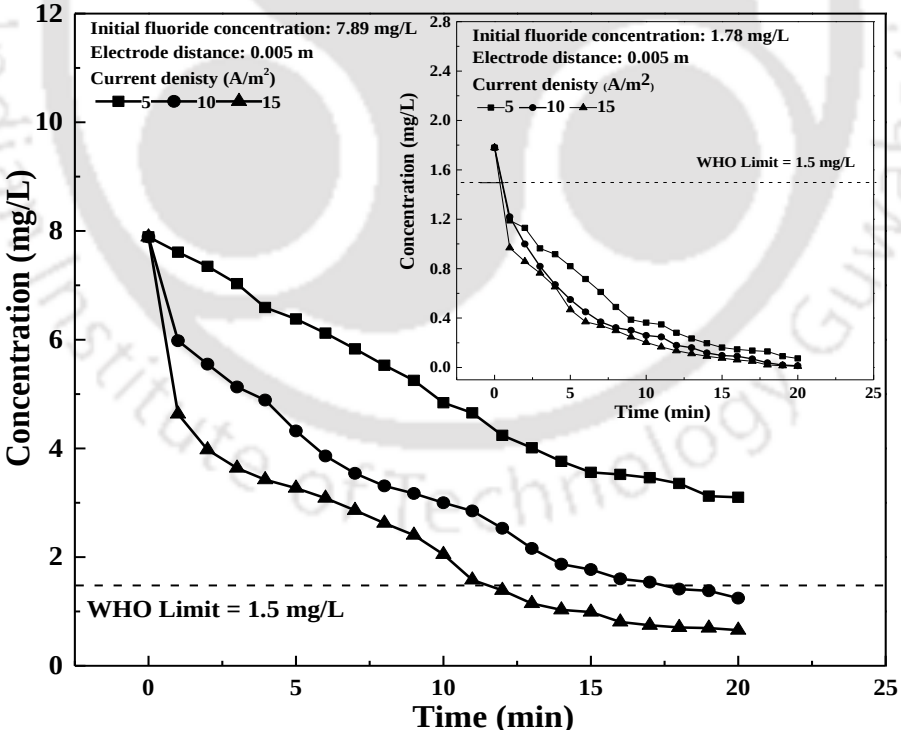


**Fig. 5.3**: **Effect on removal of fluoride with varying current density**

Similarly, for an initial fluoride concentration of 7.89 mg/L the concentrations reduced to 0.656, 1.245 and 3.1 mg/L for current densities 15, 10 and 5 A/$m^2$, respectively.

### 5.2.3 Effect of pH

The pH of a solution is an important parameter that needs to be considered for the removal of fluoride by electrocoagulation. **Fig. 5.4** shows the effect of initial pH on the removal of fluoride during electrocoagulation for the water sample having a fluoride concentration of 7.89 mg/L. The removal of fluoride depends on initial pH and increase of pH during electrocoagulation. In aqueous solution fluoride is present in HF and $F^-$ form. Speciation of fluoride will change with pH of solution and redox potential. Similarly, changes will be seen for the aluminum ion. The final concentration of fluoride in the solution for pH = 3.89 was 0.71 mg/L whereas the water in its normal pH = 7.9 had a fluoride concentration of 0.43 mg/L. As evident, the uptake of fluoride in acidic medium was higher suggesting that apart from adsorption, sweep coagulation and coprecipitation are also responsible for the removal of fluoride. Freshly formed $Al(OH)_3$ has very less solubility and gets polymerized to $Al_n(OH)_{3n}$, resulting into dense flocks with large surface area thereby aiding the removal of fluoride. Above pH 9, the soluble species $Al(OH)_4^-$ and $AlO_2^-$ are the predominant species thereby decreasing the removal of fluoride [133] . As seen from the **Fig. 5.4,** a concentration of 1.07 mg/L was observed at higher pH of 11.8.

**Figure 5.4 (inset)** shows the change in pH value as electrocoagulation proceeded. Studies were done for a fluoride concentration of 7.89 mg/L at three different current densities of 5, 10 and 15 A/$m^2$. From the **Figure 5.4 (inset)** it seems that variation of pH with time remains unaltered. However, marginal increase in pH was observed with at higher current density. This was due to the fact that higher current density favors more formation of hydroxyl ions than that of lower one.

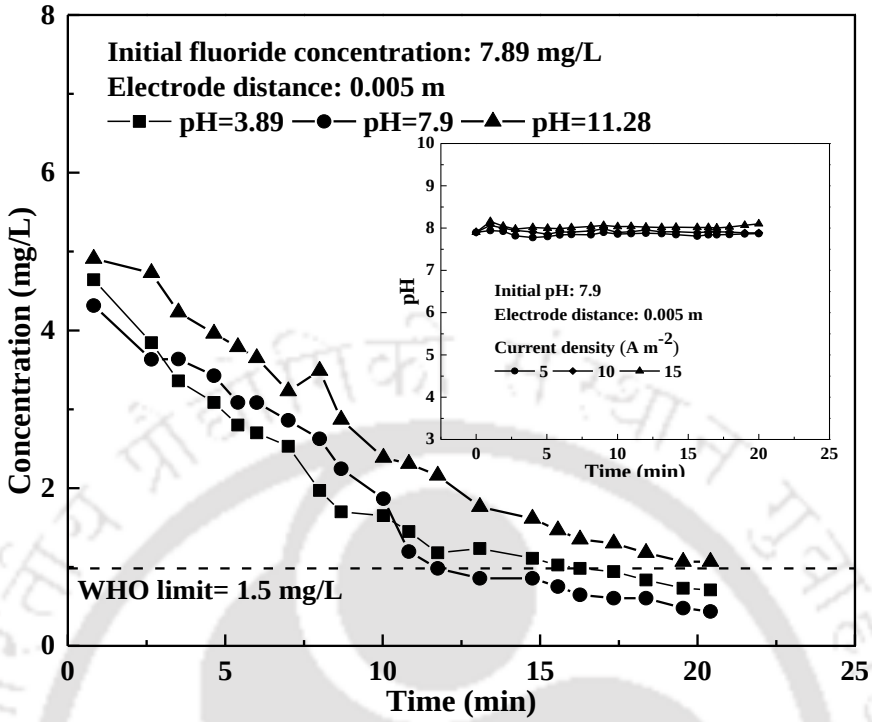


**Fig. 5.4: Effect on removal of fluoride with varying initial pH values**

## 5.3 Electrode corrosion and variation of film thickness

Due to the application of potential across the electrodes oxidation of the anode occurs which results in the corrosion of the electrode during electrocoagulation. Studies on the corrosion of electrodes helps to know about the expenditure associated with the EC process and also gives an overall idea on the lifetime of the electrode material. Corrosion of the electrodes can be defined as the weight loss (mg) of the electrodes due to anodic oxidation. As seen from **Fig. 5.5a**, corrosion of the electrodes increased at high fluoride concentrations and high current densities. This was due to the increased dissolution of the electrodes. A maximum corrosion of 5.21, 5.85 and 6.47 mg was observed for the water with fluoride concentrations of 1.46, 4.79 and 7.89 mg/L respectively, at a current density of 15 A/m$^2$.

During the electrocoagulation process a gelatinous hydroxide species is produced due to the anodic oxidation. This gelatinous hydroxide sticks to the surface of the electrode and grows with increasing electrocoagulation time. This hydroxide adhered to the membrane surface in the form of a film thereby creating an additional barrier during the electrocoagulation process. Hence, the thickness of this film has to be taken into account during the process operation. Film thickness can be presented by the equation [133].

$$t = \frac{m_1 - m_2}{\rho \times A} \times 10^{-6} \qquad 5.6$$

Where, t = Film-thickness, µm

$m_1$ = Weight of the electrodes immediately after the electrocoagulation experiment, mg

$m_2$ = Weight of the electrodes after the electrocoagulation experiment after cleaning, mg

ρ = Density of the film formed over the electrode surface, g/L

A = Area of the electrodes, $m^2$

**Fig. 5.5 b** shows the change of film-thickness over the electrode surface at different current densities for an initial fluoride concentrations of 1.78, 4.79 and 7.89 mg/L. It was seen that, film-thickness increased from 0.206 - 0.305 µm, 0.267 - 0.325 µm and 0.308 - 0.355 µm respectively for the initial fluoride concentrations of 1.78, 4.79 and 7.89 mg/L respectively, with an increase in current density from 5 to 15 $A/m^2$. An increase in the current density enhanced the anodic oxidation which caused an increase in the production off gelatinous hydroxide. This hydroxide in turn attached itself to the electrode surface as a film and this film thickness increased with increasing electrocoagulation time.

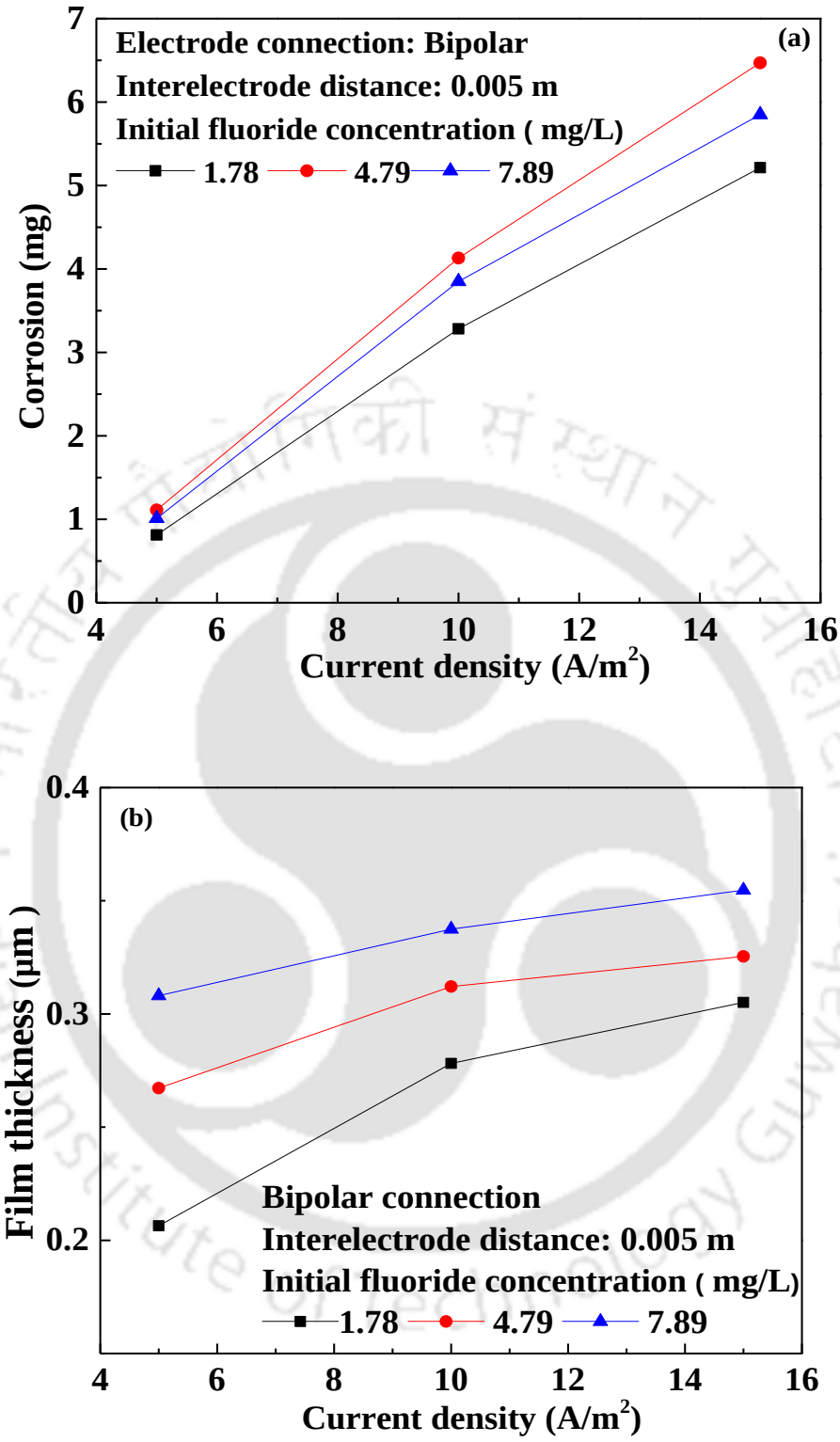


**Fig. 5.5: (a) Corrosion over electrode surface with different current densities (b) Variation of film-thickness**

## 5.4 Estimation of energy consumption and operating cost

Feasibility of the electrocoagulation process depends on the total cost incurred during the operation of the entire treatment process. Operating cost mainly includes cost of electrode, chemical, electricity, sludge disposal and fixed cost. For simplicity, this study includes the electrode material cost and electricity charges for determining operating cost of this EC process [133]. Operating cost can be expressed as

$$\text{Operating cost} = p \times C_{Electrode} + q \times C_{Energy} \quad 5.6$$

Where, $C_{Electrode}$ and $C_{Energy}$ are consumption quantities of electrode material and electricity required for fluoride removal. ‘‘p” is the price of electrical energy (0.0936 US$/kW. h) and ‘‘q” the price of electrode material (2.0466 US$/kg of Al) for the state of Assam as on August 2017. Cost due to electrical energy, $C_{Energy}$ is given as

$$C_{Energy} = \frac{Vi \times I \times t}{V_L} \quad 5.7$$

Where, V is the applied voltage ($V_i$), I is the current (A), t is the time (s) and $V_L$ is the volume of drinking water used for electrocoagulation ($m^3$). Cost for electrode was calculated from the Faraday’s law as

$$C_{Electrode} = \frac{I \times t \times M_w}{z \times F \times V_L} \quad 5.8$$

Where, I is the current (A), t is the electrolysis time (s), $M_w$ is the molecular mass of Aluminium (26.98 g/mol), z is the number of electron transferred (z = 3), F is the Faraday’s constant (96487 C/mol) and $V_L$ is the volume ($m^3$) of EC solution.

**Fig. 5.6** shows the variation of operating costs at different current densities for an initial fluoride concentrations of 1.78 mg/L at the end of 20 min of EC operation. With increased current density, energy cost increased due to higher energy consumptions. Similarly, electrode

cost increased at high current densities due to more dissolution of electrode into the solution. Total operating costs were found to increase as 0.00736 US$/m$^3$, 0.01644 US$/m$^3$ and 0.027 US$/m$^3$ with increasing current densities of 5 A/m$^2$, 10 A/m$^2$ and 15 A/m$^2$, respectively.

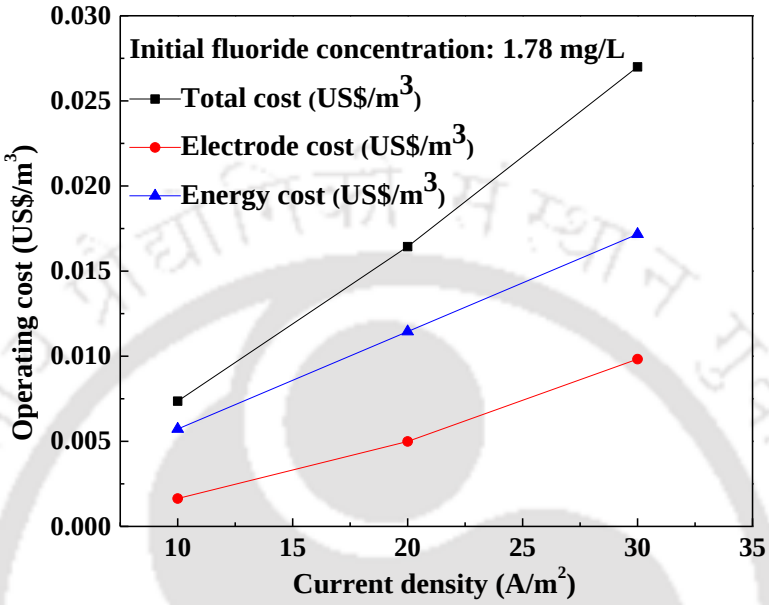


**Fig. 5.6: Cost for the treatment of drinking water containing fluoride of 1.78 mg/L at different current densities, interelectrode distance 0.005 m; duration of the experiment: 20 min; temperature: 25 ºC.**

### 5.5 Characterization of membrane (before and after operation)

FESEM analysis of the membranes before filtration suggested that the pore size of 0.06 µm, 1. 26 µm and 18 µm for the polymer - nanoparticle coated ceramic membrane (PNM), polymer coated

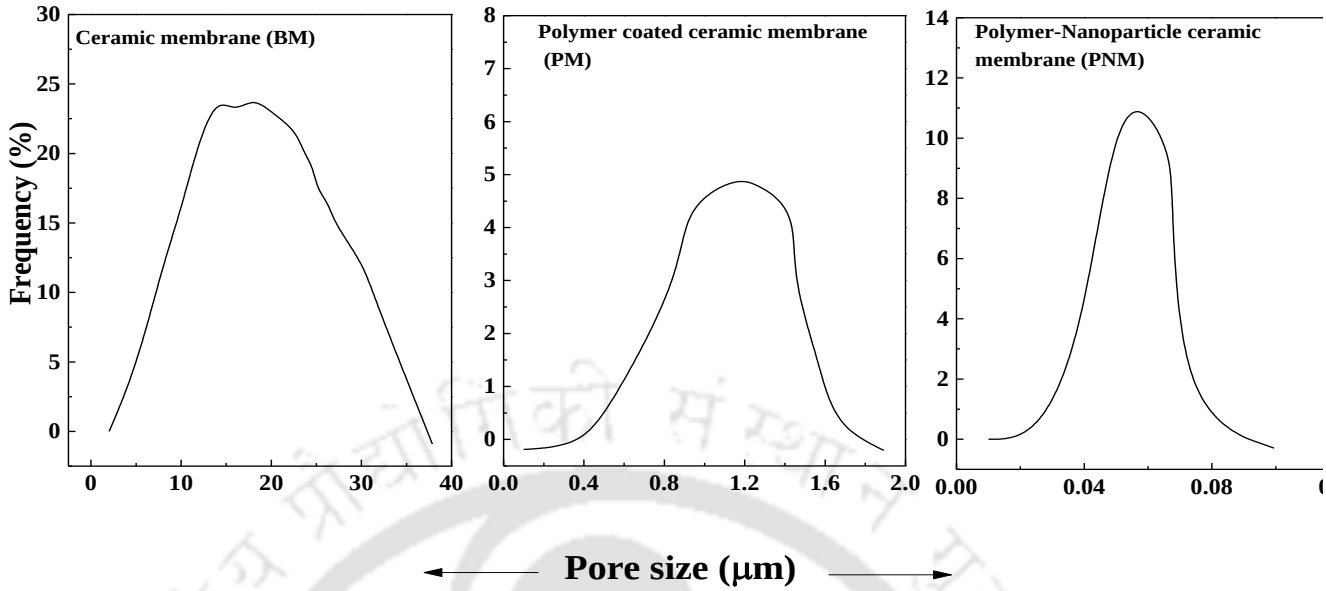


**Fig. 5.7: Pore size distribution of the prepared membranes**

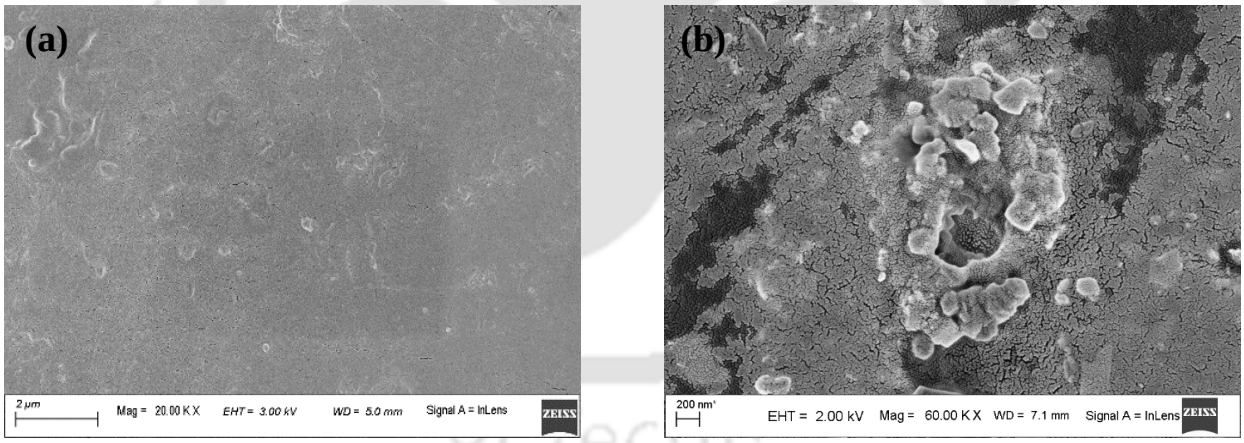


**Fig. 5.8: FESEM images of (a) polymer-nanoparticle coated ceramic membrane before filtration (b) polymer-nanoparticle coated ceramic membrane after filtration**

ceramic membrane (PM) and bare ceramic membrane (BM) respectively **Fig. 5.7 (a, b, c).** Flocks size ranged from 0.4 - 10.08 µm hence the nanoparticle-polymer coated ceramic membrane was used for carrying out the filtration process. **Fig. 5.8 (a, b)** showed changed morphology of the used membrane clarifying the successful retention of agglomerated flocks generated during electrocoagulation process. As seen from the figure 5.8 a, the surface of the membrane had visible pores before microfiltration, however, after the microfiltration of the electrocoagulated water, a layer of flocks generated during the treatment process deposited on the membrane surface.

## 5.6 Filtration of flocks

The flocks produced during the electrocoagulation treatment were analyzed using Delsa nano size analyzer to know about the particle size distribution of the suspended flocks generated at current densities of 5 $A/m^2$, 10 $A/m^2$ and 15 $A/m^2$ for initial fluoride concentrations of 1.78 mg/L and 7.89 mg/L at the end of 20 min EC operation. As seen from **Figs. 5.9a and 5.9b**, the amount of flocks produced during electrocoagulation process increased with increasing fluoride concentration and current densities. Flocks size ranged from 0.4-10.08 µm and 3.44 - 13.27 µm for initial fluoride concentrations of 1.78 mg/L and 7.89 mg/L, respectively. The larger particles in the range of 1-13 µm may agglomerate and settle down after 30 min but it is quite difficult to settle the smaller particles (<1 µm) even after 12 h [162, 163].

Electrocoagulation process treats the contaminated drinking water and successfully removes the unwanted fluoride however, the quality of water obtained was found to be unfit for consumption. The main reason being the presence of the suspended flocks in water. A favourable and easy method to make this electrocoagulated water fit for consumption purpose would be to remove these suspended flocks by filtration process using indigenously prepared membranes as discussed in **section 3.2** of **Chapter 3**.

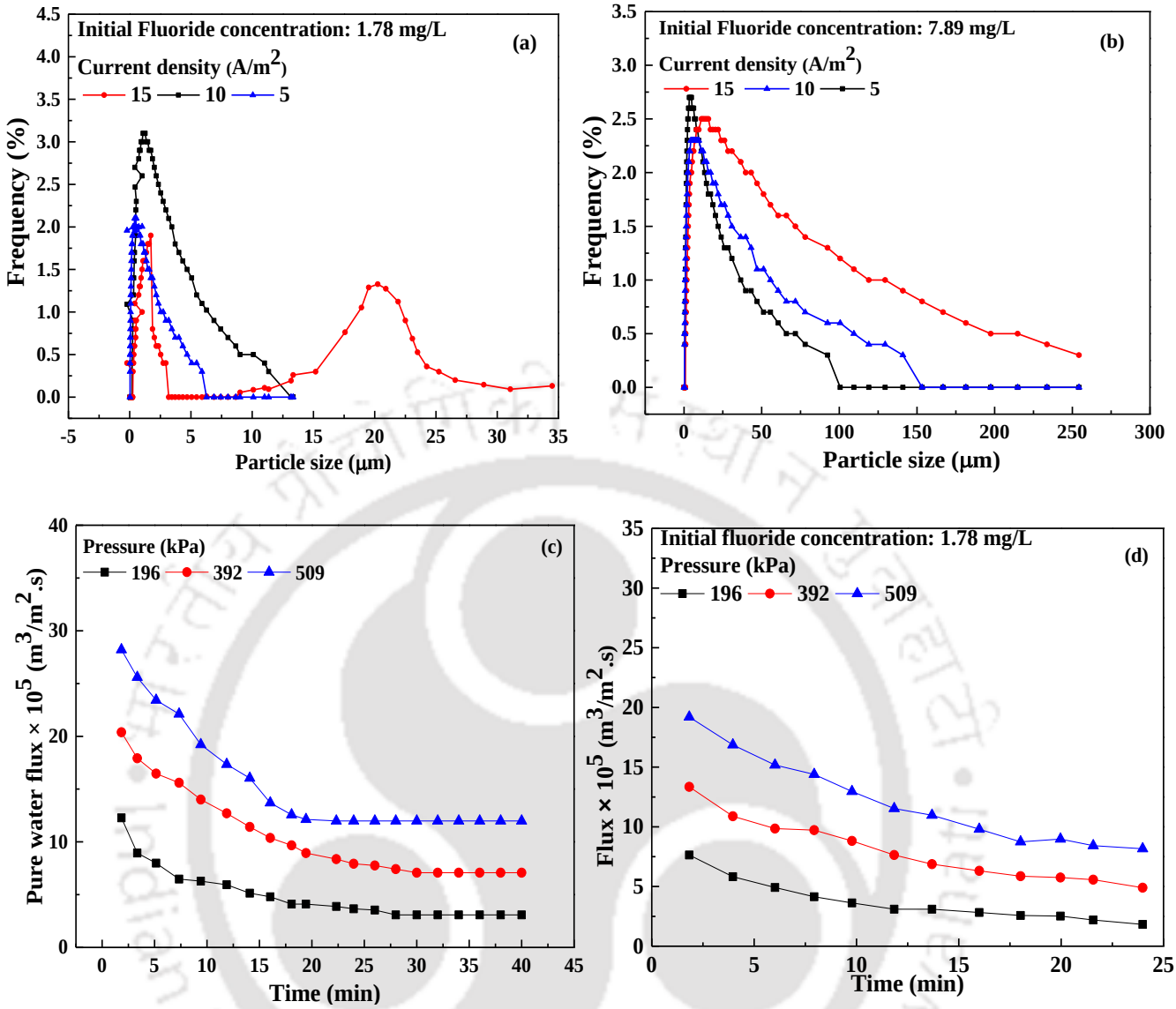


**Fig. 5.9: Particle size distribution of flocks generated during electrocoagulation for an initial concentration of (a) 1.78 mg/L (b) 7.89 mg/L (c) Pure water flux profile (d) Flux declination profile during microfiltration**

Pore size distribution of membranes were determined using the imageJ software. The pore size were found to be 0.06 µm, 1. 26 µm and 18 µm for the polymer-nanoparticle coated ceramic membrane (PNM), polymer coated ceramic membrane (PM) and bare ceramic membrane (BM) respectively as discussed in **section 5.5**. Hence, the nanoparticle-polymer coated ceramic membrane was utilized for further filtration process as we had flocks in the size range of 0.4 µm. A cross flow filtration setup was used to study the batch microfiltration experiments is shown in **Chapter 2**. A beaker was placed on a weighing balance to collect the permeate solution which was used to quantify the weight of the permeate after definite time intervals A batch of 1L was used to carry out the study. The pure water flux was determined at three different pressures of 196, 392 and 509 kPa **(Fig. 5.6c).** The applied pressure was controlled by utilizing the adjustable valves. For every pressure, the amount of water collected through the membrane at a definite interval of time was measured. The flux studies suggested that the permeate flux declined with time for the given operating pressure differentials **(Fig. 5.6d)**. Filtration studies suggested a decrease in flux from $7.8 \times 10^{-5}$ to $1.8 \times 10^{-5}$ $m^3/m^2.s$, $13.35 \times 10^{-5}$ to $4.9 \times 10^{-5}$ $m^3/m^2.s$ and $19.19 \times 10^{-5}$ to $8.16 \times 10^{-5}$ $m^3/m^2.s$ when the pressure increased from 196, 392 and 509 kPa respectively. As evident flux declination was more at higher pressure differentials. The decrease in flux with time was due to the deposition of suspended flocks on the surface of the membrane which blocked the active pores of the membranes. The membranes were washed after 3 runs to remove the attached flocks from the membrane surface.

### 5.7 Flocks characterization

The white precipitate formed during the electrocoagulation process was taken out after filtration for further characterization to ensure the removal of fluoride. The collected flock were taken in a petridish and dried in a hot air oven for 12 h to remove moisture. The dried flocks obtained were grinded and then analyzed using FTIR and EDX.

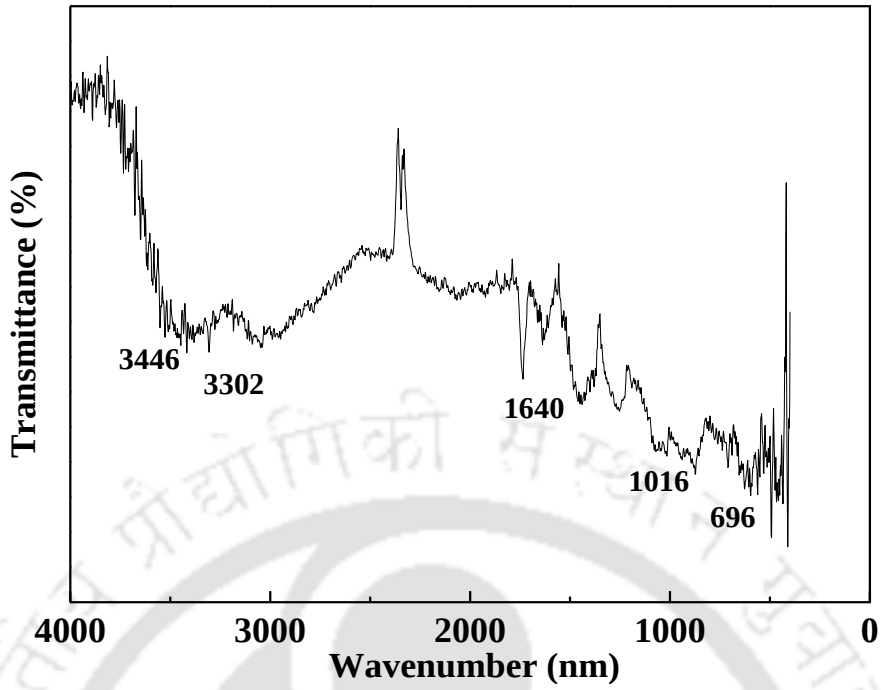


**Fig. 5.10: FT-IR spectra of the electro coagulated sludge left behind after filtration**

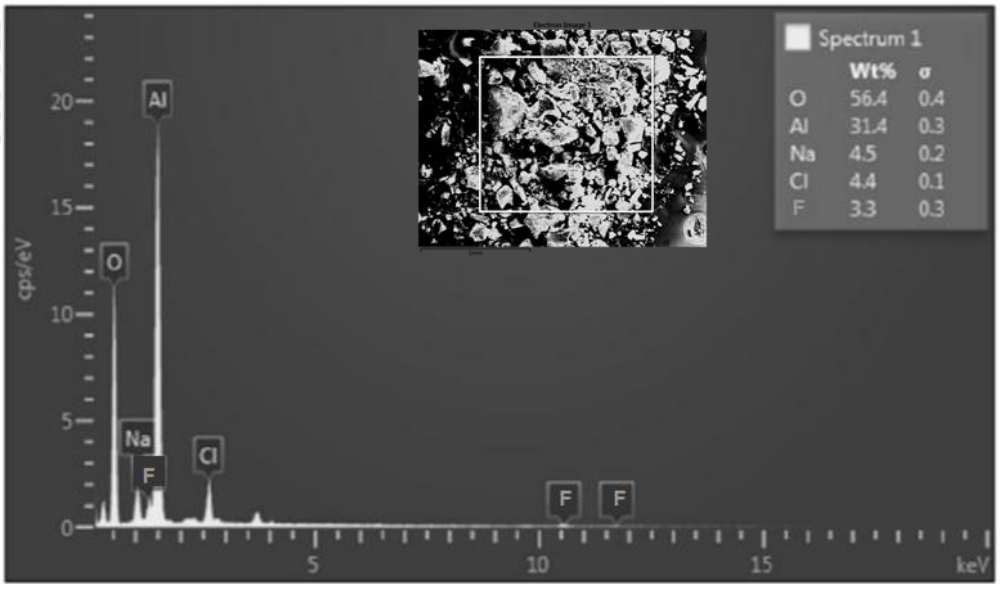


**Fig. 5.11: EDX spectra of the electro coagulated sludge left behind after filtration**

FTIR analysis was performed with wave numbers ranging from 4000 to 450 $cm^{-1}$ (**Fig. 5.10**). Peaks at 3446, 1020 and 609 $cm^{-1}$ corresponding to H–O–H, Al–O and Al–F–Al bond stretching, respectively. Peaks at 878 $cm^{-1}$ corresponded to Fe-O which confirmed the presence of fluoride complexes precipitated at the bottom of the EC tank. The EDX (**Fig. 5.11**) analysis provides a qualitative insight about the elements present in the flock and indicated the presence of elements like fluoride, aluminium, sodium, chloride and carbon. The presence of aluminum and carbon are mainly due to the formation of aluminum hydroxide complex and carbon black tape Sodium and chlorine presence were due to the NaCl used as a conducting medium during the electrocoagulation process. The presence of fluoride in the flocks suggested the successful removal by electrocoagulation process.

### 4.8 Quality of electrocoagulated and filtered water

The quality of the electrocoagulated water and the filtrate obtained after membrane filtration were analyzed. The water quality parameters were measured in terms of pH, conductivity, TDS, turbidity and dissolved oxygen for the initial fluoride concentration of 7.89 mg/L and shown in **Table 5.2**. Observations from **Table 5.2** suggested that electrocoagulated samples were not fit for drinking purpose. The properties such as pH, conductivity, TDS, turbidity and D.O. had values of 8.10 - 7.87, 6.06 - 4.40 mS/cm, 1310 - 500 mg/L, 12 - 7.6 NTU and 26.1 - 12.3 mg/L respectively. However, after filtration, the treated water quality obeyed the drinking water specification with pH, conductivity, TDS, turbidity and D.O. had values of 8.05 - 7.08, 2.94 - 1.50 mS/cm, 600 - 421 mg/L, 0.8 - 0.2 NTU and 14.3 - 6.5 mg/L respectively. Similarly, water samples with varying initial

**Table 5.2: Quality of electrocoagulated solution and permeate of membrane filtration**

| **Parameters** | **Electrocoagulated water** | | | **Filtered water** | | | |
|---|---|---|---|---|---|---|---|
| **Current density ($A/m^2$)** | **15** | **10** | **5** | **15** | **10** | **5** | **Drinking water limits, WHO [134]** |
| pH | 8.10 | 7.88 | 7.87 | 8.05 | 7.16 | 7.08 | 6.5-8.2 |
| Conductivity (mS/cm) | 6.06 | 5.21 | 4.40 | 2.94 | 2.60 | 1.50 | 0.2 -2.0 |
| TDS (mg/L) | 1310 | 741 | 500 | 600 | 550 | 421 | 500-700 |
| Turbidity ( NTU) | 12 | 9.6 | 7.6 | 0.8 | 0.5 | 0.2 | 1 |
| D.O (mg/L) | 26.1 | 15.1 | 12.3 | 14.3 | 14.6 | 6.5 | 0-15 |
| **Initial pH** | **3.86** | **7.9** | **11.28** | **3.86** | **7.9** | **11.28** | **Drinking water limits, WHO [134]** |
| pH | 8.05 | 8.6 | 10.22 | 7.9 | 7.2 | 8.07 | 6.5-8.2 |
| Conductivity (mS/cm) | 5.7 | 5.21 | 6 | 4.94 | 2.6 | 4.87 | 0.2 -2.0 |
| TDS (mg/L) | 2850 | 2741 | 3080 | 800 | 600 | 781 | 500-700 |
| Turbidity ( NTU) | 15.87 | 9.6 | 9.1 | 0.6 | 0.5 | 0.45 | 1 |
| D.O (mg/L) | 18.1 | 15.1 | 13.3 | 10 | 14.6 | 15 | 0-15 |

pH values of 3.86, 7.9 and 11.28 were also found to have drinking water specifications after filtration. Membrane processes such as dialysis, nanofiltration and reverse osmosis have been reported which successfully lowered the levels of fluoride to 0.2 mg/L [143, 153, 156]. Coagulation and precipitation process like the Nalgonda technique lowered the fluoride limits to 1 mg/L [154, 155]. Ion exchange and electrocoagulation techniques have also been used. However, the present work reduced fluoride to very low concentrations of 0.009 mg/L.

**Table 5.3: Comparative table showing fluoride removal for various techniques**

| Technique | Initial Concentration (mg/L) | Final Concentration (mg/L) | Reference |
|---|---|---|---|
| **Membrane process** | | | |
| Reverse Osmosis | 17 | 0.2 | [156] |
| Electro-Dialysis | 20.6 | 0.8 | [153] |
| Dialysis | >30 | 1.5 | [143] |
| **Coagulation and precipitation** | | | |
| Nalgonda technique (Large scale, Community level and Household level) | 1.5-20 | 1-1.8 | [155] [154] |
| **Ion-exchange process** | | | |
| Organic-inorganic type | 1.96 | 3 | [158] |
| **Electrocoagulation process** | | | |
| Al electrode and NaCl conducting agent | 15 | 2 | [157] |
| Al electrode and NaCl conducting agent | 2-10 | 1 | [31] |
| **Al electrode and NaCl conducting agent** | **1.49-7.89** | **0.009** | **Present work** |

# Chapter 6

# Treatment of drilling effluent using electrocoagulation followed by microfiltration

# Treatment of drilling effluent using electrocoagulation followed by microfiltration

*This chapter presents the application of the fabricated ceramic membrane for the microfiltration of electro coagulated drilling fluids for the removal of oil, grease and other heavy metals. Drilling effluent containing oil, grease along with metals like Na, Cr, Cu, Pb and Ni were pre-treated using the electrocoagulation technique followed by dead end microfiltration through an indigenously prepared ceramic membrane. Pre-treatment involved varying the working parameters such as current density (20 - 80 A/m$^2$), electrode distance (0.005 - 0.2 m) and initial pH (3.6 - 8.7). Microfiltration was carried out to remove the flocks from the electrocoagulated water at three different pressures of 98,196 and 194 kPa. Flux declination ratio and flux recovery ratio were also determined. In addition to a detailed characterization, studies were also done on the corrosion and operating costs of the electrocoagulation process to investigate the power consumption and electrode material consumption at different operating conditions.*

## 6.1 Experimental

### 6.1.1 Materials and methods

Effluent water from the drilling site of Barekuri, Oil India Limited (OIL) was collected on 29$^{th}$ August, 2017. The obtained sample was from a drilling location TAU having a well depth of 3364 m. Obtained effluent samples had very high quantity of suspended solids, TDS, sulphates, chlorides, COD and BOD. The oil and grease content was around 35 mg/L. The initial concentration of all the components of the feed was determined and reported in **section 6.5**.

### 6.1.2 Measurement and analysis

The concentration of oil and grease in the effluent after EC treatment was determined using UV-Vis spectrophotometer (Make: Perkin Elmer). The quality of the treated effluent after electrocoagulation and microfiltration were studied in terms of turbidity, conductivity, salinity, TDS, D.O and pH using a water analysis kit (Make: VSI electronics pvt. Ltd.). Characterization on the produced flocks during EC process and the membrane used for microfiltration were done using EDX (Make: Leo), FESEM (Make: Leo) and Delsa Nano (Make: Beckman Coulter).

### 6.1.3 Membrane preparation

The basic membrane preparation technique has already been discussed in **Section 2.1.3** of **Chapter 2,** however the sintering temperature has been varied in this particular study to obtain four membranes at different sintering temperature. Fly ash obtained from NTPC was mixed with sodium carbonate, boric acid, sodium metasilicate and alumina using a mortar and pastel. The obtained mixture was mixed with a definite amount of Millipore and casted on an MS ring to form disk shaped membranes. This membrane was then removed from the MS ring very carefully and the placed in a hot air oven at a temperature of 110 $^{o}$C to remove the water and excess moisture content for 12 h. The dried membrane was then sintered at three different temperatures of 700, 800, 900 and 1000 $^{o}$C for 12 h. The obtained membranes were then polishes and washed before being used for microfiltration studies.

### 6.1.4 Electrocoagulation bath

The collected effluent from OIL was pre-treated using electrocoagulation before being filtered using a ceramic membrane. The basic pre-treatment method using electrocoagulation has already been discussed in **section 5.1.4**. The set up consisted a rectangular box of dimensions 0.23 m × 0.08 m × 0.04 m with a holding capacity of 600 ml. Aluminium sheets of dimension 0.07 m × 0.77 m × 0.001 m with an inter-electrode distance of 0.005 m were used as the electrode which were connected to a direct current power source. The EC process was carried out maintain various operating parameters to study the removal of oil and grease during the electrocoagulation process. Thus, EC was carried out by varying the parameters such as current density, electrode distance and initial pH.

### 6.1.5 Oil removal mechanism by electrocoagulation

Electrocoagulation (EC) process utilizes the benefits of flocculation and coagulation for the removal of oil and grease from water. The process involves the usage of Al electrodes which when under the influence of a potential difference results in the generation of flocculating species from the anode. Freshly formed amorphous Al(OH)$_3$ "sweep flocs" have large surface areas which is beneficial for a rapid adsorption of soluble organic compounds and trapping of colloidal particles The hydrogen and oxygen gas produced during the EC process further aids in the removal of oil and grease from aqueous solutions [181, 182].

## 6.2 Results and discussion

### 6.2.1 Effect of current density, electrode distance and initial pH on removal of oil and grease

Three important parameters i.e. current density (20 - 80 A/m$^2$), electrode distance (0.005 - 0.02 m) and initial pH (3.6 - 8.7) were considered when studying the removal of oil and grease from effluent water. All the varying parameters were studied experimentally for an operating time period of 20 min. During the EC process flocks are produced due to anodic oxidation which helps in the capturing of oil and grease from the aqueous solution. Thus more is the current density, more flocks will be produced and hence more removal of oil and grease will be observed. As seen from the **Figure 6.1a**, with an increase in current density as 20, 50 and 80 A/m$^2$ the final concentration of oil in the effluent reduced to 29.3, 27.9 and 26.86 mg/L respectively, from an initial concentration of 35 mg/L. More is the applied current density, more is the anodic oxidation resulting in the dissolution of the sacrificial anode facilitating the production of aluminium hydroxide flocks which aid in the removal of oil from effluent [181, 182].

Electrode distance also plays an important role in the removal of oil and grease from effluent water. The more is the distance in between the electrodes, more is the current required to produce aluminium hydroxide responsible for the removal of oil from effluent. **Figure 6.1b** shows the effect of varying electrode distance with a constant current density of 80 A/m$^2$ and a constant operating time of 20 min. At the same current density, the least flocks would be produced by the highest electrode distance which is well explained in the figure. The removal of oil is not much effected when the electrode distance was increased from 0.005 to 0.02 m, as the concentrations were reported to differ by a mere 0.64 mg/L [187, 188].

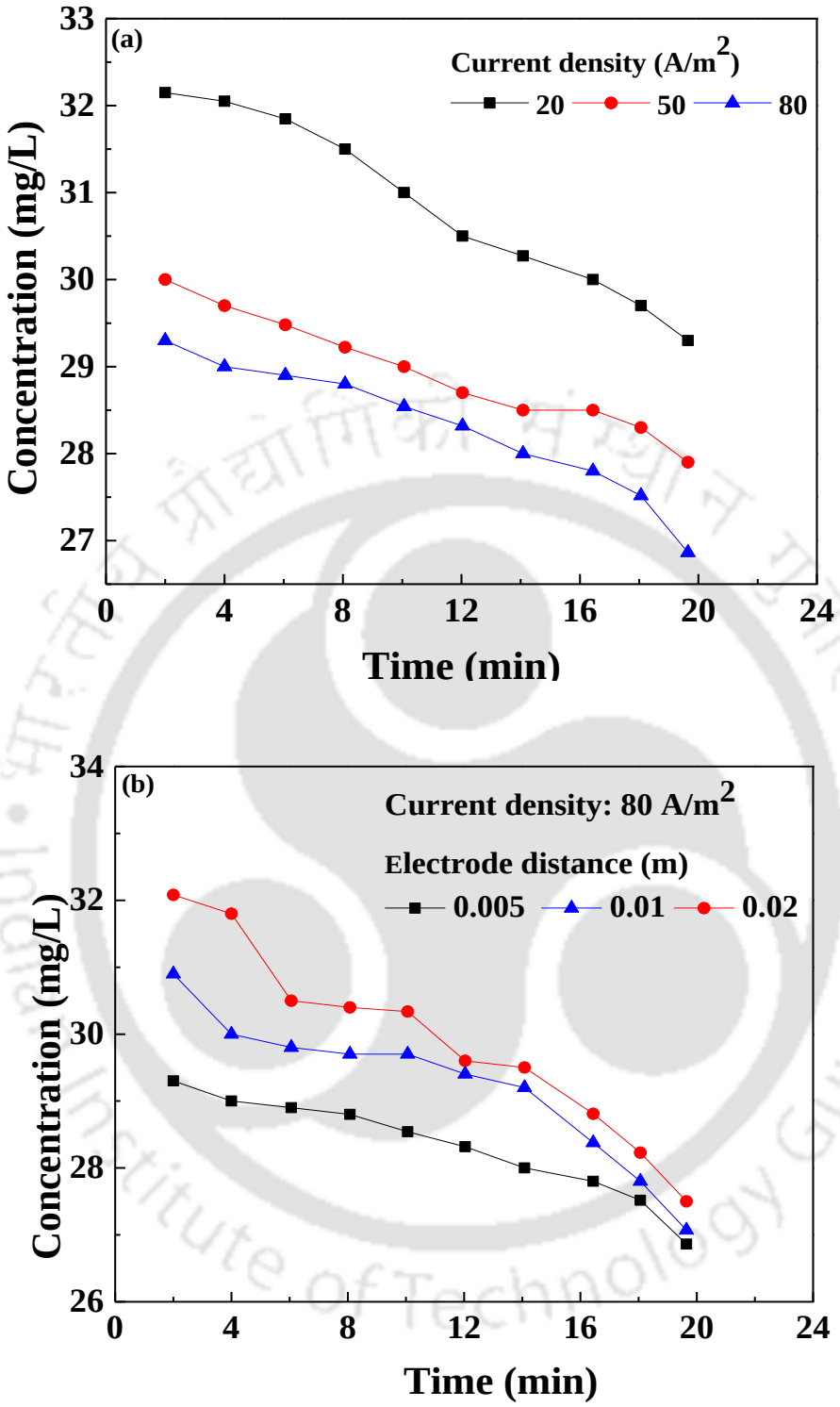

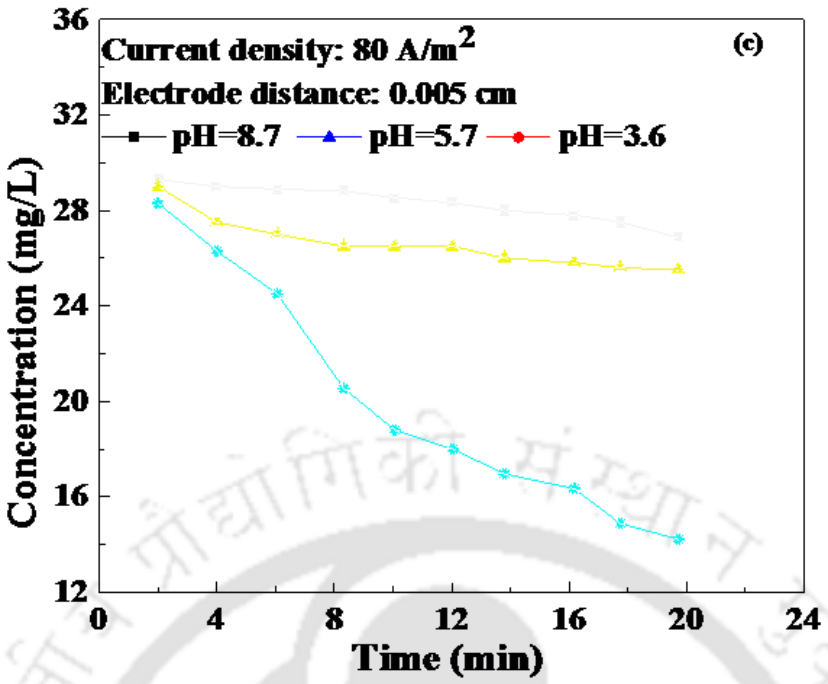


**Fig. 6.1: Variation of concentration with time at different operating parameters of (a) Current density (b) Electrode distance and (c) Initial pH**

pH plays a major role in the removal of contaminants from a solution. Two major pH related mechanisms have been suggested for removal performance during electrocoagulation process.

These interactions are precipitation and adsorption, each being suggested for a separate pH range. Flocculation in the low pH range is caused due to the precipitation of the hydroxides and the contaminants while at higher pH range (>6.5) adsorption is dominant. The abundant aluminum species are $Al^{3+}$, $Al(OH)_2^{2+}$and $Al(OH)^{2+}$ for a solution pH of 2 - 4 and for pH between 4-9 major species include $Al_{13}O_4(OH)_{24}^{7+}$ which get precipitated as $Al(OH)_3$ (s). For initial pH of 3.6, maximum removal was observed with a final residual concentration of 10.21 mg/L (**Fig. 6.1c**) [164].

### 6.2.2 Effect of current density, electrode distance and initial pH on removal of chlorides, TSS and sulphates

Studies were done to see the effect of current density, electrode distance and initial pH on the removal of chlorides, total suspended solids and sulphates present in the effluent water. As seen from **Figure 6.2a,** with an increase in current density (20 - 80 $A/m^2$) the concentration of chlorides reduced from 1374 mg/L to 1274.6 mg/. The concentration of chlorides increased to 1600 mg/L at acidic pH. Similarly, with increasing electrode distance the removal of chlorides were reduced due to the lesser production of hydroxides. Th

The amount of suspended solids however, increased from 150 - 250 mg/L with an increase in current density (20 - 80 $A/m^2$) due to more production of aluminium. Similar observations were made for changing pH values. At acidic pH the TSS concentration increased due to high flocculation by precipitation with a concentration of 630 mg/L whereas at basic pH the concentration was low. Increasing the electrode distance from 0.005 to 0.02 m resulted in the decrease in TSS from 283 to 225 mg/L **(Fig 6.2b**).

The sulphates concentration dropped to 18189 mg/L at acidic pH whereas it increased to 18218 at basic pH. Similar observations were made with electrode distance where increase in electrode distance from 0.005 to 0.02 m resulted in a decrease in removal of sulphates. Current density increase from 20 – 80 $A/m^2$, the concentration of sulphates decreased from 18245 mg/L to 18218 mg/L (**Fig. 6.2c**).

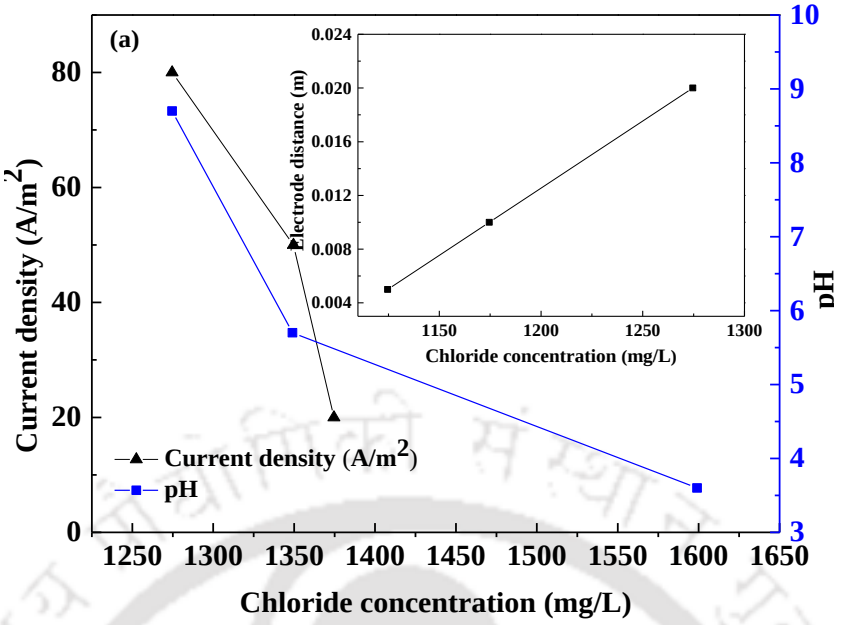


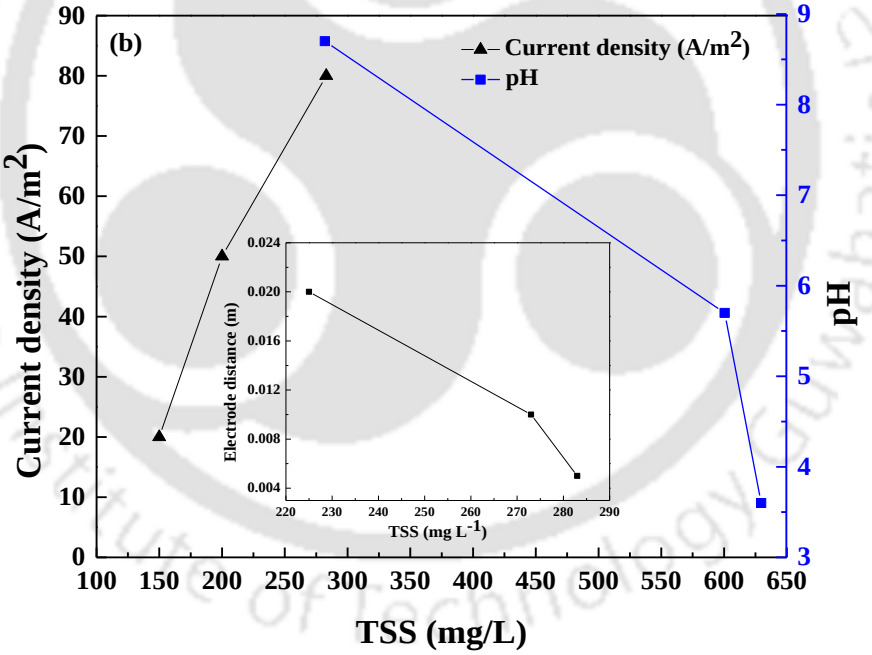

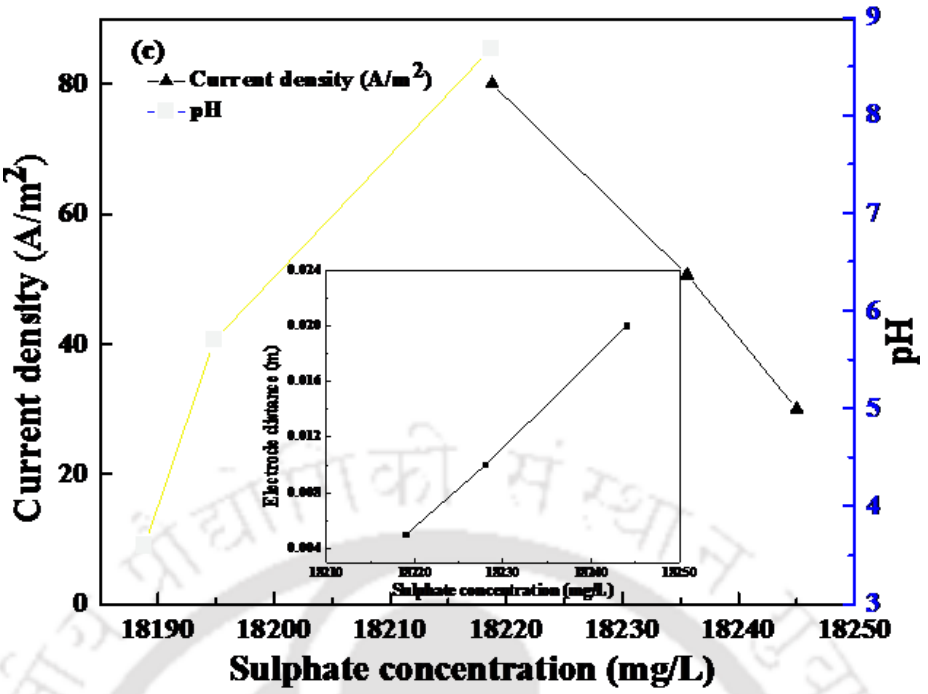


**Fig. 6.2: Effect of current density, pH and electrode distance on the (a) Chloride concentration (b) TSS and (c) Sulphate concentration**

### 6.2.3 Estimation of corrosion, film thickness, energy consumption and operating cost

In order to determine the lifetime of the electrocoagulation process it is necessary to carry out the corrosion studies on the used electrodes. As electrocoagulation proceeds, there will be a weight loss of the electrodes which shall determine the amount of corrosion the electrodes. It may be seen from the **Figure 6.3a** that with an increase in current density from 20 to 80 A/m$^2$ the corrosion increased from 24.5 to 71.11 mg. This is because of the fact that at higher current densities more anodic dissolution occurs thereby resulting in the weight loss of the electrodes. However, at increasing electrode distances the amount of corrosion of the electrodes reduced drastically. Low electrode distance of 0.005 m had corrosion of 71.11 mg whereas with an increase in electrode distance to 0.02 m, corrosion decreased to 37.6 mg.

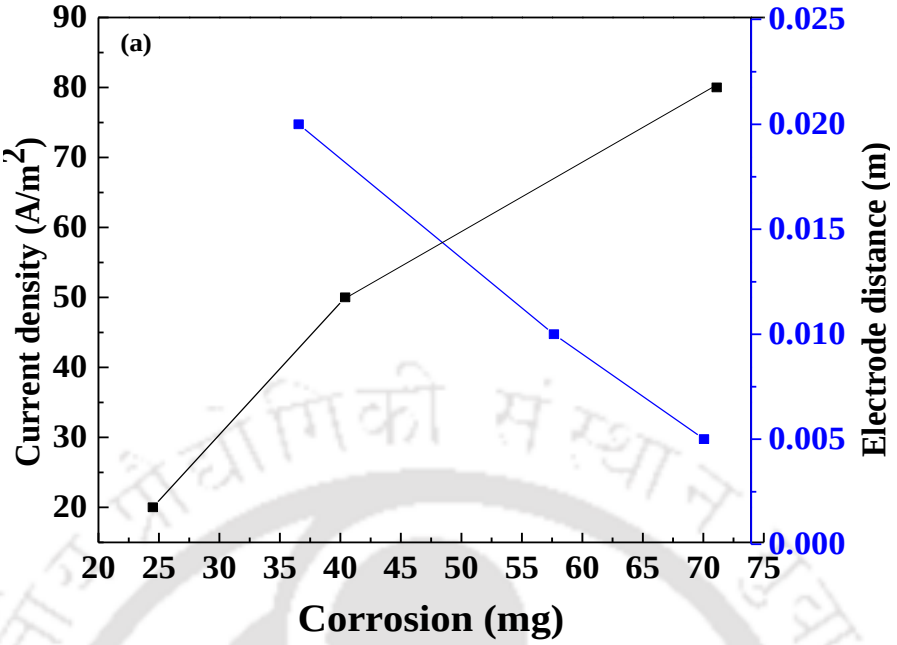


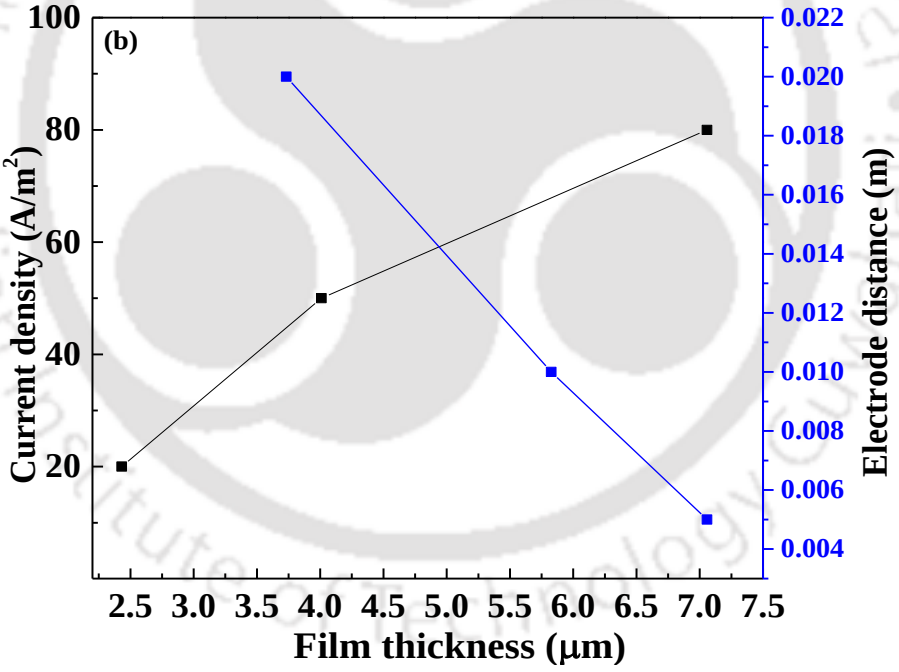

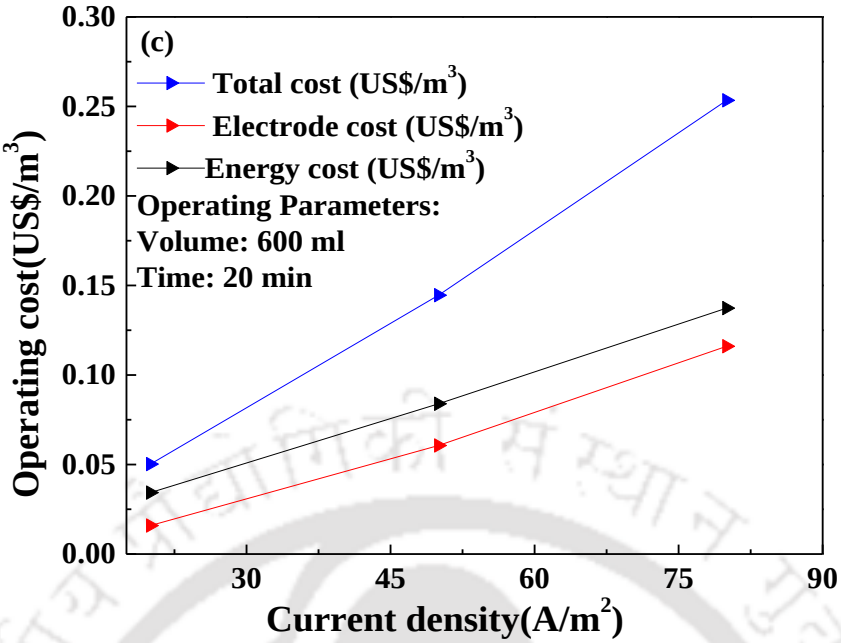


**Fig. 6.3: Effect of current density and electrode distance on (a) Corrosion (b) Film thickness and (c) Operating cost variation with current density**

During the EC process a gelatinous layer formed on the surface of the electrodes which forms an additional barrier towards the formation of aluminum hydroxide. The film thickness of this gelatinous layer formed over the electrode surface has already been mentioned in our previous work. The film thickness increased from 2.43 to 7.05 µm when the current density increased from 20 to 80 A/m$^2$. An increase in electrode distance resulted in low thickness of gel layer and a decrease in electrode distance resulted in a high gel layer thickness. Gel layer of thickness 7.05 and 3.73 µm were formed when electrode distance were maintained at 0.005 and 0.02 m, respectively (**Fig. 6.3b**).

**Figure 6.3c** shows the variation of operating costs at different current densities at the end of 20 min of EC operation for a working volume of 600 ml effluent. With increased current density energy cost increased due to higher energy consumptions. Calculation for the costs were done as per our previous work [191]. The cost of electricity consumptions and electrode material were taken as per their price in the year 2017 which were 0.0936

US$/Kwh and 2.046 US $/Kg of Al. As seen, the electrode cost and energy cost increases with increasing current density due to higher anodic oxidations and more energy consumptions. The total cost as a result increased from 0.0502 to 0.253 US$/$m^3$ when current density increased from 20 to 80 A/$m^2$.

### 6.3. Water permeation experiment

#### 6.3.1. Porosity

The porosity of the membranes prepared at 700, 800, 900 and 1000 $^oC$ were determined using the Archimedes's principle. The porosity can be determined using the following equation

$$P=\frac{M_c-M_d}{M_c-M_s}\times 100\ \% \qquad 6.1$$

Where, $M_c$ is the mass of the ceramic membrane saturated with water, $M_d$ is the dry mass of the ceramic membrane and $M_s$ is the mass of the suspended membrane taken at its dipping condition into water. The membranes were first weighed in air followed by suspending the membranes in water to measure the suspended weight .The membranes were then soaked in water for 24 h, removed from water and measured again for the soaked weight.

**Figure 6.4a** shows the variation of the bulk porosity with sintering temperature for the ceramic membranes prepared by paste method. As seen from the figure, it is evident that with an increase in sintering temperature, the porosity of the ceramic membrane decreased. A decrease from 55 % to 30.13 % was seen when the sintering temperature increased from 700 to 1000 $^oC$. This decrease in porosity is because of the fusion of the membrane constituents at higher temperatures. When the sintering temperature is increased more melting of the membrane constituents shall occur resulting in removal of the existing voids and thereby leading to structural densification.

### 6.3.2 Hydraulic permeability

Hydraulic permeability variation at different sintering temperatures were also determined. The hydraulic permeability was estimated by using the following equation

$$J_p = \frac{\varepsilon r^2 \Delta P}{8\mu l} = L_p \Delta P \qquad 6.2$$

Where, $J_p$ is the flux across the membrane in $m^3/m^2.s$, $\Delta P$ is the transmembrane pressure in kPa, $\varepsilon$ is the porosity of the ceramic membrane ($\varepsilon = n\pi r^2$), $\mu$ is the viscosity of water, $l$ is the length of the pore. As seen from **Fig. 6.4 (top inset)** the hydraulic permeability increased with an increase in the sintering temperature. The hydraulic permeability increased from 5.7 $\times 10^{-9}$ m/Pa.s to 2.47 $\times 10^{-8}$ m/Pa.s when the sintering temperature increased from 700 to 1000 $^oC$. This increase in the hydraulic permeability was because of the fact that with an increase in sintering temperature the pore size of the ceramic membranes increased resulting in a increase in the permeate flux of the ceramic membrane. The hydraulic permeability was also determined after microfiltration of electrocoagulated oil samples and it was found that the values decreased from 2.30 $\times 10^{-9}$ to 4.00$\times 10^{-9}$ m/Pa.s respectively, when the sintering temperature of the ceramic membrane increased from 700 to 1000 $^oC$. It was already reported in our previous work **Chapter 2**, that void spaces were created more when ceramic membranes were prepared by paste method. Also reports from FESEM analysis suggested that with an increase in sintering temperature, the size of the pores increased which has been discussed in details in the section below.

### 6.3.3 The average pore size

The average pore size of the ceramic membranes were determined using water permeation experiments and imageJ software for SEM analysis. For the water permeation experiments, the equation used for the determination of the pore size is as follows

$$r = \left(\frac{8\mu l L_p}{\epsilon}\right)^{0.5} \quad 6.3$$

Where, μ is the viscosity of water, $l$ is the length of the pore, $L_p$ is the hydraulic permeability and ε is the porosity of the membrane. **Figure 6.4 (bottom inset)** shows the variation of pore sizes with sintering temperature. As seen the pore size increases with an increase in sintering temperature. This is because of large voids created at higher temperatures due to burning off of CaO. The **Fig. 6.4 (bottom inset)** shows that the average pore size for both the methods of pore size determination agreed with the assumption. Pore size increased from 1.175 μm to 24.76 μm for temperature changes from 700 to 1000 $^{o}$C by imageJ software and from 0.72 μm to 1.87 μm for temperature changes from 700 to 1000 $^{o}$C for water permeation experiments. Moreover, the figure suggests that pore sizes obtained by imageJ software were considerably high from the water permeation experiments. This is because the software mainly determines pore size based on surface pore which may or may not extend throughout the entire membrane whereas the water permeation experiment considers the continuous pores that are involved in the microfiltration of permeate.

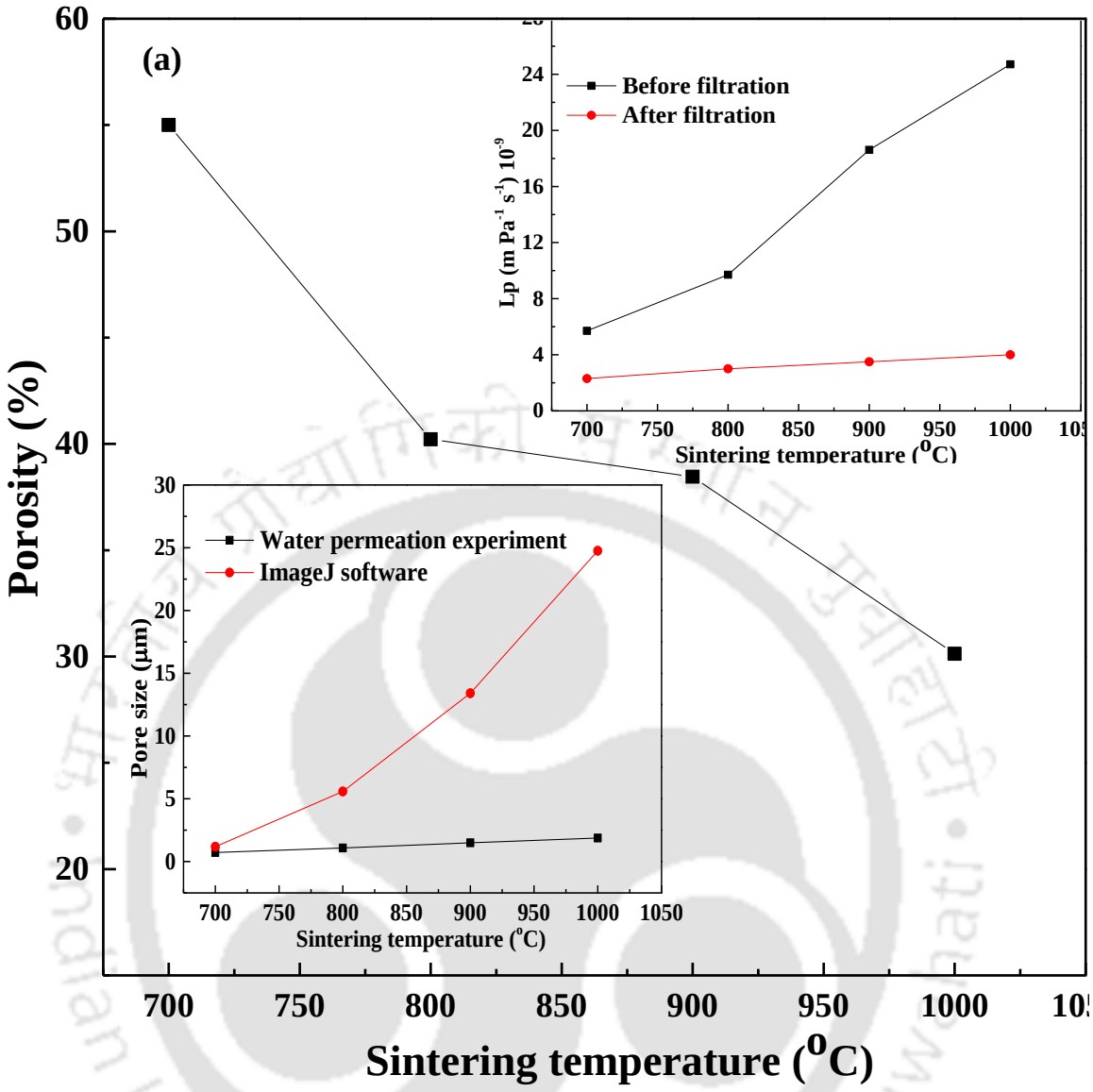


**Fig. 6.4: Porosity of membranes at different sintering temperatures, inset (top): Variation of hydraulic permeability (Lp) at various sintering temperatures, inset (bottom): Variation of average pore size obtained from FESEM images and water permeation test for different membranes**

### 6.3.4 Permeation experiment

Permeation experiments were carried out using the electrocoagulated sample of effluent at 80 A/$m^2$. Each of the membranes sintered at 700, 800, 900 and 1000 $^oC$ were used for the permeation experiments in a batch mode. Trans-membrane pressures were maintained at three different pressures of 98,196 and 194 kPa. Before using each membrane, water permeation was done using deionized water at a transmembrane pressure of 392 kPa in order to ensure that the pores were unblocked for the effluent permeation experiments. It was observed that initially the membrane flux was very high and as the microfiltration experiments progressed it gradually reduced and reached a final steady state value. Steady state flux was achieved within 20 min of operation. The permeate flux (**Fig. 6.5**) followed an increasing trend for higher sintering temperatures because at higher sintering temperatures, the pore size increased. As evident, at a pressure of 98 kPa the permeate flux increased from 264 to 423 L/h.$m^2$ when sintering temperatures increased from 700 to 1000 $^oC$. However, with time there was a decline in flux due to the fact that the deposition of suspended particles over the membrane surface restricted the permeate flux by blocking the active pores of the membranes. Again, increase in permeate flux with pressure is due to the more driving force.

### 6.3.5 Permeate flux profile after MF experiments

In order to determine the usability of the membrane, the pure water flux profiles before and after microfiltration studies were determined. **Figure 6.6a** shows the pure water flux of the ceramic membrane before and after the microfiltration experiment. As observed from the **figure 6.6b**, there is a decline in the flux after microfiltration of electrocoagulated samples. As seen, for the pressure 98 kPa the steady state flux of 264 L/h.$m^2$ was reached at 16 min

(**Fig. 6.6c**), the decrease in flux with time was due to the deposition of flocks on the membrane surface.

Pure water flux had a steady state value of 2011.75 L/h.m$^2$ at 20 min, however after microfiltration of EC sample, the flux was reduced to 811 L/h.m$^2$ at 10 min. This declination in flux profile was evident for all the membranes. The decrease in flux after usage was due to the deposition of the suspended flocks of the EC samples on the surface of the membrane thereby blocking the active pores which were available for the filtration process.

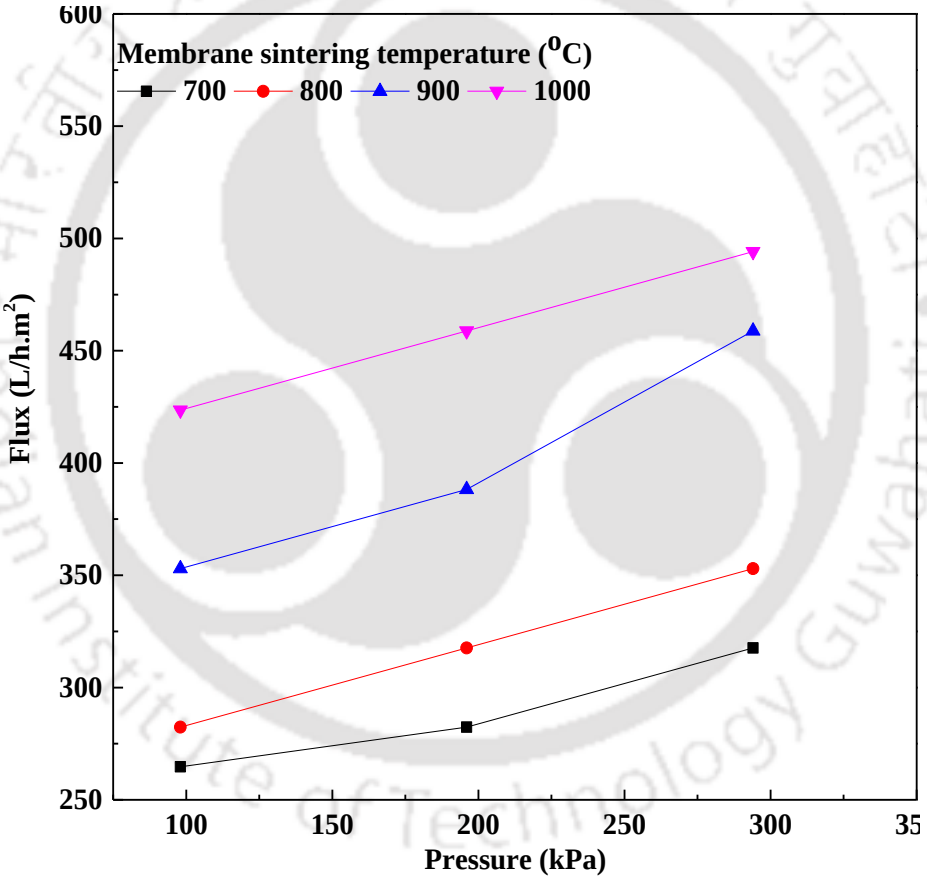


**Fig. 6.5: Variation of permeate flux with pressure for MF membranes sintered at different temperatures**

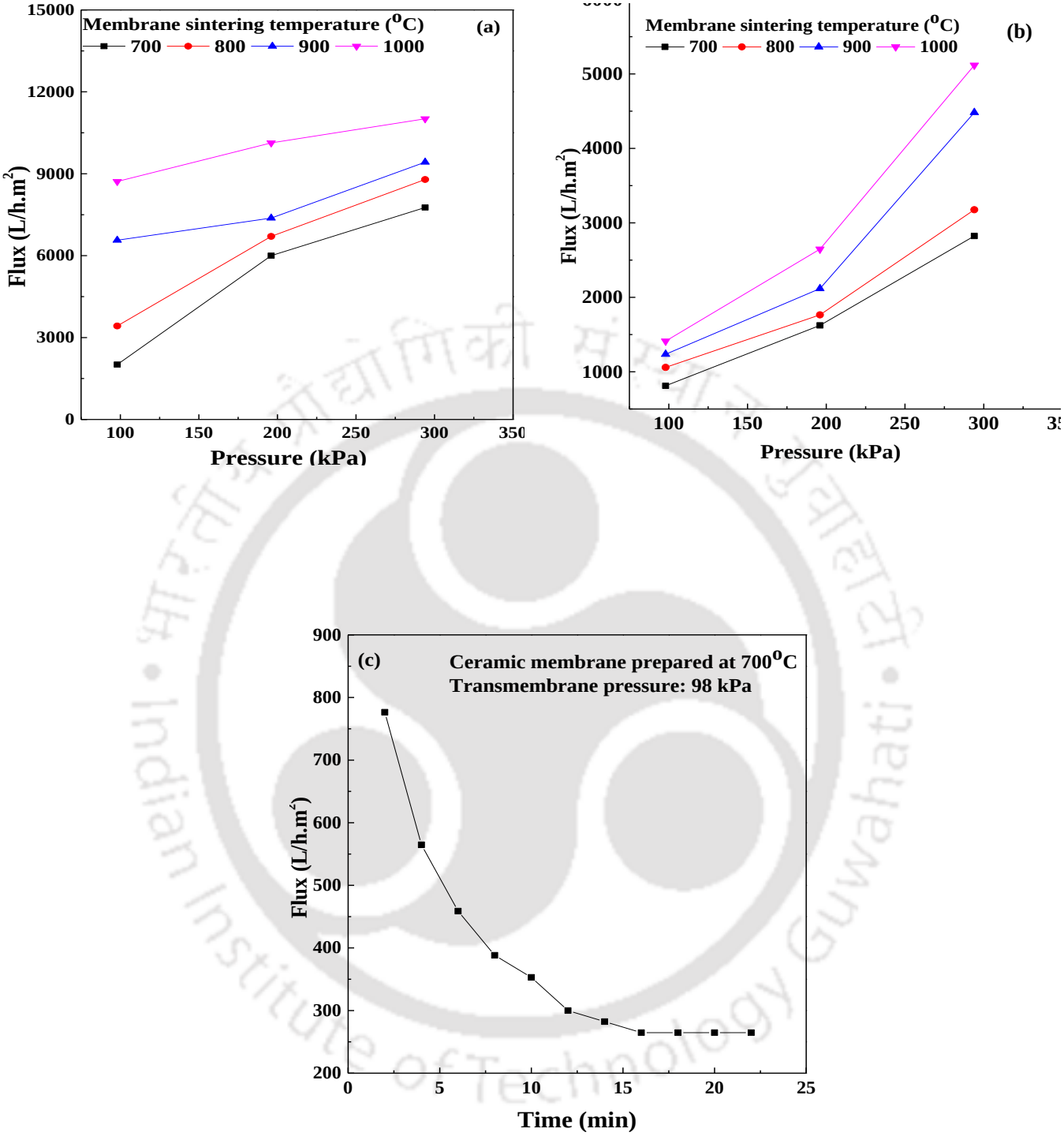


**Fig. 6.6: Pure water flux of the membranes at different sintering temperatures (a) Before microfiltration of EC sample, (b) After microfiltration of EC sample (c) Pure water flux for the ceramic membrane prepared at 700 °C for TMP of 98 kPa**

To quantify the results, flux decline ratio (FDR) and flux recovery ratio (FRR) were determined using the following equations [189, 190].

$$\text{Flux decline ratio (FDR)} = \frac{J_I - J_F}{J_I} \quad 6.4$$

$$\text{Flux recovery ratio (FRR)} = \frac{J_F}{J_W} \quad 6.5$$

Where, $J_I$ is the initial permeate flux, $J_F$ is the steady state permeate flux and $J_W$ is the pure water flux. It can be observed from **Table 6.1**, that FDR of 0.659 - 0.745, 0.6 - 0.75, 0.778 - 0.837 and 0.76 - 0.854 was observed for the membranes sintered at 700, 800, 900 and 1000$^o$C respectively, at pressure of 98 - 294 kPa indicating that 75 - 85 %of the initial flux was lost during the microfiltration of the electrocoagulated samples. Similarly, FRR of 0.131 - 0.041, 0.082 - 0.040, 0.054 - 0.049 and 0.048 - 0.044 was observed for the membranes sintered at 700, 800, 900 and 1000 $^o$C respectively, that the cleaning of membrane is in-effective. The organic solutes, responsible for fouling, deposit over the membrane surface forming a thick cake layer which needs to be scraped out and the membrane surface needs to be washed rigorously to retain atleast 50% of the former flux properties.

### 6.4 Flock characterization and membrane characterization (before and after filtration)

Flock size of the electrocoagulated samples were determined using DelsaNano. The size of the flocks varied from 2.61 to 5.83 µm when the applied current density for electrocoagulation varied from 20 to 80 A/m$^2$. As evident from Fig. 6.7a the size variation curve was bimodal in nature. Similarly, flock size was 124.49 µm at a pH of 3.6 and 11.87 µm at pH of 5.7 flocks. The EDX analysis provides a qualitative insight about the elements present in the flock **(Fig. 6.7b).** The membranes prepared at different sintering temperatures were analyzed using XRD (**Fig. 6.7c**).

**Table 6.1: Flux decline ratio (FDR) and flux recovery ratio (FRR) at different transmembrane pressure for the membranes prepared at 700, 800, 900 and 1000°C**

| Membrane sintering temperature (°C) | Transmembrane pressure (kPa) | FDR | FRR |
|---|---|---|---|
| 700 | 98 | 0.659 | 0.131 |
| | 196 | 0.742 | 0.047 |
| | 294 | 0.746 | 0.041 |
| 800 | 98 | 0.600 | 0.082 |
| | 196 | 0.719 | 0.047 |
| | 294 | 0.75 | 0.040 |
| 900 | 98 | 0.778 | 0.054 |
| | 196 | 0.842 | 0.053 |
| | 294 | 0.837 | 0.049 |
| 1000 | 98 | 0.760 | 0.048 |
| | 196 | 0.750 | 0.045 |
| | 294 | 0.854 | 0.044 |

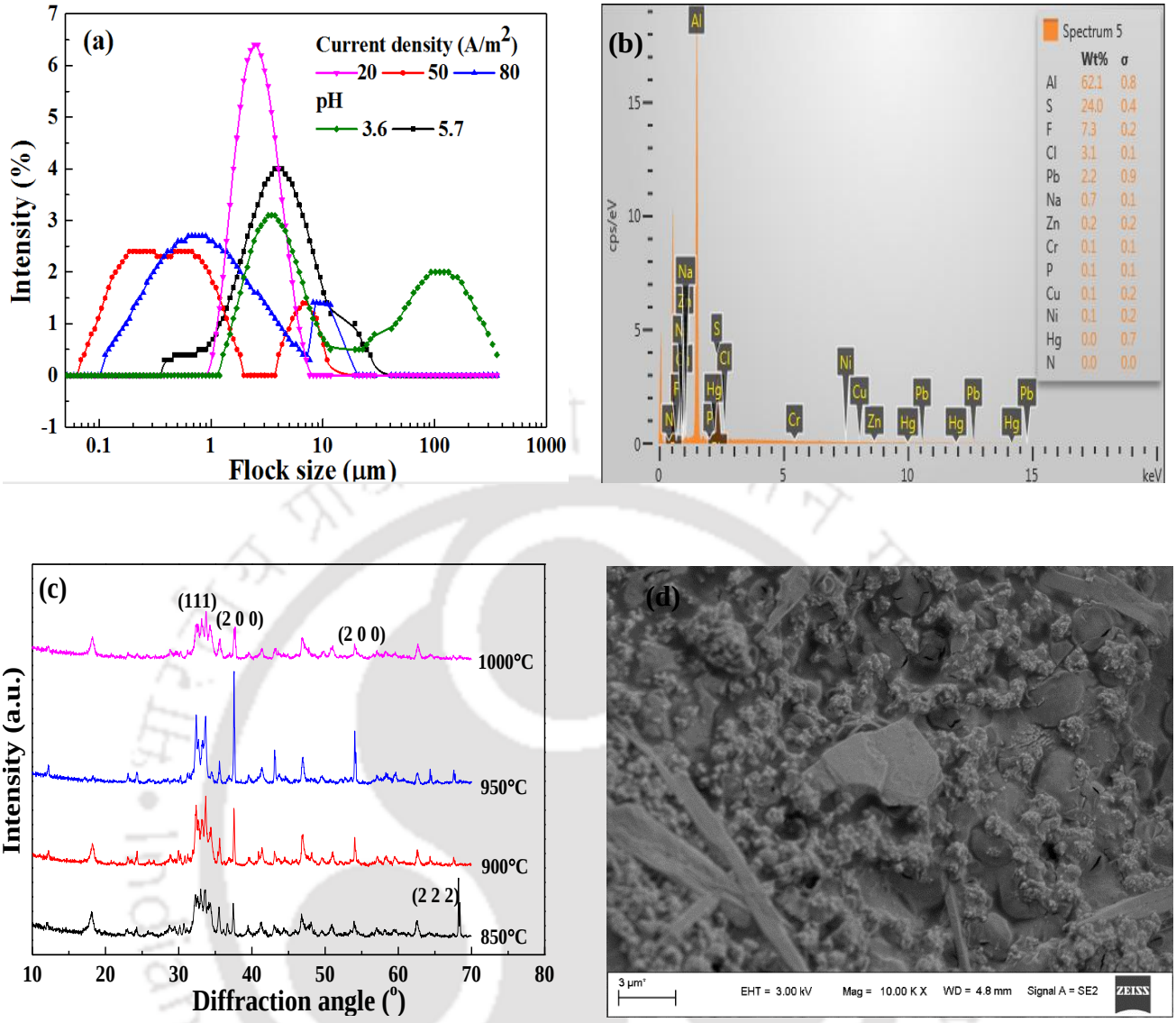


**Fig. 6.7: (a) XRD figure of membrane prepared from fly ash at different sintering temperature (b) EDX analysis of flocks filtered by fly ash membrane (c) Particle size distribution of flocks produced during EC process (d) FESEM image of membrane after microfiltration**

As seen, the crystalline nature increased with an increase in sintering temperature form 700 to 1000 $^{o}$C. Phases (111), (200) and (222) were present which corresponded to the calcium oxide,

dicalciumsilicates. **Figure 6.7d** shows the membrane after microfiltration experiment. As evident from the image, a layer of filtered flocks covers the membrane top layer which can be removed easily by washing.

### 6.5 Performance of hybrid process

The quality of the feed and electro-coagulated water were determined and compared along with the available state pollution control board (SPCB) permissible limits. **Table 6.2** shows the obtained results. As can be seen from the table, TDS values decreased from 3230 to 2780 mg/L. Conductivity of the feed increased from 2.65 to 6.19 which was due to the addition of NaCl, salinity remained more or less the same. pH was within permissible limits for all the sets of experiments. Turbidity increased from 28.1 to 71.6 because of large amounts of flocks produced during the electrocoagulation process. Metals like sodium, chromium, copper, lead, nickel were brought down within their permissible limits by electrocoagulation. The concentration of oil and grease was reduced from 35 mg/L to 14.2 mg/L in just 20 min. A further long duration of the experiment till 30 min suggested the concentration of oil and grease to be below the permissible limits of 110 mg/L. It was found that a large number of work has been done for the treatment of oily water in the past using the EC process. Electrocoagulation on refectory oily wastewater and vegetable oil refinery wastewater having and initial oil concentration of 100-250 mg/L and 2648-3880 mg/L [182, 171]. Similar work was done for initial oil concentrations of 250,000 mg/L, 100-2100 mg/L, 1500-6000 mg/L and 200 mg/L **(Table 6.3)** [172, 206, 207]. Each of these samples were treated using electrocoagulation process and a removal of 85-98 % was achieved in all the

**Table 6.2: Different properties for oily water at different operating parameters after electrocoagulation**

| Parameter / Property | Feed (without salt) | J = 20 A/m$^2$ | J = 50 A/m$^2$ | J = 80 A/m$^2$ | D = 0.01 cm | D = 0.02 cm | pH = 3.6 | pH = 5.7 | Permissible limits | |
|---|---|---|---|---|---|---|---|---|---|---|
| | | | | | | | | | Drinking water [200-203] | Discharged wastewater [200-203] |
| Conductivity (mS/cm) | 2.65 | 6.14 | 6.19 | 6.20 | 7.05 | 6.11 | 5.60 | 5.62 | 1.4 [WHO] | 1.4 [WHO] |
| TDS (ppm) | 3230 | 3130 | 3100 | 3070 | 3550 | 3040 | 2800 | 780 | 1000 [WHO] | 2000 [WHO] |
| Salinity (ppt) | 2.03 | 4.69 | 4.37 | 4.68 | 5.24 | 4.60 | 4.19 | 4.23 | 0.67 [WHO] | 0.46 [WHO] |
| pH | 8.72 | 8.80 | 8.80 | 8.15 | 9.70 | 9.04 | 7.20 | 7.59 | 8.5 [BIS] | 9 [WHO] |
| D.O. (ppm) | 93.7 | 26.1 | 22.4 | 16.7 | 12.0 | 8.5 | 18.6 | 11.2 | 15 [WHO] | >5 [WHO] |
| Turbidity (NTU) | 28.1 | 32.3 | 49.3 | 88.3 | 36.6 | 47.7 | 60.3 | 71.6 | 1 [WHO] | 5 [WHO] |
| % Sodium (mg/L) | 68.4 | 65 | 58 | 50 | 59 | 62 | 40 | 48 | NA | 60 [CPCB] |
| Oil & Grease (mg/L) | 35 | 29.8 | 28 | 26.82 | 27.07 | 29 | 14.2 | 25.5 | 0.5 [BIS] | 10 [CPCB] |
| Phenolics (mg/L) | 12.2 | 10 | 7.5 | - | 5 | 10.8 | 1 | 2.8 | 0.002 [BIS] | 1.2 [CPCB] |
| Cyanides (mg/L) | 0.002 | - | - | - | - | - | - | - | 0.05 [BIS] | 0.2 [CPCB] |
| Fluorides (mg/L) | 0.40 | - | - | - | - | - | - | - | 1.5 [BIS] | 1.5 [CPCB] |
| Sulphides (mg/L) | 0.007 | - | - | - | - | - | - | - | 0.05 [BIS] | 2 [CPCB] |
| Chromium (Hexa) (mg/L) | 0.9 | 0.1 | - | - | 0.3 | 0.45 | 0.1 | 0.3 | 0.1 [BIS] | 0.1 [CPCB] |
| Chromium (Total) (mg/L) | 1.2 | 0.6 | 0.4 | - | 0.5 | 0.7 | - | - | 1 [BIS] | 1 [CPCB] |
| Copper (mg/L) | 0.17 | - | - | - | - | - | - | - | 0.2 [BIS] | 0.2 [CPCB] |
| Lead (mg/L) | 0.04 | - | - | - | - | - | - | - | 0.01 [BIS] | 0.1 [CPCB] |
| Mercury (mg/L) | - | - | - | - | - | -- | - | - | 0.001 [BIS] | 0.01 [CPCB] |
| Nickel (mg/L) | 0.36 | - | - | - | - | - | - | - | 0.02 [BIS] | 3 [CPCB] |

**Table 6.3**: **Types of oil water treated using the electrocoagulation method**

| **Type of oil water** | **Initial feed concentration (mg/L)** | **Reference** |
|---|---|---|
| Refectory oily wastewater | 100 - 200 | [182] |
| Vegetable oil refinery industry wastewater | 2648 - 3880 | [171] |
| Palm oil mill effluent | 250,000 | [172] |
| Crude oil | 500 | [166] |
| Synthetic oil (lubricant oil (REPSOL ELITE TDI 15W40) + soluble oil (SOL 1000)) | 1500 - 6000 | [206] |
| Synthetic oil (paraffin oil + Oleic acid + Triethanolamine) | 200 | [207] |
| Restaurant oil water in Hong Kong | 100 - 2100 | [208] |
| **Drilling wastewater from Barekuri, India** | **35** | **Present work** |

cases. However, the EC experiments were performed for a longer period of time of 45-60 min in comparison to the present work of 20 min. Literature review suggested that although a large experiments were performed on oil wastewater, however no work was done till date on drilling waste water. The present sample had oil concentration of 35 mg/L which was brought down to 14 mg/L in 20 min of operation. Hence, EC process can be opted as a viable option for the treatment of oil water from drilling sites.

# Chapter 7

# Application of electrocoagulation-microfiltration process for the treatment of effluent water from steel plant

# *Chapter 7*

# Application of electrocoagulation-microfiltration process for the treatment of effluent water from steel plant

This chapter presents the application of the prepared membrane in the microfiltration of electro coagulated effluent water from steel industry. Effluent water from Tata Steel Limited had chloride, sodium, potassium, manganese, magnesium, pH, TDS, sulphate, calcium and iron. This effluent water was treated by a lab scale batch process of electrocoagulation followed by microfiltration of the electro-coagulated sample. The microfiltration process utilized a membrane prepared from fly ash. Removal studies were performed considering the operating parameters current density, run time and electrode distance. An estimation of corrosion, energy consumption and operating cost for the electrocoagulation process were also performed. Microfiltration studies were carried out at three different transmembrane pressure (TMP) of 103, 117 and 196 kPa. Filtered flocks were characterized to confirm the removal of heavy metals from the effluent water.

## 7.1 Experimental

### 7.1.1 Materials and methods

The water samples were collected from a steel industry with high initial concentrations of chloride, sodium, TDS, calcium and sulphate of 3739, 2370, 6076, 172.6 and 605.1 ppm respectively. In addition to these, metals such as potassium, iron, manganese and magnesium were also found in the water samples. A measured quantity (600 ml) of the effluent water sample was taken into the electrocoagulation setup. Current density was maintained in the range of 10 - 50 $A/m^2$ and all the experiments were performed at room temperature. Electrocoagulation was carried out for a time period of 20 min which were

then analyzed using atomic absorption spectroscopy (AAS). No additional conducting medium was added as the obtained samples had a sufficiently high conductivity of 4.59 mS/cm. Electrodes were washed with $H_2SO_4$ and rubbed with abrasive paper (C220) in order to ensure the complete removal of impurities before every experiment. The used electrodes were replaced after a run of 5 - 6 experiments. The membrane used for microfiltration of electro-coagulated sample were prepared using fly ash as mentioned in **Chapter 2**.

### 7.1.2 Membrane preparation

The obtained fly ash was mixed with appropriate additives such as sodium carbonate, calcium carbonate, boric acid and sodium metasilicate as discussed in **Chapter 2** of the thesis to increase the mechanical strength of the prepared membranes and incorporating a porous structure. The obtained powder was then mixed with Millipore water to form a paste having a consistency well enough to take the shape of a disk when placed in a MS ring. The casted membrane was kept overnight to dry under a uniform weight of 1-2 kg. The dried circular disks were removed from the MS ring and kept in an oven for drying at 110 $^{o}$C for 12 h which was followed by sintering at 850 $^{o}$C for 6 h. Obtained membrane had a diameter of 56 mm and a thickness of 7 mm. These membranes were then polished and abraded using a C220 abrasive paper on the edges to fit into the microfiltration set up. Once polished and abraded, the membranes were sonicated for 20 min to remove any loose particles adhering to the membrane surface. The sonicated membranes were pat dried and the left in the oven overnight for drying.

### 7.1.3 Measurement and analysis

The residual concentration of the metals were determined using atomic absorption spectroscopy (AAS, Make: Varian). Quality of the untreated and treated water such as pH, conductivity, turbidity were determined using a microprocessor based water analysis kit (VSI electronics Pvt. Ltd., Mohali, Chandigarh). Morphological properties of the flocks from the electrocoagulation unit and the membranes used for filtration were carried out by a field emission scanning electron microscope (FESEM, Make: LEO). Energy dispersive X-ray (EDX) was performed to identify the elemental composition of the flocks obtained from the electrochemical unit. Delsa Nano ((Beckman Coulter) was utilized for the measurement of particle size distribution.

### 7.1.4 Theoretical

In order to verify the declination of flux during the microfiltration process, a resistance-in-series model has been adopted [193]. The permeate flux is given by the following equation

$$J_p(t) = \frac{\Delta P}{\mu(R_m + R_c(t))} \qquad 7.1$$

Where, $J_p$ is the permeate flux at a time $t$, $\Delta P$ is the transmembrane pressure, $\mu$ is the viscosity of pure water, $R_m$ is the membrane hydraulic resistance and $R_c(t)$ is the resistance due to concentration polarization at a time $t$. The steady state concentration polarization is given as

$$R_c^s = \frac{\Delta P}{\mu J_p^s} - R_m \qquad 7.2$$

$$R_c(t) = \frac{\Delta P}{\mu J_p(t)} - R_m \qquad 7.3$$

Considering the rate of growth of resistance due to concentration polarization to be directly proportional to $R_c^s$-$R_p$

$$\frac{dR_c}{dt} \infty (R_c^s - R_p) \qquad 7.4$$

Which can be integrated to get the following equation

$$R_c(t) = R_c^s[1 - \exp(-at)] \qquad 7.5$$

Where the parameter 'a' determines the rate at which the polarization resistance grows with time and can be estimated by the slope of the linear plot of $\ln[R_c^s/R_c^s - R_c(t)]$ versus 't'

### 7.2 Pre-treatment

#### 7.2.1 Electrocoagulation bath

An electrocoagulation setup having dimension of 0.23 m × 0.08 m × 0.04 m with a working volume of about 600 ml was used to carry out the experiments. Four aluminium sheets of 0.07 m × 0.77 m × 0.001 m with an inter-electrode distance of 0.005 m and a bipolar connection were used as electrodes for electrocoagulation. The assembly of electrodes was connected to DC power source (Crown, DC regulated power supply, 0-30 V/2A) to constitute the electrochemical cell.

Removal of metals by electrocoagulation process was studied considering the effect of parameters such as current density, electrode distance and run time. Experiments were carried out for a period of 20 min with samples being withdrawn in every 2 min and analyzed by AAS for the detection of concentration of different metals in the sample. Flocks thus obtained by the electrocoagulation process were dried at 110 $^{o}$C and further characterized using EDX to confirm the uptake of various metals by the produced flocks.

## 7.3 Results and discussion

### 7.3.1 Effect of current density

Current density plays an important role in the electrocoagulation process. The generation of flocks, rate of generation of flocks, growth of flocks and generation of bubbles and thereby the efficiency of the EC process are all controlled by current density. More is the applied current density, more is the anodic oxidation resulting in the dissolution of the sacrificial anode and the production of metal hydroxides which facilitates the removal of metals from the solution. As evident from **Fig. 7.1**, the uptake of metals by aluminium hydroxide increases with an increasing current density. For a current density variation from 10 - 50 $A/m^2$ the final concentration for Na, Mg, Ca, K and Fe reduced from 507 - 449, 90 - 54, 97 - 18, 90 - 35 and 10 - nil mg/L respectively after a run time of 20 min (**Fig 7.1 a, b and c**). The concentration of Mn was found to be completely absent at high current densities of 30 and 50 $A/m^2$ (**Fig. 7.1 b and c**).

### 7.3.2 Effect of electrode distance

Inter-electrode distance is another important parameter controlling the electrocoagulation process. At higher electrode distance more current is required to produce the aluminium hydroxide by the oxidation of the sacrificial anode which helps in the removal of metals from aqueous solutions. **Figure 7.2** shows the effect of inter-electrode distance at a constant current density and a variation of electrode distance from 0.005 - 0.02 m. At a constant current density of 10 $A/m^2$, the amount of aluminium hydroxide formed will be less with an increase in electrode distance. As evident from the figure, the removal of metals decreases at higher electrode distance. The final concentration at the end of 20 min run time for the metals

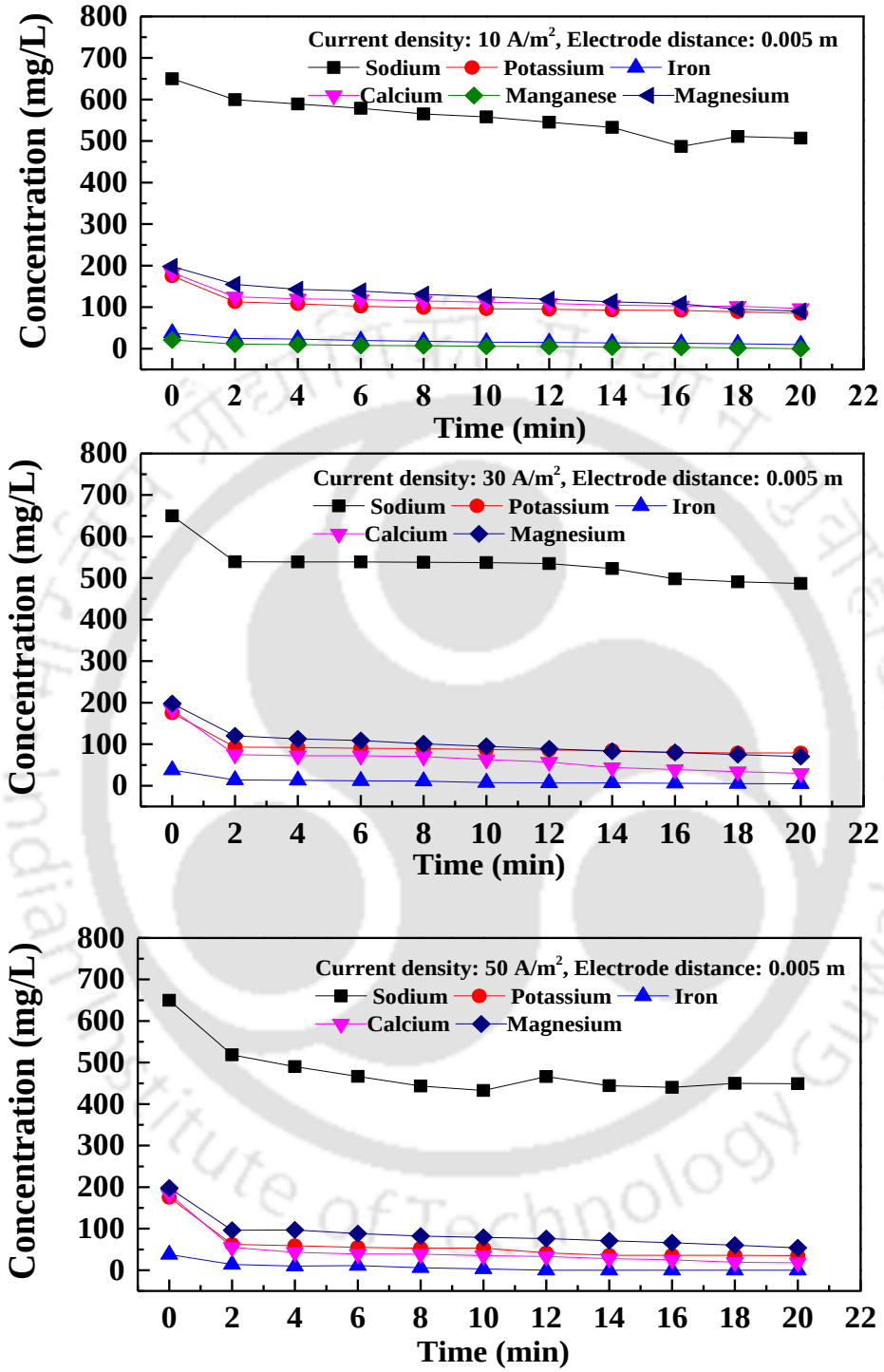


**Fig. 7.1: Effect of current density and run time on the removal of metals from effluent water sample**

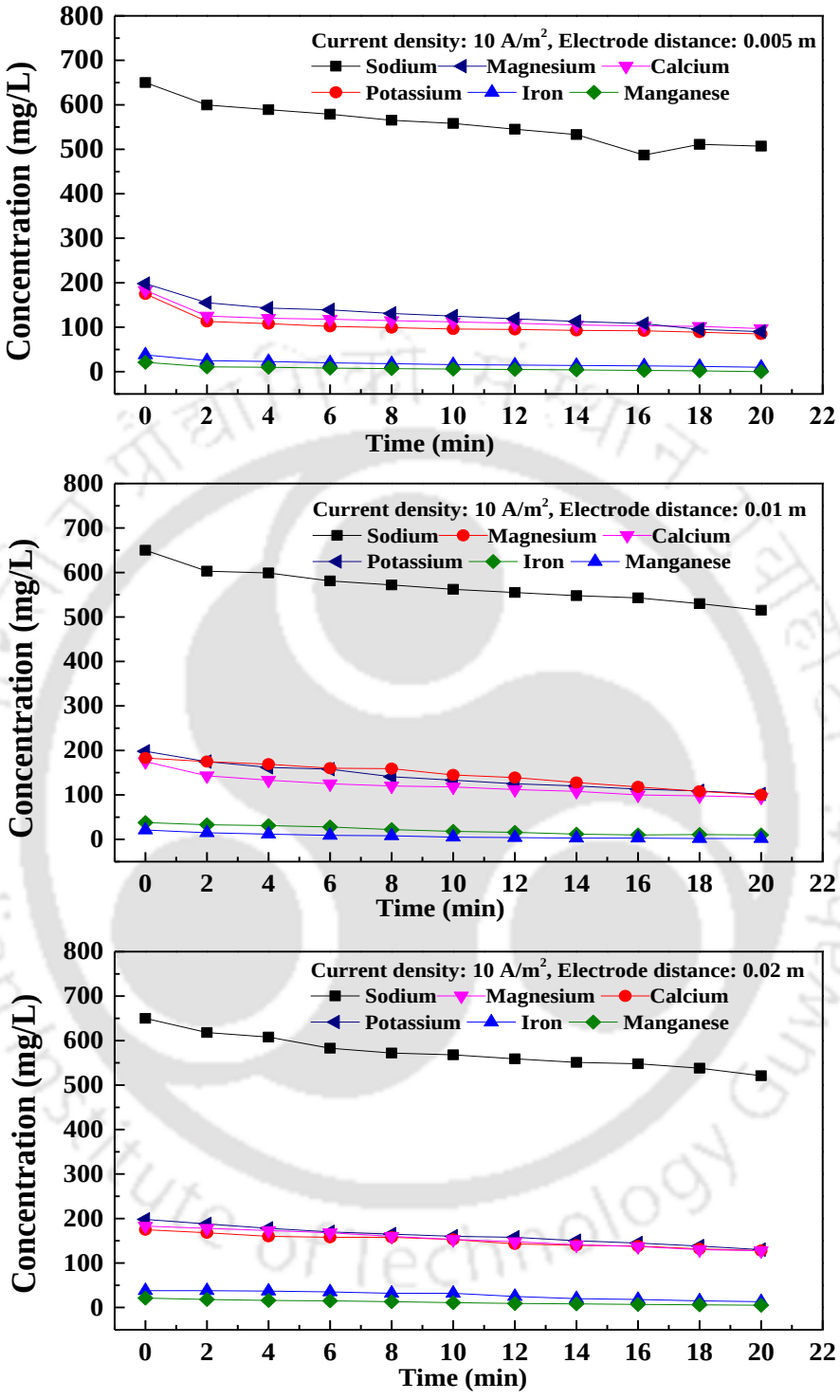


**Fig. 7.2: Effect of electrode distance and run time on the removal of metals from effluent water sample**

Na, Mg, Ca, K, Fe and Mn were found to vary as 507 - 521, 90 - 223, 97 - 135, 90 - 128, 10 - 17 and 0 - 16 mg/L (**Fig. 7.2 a, b and c**).

### 7.3.3 Variation of pH, TDS, chlorides and sulphates with varying current density

**Figure 7.3 a** shows the variation in pH with the progression of electrocoagulation. Current densities were varied from 10-50 A/m$^2$ to study the variation of pH. **Figure 7.3 a** shows that the pH values decreases with time and finally reaches values of 7.3, 7.1 and 7 for current densities of 10, 30 and 50 A/m$^2$, respectively. This water molecules coordinate with the $Al^{3+}$ ion and result in the formation of an aqua complex hexa-aqua ion $(Al(H_2O)_6)^{3+}$ and leads to increased dissociation of the water molecule with elimination of the proton [204]. This $H_3O^+$ accumulation in the solution leads to the decrease of its pH.

A similar decreasing trend was observed for the TDS values. With an increase in the current density values, the total dissolved solids decreased. As seen from **Figure 7.3b** the TDS values decreased from 2530 ppm to 2110 ppm, 2092 ppm and 2030 ppm for the current densities of 10, 30 and 50 A/m$^2$ respectively with a run time of 20 min. The decrease was mainly because of the capturing of dissolved solids by the metal hydroxides produced during EC. At higher current densities more metal hydroxides were produced and hence more TDS were removed.

Chlorides and sulphates were determined using the titration method. **Table 7.1** shows the changes in the values of chlorides and sulphates for the operating parameters of current density and electrode distance. The concentration of chlorides and sulphates decreased from 1299-1249 ppm and 1099-821 ppm respectively when current densities were increased from 10-50 A/m$^2$. However, at higher electrode distance of 0.2 m the concentrations of both chlorides and sulphates were found to be much higher when compared to the concentrations at an electrode distance of 0.005 m. Metals such as iron,

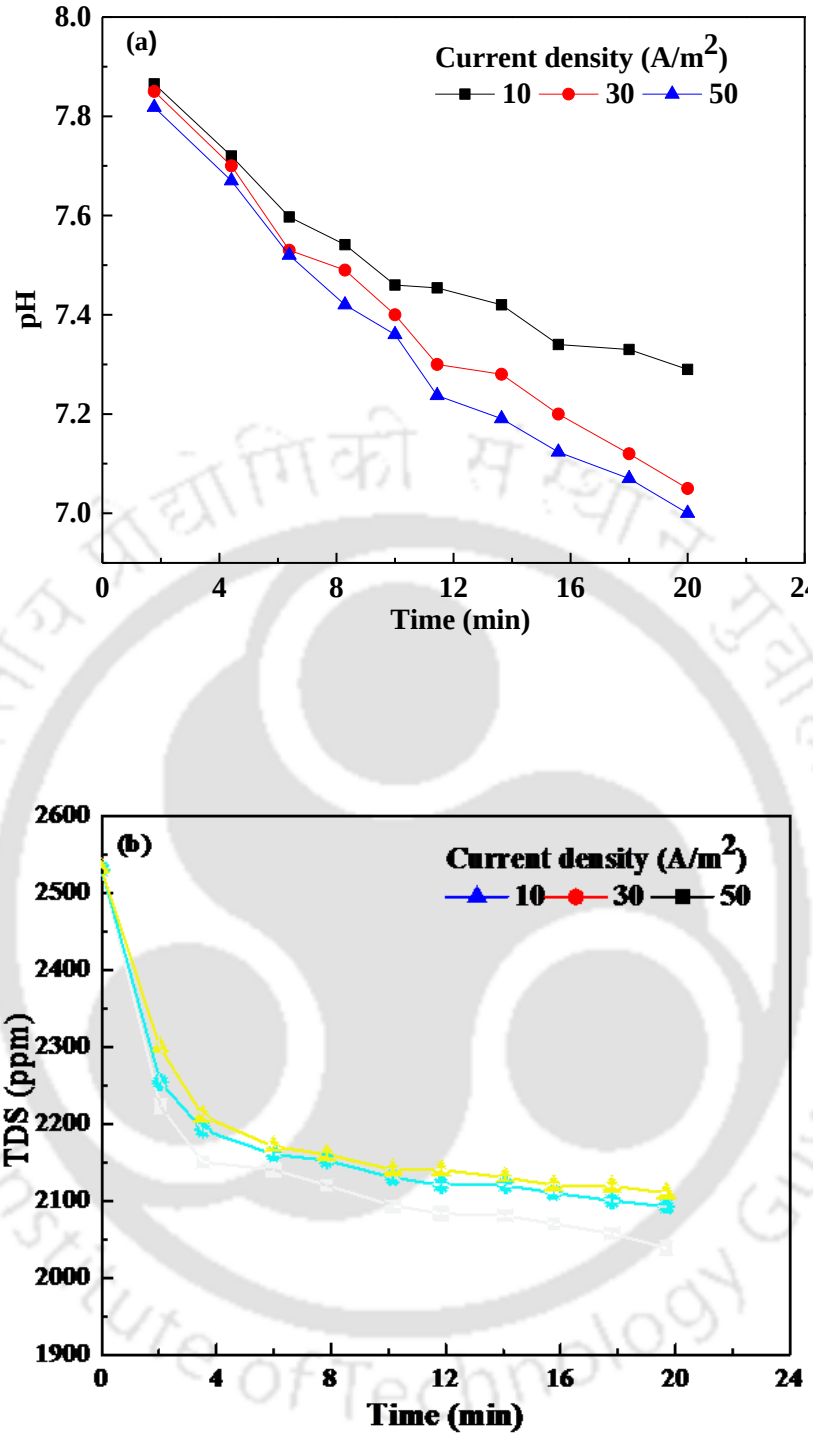


**Fig. 7.3: Changes in (a) pH and (b) TDS with changing current density**

**Table 7.1: Comparative table showing the concentration of chlorides, sulphates and metals in feed and after electrocoagulation along with their permissible limits.**

| **Parameters** | **Feed** | **Electrocoagulated** | | | **Permissible limit** | |
|---|---|---|---|---|---|---|
| **Current density ($A/m^2$)** | **None** | **10** | **30** | **50** | **Drinking water [193, 195, 198]** | **Discharged wastewater into surface water [194, 196]** |
| Chlorides (mg/L) | 1299 | 1281 | 1274 | 1249 | 1000 [BIS] | 1500 [EPA] |
| Sulphates (mg/L) | 1099 | 1058 | 986 | 821 | 400 [BIS] | 1500 [EPA] |
| Sodium (mg/L) | 650 | 507 | 487 | 449 | 200 [WHO] | 200 [EPA] |
| Potassium (mg/L) | 175 | 90 | 78.8 | 54 | 12 [WHO] | NA |
| Iron (mg/L) | 38 | 10 | 4.8 | 0 | 0.3 [ISI, BIS] | 2 [EPA] |
| Calcium (mg/L) | 183 | 97 | 30 | 18 | 200 [WHO, BIS] | NA |
| Magnesium (mg/L) | 198 | 90 | 70 | 54 | 50-100 [WHO, BIS ] | 150 [WHO] |
| Manganese (mg/L) | 21 | 0 | 0 | 0 | 0.3 [BIS] | 0.2 [EPA] |
| **Electrode distance (m)** | **None** | **0.005** | **0.01** | **0.02** | **Drinking water** | **Discharged wastewater into surface water** |
| Chlorides (mg $L^{-1}$) | 1299 | 1281 | 1288 | 1293 | 1000 [BIS] | 1500 [EPA] |
| Sulphates (mg $L^{-1}$) | 1099 | 1058 | 986 | 82 | 400 [BIS] | 1500 [EPA] |
| Sodium (mg/L) | 650 | 507 | 507 | 521 | 200 [WHO] | 200 [EPA] |
| Potassium (mg/L) | 175 | 90 | 102 | 130 | 12 [WHO] | NA |
| Iron (mg/L) | 38 | 10 | 10 | 13 | 0.3 [ISI, BIS] | 2 [EPA] |
| Calcium (mg/L) | 183 | 97 | 95 | 128 | 200 [WHO, BIS ] | NA |
| Magnesium (mg/L) | 198 | 90 | 100 | 129 | 50-100 [WHO, BIS] | 150 [WHO] |
| Manganese (mg/L) | 21 | 0 | 2 | 5 | 0.3 [BIS] | 0.2 [EPA] |

calcium, magnesium and manganese were reduced to the desired permissible limits, sodium and potassium however remained more than the desired permissible limits. Both

these elements are essential for plants. No specific limits were confirmed for these elements to be used in irrigation as crops have high tolerances for both sodium and potassium. However, large quantities of sodium may be harmful [204].

### 7.3.4 Estimation of corrosion, film thickness, energy consumption and operating cost

Study on the corrosion of electrodes gives the overview of the lifetime of the EC process. It is usually determined in terms of weight loss of the electrode during the electrocoagulation process. Corrosion generally increases with higher current densities and high initial concentrations of metals in the sample water, however with higher electrode distance the corrosion decreases. The increase in corrosion is due to increases dissolution of electrodes at higher current densities. As seen from **Figure 7.4a** the corrosion increased from 17.2 mg to 27.2 mg when the current density increased from 10 to 50 A/m$^2$. A reverse case with a lesser corrosion was observed when electrode distance increased from 0.005 m to 0 0.02 m as 27.2 mg to 19 mg, respectively.

A layer of gelatinous hydroxide surrounds the electrode as the EC process continues. With increasing run time more hydroxides are produced which get adhered on to the surface of the electrode and create an additional barrier for the anodic oxidation, thereby reducing the efficiency of the EC process. Film thickness can be presented by the equation as reported in our previous work [192]. **Fig. 7.4b** shows the variation of film-thickness over electrode surface at different current densities. It was evident that the film-thickness increased from 3.86 µm to 6.1 µm with an increase in current density from 10 to 50 A/m$^2$. An enhancement in the current density favored the anodic oxidation which caused an increase in the production off gelatinous hydroxide. This hydroxide in turn attached itself to the electrode surface as a film and this film thickness increased with increasing electrocoagulation time. Also at higher electrode distance lesser gelatin hydroxide was

produced at 4.27 mg for 0.02 m electrode distance when compared to 6.1 mg at 0.005 m both at a current density of 50 A/m$^2$ and a run time of 20 min.

**Figure 7.4c** shows the variation of operating costs at different current densities at the end of 20 min of EC operation. With increased current density energy cost increased due to higher energy consumptions. Energy cost, electrode cost and the total cost were calculated as **Chapter 5**. Similarly, electrode cost increased with current density due to increased dissolution of electrode into the solution. Total operating costs were found to increase from 0.05821 - 0.16745 US$/m$^3$with increasing current densities of 10 - 50 A/m$^2$.

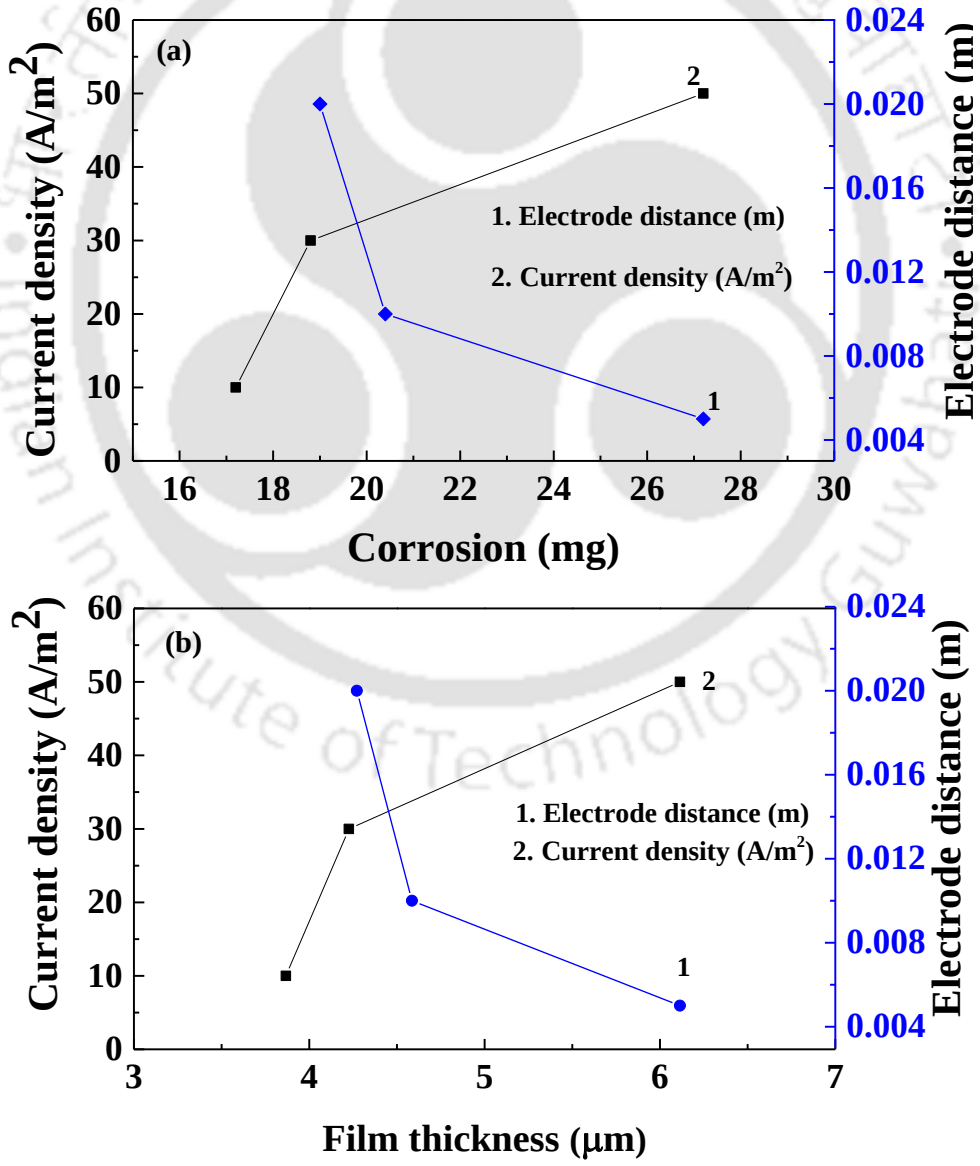

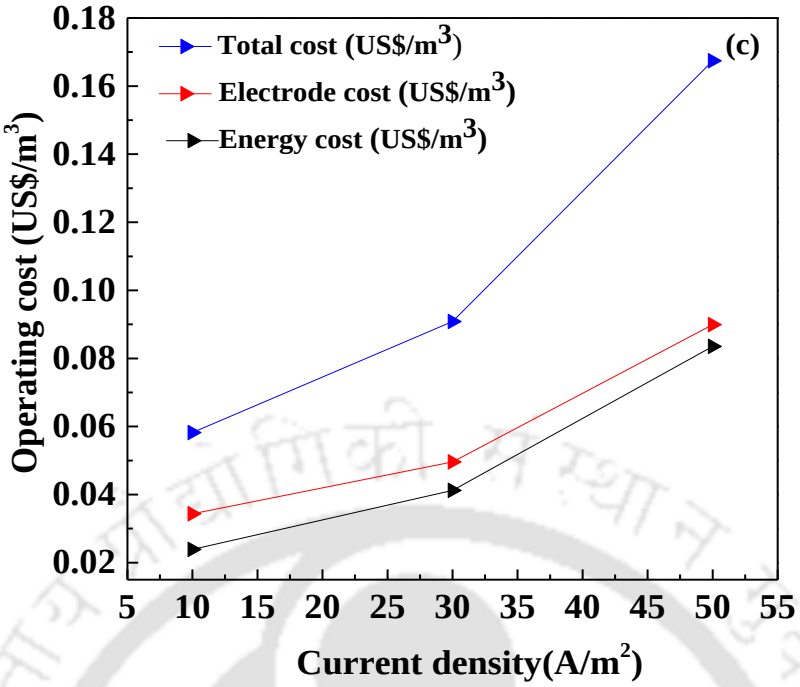


**Fig. 7.4: Effect of current density and electrode distance on (a) Corrosion (b) Film thickness and (c) Operating cost variation with current density**

### 7.3.5 Effect of transmembrane pressure (TMP) on microfiltration of electro-coagulated water

Permeate flux was measured during the microfiltration process of the electro-coagulated water samples. A flux declination for the initial 10 - 12 minutes was observed beyond which it remained almost constant. Three electro-coagulated samples treated at a current density of 10, 30 and 50 A/m$^2$ were filtered through the prepared membrane at three varying pressures of 103, 117 and 196 kPa. The samples of water consisted of coagulated species which aided in the process of concentration polarization during microfiltration. Thereby resulting in the flux decline. **Figure 7.5** shows that permeate flux decline is more pronounced at higher transmembrane pressure. This is because of the fact that at higher operating pressures, more coagulants are convected towards the membrane surface due to

enhanced driving force, leading to augmented concentration polarization and sharp flux decline. As seen for sample electro-coagulated at 10 A/m$^2$ the steady state permeate flux increased from 122 to 1146 L/m$^2$·h with increase in TMP from 103 to 196 kPa. However steady state flux decreased for the samples treated at 30 and 50 A/m$^2$ as these samples had higher amounts of coagulants produced during EC process in comparison to the sample treated at 10 A/m$^2$ resulting in lower values of steady state flux.

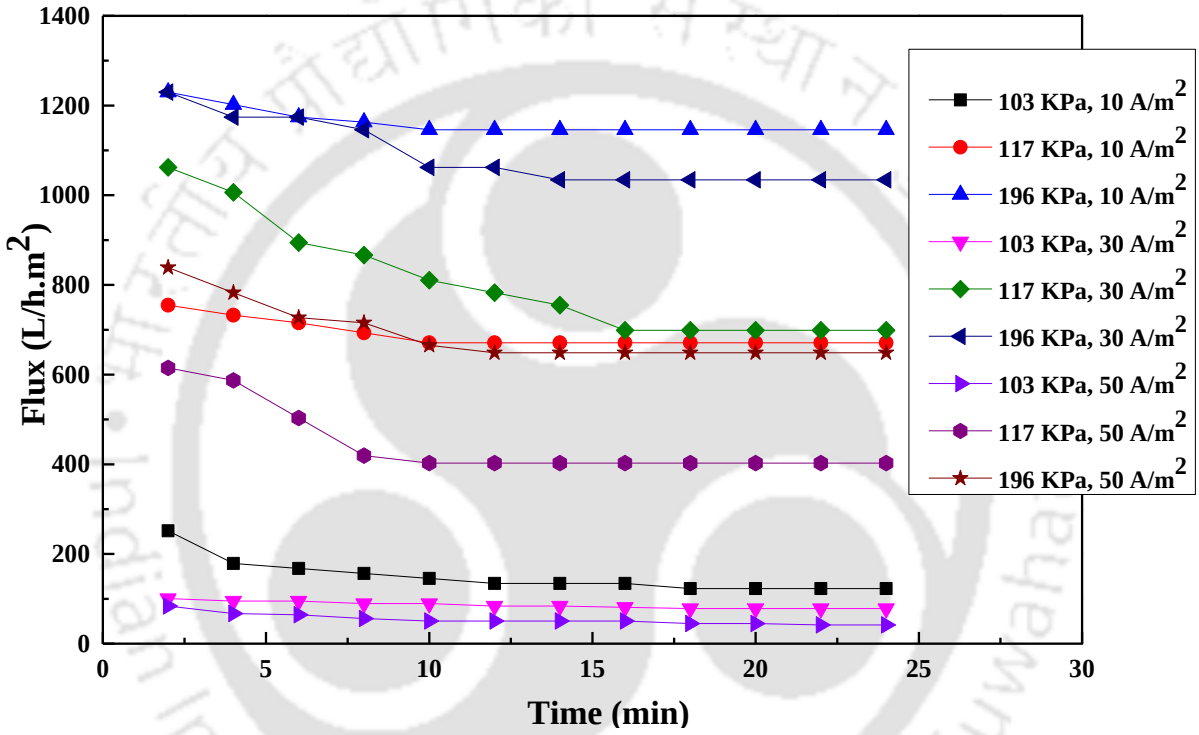


**Fig. 7.5: Flux declination profile for samples treated with current densities of 10, 30 and 50 A/m$^2$**

### 7.3.6 Washing and flux recovery

In order to determine the efficiency of the membrane, it is necessary that the membrane is washed from time to time. To quantify the results, flux decline ratio (FDR) and flux recovery ratio (FRR) are used. FDR and FRR can be determine d using the equations below

Flux decline ratio (FDR) = $\frac{J_{pi} - J_{pf}}{J_{pi}}$ 7.6

Flux recovery ratio (FRR) = $\frac{J_{pf}}{J_w}$ 7.7

**Table 7.2: Flux decline ratio and flux recovery ratio for samples treated with current densities of 10, 30 and 50 A/m$^2$**

| **Sample type based on applied current density (A/m$^2$)** | **Transmembrane pressure (kPa)** | **FDR** | **FRR** |
|---|---|---|---|
| 10 | 103 | 0.511 | 0.733 |
| | 117 | 0.111 | 0.649 |
| | 196 | 0.068 | 0.683 |
| 30 | 103 | 0.222 | 0.467 |
| | 117 | 0.342 | 0.676 |
| | 196 | 0.159 | 0.617 |
| 50 | 103 | 0.500 | 0.250 |
| | 117 | 0.345 | 0.389 |
| | 196 | 0.226 | 0.387 |

recovery. High FRR values at all experimental conditions signify that the cleaning of membrane is effective in all conditions. The organic solutes, responsible for fouling, deposit loosely over the membrane surface and get cleaned during washing. Where, $J_{pi}$ is the initial permeate flux, $J_{pf}$ is the steady state permeate flux and $J_w$ is the pure water flux. FDR value closer to 0 signifies that the membrane offers low fouling. FRR value close to 1 signifies that cleaning process can successfully recover most of the membrane permeability. It can be observed from Table 7.2, that the highest FDR is 0.511 indicating only 51.1 % of the initial permeate flux is lost during microfiltration. As seen, during the prolonged use of the membrane a flux decline from 6.8 % to 51.1 % was observed. In this case, the highest FRR value was around 0.73, signifying efficient flux

### 7.3.7 Analysis of various resistances

**Table 7.3** shows the variation of resistance due to concentration polarization at different operating conditions of transmembrane pressure and type of electro-coagulated sample. An increase in TMP results in the decrease in the concentration polarization values. For example, the sample treated with current density of 10 A/m$^2$ had the $R_c$ values decreased from 0.532 to 0.282 with a reduction of 46.99 %. Increased TMP results into more convection and deposition of lesser solutes on the membrane surface, thereby, decreasing the polarization layer resistance.

It is evident from **Table 7.3** that resistance due to concentration polarization is more dominant for electro - coagulated effluent having more flocks (50 A/m$^2$) whereas membrane resistance is dominant for electro - coagulated effluent having less flocks (10 A/m$^2$). For the sample of effluent electro - coagulated at 10 A/m$^2$ and filtered at 196 kPa, membrane resistance and resistance due to concentration polarization were 71.8 % and 28.3 %, respectively. Variation of concentration polarization resistance with time is

presented in **Fig. 7.6**. Three electro-coagulated samples treated at a current density of 10, 30 and 50 A/$m^2$ each at three different operating pressure of 103, 117 and 196 kPa have been shown. It can be observed from the figure that, polarization resistance increases at initial time of filtration and then decreases later on, ultimately assuming a steady state value. This was due to the formation of a layer of the suspended flocks on the membrane surface with the progression of time.

**Table 7.3: Characteristics of fouling resistance at different operating conditions**

| **Sample type based on applied current density (A/$m^2$)** | **Transmembrane pressure (kPa)** | **$R_m/R_T$** | **$R_c/R_T$** | **k** |
|---|---|---|---|---|
| 10 | 103 | 0.468 | 0.532 | 0.618 |
| | 117 | 0.609 | 0.390 | 0.506 |
| | 196 | 0.718 | 0.282 | 0.492 |
| 30 | 103 | 0.297 | 0.702 | 0.586 |
| | 117 | 0.635 | 0.365 | 0.648 |
| | 196 | 0.648 | 0.352 | 0.570 |
| 50 | 103 | 0.159 | 0.840 | 0.552 |
| | 117 | 0.365 | 0.634 | 0.390 |
| | 196 | 0.352 | 0.593 | 0.192 |

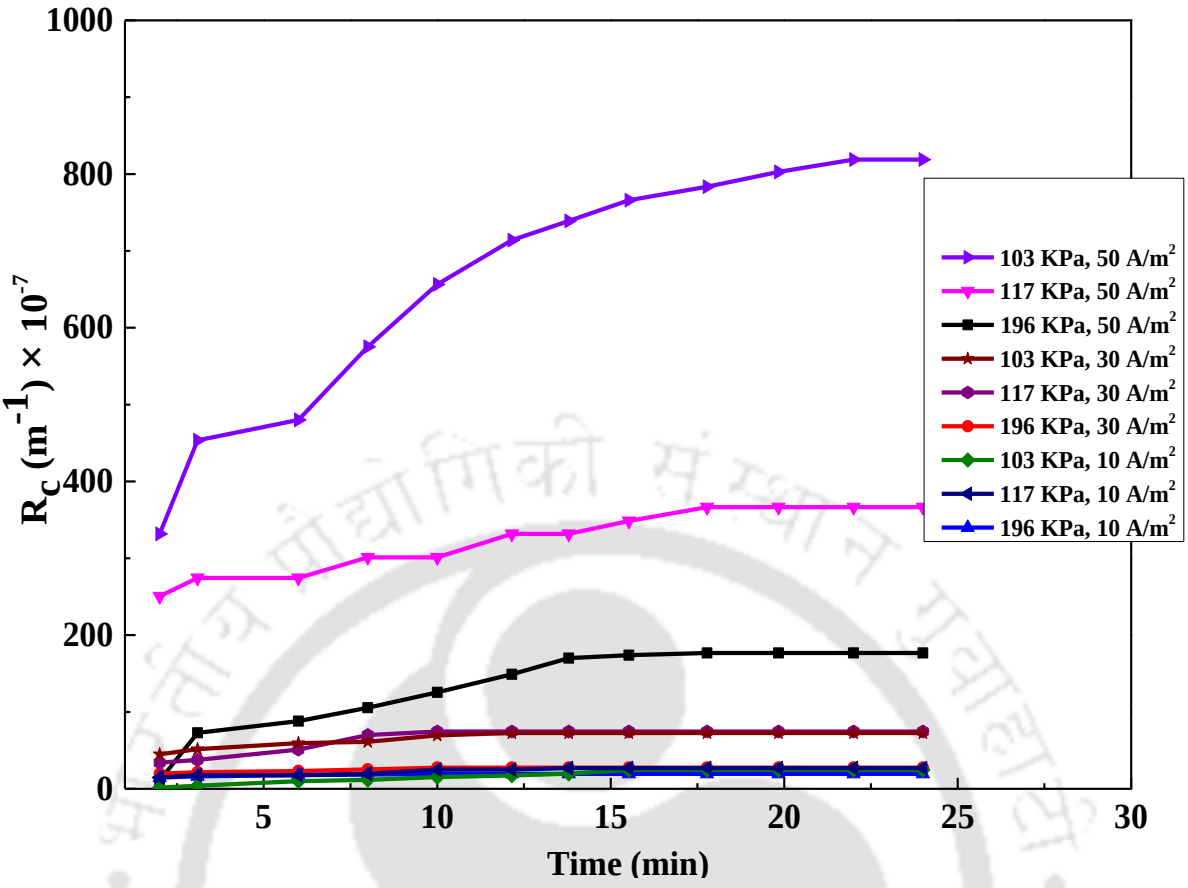


**Fig. 7.6: Resistance due to concentration polarization samples treated with current densities of 10, 30 and 50 A/m$^2$**

### 7.3.8 Flock characterization and membrane characterization (before and after filtration)

Flock size was measured using delsa - nano. The size of the flocks varied from 28.2 to 62.25 µm when the applied current density for electrocoagulation varied from 10 to 50 A/m$^2$. As evident from **Fig. 7.7 a** the size variation curve was bimodal in nature. This behavior was explained by the fact that the small sized flocks at around 2.8 µm produced during the initial phase of EC process tends to agglomerate and form flocks the large sized flocks as indicated by the second nodes in the curves**.** The energy mapping analysis provides a qualitative insight about the elements present in the flock**. Fig. 7.7 b** indicates

the presence of elements calcium, magnesium, sodium, manganese, iron and potassium. The presence of all these metals in the in the flocks suggested the successful removal by electrocoagulation process.

The membrane utilized for the filtration of the electro-coagulated sample had a pore size of 20 µm which was sufficient enough to aid in the removal of the flocks produce during the electrocoagulation process. Morphological study **Fig. 7.7 c and d** of the membrane before and after filtration was carried out using the FESEM analysis. The studies suggested that the top layer of the membrane was covered by a layer of flocks produced during the electro-coagulation process. This suggested a successful removal of the generated flocks during electrocoagulation by the prepared ceramic membrane.

### 7.3.9 Quality of electro-coagulated and filtered water

The quality of the electro-coagulated water and the filtrate obtained after membrane filtration were analyzed in terms of pH, conductivity, TDS, turbidity, salinity and dissolved oxygen and shown in **Table 7.4**. The properties of electro-coagulated water such as pH, conductivity, TDS, turbidity, salinity and D.O. had values of 7.29 -7, 4.47 - 4.45 mS/cm, 2110 - 2030 mg/L, 54 - 95.7 NTU, 3.44 - 3.34 and 18.8 - 12.8 mg/L respectively. The pH and D.O. values increased after filtration, however the turbidity was completely removed after filtration. Similarly conductivity, TDS and salinity values were found to be lower than the electro-coagulated samples.

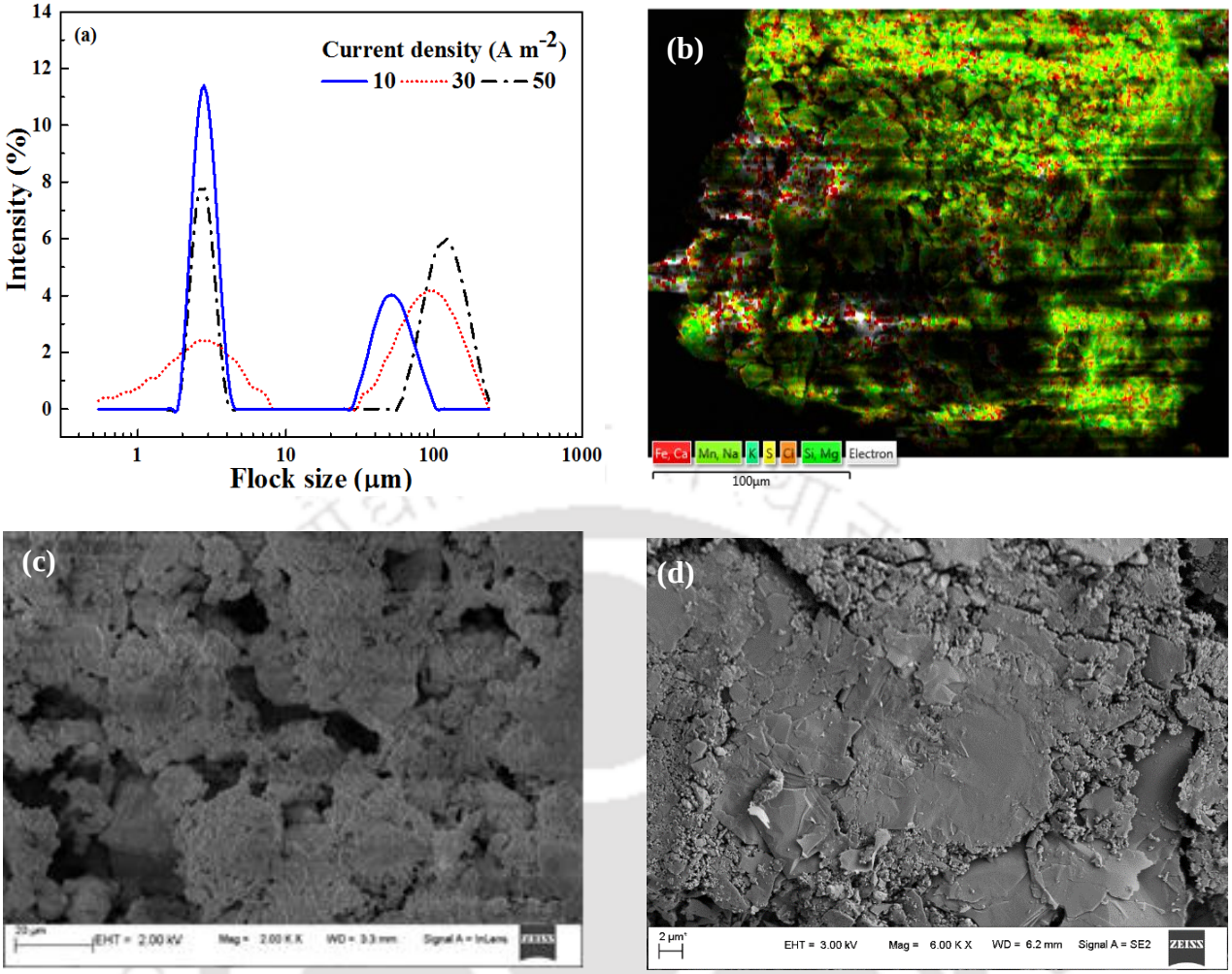


**Fig. 7.7: (a) Size distribution of flocks produced during electrocoagulation (b) Energy mapping of sludge filtered by membrane, FESEM image of membrane (c) before microfiltration (d) after microfiltration**

**Table 7.4: Comparative table showing the quality of effluent water as feed, after electro-coagulation and after filtration.**

| **Parameters** | **Feed** | **Electrocoagulated** | | | **Filtered** | | | **Permissible limit** | |
|---|---|---|---|---|---|---|---|---|---|
| **Current density ($A/m^2$)** | **None** | **10** | **30** | **50** | **10** | **30** | **50** | **Drinking water [193, 195, 198]** | **Discharged wastewater into surface water [194, 196]** |
| Turbidity (NTU) | 0.5 | 54.4 | 83.60 | 95.7 | 0 | 0 | 0.1 | 0 - 1 [WHO] | 5 [WHO] |
| Conductivity (mS/cm) | 4.59 | 4.57 | 4.44 | 4.45 | 4.27 | 4.23 | 4.13 | 1.4 [WHO] | 1 [WHO] |
| TDS (mg/L) | 2530 | 2110 | 2092 | 2030 | 2000 | 1980 | 1890 | 1000 [WHO] | 2000 [WHO] |
| Salinity (ppt) | 3.32 | 3.44 | 3.33 | 3.34 | 3.22 | 3.17 | 3.13 | 0.67 [WHO] | 0.46 [WHO] |
| D.O (mg/L) | 15.5 | 18.8 | 14.8 | 12.8 | 30.1 | 24.3 | 33.1 | 0-15 [WHO] | >5 [WHO] |
| pH | 7.65 | 7.29 | 7.05 | 7 | 8.14 | 7.76 | 7.95 | 6.5 - 8.5 [WHO,BIS] | 6 - 9 [WHO] |
| **Electrode distance (m)** | **None** | **0.01** | | **0.02** | **0.01** | | **0.02** | **Drinking water** | **Discharged wastewater into surface water** |
| Turbidity (NTU) | 0.5 | 105.6 | | 153.4 | 0 | | 0 | 0 - 1 [WHO] | 5 [WHO] |
| Conductivity (mS/cm) | 4.59 | 4.20 | | 4.24 | 4 | | 4.26 | 1.4 [WHO] | 1 [WHO] |
| TDS (ppt) | 2530 | 2110 | | 2120 | 2010 | | 2050 | 1000 [WHO] | 2000 [WHO] |
| Salinity (mg/L) | 3.32 | 3.15 | | 3.20 | 3.19 | | 3.19 | 0.67 [WHO] | 0.46 [WHO] |
| D.O (mg/L) | 15.5 | 11.2 | | 8.9 | 30.2 | | 28.4 | 0-15 [WHO] | >5 [WHO] |
| pH | 7.65 | 7.52 | | 7.70 | 7.85 | | 7.98 | 6.5 - 8.5 [WHO,BIS] | 6 - 9 [WHO] |

# Chapter 8

# Conclusion, Summary and Scope of future work

# *Chapter 8*

## Summary, Conclusions and Future scope of work

*This chapter is divided into three parts; the first section is named as summary, which contains a brief gist of all the work presented in this thesis. Second section named as conclusions restrains the winding up of all the chapters and provides the inferences drawn from various work presented in this thesis. Last section is about suggestions towards the future scope.*

## 8.1 Summary

This work dealt with the preparation, characterization and applications of inexpensive ceramic membranes mainly from industrial waste such as fly ash. Extensive characterization was carried out using the prepared ceramic membranes by FESEM, TGA, XRD, EDX, Porosity etc. and indicated that the prepared membranes possessed desired properties for MF applications. The prepared ceramic membranes were used for the clarification of tomato juice. Providing adequate product quality and lower fouling. The left behind waste from tomato juice clarification process were used in the preparation of adsorbents for the removal of Co (II) from aqueous solutions. Prepared ceramic membranes were also coated with a thermo responsive polymer and BSA rejection properties were studied for the aforesaid composite membrane. Fluoride contaminated drinking water, drilling effluent rich in oil and grease and effluent water from steel industry were pretreated by electrocoagulation process. Prepared membranes were used for dead end of microfiltration of the pretreated drinking water and industrial wastewater. The major conclusions obtained from this study is summarized chapter wise and shown below.

## 8.2 Conclusion

***Chapter 2***

1. Contribution of fouling resistance was in between 98 % and 96 %, adsorption resistance 0.09 % to 0.33 %, pore plugging resistance from 0.33 % to 0.91 % and membrane resistance from 0.6 % to 2 % of overall total resistance.
2. Membrane pore sizes varied as MB1> MB2 >MB3 and accordingly permeate size changed as 10.36 µm, 1.04 µm and 220 nm respectively for MB1, MB2 and MB3.
3. Properties like color, clarity, density and suspended solids almost had a change of about 2-3 % from fresh juice properties.
4. Membrane MB2 was found to be more suitable for the clarification of tomato juice with better flux decline ratio (FDR) and flux recovery ratio (FRR) values of 0.68 and 0.77, respectively.

***Chapter 3***

1. Temperature had a profound effect on the filtration rate. A change in flux was observed from $0.03 \times 10^3$ L/h. $m^2$ to $0.49 \times 10^3$ L/h. $m^2$ for membrane M-5, $0.1 \times 10^3$ L/h. $m^2$ to $0.14 \times 10^3$ L/h. $m^2$ for membrane M-10, $0.19 \times 10^3$ L/h. $m^2$ to $1.39 \times 10^3$ L/h. $m^2$ for membrane M-15 and $0.7 \times 10^3$ L/h. $m^2$ to $1.68 \times 10^3$ L/h. $m^2$ for membrane M-20 as temperature increased from 25ºC to 90 ºC.
2. Above LCST the flux achieved was highest for membrane MB-20 at about $1.68 \times 10^3$ L/h.$m^2$ than at temperatures below LCST.
3. Percent BSA rejection was found to vary from 15 % to 5 % for membrane M-5 from 25 ºC to 90 ºC. Similar changes were observed for membrane M-10 with %

rejection changing from 21% to 7%, membrane M-15 from 68 % to 27.8 % and membrane M-20 from 69 % to 30 %.

4. A very good rejection of 68 % was observed for membrane M-15. Hydraulic permeability of the membrane M-15 decreased with an increase in dip coating time and increased with an increase in operating temperature.

***Chapter 4***

1. Adsorbents were prepared from tomato, carrot waste and PET by chemical activation method.
2. Activated carbon from carrot waste (ACW), activated tomato waste (ATW) and composite (APTC) gave a removal of 24 %, 37 % and 67 % respectively at an adsorbent dose of 1.2 g/L, 0.6 g/L and 0.8 g/L respectively.
3. The prepared adsorbents followed second order kinetics and Langmuir isotherm with an adsorption capacity of 312.50 mg/g for APTC which was significantly high in comparison to ACW and ATW with adsorption capacities of 56.17 and 170.06 mg/g respectively.
4. Cost estimation suggested that the prepared composite adsorbents is priced at 58.93 US$ per kg of adsorbent produced which is far less than the activated carbon available in the market at 172.96 US$ per kg of adsorbent.

***Chapter 5***

1. Defluoridation of contaminated drinking water was carried out with initial fluoride concentrations of 1.78, 4.79 and 7.89 mg/L.

2. Maximum removal at current density 15 A/$m^2$, inter-electrode distance of 0.005 m and NaCl concentration of 1.95 g/L resulting in final fluoride concentrations reduced to 0.009, 0.335 and 0.656 mg/L.
3. Filtered electro coagulated waster obeyed the drinking water specification as per WHO with pH, conductivity, TDS, turbidity and D.O. had values of 8.05 - 7.08, 2.94 - 1.50 mS/cm, 600 - 421 mg/L, 0.8 - 0.2 NTU and 14.3 - 6.5 mg/L.
4. Filtration studies suggested an increase in flux from 7.98 × 10-5 to 19.19 × 10-5 m3/m2.s when the pressure increased from 196 to 509 kPa.
5. The proposed hybrid technique was able to reduce the fluoride concentration of contaminated drinking water to below permissible limit of 1.5 mg/L.

***Chapter 6***

1. Electrocoagulation of effluent water from Tata Steel Limited resulted in lowering of the concentration of oil and grease from 35 mg/L to 14.2 mg/L in just 20 min. TDS values decreased from 3230 to 2780 mg/L.
2. Four different membranes prepared at sintering temperatures of 700, 800, 900 and 1000$^oC$ were utilized for the microfiltration studies. Trans-membrane pressures were maintained at three different pressures of 98,196 and 194 kPa. At a pressure of 98 kPa the permeate flux increased from 264 to 423 L/h.$m^2$ when sintering temperatures increased from 700 to 1000$^oC$.
3. 75-85 % of the initial flux was lost during the microfiltration of the electro-coagulated samples.
4. Low FRR values ranging from 0.040-0.131 suggested that thorough cleaning of membranes is necessary as the oily flocks produced during electrocoagulation

process strongly adhered to the membrane surface thereby resulting in the FRR values.

***Chapter 7***

1. At a current density of 50 A/m$^2$, inter-electrode distance of 0.005 m and run time of 20 min the concentrations of Na, Mg, K and Ca were reduced to 449, 54, 35 and 18 ppm respectively, whereas Mn and Fe were found to be completely removed.
2. The TDS concentrations were lowered to 2100, 2092 and 2070 ppm from an initial concentration of 2530 ppm at current densities of 20, 30 and 50 A/m$^2$, respectively.
3. Microfiltration studies were carried out at pressures of 103, 117 and 196 kPa. Membrane resistance contributed to about 71.8 % of the total offered resistance.
4. Produced flocks were analyzed using energy mapping which confirmed the presence of metals like calcium, magnesium, sodium, manganese, iron and potassium.

## 8.3 Future scope of work

Research findings in this work provided a good number of insights with respect to fabrication and applications of comparatively low cost ceramic and polymer ceramic composite membranes. Few research areas for future work are presented as follows:

***Preparation of tubular ceramic membranes***

1. Preparation and characterization of tubular ceramic membranes of a suitable composition using the extrusion method.

2. Study the impact of various membrane preparation parameters on the strength of the finished membranes.
3. To utilized methods such as rapid thermal processing (RTP) technique to reduce the overall sintering time of the prepared membranes.

***Preparation of pH responsive polymer ceramic membrane***

1. Composite polymer ceramic membrane can be prepared by the dip coating method.
2. Effect of parameters such as dipping time, polymer weight % and dipping method on the structural and morphological properties of the membrane.

***Preparation of dual responsive composite ceramic membranes***

1. Dual sensitivity of the ceramic membranes can be brought about by coating the membrane surface with a responsive pH-thermo responsive polymer
2. Study the simultaneous effect of temperature and pH on the morphology and the structure of the membrane.

***Continuous mode of electrocoagulation-microfiltration***

1. A continuous mode set up for the electrocoagulation and microfiltration must be utilized for the treatment for drinking water and industrial wastewater.
2. Operating parameters such as flow rate, electrocoagulation time etc. can be taken into consideration to determine the optimal parameters
3. Comparative study for the use of different type of electrode material for the same effluent and the same operating parameters.
4. Study the effect of adding precipitating agents like polyelectrolytes on the overall efficiency in the removal of toxic pollutants from wastewater.
5.

***Comparative study of adsorbents from food waste***

1. Utilize different type of agricultural and food waste for the preparation of adsorbents
2. Detailed characterization of the prepared adsorbents for a comparative study on the structural and morphological properties.
3. Cost analysis of the prepared adsorbents.
4. Regeneration study can be carried out for the re-usability of the adsorbents.

***Rigorous cost analysis***

1. A thorough cost analysis on the ceramic membrane preparation can be carried out for different type of raw materials used.
2. Detailed cost estimation for the electrocoagulation process considering parameters such as variation of electrode material, electrocoagulation time, precipitating agent used etc. can also be done.

# References

[1] M. Mulder, Basic principles of membrane technology, Kluwer Academic Publishers, Dordrecht, 1991.

[2] M. Cheryan, Ultrafiltration and microfiltration handbook, Technomic publishing Co. Inc. Lancaster, Pennsylvania, U.S.A, 1998.

[3] S.P. Nunes and K.V. Pinemann (Eds.), Membrane technology in the chemical industry, Wiley-VCH Verlag Gmbh, 2001.

[4] G. Pearce, Introduction to membranes: Membrane separation processes, CRC Press. Inc., Corporative Blvd., N.W., Boca Raton, Florida, 2000.

[5] Sh. K. Amin, H.A.M. Abdallah, M.H. Roushdy, S.A. El-Sherbiny, An Overview of production and development of ceramic membranes, IJAER, 11 (2016) 7708-7721

[6] P. Monash, G. Pugazhenthi, P. Saravanan, Various fabrication methods of porous ceramic supports for membrane applications, Reviews in chemical engineering, 29 (2013) 357-383

[7] Manohar, Development and characterization of ceramic membrane, International Journal of Modern Engineering Research, 2 (2012) 1492-1506

[8] R. Mallada, M. Menendez, Inorganic Membranes: Synthesis, Characterization and Applications, membrane science and technology, Series 13, Elsevier, The Netherlands, 2008.

[9] G. Singh, V.K. Bulasara, Preparation of low-cost micro-filtration membranes from fly ash, Desalin. Water Treat. 53 (2015) 1204-1212.

[10] N.P. Xu, W.H. Xing, Separation Technology and Application of Inorganic Membrane, Chem. Indus. Press (2003).

[11] J.H. She, T. Ohji, Fabrication and Characterization of Highly Porous Mullite Ceramics. Mater. Chem. Phys. 80 (2003) 610-614.

[12] Z. Xie, Study on Binder Removal Process of Ceramics Injection Molding. Bull. Chin. Ceram. Soc. 2 (1998) 18-21.

[13] Y.F. Liu , X.Q. Liu, H. Wei, G.Y. Meng , Porous Mullite Ceramics from National Clay Produced by Gelcasting. Ceram. Int. 27 (2001) 1-7.

[14] Y. Yoshino, T. Suzuki, B.N. Nair, H. Taguchi, N. Itoh , Development of tubular substrates, silica based membranes and membrane modules for hydrogen separation at high temperature. J. Membr. Sci. 267 (2005) 8-17.

[15] S. Li, H. Du, A. Guo, H. Xu, D. Yang, Preparation of self-reinforcement of porous mullite ceramics through in situ synthesis of mullite whisker in flyash body. Ceram. Int. 38 (2012) 1027-1032.

[16] Y. Dong, S. Hampshire , B. Z. Lin, Z. Ji , X. Zhang, Recycling of flyash for preparing porous mullite membrane supports with titania addition. J. Hazard Mater. 180 (2010) 173-180.

[17] S. Li, N. Li, Influences of composition of starting powders and sintering temperature on the pore size distribution of porous corundum-mullite ceramics. Sci. Sinter. 37 (2005) 173-180.

[18] V. Simitiy, N. Jumate, V. Moldovan, G. Thalmaier ,N. Sechel , Characterization of gradual porous ceramic structures obtained by powder sedimentation . J. Mater. Sci. Technol. 28 (2012) 362.

[19] Q. Chang, Y. Yang , X. Zhang , Y. Wang , J. Zhou, X. Wang , S. Cerneaux , L. Zhuc, Y. Dong, Effect of particle size distribution of raw powders on pore size distribution and bending

strength of Al2O3 micro-filtration membrane supports. J. Eur. Ceram. Soc. 34 (2014) 3819-3825.

[20] W. Yan and N. Li, Pore-size distribution and strength of porous mullite ceramics. Am. Ceram. Soc. Bull. 85 (2006) 9401-9406.

[21] M.T. Colomer , Nanoporous anatase ceramic membranes as fast-proton-conducting materials. J. Eur. Ceram. Soc. 26 (2006) 1231.

[22]V.V. Kharton, A.A. Yaremchenko, A.V. Kovalevsky, A.P. Viskup, E.N. Naumovich, P.F. Kerko, Perovskite-type oxides for high-temperature oxygen separation membranes. J. Memb. Sci. 163 (1999) 307-317.

[23] D. Vasanth, R. Uppaluri, G. Pugazhenthi, Influence of Sintering Temperature on the Properties of Porous Ceramic Support Prepared by Uniaxial Dry Compaction Method Using Low-Cost Raw Materials for Membrane Applications. Sep. Sci. Technol. 46 (2011) 1241-1249.

[24] S. Khemakhem, A. Larbot, R.B. Amar, New ceramic microfiltration membranes from Tunisian natural materials: Application for the cuttlefish effluents treatmen. Ceramics Intl. 35 (2009) 55-61.

[25] A.S. Chichkan, V.V. Chesnokov, E.Y. Gerasimov, V.N. Parmon , Production of nanoporous ceramic membranes using carbon nanomaterials . Dokl. Phys. Chem. 450 (2013) 135-137.

[26] N. Saffaj, S.A. Younssi, A. Albizane, A. messouadi, M. Bouhria, M. Persin, M. Cretin, A. Larbot. Preparation and characterization of ultrafiltration membranes for toxic removal from wastewater. Desalin. 168 (2004) 259-263.

[27] N. Saffaj, M. Persin, S.A. Younsi, A. Albizane, M. Cretin, A. Larbot, New ceramic microfiltration membranes from Tunisian natural materials: Application for the cuttlefish effluents treatment, Appl. Clay Sci. 31 (2006) 110-119 .

[28] T. Tsuru, T. Hino, T. Yoshioka, M. Asaeda, Permporometry characterization of microporous ceramic membranes. J. Membr. Sci. 186 (2001) 257-265.

[29] Global tomato production in 2013, Crops/World/2013 FAOSTAT. UN Food and Agriculture Organization. 2015.

[30] B.K. Nandi, B. Das, R. Uppaluri, M.K. Purkait, Micro-filtration of mosambi juice using low cost ceramic membrane. J. Food Eng. 95 (2009) 597-605.

[31] D. Ghosh , M.K. Sinha , M.K. Purkait, A comparative analysis of low-cost ceramic membrane preparation for effective fluoride removal using hybrid technique, Desalin. 327 (2013) 2-13.

[32] N. Subriyer, Treatment of domestic water using ceramic filter from natural clay and fly-ash. J. Eng. Studies Res. 19 (2013) 71-75.

[33] J. Fang, G. Qin, W. Wei, X. Zhao, Preparation and characterization of tubular supported ceramic micro-filtration membranes from fly ash. Sep. Purif. Technol. 80 (2011) 585-591.

[34] Y. Dong, S. Hampshire, J. Zhou, Z. Ji, J. Wang, G. Meng , Sintering and characterization of flyash-based mullite with MgO addition. J. Eur. Ceram. Soc. 31 (2011) 687-695.

[35] I. Jedidi , S. Saidi , S. Khmakem , A. Larbot , N.E. Ammar , A. Fourati , A. Charfi , R. B. Amar, New ceramic micro-filtration membranes from mineral coal fly ash . Arabian J. Chem. 2 (2009) 31-39.

[36] L. Zhua, Y. Dong, S. Hampshire, S. Cerneaux, L. Winnubst , Waste-to-resource preparation of a porous ceramic membrane support featuring elongated mullite whiskers with enhanced porosity and permeance. J. Eur. Ceram. Soc. 35 (2015) 711-721.

[37] F. Vaillant, A. Millan, M. Dornier, M. Decloux, M. Reynes, Strategy for economical optimisation of the clarification of pulpy fruit juices using crossflow micro-filtration. J. Food Engg. 48 (2001) 83-90.

[38] G.T. Vladisavljevic, P. Vukosavljevic, B. Bukvic, Permeate flux and fouling resistance in ultra-filtration of depectinized apple juice using ceramic membranes. J. Food Engg. 60 (2003) 241-247.

[39] A. Cassano, E. Drioli, G. Galaverna, R. Marchelli, G.D. Silvestro, P. Cagnasso, Clarification and concentration of citrus and carrot juices by integrated membrane processes. J. Food Engg. 57 (2003) 153-163.

[40] B. Jiao, A. Cassano, E. Drioli , Recent advances on membrane processes for the concentration of fruit juices: A review, J. Food Engg. 63 (2004) 303-305.

[41] A. Cassano, C. Conidi, E. Drioli, Clarification and concentration of pomegranate juice (Punica granatum L.) using membrane processes. J. Food Engg. 107 (2011) 366-373.

[42] P. Onsekizoglua, K.S. Bahcecib, M.J. Acara, Clarification and the concentration of apple juice using membrane processes: A comparative quality assessment. J. Membr. Sci. 352 (2010) 160-165.

[43] K. Riedl, B. Girard, R.W. Lencki, Influence of membrane structure on fouling layer mo[44] F. Vaillanta, M. Cissea, M. Chaverri, A. Perez, M. Dornier, F. Viquez, C.D. Mayera,

Clarification and concentration of melon juice using membrane processes, Innov. Food Sci. & Emerg. Technol. 6 (2005) 213.

[45] A. Cassano, E. Drioli, G. Galaverna, R. Marchelli, G.D. Silvestro, P. Cagnasso, Clarification and concentration of citrus and carrot juices by integrated membrane processes. J. Food Engg. 57 (2003) 153-163.

[46] A. Bottino , G. Capannelli, A. Turchini, P.D. Valleb, M. Trevisanc, Integrated membrane processes for the concentration of tomato juice, Desalination 148 (2002) 73-77.

[47] S.S. Koseoglu, J.T. Lawhon, E.W. Lusas, Use of membranes in citrus juice processing, Food Technology 44 (1990) 90-97.

[48] C.C. Pereira, J.M. Rufino, A.C. Habert, A. Nobrega, L.M.C. Cabral, C.P. Borges, Membrane for processing tropical fruit juice, Desalination 148 (2002) 57-60.

[48] D.E. Kirk, M.W. Mongomery, M.G. Kortekaas, Clarification of pear juice by hollow fiber ultra-filtration, J. of Food Scie. 48 (1983) 1663-1666.

[49] L. Carneiro, I.D. Sa, F.D. Gomes, V.M. Matta, L.M.C. Cabral, Cold sterilization and clarification of pineapple juice by tangential micro-filtration, Desalination 148 (2002), 93-98.

[50] F.Y. Ushikubo, A.P. Watanabe, L.A. Viotto, Micro-filtration of umbu (Spondias tuberose Arr. Com.) juice, J. of Membr. Sci. 288 (2007) 61-66.

[51] A. Cassano, M. Marchio, E. Drioli, Clarification of blood orange juice by ultra-filtration: analyses of operating parameters, membrane fouling and juice quality, Desalination 212 (2007) 15-27.

[52] A. Kozak, S. Banvolgyi, I. Vincze, I. Kiss, E. Bekassy-Molnar, G. Vatai, Comparison of integrated large scale and laboratory scale membrane processes for the production of black currant juice concentrate, Chemical Engineering & Processing: Process Intensification 47 (2008) 1171-1177.

[53] P.A. Vesilind, The Rosin-Rammler particle size distribution. Resor. Recovery Conserv. 5 (1980) 275-277.

[54] R.S. Faibish, Y. Cohen, Fouling resistant ceramic supported polymer membranes for ultrafiltration of oil-in-water microemulsions, J. Membr. Sci. 185 (2001) 129-143.

[55] Y. Matsumoto, M. Sudoh, Y. Suzuki, Preparation of composite UF membranes of sulfonated polysulfone coated on ceramics, J. Membr. Sci. 158 (1999) 55-62.

[56] S. Sachdeva, A. Kumar, Synthesis and modeling of composite poly(styrene-coacrylonitrile) membrane for the separation of chromic acid, J. Membr. Sci. 307 (2008) 37-52.

[57] L.L. Yang, Y.J. Zhao, S.Y. Zhou, M.S. Li, Y. Chen, W.H. Xing, Preparation of pH-responsive ceramic composite membranes by grafting acrylic acid onto $\alpha$-alumina membranes, Chinese Sci. Bull, 54 (2009) 2147-2149.

[58] W. Yoshida, Y. Cohen, Ceramic-supported polymer membranes for pervaporation of binary organic/organic mixtures, J. Membr. Sci.213 (2003) 145-157.

[59] Sterlitech Corporation, USA, http://www.sterlitech.com/ (May 2008).

[60] M. Goldman, D. Fraenkel, G. Levin, A zeolite/polymer membrane for separation of ethanol–water azeotrope, J. Appl. Polym. Sci. 37 (1989) 1791-1800.

[61] K.M. Song, W.H. Hong, Dehydration of ethanol and isopropanol using tubular type cellulose acetate membrane with ceramic support in pervaporation process, J. Membr. Sci. 123 (1997) 27-33.

[62] Y. Zhu, R.G. Minet, T.T. Tsotsis, A continuous pervaporation membrane reactor for the study of esterification reactions using a composite polymeric/ceramic membrane, Chem. Eng. Sci. 51 (1996) 4103-4113.

[63] Y. Zhu, H. Chen, Pervaporation separation and pervaporation–esterification coupling using crosslinked PVA composite catalytic membranes on porous ceramic plate, J. Membr. Sci. 138 (1998) 123-134.

[64] S. Ulutan, T. Nakagawa, Separability of ethanol and water mixtures through PTMSP-silica membranes in pervaporation, J. Membr. Sci. 143 (1998) 275-284.

[65] S. Sakohara, F. Muramoto, T. Sakata, M. Asaeda, Separation of acetone/water mixture by thin acrylamide gel membrane prepared in pores of thin ceramic membrane, J. Chem. Eng. Jpn. 23 (1990) 40-45.

[66] H. Kanazawa, Y. Kashiwase, K. Yamamito, Y. Matsushima, Temperature-responsive liquid chromatography. Effects of hydrophobic groups in N-isopropylacrylamide copolymer modified silica, Anal. Chem. 68 (1997) 823-830.

[67] A.M. Voice, J.P. Southall, V. Rogers, K.H. Matthews, G.R. Davies, J.E. Mcintyre, I.M. Ward, Thermoreversible polymer gel electrolytes, Polymer 35 (1994) 3363-3372.

[68] H.G. Schild, Poly(N-isopropylacrylamide): experiment, theory and application, Prog. Polym. Sci. 17 (1992) 163-249.

[69] Y. Hirose, G. Giannetti, J. Marguardt, T. Tanaka, Migration of ions and pH gradients in gels under stationary electric fields, J. Phys. Soc. Jpn. 61 (1992) 4085-4097.

[70] J.P. Gang, J. Kawakami, V.G. Sergeyev, Y. Osada, Electroconductive organgel: Preparation and properties of charge transfer complex gel in an organic-solvent, Macromolecules 24 (1991) 5246-5250.

[71] M. Kamachi, K. Takemoto, R.M. Ottenbrite, M. Kamachi (Eds.), Magnetic polymers in: Functional Monomers and Polymers, Marcel Dekker, New York, 1997, 149.

[72] A. Suzuki, T. Tanaka, Phase translation in polymer gels induced by visible Light, Nature 346 (1990) 345-347.

[73] Y. Ito, S. Kotera, M. Inaba, K. Kono, Y. Imanish, Control of pore size of polycarbonate membrane with straight pores by poly(acrylic acid) grafts, Polymer 31 (1990) 2157-2161.

[74] A.M. Mika, R.F. Childs, J.M. Dickson, B.E. McCarry, D.R. Gagnon, A new class of polyelectrolyte-filled microfiltration membranes with environmentally controlled porosity, J. Membr. Sci. 108 (1995) 37-56.

[75] G. Chen, A.S. Hoffman, Graft-copolymers that exhibit temperature-induced phase transition over a wide range of pH, Nature 373 (1995) 49-52.

[76] S. Zhou, A. Xue, Y. Zhang, M. Li, J. Wang, Y. Zhao, W. Xing, Fabrication of temperature-responsive ZrO2 tubular membranes, grafted with poly(N-isopropylacrylamide) brush chains, for protein removal and easy cleaning, J. Membr. Sci. 450 (2014) 351-361.

[77] Y. Zhao, S. Zhou, M. Li, A. Xue, Y. Zhang, J. Wanga, W. Xing, Humic acid removal and easy-cleanability using temperature responsive ZrO2 tubular membranes grafted with poly(N-isopropylacrylamide) brush chains, Water Res. 47 (2013) 2375-2386.

[78] F. Kursun, N. Isiklan Development of thermo-responsive poly(vinyl alcohol)-g-poly(N-isopropylacrylamide) copolymeric membranes for separation of isopropyl alcohol/water mixtures via pervaporation, J. Ind. Eng. Chem. 41 (2016) 91-104.

[79] X. Wang, J. Huang, X. Chen, X. Yu, Graft polymerization of N-isopropylacrylamide into a microporous polyethylene membrane by the plasma method: technique and morphology, Desalination, 450 (2002) 337-343.

[80] L. Liang, X. Feng, L. Peurrung, V. Viswanathan, Temperature-sensitive membranes prepared by UV photopolymerization of N-isopropylacrylamide on a surface of porous hydrophilic polypropylene membranes, J. Membr. Sci.162 (1999) 235-246.

[81] X. Yuan, W. Li, Z. Zhu, N. Han, X. Zhang, Thermo-responsive PVDF/PSMA composite membranes with micro/nanoscale hierarchical structures for oil/water emulsion separation, Coll. Surf. A: Physicochem. Eng. Aspects, 516 (2017) 305-316.

[82] L. Klouda, A.G. Mikos, Thermoresponsive hydrogels in biomedical applications, Eur. J. Pharm. Biopharm. 68 (2008) 34-45.

[83] N.S. Kotrappanavar, S. Roy, M.B. Patil, M.N. Nadagouda, W.E. Rudzinski, T.M. Aminabhavi, Cellulose acetate-coated α-alumina ceramic composite tubular membranes for wastewater treatmen. Desalination, 281 (2011) 348-353.

[84] G.C. Steenkamp, K. Keizer, H.W.J.P. Neomagus, H.M. Krieg, Copper(II) removal from polluted water with alumina/chitosan composite membranes, J. Memb. Sci. B 197 (2002) 147-156

[85] N. Zhang, S. Huber, A. Schulz, R. Luxenhofer, R. Jordan, Cylindrical Molecular Brushes of Poly(2-oxazoline)s from 2-Isopropenyl-2-oxazoline, Macromolecules 42 (2009) 2215-2221.

[86] Y.K. Hong, W.H. Hong, Influence of ceramic support on pervaporation characteristics of IPA/water mixtures using PDMS/ceramic composite membrane, J. Memb. Sci. 159 (1999) 29-39.

[87] M.E. Rezac, P.H. Pfromm, L.M. Costello, W.J. Koros, Aging of Thin Polyimide-Ceramic and Polycarbonate-Ceramic Composite Membranes, Ind. Eng. Chem. Res. 32 (1993) 1921-1926.

[88] S. Jana, M.K.Purkait, K. Mohanty, Clay supported polyvinyl acetate coated composite membrane by modified dip coating method: Application for the purification of lysozyme from chicken egg white. J. Membr. Sci. 382 (2011) 243-251.

[89] B.K. Nandi, R. Uppaluri and M.K. Purkait, Effects of dip coating parameters on the morphology and transport properties of cellulose acetate ceramic composite membranes, J. Membr. Sci. 330 (2009) 246-258.

[90] X. Cao, T. Zhang, Q.T. Nguyen, Y. Zhang, Z. Ping, A novel hydrophilic polymer-ceramic composite membrane 1: Acrylic acid grafting membrane, J. Membr. Sci. 312 (2008) 15-22.

[91] Y. Zhu, S. Xia, G. Liu, W. Jin, Preparation of ceramic-supported poly(vinyl alcohol)–chitosan composite membranes and their applications in pervaporation dehydration of organic/water mixtures, J. Membr. Sci. 349 (2010) 341-348.

[92] G. Yohannes, S.K. Wiedmer, M. Elomaa, M. Jussila, V. Aseyev, M.L. Riekkola, Thermal aggregation of bovine serum albumin studied by asymmetrical flow field-flow fractionation, Anal. Chim. Acta. 675 (2010) 191-198.

[93] J. Goel, K. Kadirvelu, C. Rajagopal, V.K. Garg, Removal of lead (II) by adsorption using treated granular activated carbon: batch and column studies, J. Hazard. Mater., 125 (2005) 211-220.

[94] E. Malkoc, Y. Nuhoglu, M. Dundar, Batch adsorption and kinetics of chromium (VI) removal from aqueous solutions by Ocimum americanum L. seed pods, J. Hazard. Mater., 161 (2009) 709-713.

[95] S. P. Dubey, K. Gopal, Adsorption of chromium (VI) on low cost adsorbents derived from agricultural waste material: A comparative study, J. Hazard. Mater., 145 (2007) 465-470.

[96] M.A Yahya, Z.A. Qodah, C.W.Z. Ngah, Agricultural bio-waste materials as potential sustainable precursors used for activated carbon production: A review, Renew. Sustainable Energy Rev., 46 (2015) 218–235.

[97] H. Sayğili, F. Güzel, Y. Onal, Conversion of grape industrial processing waste to activated carbon sorbent and its performance in cationic and anionic dyes adsorption, J. Clean. Prod., 93 (2015) 84-93.

[98] H. Sayğili, F. Güzel, High surface area mesoporous activated carbon from tomato processing solid waste by zinc chloride activation: Process optimization, characterization and dyes adsorption, J. Clean. Prod., 113 (2016) 995-1004.

[99] G.Z. Kyzas, E.A. Deliyanni, K.A. Matis, Activated carbon produced by pyrolysis of waste potato peels: cobalt ions removal by absorption, Colloids. Surf. A Physicochem. Eng. Asp., 490 (2016)74–83.

[100] Y.S. Ho, J.C.Y. Ng, G. McKay, Kinetics of pollution sorption by biosorption: review, Sep. Purif. Methods, 29 (2000) 189–232.

[101] A. Esfandiari, T. Kaghazchi, M. Soleimani, Preparation and evaluation of activated carbons obtained by physical activation of polyethyleneterephtalate (PET) wastes, J. Taiwan Inst. Chem. Eng., 43 (2012) 631–637.

[102] Z.A. Othman, M.A. Habila, R. Ali, Preparation of activated carbon using the co-pyrolysis of agricultural and municipal solid wastes at a low carbonization temperature, Carbon, 20 (2011).

[103] M. Adibfar, T. Kaghazchi, N. Asasian, M. Soleimani, Conversion of poly (ethylene terephthalate) waste into activated carbon: chemical activation and characterization, Chem. Eng. Technol., 37 (2014) 979–986.

[104] E. Ali, K. Tahereh, S.Mansooreh, Preparation of high surface area activated carbon from polyethylene terephthalate (PET) waste by physical activation, Res. J. Chem. Environ., 15 (2011) 433-437.

[105] S. Vijayakumar, P.R. Rajakumar, Infrared spectral analysis of waste pet samples, Int. Lett. Chem. Phys. Astron., 4 (2012) 58-65.

[106] N.P. Prorokova, A.V. Khorev, S.Y. Vavilova, Chemical method of surface activation of poly(ethylene terephthalate) fibre materials, Fibre Chem., 41 (2009) 158-163.

[107] F. Zhang, H. Itoh, Adsorbents made from waste ashes and post-consumer PET and their potential utilization in wastewater treatment, J. Hazard. Mater., 101 (2003) 323-337.

[108] http://www.who.int/ipcs/publications/cicad/cicad69%20, 2017 (accessed 30.08.2017).

[109] S. Rengaraj, S. Moon, Kinetics of adsorption of Co (II) removal from water and wastewater by ion exchange resins, Water Res., 36 (2002) 1783-1793.

[110] https://www.atsdr.cdc.gov/phs/phs.asp?id=371&tid=64, 2017 (accessed 30.08.2017).

[111] D.M. Manohar, B.F. Noeline, T.S. Anirudhan, Adsorption performance of Al-pillared bentonite clay for the removal of cobalt(II) from aqueous phase, Applied Clay Sci., 31 (2006) 194-206.

[112] M. Dai, The Effect of zeta potential of activate carbon on the adsorption of dyes from aqueous solution, J. Colloid Interface Sci., 164 (1994) 223-228.

[113] M. Ghaedi, A. Daneshyar, A. Asfaram, M.K. Purkait, Adsorption of naphthalene onto high-surface-area nanoparticle loaded activated carbon by high performance liquid chromatography: response surface methodology, isotherm and kinetic study, RSC Adv., 6 (2016) 54322-54330.

[114] S. Bahrani, M. Ghaedi, M.J. Mansoorkhani, A. Asfaram, A.A. Bazrafshan, M.K. Purkait, Ultrasonic assisted dispersive solid-phase microextraction of Eriochrome Cyanine R from water sample on ultrasonically synthesized lead (II) dioxide nanoparticles loaded on activated carbon: Experimental design methodology, Ultrason. Sonochem., 34 (2016) 317-324.

[115] M. Changmai, M.K. Purkait, Kinetics, equilibrium and thermodynamic study of phenol adsorptionusing NiFe2O4 nanoparticles aggregated on PAC, J. Water Proc. Eng., 16 (2017) 90–97.

[116] A .Basker, P.S. Syed-shabudeen, P. V. Kumar, Evaluation of adsorption potential of the agricultural waste areca husk carbon for methylene blue, J. ChemTech Res., 6 (2014) 1309-1324.

[117] M. Krzywinski, N. Altman, Points of Significance: Visualizing samples with box plots, Nature methods., 11 (2014) 119-120.

[118] K.A. Krishnan, T.S. Anirudhan, Kinetic and equilibrium modelling of cobalt (II) adsorption onto bagasse pith based sulphurised activated carbon, Chem. Eng. J., 137 (2008) 257-264.

[119] I.P. Suhasini, G. Sriram, S.R. Asolekar, G.K. Sureshkumar, Biosorptive removal and recovery of cobalt from aqueous systems, Process Biochem., 34 (1999) 239-247.

[120] A. Ahmadpour, M. Tahmasbi, T.R. Bastami, J.A. Besharati, Rapid removal of cobalt ion from aqueous solutions by almond green hull, J. Hazard. Mater., 166 (2009) 925-930.

[121] A. Bhatnagar, A.K. Minocha, M. Sillanpää, Adsorptive Removal of Cobalt from Aqueous Solution by Utilizing Lemon Peel as Biosorbent, J. Biochem. Eng., 48 (2010) 181-186.

[122] N.M. Andal, S. Charulatha, Univers. J. Environ. Res. Tech., 3 (2013) 375-384.

[123] R. Lakshmipathy, N.C Sarada, Application of watermelon rind as sorbent for removal of nickel and cobalt from aqueous solution, Int. J. Miner. Process., 122 (2013) 63-65.

[124] E. Erdem, N. Karapinar, R. Donat, The removal of heavy metal cations by natural zeolites, J. Colloid Interface Sci., 280 (2004) 309-314.

[125] E. Repo, T.A. Kurniawan, J.K. Warchol, M.E.T. Sillanpää, Removal of Co (II) and Ni (II) ions from contaminated water using silica gel functionalized with EDTA and/or DTPA as chelating agents, J. Hazard. Mater., 171 (2009) 1071-1080.

[126] H. Parab, S. Joshi, N. Shenoy, A. Lali, U.S. Sarma, M. Sudersanan, Determination of kinetic and equilibrium parameters of the batch adsorption of Co (II), Cr (III) and Ni (II) onto coir pith, Process Biochem., 41 (2006) 609-615.

[127] Ö. Yavuz, Y. Altunkaynak, F. Güzel, Removal of copper, nickel, cobalt and manganese from aqueous solution by kaolinite, Water Res., 37 (2003) 948-952.

[128]. World Health Organization, Guidelines for drinking-water quality. 1, 3rd ed., (2006) 375-376.

[129]. M. Mohapatra, S. Anand, B.K. Mishra, D.E. Giles, P. Singh, Review of fluoride removal from drinking water. J. Environ. Manage., 91 (2009) 67-77.

[130]. U.K. Garg, C. Sharma, Electrocoagulation : Promising technology for removal of fluoride from drinking water-A review. Biol. Forum Int. J., 8 (2016) 248-254.

[131]. K.L. Saxena, R. Sewak, Fluoride consumption in endemic villages of India and its remedial measures. Int. J. Eng. Sci. Inv., 4 (2013) 58-73.

[132]. M. Jimenez-Reyes, M. Solache-Rios, Sorption behavior of fluoride ions from aqueous solutions by hydroxyapatite. J. Hazard. Mater., 180 (2010) 297–302.

[133]. D. Ghosh, C.R. Medhi, M.K. Purkait, Treatment of fluoride containing drinking water by electrocoagulation using monopolar and bipolar electrode connection. Chemosphere, 73 (2008) 1393-1400.

[134]. World Health Organization, Guidelines for drinking water quality, Geneva, 4th ed., (2011) 370-372.

[135]. NHMRC, ARMCANZ, Australian drinking water guidelines, National health and medical research council and the agriculture and resource management council of Australia and New Zealand, 2004.

[136]. S. Yasmin, S. Monterio, P.A. Ligimol, D.D. Souza, Fluoride contamination and fluorosis in Gaya Region of Bihar, India. Current Biotica, 5 (2011) 232-236.

[137]. A.K. Shrivastav, M.K. Sharma, An Innovative Technique for removal of fluoride from drinking water. Sci. Revs. Chem. Commun., 2 (2012) 133-140.

[138]. P. Mariappan, V. Yegnaraman, T. Vasudevan, Occurrence and removal possibilities of fluoride in ground waters of India. Poll. Res., 19 (2000) 165-177.

[139]. L. Borah, N.C. Dey, Removal of fluoride from low TDS water using low grade coal. Indian J. Chem. Technol., 16 (2009) 361-363.

[140]. X. Wu, Y. Zhang, X. Dou, M. Yang, Fluoride removal performance of a novel Fe–Al–Ce trimetal oxide adsorbent. Chemosphere, 69 (2007) 1758-1764.

[141]. C.B. Shivayogimath, S. Punage, Optimization of parameters for fluoride removal by electrocoagulation using auminum electrodes in monopolar parallel combination. Int. J. Eng. Technol., 3 (2014) 1276-1280.

[142]. V.K. Gupta, I. Ali, V.K. Saini, Defluoridation of waste waters using waste carbon slurry. Water Res., 41 (2007) 3307–3316.

[143]. M. Hichour, F. Persin, J. Sandeaux, C. Gavach, Fluoride removal from water by Donnan dialysis. Sep. Purif. Technol., 18 (2007)1–11.

[144]. K. Hu, J.M. Dickson, Nanofiltration membrane performance on fluoride removal from water. J. Membr. Sci., 279 (2006) 529–538.

[145]. A. Tor, Removal of fluoride from water using anion-exchange membrane under Donnan dialysis condition. J. Hazard. Mater., 141 (2007) 814-818.

[146]. A. Mekonen, P. Kumar, A. Kumar, Integrated biological and physicochemical treatment process for nitrate and fluoride removal. Water Res., 35 (2001) 3127-3136.

[147]. A.A.M. Daifullah, S.M. Yakout, S.A. Elreefy, Adsorption of fluoride in aqueous solutions using KMnO4 modified activated carbon derived from steam pyrolysis of rice straw. J. Hazard. Mater., 147 (2007) 633-643.

[148]. S. Kumar, A. Gupta, J.P. Yadav, Fluoride removal by mixtures of activated carbon prepared from Neem (Azadirachta indica) and Kikar (Acacia arabica) leaves. Ind. J. Chem. Technol., 14 (2007) 355-36.

[149]. M. Arora, R.C. Maheshwari, S.K. Jain, A. Gupta, Use of membrane technology for potable water production. Desalination, 170 (2004) 105-112.

[150]. E. Bazrafshan, K.A. Ownagh, A.H. Mahvi, Application of electrocoagulation process using iron and aluminum electrodes for fluoride removal from aqueous environment. J. Chem., 9 (2012) 2297-308.

[151]. A. Takdastan, S.E. Tabar, A. Neisi, A. Eslami, Fluoride removal from drinking water by electrocoagulation using iron and aluminum electrodes. Jundishapur J. Health Sci. 6 (2014) 217-218.

[152]. K.R. Bulusu, B.B. Sunderasan, B.N. Pathak, W.G. Nawlakhe, D.N. Kulkarni, V.P. Thergaonkar, Fluoride in water, defluoridation methods and their limitations, J. Inst. Engineers, 60 (1979) 1-25.

[153]. E. Ergun, A. Tor, Y. Cengeloglu, I. Kocak, Electrodialytic removal of fluoride from water: Effects of process parameters and accompanying anions. Sep. Purif. Technol., 64 (2008)147-153.

[154]. H. Mjengera, G. Meenakshi, Appropriate defluoridation technology for use in fluorotic areas in Tanzania. 3rd Water Net Symposium Water Demand Management for Sustainable Development, 2003.

[155]. N. Razbe, R. Kumar, R. Pratima, R. Kumar, Various options for removal of fluoride from drinking water. IOSR J. App. Phys., 3 (2013) 40-47.

[156]. J.J. Schoeman, Water defluoridation, water denitrification and water desalination in rural areas in South Africa. Proceedings of the third IASTED African Conference, Power and Energy System, (2010) 244-247.

[157]. F. Shen, X. Chen, P. Gao, G. Chen, Electrochemical removal of fluoride ions from industrial wastewater. Chem. Eng. Sci., 58 (2003) 987-993.

[158]. C.S. Sundaram, S. Meenakshi, Fluoride sorption using organic-inorganic hybrid type ion exchangers. J. Coll. Interf. Sci., 333 (2009) 58-62.

[159]. L.S. Millar, P. Mondal, Simultaneous arsenic and fluoride removal from synthetic and real groundwater by electrocoagulation process: Parametric and cost evaluation. J. Environmen. Manag., 190 (2017) 102-112.

[160]. U.T. Un, A.S. Koparal, U.B. Ogutveren, Electrochemical process for the treatment of drinking water. Thirteenth International Water Technology Conference, IWTC 13 (2009) 129-137.

[161]. Parameter fact sheet -fluoride.2017. http://www.delagua.org/ (accessed 29 August 2017).

[162]. G.J. Nandilar, J. Lin, A. Arshad, S.J. Couperthwaite, Evaluation of electrocoagulation for the pre-treatment of coal seam water. J. Water Process Eng., 4 (2014) 166-178.

[163]. E. Bazrafashan, H. Moein, F.K. Mostafapour, S. Nakhaie, Application of Electrocoagulation Process for Dairy Wastewater Treatment, J. Chem., 2013, 8 pages.

[164]. S. Barışçı, O. Turkay, Domestic grey water treatment by electrocoagulation using hybrid electrode combinations. J. Water Process Eng., 10 (2016) 56–66.

[165]. A.M.H. Elnenary, E. Nassef, G.F. Malash, M.H.A. Magid, Treatment of drilling fluids wastewater by electrocoagulation, Egypt. J. Pet., 26 (2017) 203-208

[166]. Y.O. Fouad, Electrocoagulation of crude oil from oil-in-water emulsions using a rectangular cell with a horizontal aluminium wire gauze anode, J. Dispers. Sci. and Technol., 34 (2012) 214-221.

[167]. P. Cañizares, F. Martínez, C. Jiménez, C.S. Manuel, A. Rodrigo, Coagulation and electrocoagulation of oil-in-water emulsions, J. Hazard . Mater., 151 (2008) 44-51.

[168]. M. Carmona, M. Khemis, J.P. Lecler, F. Lapicque, A simple model to predict the removal of oil suspensions from water using the electrocoagulation technique, Chem. Eng. Sci., 61 (2006) 1237-1246.

[169]. E. Sabah, M. Çnar, M.S. Çelik, Decolorization of vegetable oils: Adsorption mechanism of β-carotene on acid-activated sepiolite, Food Chem., 100 (2007) 1661-1668.

[160]. U.T. Un, A.S. Koparal, U.B. Ogutveren, Electrochemical process for the treatment of drinking water. Thirteenth International Water Technology Conference, IWTC 13 (2009) 129-137.

[161]. Parameter fact sheet -fluoride.2017. http://www.delagua.org/ (accessed 29 August 2017).

[162]. G.J. Nandilar, J. Lin, A. Arshad, S.J. Couperthwaite, Evaluation of electrocoagulation for the pre-treatment of coal seam water. J. Water Process Eng., 4 (2014) 166-178.

[163]. E. Bazrafashan, H. Moein, F.K. Mostafapour, S. Nakhaie, Application of Electrocoagulation Process for Dairy Wastewater Treatment, J. Chem., 2013, 8 pages.

[164]. S. Barışçı, O. Turkay, Domestic grey water treatment by electrocoagulation using hybrid electrode combinations. J. Water Process Eng., 10 (2016) 56–66.

[165]. A.M.H. Elnenary, E. Nassef, G.F. Malash, M.H.A. Magid, Treatment of drilling fluids wastewater by electrocoagulation, Egypt. J. Pet., 26 (2017) 203-208

[166]. Y.O. Fouad, Electrocoagulation of crude oil from oil-in-water emulsions using a rectangular cell with a horizontal aluminium wire gauze anode, J. Dispers. Sci. and Technol., 34 (2012) 214-221.

[167]. P. Cañizares, F. Martínez, C. Jiménez, C.S. Manuel, A. Rodrigo, Coagulation and electrocoagulation of oil-in-water emulsions, J. Hazard . Mater., 151 (2008) 44-51.

[168]. M. Carmona, M. Khemis, J.P. Lecler, F. Lapicque, A simple model to predict the removal of oil suspensions from water using the electrocoagulation technique, Chem. Eng. Sci., 61 (2006) 1237-1246.

[169]. E. Sabah, M. Çnar, M.S. Çelik, Decolorization of vegetable oils: Adsorption mechanism of β-carotene on acid-activated sepiolite, Food Chem., 100 (2007) 1661-1668.

[170]. U.T. Un, A.S. Koparal, U.B. Ogutveren, Electrochemical process for the treatment of drinking water. Thirteenth International Water Technology Conference, IWTC 13 (2009) 129-137.

[171]. Parameter fact sheet -fluoride.2017. http://www.delagua.org/ (accessed 29 August 2017).

[172]. G.J. Nandilar, J. Lin, A. Arshad, S.J. Couperthwaite, Evaluation of electrocoagulation for the pre-treatment of coal seam water. J. Water Process Eng., 4 (2014) 166-178.

[173]. E. Bazrafashan, H. Moein, F.K. Mostafapour, S. Nakhaie, Application of Electrocoagulation Process for Dairy Wastewater Treatment, J. Chem., 2013, 8 pages.

[174]. S. Barışçı, O. Turkay, Domestic grey water treatment by electrocoagulation using hybrid electrode combinations. J. Water Process Eng., 10 (2016) 56–66.

[175]. A.M.H. Elnenary, E. Nassef, G.F. Malash, M.H.A. Magid, Treatment of drilling fluids wastewater by electrocoagulation, Egypt. J. Pet., 26 (2017) 203-208

[176]. N. Moulai-Mostefa, M. Tir, Coupling flocculation with electroflotation for waste oil/water emulsion treatment. Optimization of the operating conditions, Desalination, 161 (2004) 115-121.

[177]. X. Xu, X. Zhu, Treatment of refectory oily wastewater by electro-coagulation process, Chemosphere, 56 (2004) 889-894.

[178]. C.L. Lai, S.H. Lin, Treatment of chemical mechanical polishing wastewater by electrocoagulation: system performances and sludge settling characteristics, Chemosphere, 54 (2004) 235-242.

[179]. C.L. Yang, Electrochemical coagulation for oily water demulsification, Sep. Purif. Technol., 54 (2007) 388-395.

[180]. M. Kobya, O.T. Can, M. Bayramoglu, Treatment of textile wastewaters by electrocoagulation using iron and aluminum electrodes, J. Hazard. Mater., 100 (2003) 163-178.

[181]. M.Y.A. Mollah, P. Morkovsky, J.A.G. Gomes, M. Kesmez, J. Parga, D.L. Cockec, Fundamentals, present and future perspectives of electrocoagulation, J. Hazard. Mater., 114 (2004) 199-210.

[182]. M. Kobya, H. Hiz, E. Senturk, C. Aydiner, E. Demirbas, Treatment of potato chips manufacturing wastewater by electrocoagulation, Desalination, 190 (2006) 201-211.

[183]. Q. Zuoa, X. Chena, W. Li, C. Guohua, Combined electrocoagulation and electroflotation for removal of fluoride from drinking water, J. Hazard. Mater., 159 (2008) 452-457.

[184]. A. Aouni, C. Fersi, B. Mourad, A. Sik, D. Mahmoud, Treatment of textile wastewater by a hybrid electrocoagulation/nanofiltration process, J. Hazard. Mater., 168 (2009) 868-874.

[185]. W. Den, C. Wang, Removal of silica from brackish water by electrocoagulation pretreatment to prevent fouling of reverse osmosis membranes, Sep. Purif. Technol., 59 (2008) 318-325.

[186]. R. Mukherjee, M. Mondal, A. Sinha, S. Sarkar, S. De, Application of nanofiltration membrane for treatment of chloride rich steel plant effluent, J. Environ. Chem. Eng., 4 (2016) 1-9

[187]. U.B. Öğütveren, S. Koparal, Electrocoagulation for oil-water emulsion treatment, J. Environ. Sci. Health, Part A: Environ. Sci. Eng. Toxi., 32 (1997) 2507-2520.

[188]. X. Chen, G. Chen, P L. Yue, Separation of pollutants from restaurant wastewater by electrocoagulation, Sep. Purif. Technol., 19 (2000) 65-76.

[189]. P. Tiwari, Water quality assessment for drinking and irrigation purpose, Indian J. Sci. Res., 13 (2017) 140-142.

[190]. Standards for Effluent Discharge Regulations, General Notice No.44. of 2003, The Environmental protection act, Regulations made by the Minister under sections 39 and 96 of the Environment Protection Act, (2002).

[191]. S.N. Singh, G. Srivastav, A. Bhatt, Physicochemical Determination of Pollutants in Wastewater in Dheradun, Curr. World Environ., 7 (2012) 133-138

[192]. E. Bazrafashan, H. Moein, F.K. Mostafapour, S. Nakhaie, Application of Electrocoagulation Process for Dairy Wastewater Treatment, . J. Chem., (2013), 8 pages

[193]. Drinking Water Standards of BIS (IS: 10500: 1991).

[194]. Environmental protection agency (EPA), Patuxent Wastewater Treatment Facilities: Environmental Impact Statement, Philadelphia, Pennsylvania, 1975.

[195]. Drinking Water specifications of BIS (IS: 10500:2012)

[196]. Integrated iron and steel industry effluent discharge standards, Central pollution control board of India, 2017

[197]. A. Shalaby, E. Nassef, A. Mubark and M. Hussein, Phosphate Removal from Wastewater by Electroco-agulation Using Aluminum Electrodes,. Am. J.Environ. Eng. Sci. 1 (2014) 90-98.

[198]. Drinking Water Standards of BIS (IS: 10500: 1991).

[199]. P. Cañizares, F. Martínez, C. Jiménez, C.S. Manuel, A. Rodrigo, Coagulation electrocoagulation of oil-in-water emulsions, J. Hazard . Mater., 151 (2008) 44-51.

[200]. U.B. Öğütveren, S. Koparal, Electrocoagulation for oil-water emulsion treatment, J. Environ. Sci. Health, Part A: Environ. Sci. Eng. Toxi., 32 (1997) 2507-2520.

[201]. X. Chen, G. Chen, P.L. Yue, Novel electrode system for electroflotation wastewater, Environ. Sci. Technol., 36 (2002) 778-783.

[202]. C. N. Sawyer, P. L. McCarty, and G. F. Parkin, Chemistry for Environmental Engineering. Fourth Edition, McGraw-Hill, Inc., New York, (2000).

[203]. J. Lumsden, P. Stocker, S. Tsai, The composition and morphology of pits formed on iron in an inhibited chloride solution, Appl. Surf. Sci., 7 (1981) 347-354.

[204]. M. Murugananthan, G.B. Raju, S. Prabhakar, Removal of sulfide, sulfate and sulfite ions by electro coagulation, J. Hazard. Mater., 109 (2004) 37-44.

[205]. R. Dabeka, H. Conacher, J. Lawrence, W. Newsome, A. McKenzie, H. Wagner, R. Chadha, K. Pepper, Survey of bottled drinking waters sold in Canada for chlorate, bromide,

bromate, lead, cadmium and other trace elements, Food Addit. Contam., 19 (2002) 721-732.

[206]. L.I. Eriksson, Miller's Anesthesia Elsevier Health Sciences, 1 (2009).

[207]. L. Agostinho, L. Nascimento, B. Cavalcanti, Water hardness removal for industrial use: application of the electrolysis process, Open Access Sci. Rep., 1 (2012) 460-465.

[208]. M. Al-Shannag, Z. Al-Qodah, K. Bani-Melhem, M.R. Qtaishat, M. Alkasrawi, Heavy metal ions removal from metal plating wastewater using electrocoagulation: Kinetic study and process performance, Chem. Eng. J., 260 (2015) 749-756.

[209]. L. Zhao, P.C.-Y. Chang, W.W. Ho, High-flux reverse osmosis membranes incorporated with hydrophilic additives for brackish water desalination, Desalination, 308 (2013) 225-232.

[210]. L.Y. Ng, A.W. Mohammad, C.Y. Ng, C.P. Leo, R. Rohani, Development of nanofiltration membrane with high salt selectivity and performance stability using polyelectrolyte multilayers, Desalination, 351 (2014) 19-26.

[211]. N. Hilal, H. Al-Zoubi, N. Darwish, A. Mohamma, M.A. Arabi, A comprehensive review of nanofiltration membranes: treatment, pretreatment, modelling, and atomic force microscopy, Desalination, 170 (2004) 281-308.

[212]. M. Plattes, A. Bertrand, B. Schmitt, J. Sinner, F. Verstraeten, J. Welfring, Removal of tungsten oxyanions from industrial wastewater by precipitation, coagulation and flocculation processes, J. Hazard. Mater., 148 (2007) 613-615.

[213]. X.-L. Wang, T. Tsuru, S.-i. Nakao, S. Kimura, Electrolyte transport through nanofiltration membranes by the space-charge model and the comparison with Teorell-Meyer-Sievers model, J. Membr. Sci., 103 (1995) 117-133.

[214]. A.K. Pabby, S.S. Rizvi, A.M.S. Requena, Handbook of membrane separations: chemical, pharmaceutical, food, and biotechnological applications, CRC press, (2015).

[215]. D.M. Warsinger, J. Swaminathan, E. Guillen-Burrieza, H.A. Arafat, Scaling and fouling in membrane distillation for desalination applications: A review, Desalination, 356 (2015) 294-313.

[216]. F. Manenti, M. Masi, G. Santucci, G. Manenti, Parametric simulation and economic assessment of a heat integrated geothermal desalination plant, Desalination, 317 (2013) 193-205.

[217]. G. Mouedhen, M. Feki, M.D.P. Wery, H. Ayedi, Behavior of aluminum electrodes in electrocoagulation process, J. Hazard. Mater., 150 (2008) 124-135.

[218]. P. Ganesan, J. Lakshmi, G. Sozhan, S. Vasudevan, Removal of manganese from water by electrocoagulation: adsorption, kinetics and thermodynamic studies, Can. J. Chem. Eng., 91 (2013) 448-458.

[219]. R. Katal, H. Pahlavanzadeh, Influence of different combinations of aluminum and iron electrode on electrocoagulation efficiency: Application to the treatment of paper mill wastewater, Desalination, 265 (2011) 199-205.

# *Appendix A: Calibration Curve for the determination of oil and grease in drilling effluents*

The determination of oil and grease concentration in the electro coagulated samples is determined by first preparing a calibration curve. Obtained effluent samples had an oil and grease concentration of 35 mg/L. Hence, standard oil and grease emulsions in the concentration range of 10 – 35 mg/L were prepared using Millipore water and specific amounts of effluent samples. The prepared standards thus prepared were sonicated for 7-8 h before analysis. The obtained emulsions with varied concentrations were analyzed for their absorbance using UV-Visible spectrophotometer at a wavelength of 235 nm. Subsequently, the obtained absorbance values were plotted with respect to variations in emulsion solution concentration. Figure A1 presents the obtained calibration curve in this regard. It can be observed that the absorbance varied linearly with variation in oil and grease concentration. Thus, using the obtained calibration curve, the concentration of electro coagulated samples were evaluated by measuring its absorbance.

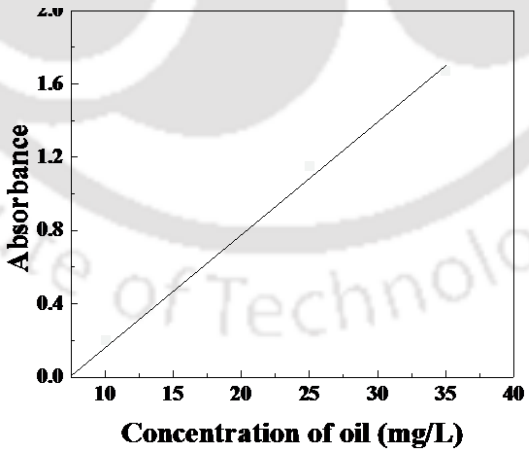


**Figure A1: Calibration curve for the evaluation of oil-water emulsion concentration in permeate samples.**

# *Appendix B: Determination of metals in steel industry effluent*

The determination of metals concentration (Na, Mg, Ca, K, Fe and Mn) in the electro coagulated samples is determined by first preparing a fresh stock solution of 1000 mg/L for each metal concentration individually. Standard solutions in the range of 10-100 mg/L as per requirement for each metal were prepared from the stock solution. The obtained standard solutions with varied concentrations were analyzed for their absorbance using Atomic absorbance spectrophotometer at the corresponding wavelength for each metal to fit the calibration values in the software analyzing the standard samples. The obtained absorbance values were plotted with respect to variations in solution concentration. Subsequently, the calibration values were used in the determination of unknown concentration of electrocoagulated samples.

# *Appendix B: Error Analysis*

Error analysis is necessary as it infers to the accuracy of calculations and reliability of reported data. Although experiments are carried out with utmost care, yet due to measurement errors, the data obtained or calculated may not be accurate. There are different types of errors viz. absolute error, relative error, systematic error and random error. Absolute error refers to the difference between the measured or inferred value of a quantity and its actual value. Relative error is the ratio of the error to the best value of the quantity. Systematic errors are the results of faulty assumptions and measuring techniques whereas random errors result from variation in the precision of measuring parameters and the slight variations that occur in successive measurements under nearly identical conditions.

**Error measurement in membrane resistance calculation**

The measurement maximum error for the estimation of membrane resistance for tomato juice clarification is about ± 2-3 %. These errors were taken under consideration considering the variations in the experimental measurements during the determination of permeate flux during MF experiments.

**Error measurements for kinetic and equilibrium models**

Error calculations were also done for the kinetic and equilibrium models for the adsorbents prepared from tomato and carrot waste. An error of ± 2 % was taken into consideration for each of the models calculated.